Water Science and Technology Library

MOMENT ANALYSIS FOR SUBSURFACE HYDROLOGIC APPLICATIONS

by

Rao S.Govindaraju and Bhabani S. Das

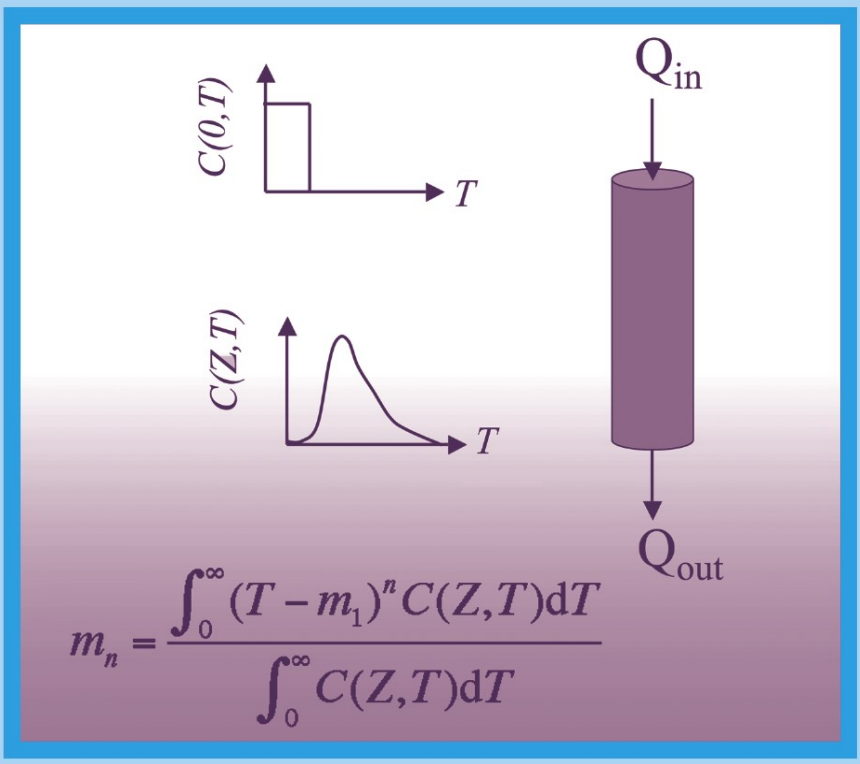

MOMENT ANALYSIS FOR SUBSURFACE HYDROLOGIC APPLICATIONS

Water Science and Technology Library

VOLUME 61

The titles published in this series are listed at the end of this volume.

MOMENT ANALYSIS FOR SUBSURFACE HYDROLOGIC APPLICATIONS

by

RAO S. GOVINDARAJU
Purdue University,
West Lafayette, IN, U.S.A.

and

BHABANI S. DAS
Indian Institute of Technology,
Kharagpur, W.B., India

Springer

A C.I.P. Catalogue record for this book is available from the Library of Congress.

ISBN 978-1-4020-5751-9 (HB)
ISBN 978-1-4020-5752-6 (e-book)

Published by Springer,
P.O. Box 17, 3300 AA Dordrecht, The Netherlands.

www.springer.com

Cover Image: A schematic of a miscible displacement setup. A typical miscible displacement (solute transport) experiment consists of the addition of a solute along with the flowing electrolyte solution through the top end of the soil column for a fixed amount of time followed by the continuation of flow with the same electrolyte solution containing no solute. The solution enters the soil column at the column surface ($Z = 0$) with a volumetric flow rate of Q_{in} and exits the column bottom end (Z) with a volumetric flow rate of Q_{out}. The concentration $[C(0,T)]$ of inflow solution as a function of time (T) is represented in the top graph and is known as the pulse-type input boundary condition. Expected concentration $[C(Z,T)]$ of the solute at depth Z as a function of time is represented in the bottom graph. This graph is called a breakthrough graph (BTC). Typically, when a BTC is bell-shaped, it resembles a probability distribution function. Different features of such BTCs may be studied using the method of moments akin to the method of moments used to describe probability distributions. This figure shows the mathematical formula for the central moments (m_n) of the order n.

Printed on acid-free paper

TABLE OF CONTENTS

PREFACE

The use of moments is quite ubiquitous, and its applications cover many areas of physical and mathematical sciences. In this regard, subsurface contaminant transport is no exception with many experimental, numerical, and theoretical studies utilizing moments to further our understanding of the subject. This book is essentially derived from a set of course notes that the senior author had developed for a graduate level course on moment analysis for subsurface contaminant transport problems.

The subject of moments, even when restricted to subsurface contaminant problems, is very vast. This book focuses on specific aspects of theoretical moment analysis for partial differential equations governing contaminant transport problems. Most of the development presented here is for one-dimensional problems, but the extension to higher dimensions can be performed in similar fashion in most cases with more investment in algebra. The motivation for this topic arises from applications in parameter estimation, and for providing insights into solute behavior. While several books discuss moments in various applications, we did not find a book that has this particular focus.

There are several other important topics in connection with moments that arise in subsurface contaminant transport, but are not addressed here. The book is almost entirely based on deterministic analysis, and stochastic theories are rarely utilized. There is no discussion on the class of solute transport problems that would result in nonlinear governing equations, as such problems are not directly addressed by the techniques discussed in this book.

Probability distributions play a key role in moment analysis. For completeness, we provide a basic review of moment generating functions as they arise in probability theory. This is the reason for the first chapter, but the emphasis is on moments along with a brief introduction to distributions that are possible candidates for solute transport models. The next two chapters serve as an introduction to Laplace and Fourier transforms, but they are presented in the context of solute transport models and, therefore, serve as introduction to topics of temporal and spatial moments for physical and chemical nonequilibrium models. The differences between flux-averaged concentrations and volume-averaged concentrations are also emphasized in these chapters.

The fourth chapter discuses similarities between travel time distributions and impulse response functions, and the use of stream tube models. Advective-dispersive models, and stochastic-advective models are presented here. Chapter 5 and Chapter 6

talk about temporal and spatial moments, respectively, with the dimensionless form of the physical and chemical nonequilibrium models serving as the motivating problem. Chapter 7 shows the utility of these techniques for cases where substantial mass transfer occurs in the vapor phase. Cases of both mobile and immobile air phases are discussed.

Chapter 8 then presents the more powerful method of moment generating differential equations. Again, temporal and spatial moments are discussed for the physical nonequilibrium model, and some cases of layered heterogeneity are examined. Chapter 9 shows applications of moments to cases when a system of partial differential equations is utilized for describing sequential chain reactions.

The remaining chapters deal with topics that are somewhat out of the ordinary use of moments. Chapter 10 explores the connection between interval computing methods and moment applications along with a few application examples. Chapter 11 deals with subsurface drainage, where the focus is primarily on unsaturated vertical flow combined with saturated groundwater flow. The governing equations have to be simplified, and the use of moments in this regard for analyzing flow data in the context of tile drains is illustrated. Chapter 12 outlines methods of reconstructing concentration distributions from the knowledge of moments.

The students that we have worked with over the years have contributed greatly to our learning. The senior author would like to specifically acknowledge (alphabetically) Mazdak Arabi, T.P. Chan, Shih-Chieh Kao, Nazmun Nahar, Rishi Parashar, Jennifer Stillman, and Shivam Tripathi for their contributions to this work. Many of them have been co-authors on manuscripts from which sections of this book have been derived, while others have provided help with analysis, computations, and figures. We also like to thank Dr. Peter J. Shouse, and Dr. Heiko M. Langner for permitting us to use a few experimental solute transport data as example calculations. Earlier drafts of this manuscript were typed by Mrs. Dinah Hackerd, and towards the end by Mrs. Judy Haan. Their patience and perseverance is appreciated. Despite our best efforts, it is likely that errors that could have crept in, and we take responsibility for them. Please bring them to our attention.

Finally, we hope that this book will serve as a useful tool for both beginners and advanced researchers interested in moment analysis.

Rao S. Govindaraju
Bhabani S. Das

CHAPTER 1

RANDOM VARIABLES AND GENERATING FUNCTIONS

1.1. INTRODUCTION TO RANDOM VARIABLES

A convenient conceptualization for studying random quantities is to first define a *sample space*, S, as the set of all possible outcomes of an experiment. Each individual outcome is called a sample point, s. An event A consists of a set of possible outcomes s, and is therefore a subset of S. Two events A_1 and A_2 are *mutually exclusive* (or disjoint) if they have no sample points in common. To every event A, one can assign a probability, denoted by $P(A)$, under the following constraints:

$$0 \leq P(A) \leq 1 \text{ for any event } A \tag{1.1.1}$$

$$P(S) = 1 \tag{1.1.2}$$

If $A_i,\ i = 1,\ 2,\ 3 \ldots$, are mutually exclusive, then

$$P(A_1 \text{ or } A_2 \text{ or } A_3 \text{ or } \ldots) = \sum_i P(A_i) \tag{1.1.3}$$

A *random variable* $X(s)$ is a single-valued numerical function that is defined for all $s \in S$, and is often called as the value of the random variable X at s. There are two kinds of random variables that are popularly used in applications – discrete and continuous. A *discrete random variable* $X(s)$ assumes denumerable (finite or infinite) number of values. For each such possible value x_i, there exists a corresponding probability p_i such that

$$P[X(s) = x_i] = p_i,\ i = 0,\ 1,\ 2,\ \ldots \tag{1.1.4}$$

The sequence $\{p_i\}$ is called the *probability mass function* of $X(s)$, and the corresponding *cumulative mass function* is

$$F_X(x) = P[X(s) \leq x] = \sum_{x_i \leq x} p_i \tag{1.1.5}$$

In the particular case when the random variable assumes only one value x_k with $p_k = 1$, then $X(s)$ is called a *degenerate distribution*, i.e. there is no uncertainty associated with it. In what follows, we will drop the reference to the sample space and simply refer to a random variable by a capital letter (X in this instance). As an example, we note that many phenomena are well-represented by the discrete *Poisson* random variable. The probability mass function of a Poisson random variable X with a single parameter λ is

$$p_k = \frac{\lambda^k}{k!} e^{-\lambda}, k = 0, 1, 2, \ldots, \lambda > 0 \tag{1.1.6}$$

The Poisson variable X may be used to describe the number of occurrences of a random quantity in unit time. The sample space is $S = \{0,\ 1,\ 2, \ldots\}$. Other common discrete distributions are listed in Table 1.1.1.

Most of our interest will be centered around the second class of random variables called *continuous random variables*. These can be defined in terms of a non-negative function $f_X(x)$ such that

$$P[a \leq X \leq b] = \int_a^b f_X(x)\ dx \tag{1.1.7}$$

Table 1.1.1. Some discrete random variables

Bernoulli random variable $S = \{0,\ 1\}$ $E[X] = p;\ \text{Var}[X] = p\ (1-p)$ $G(z) = (q + pz)$	This random variable describes an indicator function that takes a value of 1 (or success) with probability p and a value of 0 (or failure) with a probability of $q = 1 - p$. This random variable serves as the building block for many other random variables.
Binomial random variable $S = \{0,\ 1, \ldots, n\}$ $pk = \binom{n}{k} p^k (1-p)^{n-k} \quad k = 0, 1, \ldots, n$ $E[X] = np;\ \text{Var}[X] = np\ (1-p)$ $\Phi(\omega) = (q + p\omega)^n$	A random variable X denoting the number of successes in n Bernoulli trials is the Binomial random variable. Alternatively, it can be described as the sum of n independent and identically distributed Bernoulli random variables.
Geometric random variable $S = \{0,\ 1,\ 2, \ldots\}$ $p_k = p(1-p)^k\ k = 0,\ 1, \ldots$ $E[X] = \frac{1-p}{p};\ \text{Var}[X] = \frac{1-p}{p^2}$ $\Phi(\omega) = \frac{p}{1-q\omega}$	The random variable X is the number of failures before the first success in a sequence of Bernoulli trials.
Negative binomial random variable $S = \{r,\ r+1, \ldots\}$, where r is a positive integer $pk = \binom{k-1}{r-1} p^r (1-p)^{k-r}\ k = r, r+1, \ldots$ $E[X] = \frac{r}{p};\ \text{VAR}[X] = \frac{r(1-p)}{p^2}$	Here, the random variable X is the number of Bernoulli trials before the r-th success is observed.
Poisson random variable $S = \{0,\ 1,\ 2, \ldots\}$ $p_k = \frac{\lambda^k}{k!} e^{-\lambda}\ k = 0, 1, \ldots$ and $\lambda > 0$ $E[X] = \lambda;\ \text{Var}[X] = \lambda$ $\Phi(\omega) = e^{\lambda(\omega - 1)}$	The random variable X denotes the number of events occurring in unit time. This random variable also forms the basic building block for many random processes. The inter-arrival times between Poisson events is exponentially distributed.

The function $f_X(x)$ is called the *probability density function* (pdf) of the random variable X with the corresponding *cumulative distribution function* (cdf) defined as

$$F_X(x) = P[X \leq x] = \int_{-\infty}^{x} f_X(y)\, dy \tag{1.1.8}$$

and from (1.1.7),

$$P[a \leq X \leq b] = F_X(b) - F_X(a) \tag{1.1.9}$$

For proper random variables, whether discrete or continuous, we have

$$F_X(\infty) = 1 \tag{1.1.10}$$

If the cdf possesses sufficient continuity, then

$$f_X(x) = \frac{dF_X(x)}{dx} \tag{1.1.11}$$

A normal (or Gaussian) random variable Y is described by the following pdf

$$f_Y(y) = \frac{1}{\sqrt{2\pi}\sigma} \exp\left[-\frac{(y-\mu)^2}{2\sigma^2}\right], -\infty \leq y \leq \infty \ldots. \tag{1.1.12}$$

where μ and σ^2 are the parameters of the distribution. Thus, a random variable is characterized by the parameters and functional form of its distribution. The Gaussian random variable belongs to a more general class of exponential-type distributions described briefly in Appendix A.

A function of random variable is itself a random variable. If X and Y are random variables and $Y = g(X)$ where $g(\cdot)$ is a monotonic function, then the pdf of Y in terms of the pdf of X can be easily expressed as a derived distribution

$$f_Y(y) = f_X(x)\left|\frac{dx}{dy}\right| \tag{1.1.13}$$

where $x = g^{-1}(y)$. Consider, for instance, a log-normal random variable X that is defined as $Y = \ln X$ where Y is normally distributed in equation (1.1.12). Using (1.1.13), the pdf of the log-normal random variable X is obtained as

$$f_X(x) = \frac{1}{x\sigma\sqrt{2\pi}} \exp\left[-\frac{(\ln x - \mu)^2}{2\sigma^2}\right], \quad x \geq 0 \tag{1.1.14}$$

Table 1.1.2 provides a list of some of the common continuous probability density functions that are encountered in practice.

Table 1.1.2. Some continuous random variables

Uniform random variable
$S = [a, b]$
$f_X(x) = \frac{1}{b-a}\ a \le x \le b$
$E[X] = \frac{a+b}{2}$; $\mathrm{Var}[X] = \frac{(b-a)^2}{12}$
$\Phi_X(\omega) = \frac{e^{j\omega b} - e^{j\omega a}}{j\omega(b-a)}$

Exponential random variable
$S = [0, \infty]$
$f_X(x) = \lambda e^{-\lambda x}\ \ x \ge 0\ and\ \lambda = 0$
$E[X] = \frac{1}{\lambda}$; $\mathrm{Var}[X] = \frac{1}{\lambda^2}$
$\Phi_X(\omega) = \frac{\lambda}{\lambda - j\omega}$

Gaussian (normal) random variable
$S = (-\infty, +\infty)$
$f_X(x) = \frac{e^{-(x-\mu)^2/2\sigma^2}}{\sqrt{2\pi}\sigma}\ \ -\infty < x < \infty$ and $\sigma > 0$
$E[X] = \mu$; $\mathrm{Var}[X] = \sigma^2$
$\Phi_X(\omega) = e^{j\mu\omega - \sigma^2\omega^2/2}$

Gamma random variable
$S = (0, \infty)$
$f_X(x) = \frac{\lambda(\lambda x)^{\alpha-1} e^{-\lambda x}}{\Gamma(\alpha)}$
where $\Gamma(z)$ is the gamma function
$E[X] = \alpha/\lambda$; $\mathrm{Var}[X] = \alpha/\lambda^2$
$\Phi_X(\omega) = \frac{1}{(1 - j\omega/\lambda)^\alpha}$

Chi-square random variable with k degrees of freedom
$S = (0, +\infty)$
$f_X(x) = \frac{x^{(k-2)^2} e^{-x/2}}{2^{k/2}\,\Gamma(k/2)}\ x > 0$
$\Phi_X(\omega) = \left(\frac{1}{1 - j2\omega}\right)^{k/2}$
Remarks: The sum of k mutually independent, squared zero – mean, unit – variance Gaussian random variables is a chi-square random variable with k degrees of freedom. This is a special case of the Gamma random variable with $\alpha = k/2$, k is a positive integer and $\lambda = 1/2$.

Rayleigh random variable
$S = [0, \infty]$
$f_X(x) = \frac{x}{\alpha^2} e^{-x^2/2\alpha^2}\ \ x \ge 0\ \alpha > 0$
$E[X] = \alpha\sqrt{\pi/2}$; $\mathrm{Var}[X] = (2 - \pi/2)\alpha^2$

One can define two discrete random variables on the same sample space. Their *bivariate probability distribution* $\{p_{ij}\}$ is defined as

$$p_{ij} = P[X = x_i \text{ and } Y = y_j],\ \ i, j = 0, 1, \ldots \tag{1.1.15}$$

with

$$\sum_i \sum_j p_{ij} = 1 \tag{1.1.16}$$

The *marginal sequences* or *marginal distributions* of p_i and q_j are defined as

$$p_i = \sum_j p_{ij} = \sum_j P[X = x_i, Y = y_j] = P[X = x_i] \tag{1.1.17}$$

$$q_j = \sum_i p_{ij} = \sum_i P[X = X_i, Y = y_j] = P[Y = y_j] \tag{1.1.18}$$

The *conditional probability distribution* of Y given $X = x_i$ is

$$P[Y = y_j | X = x_i] = \frac{P[X = x_i,\ Y = y_j]}{P[X = x_i]} = \frac{p_{ij}}{p_i},\ \text{for } p_i > 0 \tag{1.1.19}$$

The two random variables X and Y are independent if the knowledge of one of them has no influence on our estimate of the other, i.e.

$$P[Y = y_j \,|\, X = x_i] = P[Y = y_j] \tag{1.1.20}$$

or

$$P[X = x_i, Y = y_j] = p_{ij} = p_i p_j \tag{1.1.21}$$

Similar definitions hold when X and Y are continuous random variables. A *joint pdf* $f_{X,Y}(x, y)$ is defined so that

$$P[x_1 \le X \le x_2, y_1 \le Y \le y_2] = \int_{y_1}^{y_2} \int_{x_1}^{x_2} f_{X,Y}(x, y)\ dx\ dy \tag{1.1.22}$$

In addition,

$$\int_{-\infty}^{\infty} \int_{-\infty}^{\infty} f_{X,Y}(x, y)\ dx\ dy = 1 \tag{1.1.23}$$

The joint cdf of two continuous random variables X and Y is

$$F_{X,Y}(x, y) = P[X \le x, Y \le y] = \int_{-\infty}^{y} \int_{-\infty}^{x} f_{XY}(x', y') dx'\ dy' \tag{1.1.24}$$

For instance, two jointly distributed Gaussian random variables X and Y have a joint pdf given by

$$f_{X,Y}(x, y) = \frac{1}{2\pi\sigma_x\sigma_y\sqrt{1-\rho_{XY}^2}} \cdot$$
$$\exp\left\{-\frac{1}{2(1-\rho_{XY}^2}\left[\left(\frac{x-\mu_x}{\sigma_x}\right)^2 - 2\rho_{XY}\left(\frac{x-\mu_x}{\sigma_x}\right)\left(\frac{y-\mu_y}{\sigma_y}\right)\left(\frac{y-\mu_y}{\sigma_y}\right)^2\right]\right\}$$
$$-\infty \le x, y \le \infty \tag{1.1.25}$$

where μ_x, μ_y, σ_x, σ_y, and ρ_{XY} are the five parameters of this model. In the (x, y) space, the joint pdf is centered at (μ_x, μ_y). Note that the pdf is constant if the argument of the exponential term is a constant. When $\rho_{XY} = 0$, the equal pdf contour is an ellipse whose principal axes are parallel to the x and y axis. When $\rho_{XY} \neq 0$, the major axis of the ellipse of equal pdf is oriented at an angle θ given as

$$\theta = \frac{1}{2}\ arc\ \tan\left(\frac{2\ \rho_{XY}\ \sigma_x\ \sigma_y}{\sigma_x^2 - \sigma_y^2}\right) \tag{1.1.26}$$

Just as in the discrete case, marginal density functions are defined as follows for jointly distributed continuous random variables

$$f_X(x) = \int_{-\infty}^{\infty} f_{X,Y}(x, y)\ dy \tag{1.1.27a}$$

$$f_Y(y) = \int_{-\infty}^{\infty} f_{X,Y}(x, y)\ dx \tag{1.1.27b}$$

For example, the marginal pdf of X from (1.1.25) is obtained as

$$f_X(x) = \frac{1}{\sqrt{2\pi}\ \sigma_x} \exp\left[-\frac{(x-\mu_x)^2}{2\sigma_x^2}\right] \tag{1.1.28}$$

which has the same form as (1.1.12)

For continuous random variables, conditional probability density functions are defined as

$$f_X(x/y) = \frac{f_{X,Y}(x, y)}{f_Y(y)},\ f_Y(y) > 0 \tag{1.1.29a}$$

$$f_Y(y/x) = \frac{f_{X,Y}(x, y)}{f_X(x)},\ f_X(x) > 0 \tag{1.1.29b}$$

It follows that the conditional cdf of X is given by

$$F_X(x/y) = \lim_{h \to 0} F_X(x\,|y < Y \leq y + dh) = \frac{\int_{-\infty}^{x} f_{X,Y}(x', y)\ dx'}{f_Y(y)} \tag{1.1.30}$$

For instance, using (1.1.25), (1.1.28) and (1.1.29a) the conditional pdf of X given $Y = y$ is

$$f_X(x|y) = \frac{1}{\sqrt{2\sigma_x^2(1-\rho_{XY}^2)}} . \exp\left\{-\frac{1}{2(1-\rho_{xy}^2)\sigma_x^2}\left[x - \rho_{XY}\frac{\sigma_x}{\sigma_y}(y-\mu_y) - \mu_x\right]^2\right\} \tag{1.1.31}$$

Two continuous random variables X and Y are independent if

$$f_{X,Y}(x, y) = f_X(x)\ f_Y(y) \tag{1.1.32}$$

The concept of joint distributions can be extended to many random variables leading to multivariate distributions. Thus, if $X_1, X_2, \ldots, X_n$ are a sequence of random variables then their joint cdf and pdf are related as

$$F_{X_1,X_2,\ldots,X_n}(x_1, x_2, \ldots, x_n) = P[X_1 \le x_1, X_2 \le x_2, .., X_n \le x_n]$$
$$= \int_{-\infty}^{x_n} \int_{-\infty}^{x_{n-1}} \cdots \int_{-\infty}^{x_2} \int_{-\infty}^{x_1} f_{X_1,X_2,\ldots,X_n}(x_1', x_2', .., x_n') dx_1', dx_2', .., dx_n' \tag{1.1.33}$$

1.2. EXPECTATION

Mathematically, the *expectation* of a random variable, when it exists, is defined for a discrete random variable as

$$E[X] = \sum_i x_i p_i \tag{1.2.1}$$

and for a continuous random variable as

$$E[X] = \int_{-\infty}^{\infty} x\, f_X(x)\, dx \tag{1.2.2}$$

Thus the expected value of a Poisson random variable whose probability mass function is given by (1.1.6) is

$$E[X] = \sum_{k=0}^{\infty} k \frac{\lambda^k}{k!} e^{-\lambda} = \lambda \tag{1.2.3}$$

More generally, the expectation of a function of a random variable $g(X)$ is defined as follows for X a discrete and continuous random variable, respectively.

$$E[g(X)] = \begin{matrix} \sum_i g(x_i)\, p_i \\ \int_{-\infty}^{\infty} g(x)\, f_X(x)\, dx \end{matrix} \tag{1.2.4}$$

In particular, equation (1.2.4) may be used to define the n-th *moment* of a random variable X as

$$\mu_n = E[X^n] = \sum_i x_i^n\, p_i, \text{ for } X \text{ discrete} \tag{1.2.5a}$$

$$= \int_{-\infty}^{\infty} x^n f_X(x)\, dx, \text{ for } X \text{ continuous} \tag{1.2.5b}$$

The zeroth moment, for which $n = 0$ in (1.2.5a,b), $\mu_0 = 1$ by definition of a random variable. The first moment $\mu_1 (n = 1)$ is called the *mean* or *expectation* of the random variable. The *variance* of a random variable is defined as

$$Var[X] = \sigma_x^2 = E[(X - E[X])^2] = E[X^2] - E^2[X] \tag{1.2.6}$$

where σ_x is called the standard deviation of X. Moments are measures of central tendencies of a distribution, and play a key role in the concepts presented in this book. For instance, consider the random variable Y defined by the Gaussian pdf in (1.1.12). The distribution is symmetric about the parameter μ_y.

$$E[Y] = \mu_y \tag{1.2.7}$$

Since (1.1.12) is a pdf, we have

$$\int_{-\infty}^{\infty} \frac{1}{\sqrt{2\pi}\ \sigma_y} \exp\left[-\frac{(y-\mu_y)^2}{2\sigma_y^2}\right] dy = 1 \tag{1.2.8}$$

Differentiating both sides of (1.2.8) with respect to σ_y and rearranging, we obtain

$$Var[Y] = E[(Y-\mu_y)^2] = \sigma_y^2 \tag{1.2.9}$$

Next, consider the log-normal random variable X that was defined in (1.1.14) through the transformation $Y = \ln\ X$ or $X = e^Y$. Then from (1.2.4),

$$E[X] = \mu_X = \int_{-\infty}^{\infty} e^y f_y(y)\ dy = \exp\left[\mu_y + \frac{\sigma_y^2}{2}\right] \tag{1.2.10}$$

$$\begin{aligned} Var[X] = \sigma_x^2 &= \int_{-\infty}^{\infty} (e^y - \mu_x)^2\ f_y(y)\ dy \\ &= \int_{-\infty}^{\infty} e^{2y}\ f_y(y)\ dy - \mu_x^2 \\ &= \exp\left(2\mu_y\right)\left[\exp\left(2\sigma_y^2\right) - \exp\left(\sigma_y^2\right)\right] \end{aligned} \tag{1.2.11}$$

Conversely, the following relationships hold between the means and variances of the two random variables X and Y in this case

$$\mu_y = \ell n \frac{\mu_x}{\sqrt{1+\sigma_x^2/\mu_x^2}} \tag{1.2.12}$$

$$\sigma_Y^2 = \ell n\left(1 + \frac{\sigma_x^2}{\mu_x^2}\right) \tag{1.2.13}$$

Along with moments, it is often convenient to define *central moments*. The n-th central moment of a random variable X is

$$m_n = E[(X - E[X])^n],\ \ n = 1, 2, 3\ldots \tag{1.2.14}$$

From (1.2.6), we observe that the variance of X is its second central moment. Another measure of central tendency that is of interest is expressed in terms of *factorial moments*. The r-th factorial moment is defined as

$$\alpha_r = E[X(X-1)(X-2)\ldots(X-r+1)],\ \ r = 1, 2, 3 \tag{1.2.15}$$

Factorial moments are related to ordinary moments. For instance

$$E[X] = \alpha_1 \tag{1.2.16}$$

$$Var[X] = \alpha_2 + \alpha_1 - \alpha_1^2 \tag{1.2.17}$$

For multiple random variables, conditional expectations can be defined. Thus, the *conditional expectation* of Y given X is

$$E[Y\,|X = x_i\,] = \sum_j\ y_j\ \frac{p_{ij}}{p_i},\ \ p_i > 0 \tag{1.2.18a}$$

$$E[Y|X = x] = \int_{-\infty}^{\infty} y \frac{f_{XY}(x, y)}{f_X(x)}\ dy,\ \ f_X\,(x) > 0 \tag{1.2.18b}$$

Expectation is a linear operation, i.e., if $X_1, X_2, \ldots, X_n$ are random variables, then

$$E[a_0 + a_1X_1 + a_2X_2 + \ldots + a_nX_n] = a_0 + a_1\ E[X_1] + \ldots + a_n\ E[X_n] \tag{1.2.19}$$

When several variables are involved, we use *joint moments* to summarize their behavior. The *jk*-th joint moment of two random variable X and Y is defined as

$$E[X^jY^k] = \sum_i \sum_m\ x_i^j\ y_m^k\ p_{im},\ \ X \text{ and } Y \text{ discrete} \tag{1.2.20a}$$

$$= \int_{-\infty}^{\infty} \int_{-\infty}^{\infty} x^j y^k\ f_{X,Y}\ (x, y)\ dxdy,\ \ X \text{ and } Y \text{ continuous} \tag{1.2.20b}$$

For $j = k = 1$ in (1.2.20), *E[XY]* is called the correlation of X and Y. If $E[XY] = 0,\ X$ and Y are called *orthogonal random variables*. The *jk*-th central moment of X and Y is defined as $E[(X - E[X])^j(Y - E[Y])^k]$. The *covariance* of X and Y is their joint central moment for $j = k = 1$,

$$\begin{aligned} Cov[X, Y] =& E[(X - E[X])(Y - E[Y])] \\ =& E[XY] - E[X]E[Y] \end{aligned} \tag{1.2.21}$$

If X and Y are independent, then $Cov[X, Y] = 0$.

The *correlation coefficient* of the two random variables X and Y is

$$\rho_{X,Y} = \frac{Cov[X, Y]}{\sigma_x\sigma_y} \tag{1.2.22}$$

If $\rho_{X,Y} = 0$, then X and Y are uncorrelated.

Consider a random variable U that is a linear combination of random variables $X_1, X_2, \ldots, X_n$.

$$U = a_1X_1 + a_2X_2 + \ldots + a_nX_n \tag{1.2.23}$$

Then

$$Var[U] = \sum_{i=1}^{n} \sum_{j=1}^{n} a_i a_j \; Cov\left[X_i, X_j\right] \tag{1.2.24}$$

If the random variables $X_1, X_2, \ldots, X_n$ are independent,

$$Var[U] = \sum_{i=1}^{n} a_i^2 \; \sigma_{X_i}^2 \tag{1.2.25}$$

1.3. THE CHARACTERSITIC FUNCTION

The *characteristic function* of a random variable X is defined as

$$\phi_X(\omega) = E[e^{j\omega X}] = \int_{-\infty}^{\infty} e^{j\omega x} f_X(x) \; dx \tag{1.3.1}$$

where $j = \sqrt{-1}$, and ω is a parameter that is as yet unspecified. The characteristic function may be interpreted as the *Fourier transform* of the probability density function $f_X(x)$ where X can take values in the range $-\infty \leq x \leq \infty$. A more formal description of the Fourier transform is given in Chapter 3. Since $f_X(x)$ and $\phi_X(\omega)$ are *Fourier transform pairs*, the pdf can be recovered from the characteristic function by an inversion formula

$$f_X(x) = \frac{1}{2\pi} \int_{-\infty}^{\infty} \phi_X(\omega) e^{-j\omega x} \; d\omega \tag{1.3.2}$$

The pdf of a random variable is therefore completely defined by its characteristic function.

If X is a discrete random variable taking on values x_k with probability p_k, then one can define a discrete Fourier transform as follows

$$\phi_X(\omega) = \sum_{k} e^{jwx_k} \cdot p_k \tag{1.3.3}$$

In particular, if the discrete random variable X is integer-valued, then the characteristic function is

$$\phi_X(\omega) = \sum_{k} e^{j\omega k} \; p_k \tag{1.3.4}$$

In the above equation, it can be observed that the Fourier transform is a periodic function of ω with a period of 2π, since

$$e^{j(\omega + 2\pi)k} = e^{j\omega k} \cdot e^{jk \cdot 2\pi} = e^{j\omega k} \tag{1.3.5}$$

where we have used the identity $e^{j\theta} = \cos\theta + j \sin\theta$.

The following discrete inversion formula expresses the *pmf* in terms of the discrete Fourier transform

$$p_k = \frac{1}{2\pi}\int_0^{2\pi} \phi_X(\omega)e^{-j\omega k}d\omega \tag{1.3.6}$$

The probabilities p_k are essentially the coefficients of the Fourier series of the characteristic function $\phi_X(\omega)$. The characteristic function of several discrete and continuous random variables are given in Tables 1.1.1 and 1.1.2, respectively.

The moments of X are easily obtained from $\phi_X(\omega)$ by expanding $exp(j\omega x)$ in a power series so that

$$\begin{aligned}\phi_X(\omega) &= \int_{-\infty}^{\infty}\left\{1 + j\omega x + \frac{(j\omega x)^2}{2!} + \frac{(j\omega x)^3}{3!} + \ldots.\right\} f_X(x)\ dx \\ &= 1 + j\omega E[X] + \frac{(j\omega)^2}{2!}E[X^2] + \frac{(j\omega)^3}{3!}E[X^3] + \ldots\end{aligned} \tag{1.3.7}$$

where it is assumed that all the moments exist and term-by-term integration is possible. Differentiating the characteristic function n times with respect to ω, the moments are obtained as

$$E[X^n] = \frac{1}{j^n}\frac{d^n}{d\omega^n}\phi_X(\omega)\,|_{\omega=0} \tag{1.3.8}$$

For example, the pdf of an exponential random variable is

$$f_X(x) = \lambda e^{-\lambda x},\ \ x \geq 0,\ \ \lambda > 0 \tag{1.3.9}$$

Its characteristic function is obtained as

$$\phi_X(\omega) = \int_0^{\infty} e^{j\omega x}\cdot\lambda e^{-\lambda x}\ dx = \frac{\lambda}{\lambda - j\omega} \tag{1.3.10}$$

Taking the derivative of $\phi_X(\omega)$ with respect to ω and setting it to zero yields

$$\frac{d\phi_X(\omega)}{d\omega}\,|_{\omega=0} = \frac{\lambda j}{(\lambda - j\omega)^2}\,|_{\omega=0} = \frac{j}{\lambda} \tag{1.3.11}$$

and the mean of X from (1.3.8) for $n = 1$ is

$$E[X] = \frac{1}{j}\frac{d\,(\phi_X(\omega))}{d\omega}\,|_{\omega=0} = \frac{1}{\lambda} \tag{1.3.12}$$

Hence the characteristic function is also a moment generating function.

The concept of the characteristic function can be extended to several random variables. If $X_1, X_2, \ldots, X_n$ are n random variables, their joint characteristic function is defined as

$$\phi_{X_1,X_2,\ldots,X_n}(\omega_1, \omega_2, \ldots, \omega_n) = E[\exp(j\omega_1 X_1 + j\omega_2 X_2 + \ldots. + j\omega_n X_n] \tag{1.3.13}$$

Thus, if X and Y are two continuous random variables with their joint pdf given by $f_{X,Y}(x, y)$, then

$$\phi_{X,Y}(\omega_1, \omega_2) = \int_{-\infty}^{\infty}\int_{-\infty}^{\infty} e^{j(\omega_1 x+\omega_2 y)}\ f_{X,Y}(x, y)\ dxdy \tag{1.3.14}$$

which can be recognized as the two-dimensional Fourier transform of $f_{X,Y}(x, y)$. The corresponding inversion formula to recover the pdf is

$$f_{X,Y}(x, y) = \frac{1}{4\pi^2}\int_{-\infty}^{\infty}\int_{-\infty}^{\infty}\phi_{X,Y}(\omega_1, \omega_2)e^{-j(\omega_1 x+\omega_2 y)}\ d\omega_1 d\omega_2 \tag{1.3.15}$$

We can define a *marginal characteristic function* as

$$\phi_X(\omega) = \phi_{X,Y}(\omega, 0),\ \text{or}\ \phi_Y(\omega) = \phi_{X,Y}(0, \omega) \tag{1.3.16}$$

A direct consequence of two random variables X and Y being independent is that their joint characteristic function factorizes into the product of their marginals, i.e.

$$\phi_{X,Y}(\omega_1, \omega_2) = \phi_X(\omega_1)\phi_Y(\omega_2) \tag{1.3.17}$$

Furthermore, if X and Y are independent, and we define a random variable Z as a linear combination of X and Y

$$Z = aX + bY \tag{1.3.18}$$

then

$$\phi_Z(\omega) = \phi_X(a\omega)\phi_Y(b\omega) \tag{1.3.19}$$

implying that the characteristic function of a sum of independent random variables can be expressed as a product of the individual characteristic functions. This is often called the convolution property of the characteristic function.

In particular, if $X_1, X_2, \ldots, X_n$ are a sequence of independent and identically distributed (iid) random variables and $Z = X_1 + X_2 + \ldots + X_n$, then

$$\phi_Z(\omega) = [\phi_X(\omega)]^n \tag{1.3.20}$$

The joint characteristic function (1.3.17) may be utilized to obtain joint moments as an extension to the case of a single random variable.

$$\phi_{X,Y}(\omega_1, \omega_2) = \sum_{i=0}^{\infty}\sum_{k=0}^{\infty}\frac{(j\omega_1)^i}{i!}\frac{(j\omega_2)^k}{k!}E[X^i Y^k] \tag{1.3.21}$$

Taking derivatives with respect to the transform parameters and setting these parameters to zero yields

$$E[X^i Y^k] = \frac{1}{(j)^{i+k}}\cdot\frac{\partial^i\partial^k}{\partial\omega_1^i\partial\omega_2^k}[\phi_{X,Y}(\omega_1, \omega_2)]\,\big|_{\omega_1=\omega_2=0} \tag{1.3.22}$$

1.4. THE LAPLACE TRANSFORM

Laplace transforms offer a convenient method for generating moments of non-negative random variables. A large number of random variables (travel times, concentrations, physical properties such as conductivities, porosities, velocities, dispersion coefficients, etc.) do not assume negative values. The Laplace transform for a non-negative random variable X is defined as

$$\mathcal{L}_X(s) = E[e^{-sx}] = \int_{-\infty}^{\infty} e^{-sx} f_X(x)\ dx \tag{1.4.1}$$

where s is a transform parameter. The Laplace transform essentially provides the same information for non-negative random variables as does the characteristic function. One can expand the exponential term into an infinite series such that

$$\begin{aligned}\mathcal{L}_X(s) &= \int_{-\infty}^{\infty} (1 - sx + \frac{s^2}{2!}\ x^2 - \frac{s^3}{3!} x^3 + \ldots) f_X(x)\ dx \\ &= 1 - s\ E[X] + \frac{s^2}{2!}\ E[X^2] - \frac{s^3}{3!}\ E[X^3] + \ldots\end{aligned} \tag{1.4.2}$$

assuming, of course, that all the moments exist and term-by-term integration is allowed. From (1.4.2), the moments are obtained as

$$E[X^n] = (-1)^n \frac{d^n}{ds^n} [\mathcal{L}_X(s)]\,|_{s=0} \tag{1.4.3}$$

Let us consider the gamma distribution for a random variable X whose pdf is given as (Table 1.1.2)

$$f_X(x) = \frac{\lambda^\alpha\ x^{\alpha-1} e^{-\lambda x}}{\Gamma(\alpha)},\ \ x \geq 0 \tag{1.4.4}$$

From (1.4.1), the Laplace transform is

$$\mathcal{L}_X(s) = \frac{\lambda^\alpha}{\Gamma(\alpha)} \int_0^\infty x^{\alpha-1} e^{-(\lambda+s)x}\ dx = \frac{\lambda^\alpha}{(\lambda+s)^\alpha} \tag{1.4.5}$$

From (1.4.3) it follows that

$$E[X] = \alpha/\lambda \tag{1.4.6}$$

and

$$E[X^2] = \frac{\alpha(\alpha+1)}{\lambda^2} \tag{1.4.7}$$

implying that the variance of the gamma random variable in this case is $Var[X] = \alpha/\lambda^2$.

It is sometimes more convenient to work with the cumulative distribution function $F_X(x)$ of a random variable X. The *Laplace-Stieltjes transform* is defined as

$$\mathcal{L}^*(s) = \int_0^\infty e^{-sx} dF_X(x), \ s \geqslant 0 \tag{1.4.8}$$

The Laplace transform uniquely defines the corresponding density function.

Let Z denote a random variable defined as the sum of two independent random variables X and Y with probability density functions $f_X(x)$ and $g_Y(y)$, respectively. The pdf of $Z(= X + Y)$ is defined by the *convolution*

$$f_Z(x) = \int_0^x f_X(x-y)\ g_Y(y)\ dy = f^* g \tag{1.4.9}$$

where the subscripts X and Y have been omitted on the last expression in (1.4.9). Then the Laplace transform of Z as

$$\mathcal{L}_Z(s) = E[e^{-sZ}] = \mathcal{L}_X(s) \cdot \mathcal{L}_Y(s) \tag{1.4.10}$$

Indeed, if we define Z as the sum of n iid. random variables $X_1, X_2, \ldots, X_n$, then

$$\mathcal{L}_Z(s) = \mathcal{L}^{\check{}}_{X_1+X_2+\ldots+X_n}(s) = [\mathcal{L}_X(s)]^n \tag{1.4.11}$$

1.5. PROBABILITY GENERATING FUNCTIONS

Generating functions are a powerful tool for analyzing random variables. The *probability generating function* (pgf) is particularly useful when dealing with discrete random variables. If X is a random variable taking integer values such that

$$P[X = k] = p_k, \ k = 0, \ 1, \ 2, \ldots. \tag{1.5.1}$$

then the pgf of X is given by the power series

$$G_X(s) = p_0 + p_1 s + p_2 s^2 + \ldots \tag{1.5.2}$$

Note that each of the p_k values lies between 0 and 1, so that the infinite series $G_X(s)$ will definitely converge for $|s| \leq 1$. It can be shown that the $G_X(s)$ uniquely defines the pmf of the random variable X. Under some regularity conditions, (1.5.2) implies

$$p_k = \frac{1}{k!} \frac{d^k G_X(s)}{ds^k}\Big|_{s=0}, \ k = 0, 1, 2, \ldots \tag{1.5.3}$$

It is clear that

$$G_X(1) = p_0 + p_1 + p_2 + \ldots = 1.0 \tag{1.5.4}$$

The power series in (1.5.2) can be thought of as an expectation

$$G_X(s) = E[s^X] \tag{1.5.5}$$

The probability generating function may be utilized to evaluate factorial moments (assuming they exist) as shown

$$E[X] = p_1 + 2p_2 + \ldots = \frac{d}{ds} G_X(s)\Big|_{s=1} \tag{1.5.6}$$

$$E[X(X-1)] = \frac{d^2}{ds^2} G_X(s)\Big|_{s=1} \tag{1.5.7}$$

and, in general

$$E[X(X-1)\ldots.(X-m+1)] = \frac{d^m}{ds^m} G_X(s)\Big|_{s=1} \tag{1.5.8}$$

In terms of the factorial moments, the variance is obtained as

$$\sigma_x^2 = E[X(X+1)] + E[X] - \{E[X]\}^2 \tag{1.5.9}$$

The concept of convolution is applicable to discrete random variables as well, and probability generating functions are useful in this regard. Suppose two discrete integer-valued random variables X and Y are described as

$$P[X = i] = p_i,\ P[Y = j] = q_j,\ i, j = 0, 1, 2, \ldots \tag{1.5.10}$$

We define their sum $Z(= X + Y)$ whose pmf is

$$P[Z = k] = r_k = p_0 q_k + p_1 q_{k-1} + \ldots + p_k q_0 \tag{1.5.11}$$

The sequence $\{r_k\}$ may be thought of as a convolution of the two sequences $\{r_k\} = \{p_k\}^*\{q_k\}$. The probability generating function of Z is the product of the probability generating functions of X and Y.

$$G_Z(s) = G_X(s)\ G_Y(s) \tag{1.5.12}$$

Indeed, if Z is the sum of n independent discrete integer-valued random variables $X_1, X_2, \ldots, X_n$, the above result can be extended as

$$G_Z(s) = G_{X_1}(s)\ G_{X_2}(s) \ldots . \mathrm{G}_{\mathrm{X_n}}(s) \tag{1.5.13}$$

Furthermore, if the random variables $X_1, X_2, \ldots, X_n$ are iid., then

$$G_Z(s) = [G_{X_1}(s)]^n \tag{1.5.14}$$

Consider a random variable X that is Poisson distributed as in (1.1.6). The probability generating function of X is given as

$$G_X(s) = \sum_{k=0}^{\infty} s^k \frac{e^{-\lambda}\lambda^k}{k!} = e^{-\lambda(1-s)} \tag{1.5.15}$$

If Y is another Poisson random variable independent of X with parameter α such that

$$P[Y = k] = \frac{e^{-\alpha}\alpha^k}{k!},\ k = 0, 1, 2, \ldots \tag{1.5.16}$$

then its probability generating function is $e^{-\alpha(1-s)}$. Defining $Z = X + Y$, the probability generating function of Z is

$$G_Z(s) = G_X(s) \cdot G_Y(s) = e^{-(\lambda+\alpha)(1-s)} \tag{1.5.17}$$

implying that Z is itself Poisson distributed with the parameter $(\lambda + \alpha)$.

To extract probabilities from the probability generating function, one can resort to (1.5.3) which involves taking repeated derivatives and can become a tedious exercise. It is, of course, much more convenient if the pgf can be expanded in a power series of s as shown in (1.5.2), so that the corresponding probabilities may be obtained by simple inspection. As an example, say the pgf of a random variable X can be expressed as

$$G(s) = \frac{P(s)}{Q(s)} \tag{1.5.18}$$

where $P(s)$ and $Q(s)$ are polynomials of degrees ℓ, and m respectively $(\ell < m)$. Setting $Q(s) = 0$ would therefore yield m roots (assumed distinct) namely $s_1, s_2, \ldots, s_m$. Then $G(s)$ in (1.5.18) can be decomposed into partial fractions as

$$G(s) = \frac{a_1}{s_1 - s} + \frac{a_2}{s_2 - s} + \ldots + \frac{a_m}{s_m - s} \tag{1.5.19}$$

where the n-th constant is given as

$$a_n = \frac{P(s_r)}{Q'(s_r)},\ r = 1, 2, \ldots, m \tag{1.5.20}$$

We note that the general term in (1.5.19) may be expressed as

$$\frac{1}{s_n - s} = \frac{1}{s_n(1 - s/s_n)} = \frac{1}{s_n}\left[1 + s/s_n + (s/s_n)^2 + \ldots\right] \tag{1.5.21}$$

for $s \leq s_n$. Thus the coefficient of s^k in (1.5.19) is

$$p_k = \frac{a_1}{s_1^{k+1}} + \frac{a_2}{s_2^{k+1}} + \ldots + \frac{a_k}{s_m^{k+1}} \tag{1.5.22}$$

If we select s_1 to be the smallest root in absolute value, then an approximate result may be obtained as

$$p_k \cong \frac{a_1}{s_1^{k+1}} \tag{1.5.23}$$

1.6. CUMULANTS AND CUMULANT GENERATING FUNCTIONS

Cumulants, like moments, are properties that are used to characterize random variables. Very frequently, the full probabilistic description, in terms of the multivariate joint probability density of a random process cannot be found easily. In many practical applications we restrict our attention to the first few moments. It is known that cumulants (or semi-invariants) of a random variable, if they exist, determine the nature of the random variable uniquely (Kendall and Stuart, 1977; Gardiner, 1985). Cumulants can be applied to a wide variety of problems and are particularly useful for studying the asymptotic properties of distributions. A brief discussion of cumulants and their relationships to moments is presented here.

The n-th cumulant, κ_n, of a random variable X can be defined through the moment generating function $M_X(\xi)$ as (Meeron, 1957; Kubo, 1962; Fox, 1975, 1976),

$$\begin{aligned} M_X(\xi) &= E[exp(\xi X)] = \sum_{n=0}^{\infty} \frac{\xi^n}{n!}\mu_n \\ &= exp\left[\sum_{n=1}^{\infty} \frac{\xi^n}{n!}\kappa_n\right] = exp\ [K(\xi)] \end{aligned} \tag{1.6.1}$$

where $K_X(\xi)$ is the *cumulant generating function*. Definitions in (1.6.1) can be generalized to multivariate distributions. If $X_1, X_2, \ldots, X_N$ are N random variables, then the moment and cumulant generating functions are related as

$$\begin{aligned} M_X(\xi_1, \xi_2, \ldots, \xi_N) &= E\left[exp\left(\sum_{j=1}^{N} \xi_j X_j\right)\right] \\ &= \sum_{*} \left(\prod_{j=1}^{N} \frac{\xi_j v_j}{v_j!}\right) \mu(v_1, v_2, \ldots, v_N) \\ &= exp\left\{\sum_{*} \left(\prod_{j=1}^{N} \frac{\xi_j v_j}{v_j!}\right) \kappa(v_1, v_2, \ldots, v_N)\right\} \\ &= exp\,[K\,(\xi_1, \xi_2, \ldots, \xi_n)] \end{aligned} \tag{1.6.2}$$

where $\sum^{*}$ denotes summation over $v_1, v_2, \ldots, v_N$ excluding $v_1 = .v_2 = ..v_N = 0$, and $K(\xi_1, \xi_2, \ldots, \xi_N)$ is the cumulant generating function. In the above equation, the following notation has been used.

$$\mu(v_1, v_2, \ldots, v_N) = E[X_1^{v_1} X_2^{v_2} \ldots X_N^{v_N}]$$
$$\kappa(v_1, v_2, \ldots, v_N) = \kappa[X_1^{v_1} X_2^{v_2} \ldots X_N^{v_N}] \tag{1.6.3}$$

The second part of (1.6.2) indicates the moment of highest order that would occur when evaluating the cumulant in terms of moments.

An alternative way of defining cumulants is through the characteristic function of a sequence of n random variables. If $\boldsymbol{\xi}$ is a vector $(\xi_1, \xi_2, \ldots, \xi_n)$ and $\boldsymbol{X}$ a vector of random variables $(X_1, X_2, \ldots, X_n)$, then the characteristic function of $\boldsymbol{X}$ is defined as

$$\phi(\boldsymbol{\xi}) = E[exp(j\boldsymbol{\xi} \cdot \boldsymbol{X})] \tag{1.6.4}$$

An important property of the characteristic function arises by considering its logarithm

$$K(\boldsymbol{\xi}) = \ell n \phi(\boldsymbol{\xi}) \tag{1.6.5}$$

After accounting for the complex number j, we recognize the left hand side of (1.6.5) as the cumulant generating function. If moments of all orders exist, then both $\phi(\boldsymbol{\xi})$ and $K(\boldsymbol{\xi})$ can be expanded in a power series. Equating the like powers of $\boldsymbol{\xi}$ yields expressions for the cumulants in terms of moments. Using (1.6.2), Meeron (1957) expressed the N-th order cumulant $\kappa[v_1, v_2, \ldots v_N]$ in terms of moments of order not higher than $\mu[v_1, v_2, \ldots, v_N]$ and laid the groundwork for use of cumulants in the context of stochastic differential equations. Most statistical estimation techniques, like the method of moments, are designed for estimating moments. Cumulants have the desirable property that if any of the random variables are uncorrelated with others, then their cumulant is zero. More explicitly, if two random variables X and Y are independent (uncorrelated), then the moment of the product factors into the product moments (i.e. $E[XY] = E[X]E[Y]$) while their cumulant $\kappa[X, Y] = 0$. Thus, moments are said to have the 'product property' while cumulants have the 'cluster property'. The cumulant generating function can also be defined in terms of the characteristic function (Gardiner, 1985). In either case, the relationship between moments and cumulants remains unaffected.

Method of moments has traditionally been a popular technique for estimating model parameters. Thus, many estimation methods have already been designed for computing moments (Jury and Sposito, 1985; Jury et al., 1991). Direct estimation of cumulants has not been attempted because of the complicated nature of the resulting expressions. Govindaraju et al. (1996) described a practical way of computing cumulants from moments. For instance, the first four cumulants are given by

$$\kappa_1 = \mu_1$$
$$\kappa_2 = \mu_2 - \mu_1^2$$
$$\kappa_3 = \mu_3 - 3\mu_1\mu_2 + \mu_1^3$$
$$\kappa_4 = \mu_4 - 4\mu_1\mu_3 - 3\mu_2^2 + 12\mu_1^2\mu_2 - 6\mu_1^4 \tag{1.6.6}$$

It can be observed that the first two cumulants are the mean and covariance respectively. Gardiner (1985) points out some useful applications of cumulants.

1.7. PROBABILITY WEIGHTED MOMENTS

We mention some other kinds of moments that have found applications in hydrology. Greenwood et al. (1979) defined *probability weighted moments* in terms of quantiles. Let X be a random variable with a cumulative distribution function $F_X(x)$, then the probability weighted moments are expressed as

$$M_{p,r,s} = E\left[X^p \{F_X(x)\}^r \{1 - F_X(x)\}^s\right] \tag{1.7.1}$$

If the inverse of the cdf is available such that if $F_X(x) = u$, $x = F_X^{-1}(u) = x(u)$ with $0 \leq u \leq 1$, then an alternate definition for probability weighted moments is

$$M_{p,r,s} = \int_0^1 [x(u)]^p u^r (1-u)^s \, du \tag{1.7.2}$$

From (1.7.1), we note that for $r = s = 0$, $M_{p,0,0}$ represents the conventional p-th moment (1.2.5b).

Useful forms of probability weighted moments are generally obtained for either r or s being equal to zero (Hosking and Wallis, 1997). For instance, we may define

$$\alpha_s = M_{1,0,s} = \int_0^1 x(u)(1-u)^s \, du \tag{1.7.3a}$$

$$\beta_r = M_{1,r,0} = \int_0^1 x(u) u^r \, du \tag{1.7.3b}$$

and compare them to the conventional definition of moments in (1.2.5)

$$E[X^n] = \int_{-\infty}^{\infty} x^n f_X(x) \, dx \tag{1.7.4}$$

Thus while conventional moments of higher orders involve successively higher powers of $x(u)$, probability weighted moments α_s and β_r raise it only to the first power while raising u or $(1-u)$ to higher powers. However, since u is bounded between 0 and 1, it is believed that probability weighted moments can be estimated more robustly from experimental data. Note that the two kinds of probability weighted moments in (1.7.3) are related to each other, so that α_s can be represented in terms of β_r $(r \leq s)$, and vice versa.

1.8. L-MOMENTS

The computation of higher order moments from experimental observations has always been fraught with uncertainty. In column experiments of solute transport, for example, the breakthrough data often exhibit very long tails involving very

low concentration values that are close to the detection limit of the measuring instrument. Consequently, the uncertainty associated with these measurements can be quite large. During the computation of higher order moments, a very large weight is assigned to these data resulting in estimates of moments that may have a large error associated with them.

To alleviate this problem to some degree, and to have a better representation of properties such as scale and shape of a distribution, Hosking (1986) developed *L-Moments* which could be expressed as linear combinations of probability weighted moments. Hosking and Wallis (1997) contend that while (1.7.3) are integrals of $x(u)$ weighted by u^r or $(1-u)^r$, more meaningful interpretations are possible by weighting $x(u)$ with *shifted Legendre polynomials* $P_r(u), r = 0, 1, 2, \ldots$, that possess the following properties:

(i) $P_r(u)$ is a polynomial of degree r
(ii) $P_r(1) = 1$ (normalization condition)
(iii) $\int_0^1 P_r(u)P_s(u)du = 0$ if $r \neq s$ (orthogonality)

These polynomials are defined by

$$P_r(u) = \sum_{k=o}^{r} (-1)^{r-k} \binom{r}{k} \binom{r+k}{r} u^k \tag{1.8.1}$$

Using these shifted Legendre polynomials as weighting functions, Hosking and Wallis (1997) defined L-Moments as

$$L_r = \int_0^1 x(u)P_{r-1}(u)du \tag{1.8.2}$$

L-Moments can be defined in terms of expectations of order statistics. Estimators for L-Moments from observations have been discussed in Hosking and Wallis (1997).

1.9. EXPERIMENTAL AND THEORETICAL MOMENTS

When discussing moments, we distinguish between *experimental* and *theoretical* moments. For instance, say the time-dependant concentration data observed at the outlet of a soil column during a steady-flow experiment are denoted by $c^*(t)$. A more careful definition of concentrations will be provided in Chapter 02. Here, we use the term loosely to describe an example involving parameter estimation from different methods. To treat the data like a pdf, we calculate the area M numerically from

$$M = \int_0^\infty c^*(t)dt \tag{1.9.1}$$

We can define normalized concentrations $c(t) = c^*(t)/M$, and treat $c(t)$ as a pdf. The nth absolute experimental moment is obtained numerically from

$$\mu_n = \int_0^\infty t^n c(t)dt \tag{1.9.2}$$

Numerical evaluation of experimental moments will be described in Section 5.4. As an illustration, we consider three 'models' as possible candidates for describing $c(t)$. These are the Fickian, lognormal, and gamma pdfs defined, respectively, as:

$$\begin{aligned} c_f(t) &= \frac{l}{2\sqrt{\pi D t^3}} \exp\left[-\frac{(l-Vt)^2}{4Dt}\right] \\ c_l(t) &= \frac{1}{\sqrt{2\pi}\sigma t} \exp\left[-\frac{(\ln t - \mu)^2}{2\sigma^2}\right] \\ c_g(t) &= \frac{\lambda^\alpha t^{\alpha-1}}{\Gamma(\alpha)} \exp(-\lambda t) \end{aligned} \tag{1.9.3}$$

We note that the models in equation (1.9.3) treat the quantity t as realizations of the random variable T. These three candidate distributions have two parameters each. The quantity l in the Fickian pdf is the length of the soil column. A brute force technique would be to minimize the squared error (MSE) between observations and model results to estimate the model parameters.

Another way to estimate model parameters would be through method of moments (MOM), the subject of this book. Expressions for the mean and variance of the log-normal and gamma pdfs can be obtained from Table 1.1.2. The expressions for the mean and variance of the Fickian pdf are as follows

$$E[T] = \frac{l}{V}; \quad Var[T] = \frac{2Dl}{V^3} \tag{1.9.4}$$

By equating the experimental moments to expressions for the first and second moments, we obtain estimates of model parameters.

Another popular alternative method of parameter estimation is called *maximum likelihood estimation* (MLE) and is briefly described in Appendix B, along with some desirable properties of estimators. Parameter estimation methods, such as MOM and MLE, would require N independent observations of the random variable T expressed as $t_i, i = 1, 2, 3, \ldots, N$. Then the MLE estimators are found to be as follows.

1.9.1 Gamma Distribution

$$\hat{\lambda} = \frac{N\hat{\alpha}}{\sum_{i=1}^{N} t_i} \tag{1.9.5a}$$

$$\ln \hat{\alpha} - \psi(\hat{\alpha}) = ln\left(\frac{1}{N}\sum_{i=1}^{N} t_i\right) - \frac{1}{N}\sum_{i=1}^{N} ln\ t_i \tag{1.9.5b}$$

where $\psi(\hat{\alpha}) = \frac{[\Gamma(\hat{\alpha})]'}{\Gamma(\hat{\alpha})}$ is the Psi (Digamma) function (Abramowitz and Stegun, 1964). Here we use the notation $\hat{p}$ to denote the estimator of a parameter p. No closed form solution is possible for (1.9.5) and a numerical technique must be adopted to solve the system of equations. A good approximation (within 1.5% of the correct value) exists in the form of

$$\hat{\alpha} \sim \frac{3 - s + \sqrt{s^2 + 18s + 9}}{12s} \tag{1.9.5c}$$

where s is the right hand side of (1.9.5b).

1.9.2 Fickian Distribution

$$\hat{V} = \frac{l}{\sum_{i=1}^{N} t_i} \tag{1.9.6a}$$

$$\hat{D} = \frac{1}{2N}\sum \frac{\left(l - \hat{V}t_i\right)^2}{t_i} \tag{1.9.6b}$$

1.9.3 Log-Normal Distribution

$$\hat{\mu} = \frac{1}{N}\sum_{i=1}^{N} ln\ t_i \tag{1.9.7a}$$

$$\hat{\sigma}^2 = \frac{1}{N}\sum_{i=1}^{N} (ln\ t_i - \hat{\mu})^2 \tag{1.9.7b}$$

To illustrate the use of MSE, MOM, and MLE techniques of parameter estimation, we use the experimental data reported in Langner et al. (1999). A series of unsaturated transport experiments was performed in four intact cores of Amsterdam silt loam (15.2 cm diameter, 30 cm length) collected from a grassland site at the A.H. Post Experimental Farm near Bozeman, Montana. Multiple breakthrough curves for tritiated water and pentafluorobenzoic acid (PFBA) were collected from each column by varying the upper and lower pressure heads, resulting in a range of flow rates and residence times. We have selected five tritiated water BTCs (Columns: I-10, I-24, IV-3, IV-5, IV-11) and two PFBA BTCs (Columns: II-3, II-5) from Langner et al. (1999). The pore water velocities for these BTCs ranged from 4.8 to 27.36 cm d^{-1}.

Figure 1.9.1 gives a visual indication of how each of the models compares with observations. It is clear that the three models fit the data reasonably well, and it is not possible to determine which one would best describe the process that led to these observations. Table 1.9.1 shows estimates of the model parameters by the two methods. The r^2 error estimate is the standard linear measure of performance between model results and observations. We note that minimization of squared errors will generally result in a better 'fit', but it does not yield analytical expressions. The MOM estimates were obtained without correcting for the inlet boundary condition in this section, and this aspect will be explored further in Section 5.3.

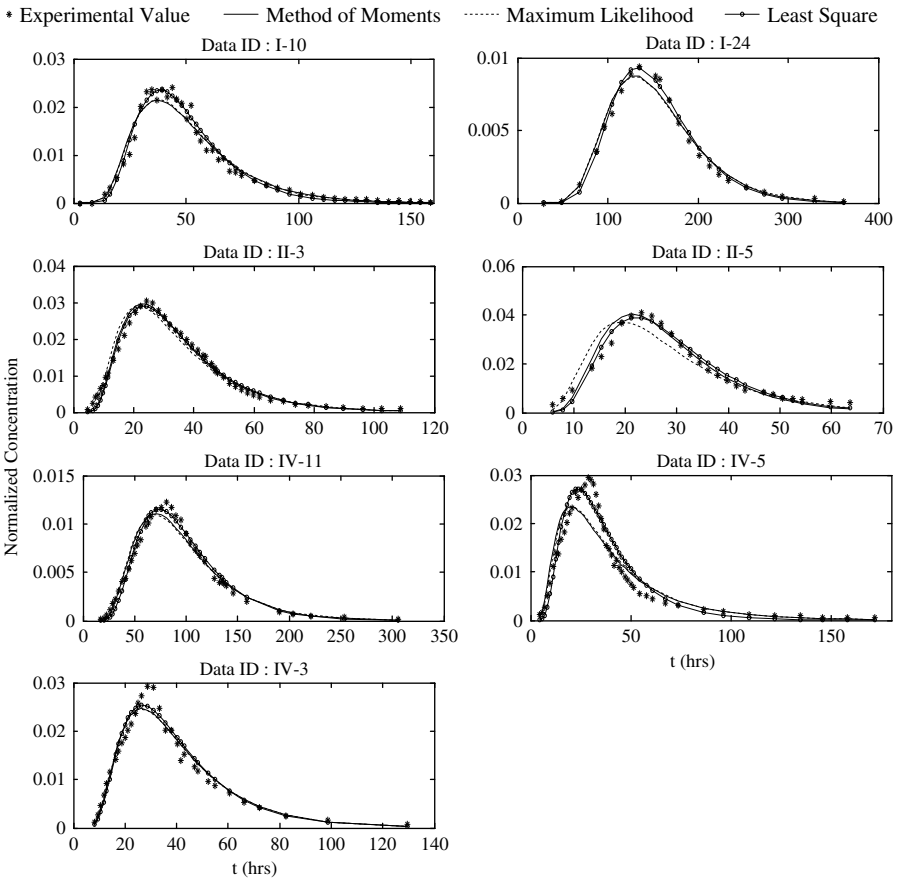

Figure 1.9.1a. Fitting of the Fickian model to the data from the seven experiments using different parameter estimation methods

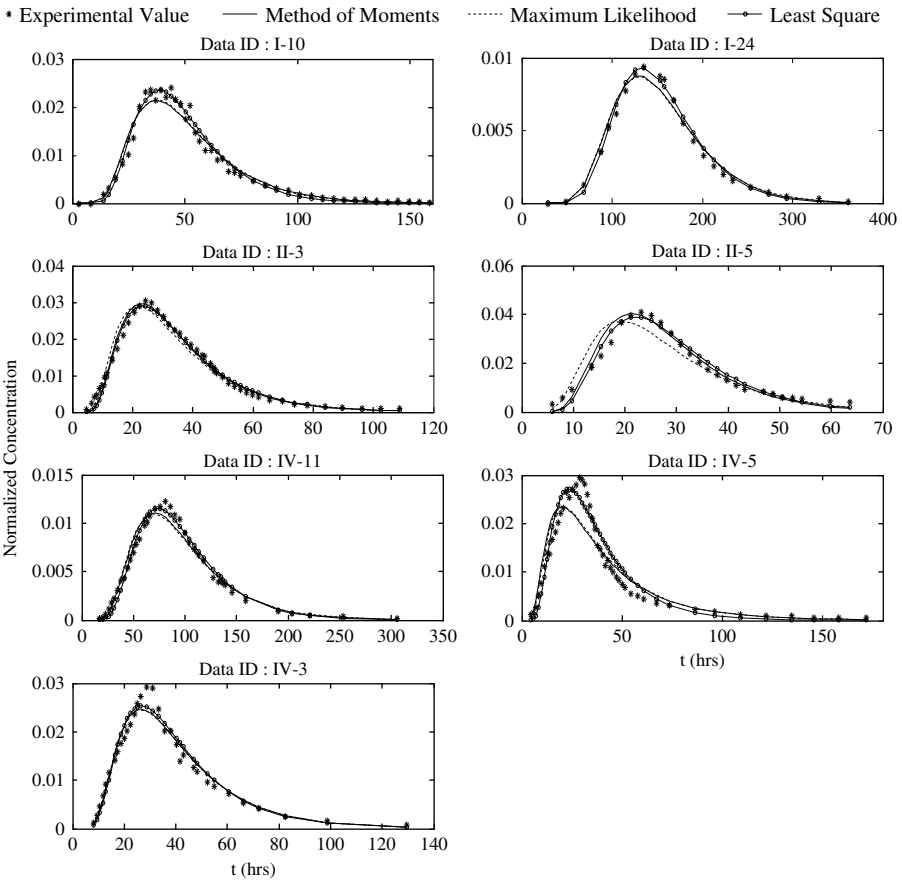

Figure 1.9.1b. Fitting of the log-normal distribution model to the data from the seven experiments using different parameter estimation methods

Table 1.9.1a. Parameter estimation results for the Fickian model

Expt→	I-10	I-24	II-3	II-5	IV-11	IV-5	IV-3
Numerical minimization of squared-errors							
D	1.202	0.215	2.707	2.152	0.72	3.103	2.543
V	0.531	0.171	0.733	0.889	0.276	0.727	0.666
r^2 error	0.98	0.990	0.980	0.965	0.98	0.933	0.954
Parameter estimation by method of moments							
D	1.463	0.252	2.734	2.263	0.834	4.624	2.695
V	0.515	0.171	0.749	0.923	0.277	0.654	0.656
r^2 error	0.966	0.980	0.980	0.959	0.963	0.857	0.951
Maximum Likelihood Estimation							
D	1.437	0.255	3.117	3.087	0.868	4.401	2.724
V	0.515	0.171	0.749	0.923	0.277	0.654	0.656
r^2 error	0.968	0.978	0.960	0.88	0.954	0.876	0.950

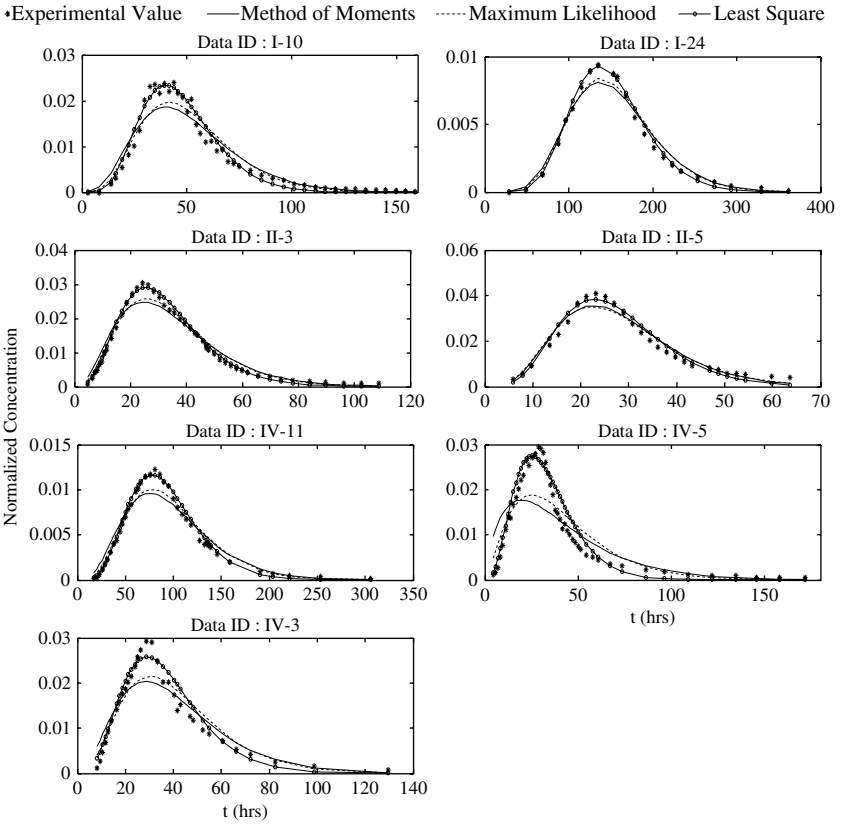

Figure 1.9.1c. Fitting of the Gamma distribution model to the data from the seven experiments using different parameter estimation methods

Table 1.9.1b. Parameter estimation results for the log-normal distribution model

Expt→	I-10	I-24	II-3	II-5	IV-11	IV-5	IV-3
			Numerical minimization of squared-errors				
μ	3.818	4.989	3.43	3.28	4.49	3.46	3.563
σ^2	0.163	0.093	0.258	0.177	0.181	0.282	0.253
r^2 error	0.981	0.992	0.988	0.970	0.985	0.944	0.960
			Parameter estimation by method of moments				
μ	3.835	4.984	3.419	3.248	4.48	3.51	3.584
σ^2	0.196	0.106	0.248	0.173	0.202	0.421	0.266
r^2 error	0.971	0.984	0.989	0.97	0.977	0.894	0.956
			Maximum likelihood estimation				
μ	3.836	4.984	3.411	3.233	4.479	3.514	3.581
σ^2	0.192	0.108	0.275	0.223	0.207	0.4	0.27
r^2 error	0.972	0.983	0.982	0.923	0.973	0.906	0.957

Table 1.9.1c. Parameter estimation results for the Gamma distribution model

Expt→	I-10	I-24	II-3	II-5	IV-11	IV-5	IV-3
			Numerical minimization of squared-errors				
α	6.653	11.256	4.586	6.035	6.283	4.206	4.689
λ	0.142	0.075	0.141	0.22	0.068	0.127	0.127
r^2 error	0.973	0.993	0.992	0.967	0.99	0.945	0.947
			Parameter estimation by method of moments				
α	4.63	8.921	3.546	5.283	4.476	1.909	3.287
λ	0.091	0.058	0.103	0.188	0.046	0.046	0.08
r^2 error	0.928	0.974	0.963	0.952	0.953	0.667	0.892
			Maximum Likelihood estimation				
α	5.328	9.511	3.927	5.096	5.053	2.563	3.83
λ	0.104	0.062	0.114	0.182	0.052	0.062	0.093
r^2 error	0.937	0.978	0.975	0.949	0.967	0.817	0.896

APPENDIX A: EXPONENTIAL DISTRIBUTIONS

Exponential-type distributions arise very commonly in first-order stochastic differential equations with random quantities. These kinds of distributions are easily motivated by considering the complete gamma function.

$$\Gamma(\alpha) = \int_0^\infty y^{\alpha-1}\ e^{-y}\ dy,\ \ \alpha > 0 \tag{A.1}$$

Integration by parts reveals

$$\Gamma(\alpha+1) = \alpha\ \Gamma(\alpha) \tag{A.2}$$

when α takes on positive integer values, then

$$\Gamma(n+1) = \int_0^\infty y^n e^{-y}\ dy = n! \tag{A.3}$$

which follows from (A.2) and because $\Gamma(1) = 1$. It can also be shown that

$$\Gamma(1/2) = \sqrt{\pi} \tag{A.4}$$

From (A.1) and (A.4), we have the relationship

$$\sqrt{\pi} = \int_0^\infty y^{-1/2}\ e^{-y}\ dy = \sqrt{2}\int_0^\infty e^{-z^2/2}\ dz \ldots \tag{A.5}$$

where the last integral is obtained from the transformation $y = z^2/2$. This last integral is symmetric about the origin and an even function of z. This leads us to the definition of the standard normal distribution i.e.

$$\int_{-\infty}^{\infty} \frac{1}{\sqrt{2\pi}}\ e^{-z^2/2}\ dz = 1 \tag{A.6}$$

The incomplete gamma function is defined as

$$\Gamma(\alpha, \beta) = \int_0^{\beta} y^{\alpha-1} e^{-y} \, dy, \;\; \alpha, p > 0 \tag{A.7}$$

Again if $\alpha - 1 = n$ is an integer, then

$$\begin{aligned} \Gamma(n+1, \beta) &= \int_0^{\beta} y^n \, e^{-y} dy = n! - \int_{\beta}^{\infty} y^n \, e^{-y} \, dy \\ &= n! \left\{ 1 - \sum_{k=0}^{n} \frac{e^{-\beta} \, \beta^k}{k!} \right\} \end{aligned} \tag{A.8}$$

which can be recognized as being described in terms of cumulative mass function of the Poisson distribution. Upon substituting $y = \beta x$ in (A.1), we have

$$\int_0^{\infty} \frac{\beta^{\alpha} \, x^{\alpha-1}}{\Gamma(\alpha)} \, e^{-\beta x} \, dx = 1 \tag{A.9}$$

The integrand is the probability density function of the two-parameter gamma distribution. Thus a random variable X is gamma-distributed if its pdf is

$$f_X(x) = \frac{\beta^{\alpha} x^{\alpha-1}}{\Gamma(\alpha)} \, e^{-\beta x}, \;\; x > 0 \tag{A.10}$$

Further, for the particular case of $\beta = 1/2$ and $\alpha = {}^{n}/_{2}$, the resulting pdf is known as the Chi-square density function with n degrees of freedom

$$f_x(x) = \frac{x^{(n-2)/2}}{2^{n/2} \left(\frac{n-2}{2}\right)!} \, e^{-x/2}, \;\; x > 0 \tag{A.11}$$

APPENDIX B: MAXIMUM LIKELIHOOD ESTIMATION

The method of moments is the main focus of this book. However, the maximum-likelihood estimation (MLE) method also plays an important role and is briefly mentioned here. Let $X_1, X_2, \ldots, X_n$ be a sequence of random variables that are independent and identically distributed (iid) with the probability density function denoted by $f_X(x; \boldsymbol{\theta})$ where $\boldsymbol{\theta} = \{\theta_1, \theta_2, \ldots, \theta_k\}$ is the parameter vector of the distribution. The joint pdf of $X_1, X_2, \ldots, X_n$ is defined as the *likelihood function*

$$L(\boldsymbol{\theta}; x) = f_X(x_i; \boldsymbol{\theta}) f_X(x_2; \boldsymbol{\theta}) \ldots f_X(x_n; \boldsymbol{\theta}) \tag{B.1}$$

The likelihood function is clearly a function of the parameter vector $\boldsymbol{\theta}$.

The problem then is one of finding an appropriate parameter set $\hat{\boldsymbol{\theta}}$ given the observed sequence $x_1, x_2, \ldots, x_n$. The statistic $\hat{\boldsymbol{\theta}}(x_1, x_2, \ldots, x_n)$ is a maximum

likelihood estimator of it maximizes the likelihood function (B.1). Thus the parameters are obtained by solving the following k equations simultaneously

$$\frac{d}{d\boldsymbol{\theta}_i} L(\boldsymbol{\theta}; x) = 0; \;\; i = 1, 2, \ldots, k \tag{B.2}$$

Since the log function is monotonically increasing, it is often more convenient to maximize the natural logarithm of the likelihood function

$$\frac{d}{d\boldsymbol{\theta}_i}[\ell n \; L(\boldsymbol{\theta}; x)] = 0; \;\; i = 1, 2, \ldots, k \tag{B.3}$$

A unique solution often exists to equation sets (B.2) or (B.3). The form of (B.3) is particularly convenient when dealing with distributions belonging to the exponential family.

There are a few desirable properties that one seeks in estimators.

Unbiasedness: The statistic or estimator $\hat{\boldsymbol{\theta}}(X_1, X_2, \ldots, X_n)$ is said to be unbiased if

$$E[\hat{\boldsymbol{\theta}}(X_1, X_2, \ldots, X_n)] = \boldsymbol{\theta} \tag{B.4}$$

Thus for instance, unbiased estimator of the sample mean is

$$\hat{\theta}_1 = \frac{1}{n}\sum_{i=1}^{n} x_i = \bar{X} \tag{B.5}$$

The MLE for the sample variance is

$$\hat{\theta}_2 = \frac{1}{n}\sum_{i=l}^{n} (x_i - \overline{X})^2 \tag{B.6}$$

The variance estimator is biased by a factor of $\frac{n-1}{n}$. However as $n \to \infty$, the bias is negligible and this estimator is said to be asymptotically unbiased.

Consistency: An estimator $\hat{\theta}_n$ of a parameter θ_0 is called consistent if it converges to θ_0 in probability, i.e. for every $\varepsilon > 0$,

$$\lim_{n\to\infty} P\left[\left|\hat{\theta}_n - \theta_0\right| > \varepsilon\right] = 0 \tag{B.7}$$

Efficiency: The efficiency of an estimator is based on its variance. If $\hat{\theta}$ is the most efficient estimate, then for any other estimate $\tilde{\theta}$, we have

$$Var\left[\hat{\theta}\right] \leq Var\left[\tilde{\theta}\right] \tag{B.8}$$

Asymptotic normality: As the sample size n tends to ∞, the pdf of the estimator $\hat{\theta}_n$ tends to be normally distributed with mean θ and variance

$$Var\left[\hat{\theta}_n\right] = \frac{1}{-E\left[\frac{d^2}{d\theta^2}\ell n \; L(\theta; X)\right]} \tag{B.9}$$

CHAPTER 2

LAPLACE TRANSFORMS FOR SOLUTE TRANSPORT MODELS

Transform methods are useful for solving linear partial differential equations. The choice of the appropriate transform depends on the kinds of boundary conditions and whether the domain is finite, infinite or semi-infinite. This chapter deals with the use of Laplace transforms, with emphasis on their role in solving partial differential equations that frequently arise in models of solute transport. In Section 1.4, Laplace transforms were introduced as moment generating functions of continuous random variables.

2.1. DEFINITION OF THE TRANSFORM AND ITS INVERSE

The Laplace transform of a function $f(t)$ is defined as

$$\mathcal{L}[f(t)] = F[s] = \int_0^\infty e^{-st} f(t)\,dt \tag{2.1.1}$$

assuming that the integral converges. This places a restriction on the class of functions for which the transform exists. The Laplace transform of many functions can be obtained by direct integration. Extensive sets of tables are available and these can be consulted for those cases where integration can be daunting.

The definition of Laplace transform in (2.1.1) suggests that it is suitable for semi-infinite domains. Clearly $f(t)$ needs to be defined for $t \geq 0$, and it is often assumed that $f(t) = 0$ for $t = 0$. Consider the unit Heaviside step function

$$H(t-b) = \begin{cases} 0, & t < b \\ 1, & t > b \end{cases} \tag{2.1.2}$$

The Laplace transform of $H(t)$ is

$$\mathcal{L}[H(t)] = \int_0^\infty e^{-st}\,dt = 1/s \tag{2.1.3}$$

If $f(t)$ in (2.1.1) is the delta-function $\delta(t-a)$, then

$$\mathcal{L}[\delta(t-a)] = \int_0^\infty \delta(t-a)e^{-st}dt = \exp(-sa) \tag{2.1.4}$$

Similarly, if $f(t) = t^n$, we have

$$\mathcal{L}[t^n] = \int_0^\infty e^{-st}t^n dt = \frac{n!}{s^{n+1}} \tag{2.1.5}$$

A partial list of Laplace transforms of some functions in provided in Table 2.1.1. A more complete list is available in references such as Abramowitz and Stegun (1964).

The inverse transform is the process of recovering the function $f(t)$ from the transform $F(s)$ and is written as

$$f(t) = \mathcal{L}^{-1}[F(s)] = \frac{1}{2\pi j}\int_{\gamma-j\infty}^{\gamma+j\infty} F(s)e^{st}ds \tag{2.1.6}$$

Table 2.1.1. A partial list of Laplace transforms of some common functions

$f(t)$	$F(s) \equiv \mathcal{L}[f(t)] \equiv \int_0^\infty f(t)e^{-st}dt$
1	$\frac{1}{s}$
$t^n \quad (n > -1)$	$n!s^{-(n+1)}$
e^{at}	$\frac{1}{s-a}$
sin ωt	$\frac{\omega}{s^2+\omega^2}$
cos ωt	$\frac{s}{s^2+\omega^2}$
sinh at = $\frac{1}{2}(e^{at} - e^{-at})$	$\frac{a}{s^2-a^2}$
cosh at = $\frac{1}{2}(e^{at} + e^{-at})$	$\frac{s}{s^2-a^2}$
$\frac{df}{dt}$	$sF(s) - f(0)$
$\frac{d^2f}{dt^2}$	$s^2F(s) - sf(0) - \frac{df}{dt}(0)$
-tf(t)	$\frac{dF}{ds}$
$e^{at}f(t)$	$F\ (s-a)$
H(t-b)f(t-b)	$e^{-bs}\ F(s)\ (b > 0)$
$\int_0^t f(t-\tau)g(\tau)d\tau$	$F(s)G(s)$
$\delta(t-b)$	$e^{-bs} \quad (b \geq 0)$
$t^{-1/2}e^{-a^2/4t}$	$\sqrt{\frac{\pi}{s}}e^{-a\sqrt{s}} \quad (a \geq 0)$
$t^{-3/2}e^{-a^2/4t}$	$\frac{2\sqrt{\pi}}{a}e^{-a\sqrt{s}} \quad (a > 0)$

where γ is a positive constant, and $j = \sqrt{-1}$. The inverse transform operation involves a line integral in the complex plane. The constant γ is chosen large enough so that all singularities of the function $F(s)$ lie to the left of the line perpendicular to the real axis at the point γ. Other than that, the integral is not dependent on γ as in Figure 2.1.1.

The evaluation of integrals involving complex variables is achieved using Cauchy's theorem. This theorem states that if $g(s)$ is analytic at all points inside and on a closed contour G, then the closed line integral is zero

$$\int_G g(s)ds = 0 \tag{2.1.7}$$

Closed line integrals are nonzero only because of singularities of $g(s)$. The *residue theorem* states that such closed line integrals (anti-clockwise direction) can be generally evaluated from the residues of the singularities s_n inside the contour (if there are no branch points)

$$\int_G g(s)ds = 2\pi i \sum_n res(s_n) \tag{2.1.8}$$

If $g(s)$ can be expressed as $R(s)/Q(s)$, and has simple poles at simple zeros s_n of $Q(s)$ inside the contour, then

$$res(s_n) = \frac{R(s_n)}{Q'(s_n)} \tag{2.1.9}$$

As shown in Figure 2.1.1, the inversion integral in (2.1.6) is over an infinite straight line to the right of all singularities of $F(s)$, and not over any closed loop. To accommodate this, the integral is computed over a semicircle, with the straight portion coincident with the infinite straight line. Letting the radius tend to infinite, the desired result is obtained by making the line integral along the arc of the semi-circle to vanish. Observing the integral in (2.1.6), $F(s) \to 0$ as $s \to \infty$, therefore

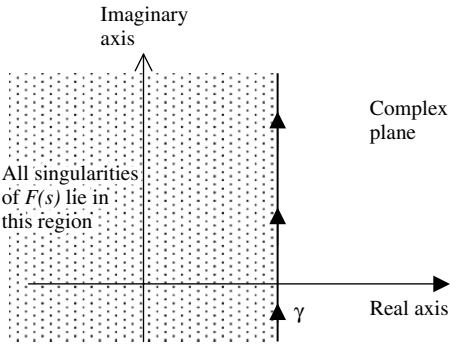

Figure 2.1.1. Schematic sketch showing the region of line integration of $F(s)$ for inverse Laplace transform operation

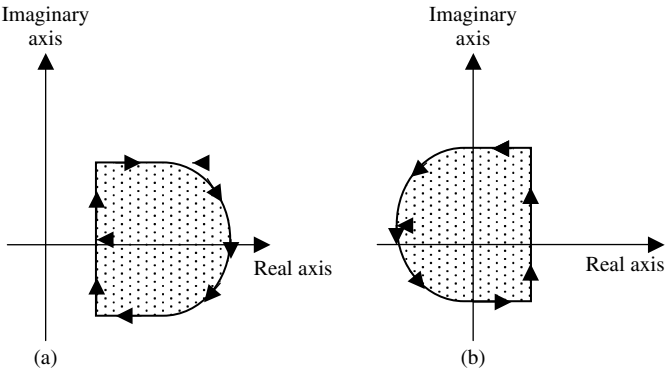

Figure 2.1.2. Closing line integrals. (a) For $t < 0$; (b) For $t > 0$

we want e^{st} to vanish as the radius of the semi-circle approaches infinity. Consider the case for $t < 0$ when e^{st} decays exponentially as the real part of s increases so the integral is closed to the right as shown in Figure 2.1.2. Note that γ was chosen so as to have no singularities to the right, so that for $t < 0$

$$f(t) = \mathcal{L}^{-1}[F(s)] = 0 \tag{2.1.10}$$

As mentioned earlier, it is required that $f(t) = 0$ for $t < 0$. For the more interesting case of $t > 0$, e^{st} will decay exponentially when $s < 0$ suggesting that we close the contour to the left (Figure 2.1.2), and account for all the singularities. From (2.1.6) and (2.1.9) we have

$$f(t) = \frac{1}{2\pi i}\int_{\gamma-\infty}^{\gamma+\infty} F(s)e^{st}ds = \frac{1}{2\pi i}\oint F(s)e^{st}ds = \sum_{n} res(s_n) \tag{2.1.11}$$

when $F(s)$ has no branch points.

Rather than compute the inverse transform, tables of Laplace transforms are generally utilized for determining inverse transforms. Numerical evaluation of (2.1.6) is possible provided the function $f(t)$ is reasonably smooth. Efficient algorithms (see Jury and Roth, 1990) are available and are often preferable to analytical evaluation through contour integration which can be quite cumbersome.

2.2. SINGULARITIES OF THE LAPLACE TRANSFORM

If the function $f(t) = e^{at}$, a simple exponential, then the growth rate a is also a singularity of its Laplace transform $F(s) = \frac{1}{s-a}$ (see Table 2.1.1). In general, the singularities of the Laplace transform correspond, in some sense, to the growth rates of $f(t)$. This is called as the singularity property.

For instance, the transform functions $\omega/\left(s^2+\omega^2\right)$ and $s/\left(s^2+\omega^2\right)$ have singularities at $s=\pm j\omega$, implying that their inverse Laplace transforms will have the form e^{st}, where $s=\pm j\omega$. Table 2.1.1 shows the inverse Laplace transforms to be $\sin\omega t$ and $\cos\omega t$ which can be expressed as linear combinations of $e^{\pm j\omega t}$ according to Euler's formulas.

When performing the inverse Laplace transform operation, we are often faced with forms that can be expressed as $F(s)=q(s)/p(s)$, where the numerator and denominator are polynomials. We expect $F(s)\to 0$ as $s\to\infty$. Thus $p(s)$ is a higher degree polynomial than $q(s)$. The use of partial fractions is particularly convenient for performing inverse Laplace transform operations. Consider the case where $p(s)$ has simple roots (i.e. no multiple roots). Then we can express $p(s)$ in terms of its n distinct roots $s_1, s_2, \ldots, s_n$ as

$$p(s)=(s-s_1)(s-s_2)\ldots(s-s_n) \tag{2.2.1}$$

The roots $s_1, s_2, \ldots, s_n$ are the simple poles of $F(s)$ whose partial-fraction expansion is

$$F(s)=\frac{q(s)}{p(s)}=\frac{a_1}{s-s_1}+\frac{a_2}{s-s_2}+\ldots.+\frac{\mathrm{a_n}}{\mathrm{s-s_n}} \tag{2.2.2}$$

where the coefficients a_i can be evaluated by the formula

$$a_i=\lim_{s\to s_i}\frac{(s-s_i)\,q(s)}{p(s)} \tag{2.2.3}$$

For simple poles, (2.2.3) can be evaluated by using L'Hospitals rule since the right hand side has a $0/0$ form in the limit.

$$a_i=\lim_{s\to s_i}\frac{\dfrac{d}{ds}\left[(s-s_i)\,q(s)\right]}{\dfrac{d}{ds}\left[p(s)\right]}=\frac{q(s_i)}{p'(s_i)} \tag{2.2.4}$$

The inverse transform for this form of $F(s)$ can be obtained as

$$f(t)=\sum_{i=1}^{n}\frac{q(s_i)}{p'(s_i)}e^{s_i t} \tag{2.2.5}$$

The shift theorem is also very useful for finding inverse transforms. If $F(s)$ is the Laplace transform of $f(t)$ then

$$\mathcal{L}^{-1}[F(as+b)]=\exp\left(\frac{-bt}{a}\right)\mathcal{L}^{-1}[F(as)]=\frac{1}{a}\exp\left(\frac{-bt}{a}\right)f\left(\frac{t}{a}\right) \tag{2.2.6}$$

The use of Laplace transforms finds applications when the functions are derivatives. Integration by parts reveals

$$\mathcal{L}\left[\frac{df}{dt}\right] = \int_0^\infty \frac{df}{dt} e^{-st} dt = sF(s) - f(0) \tag{2.2.7}$$

In a similar fashion

$$\mathcal{L}\left[\frac{d^2f}{dt^2}\right] = s\mathcal{L}\left[\frac{df}{dt}\right] - \frac{df(0)}{dt} = s^2F(s) - sf(0) - \frac{df(0)}{dt} \tag{2.2.8}$$

This process can be extended to compute higher order derivatives. Clearly, information about the function $f(t)$ and its higher order derivatives is required at $t = 0$ in the form of initial conditions. The calculations can be substantially simplified if these initial conditions are all zero.

The concept of convolution can be applied to Laplace transforms as well. Let us say we are trying to obtain the function whose Laplace transform is the product of two transforms. If

$$F(s) = \mathcal{L}[f(t)] \text{ and } G(s) = \mathcal{L}[g(t)] \tag{2.2.9}$$

then

$$\mathcal{L}^{-1}[F(s)G(s)] = \int_0^t g(t')f(t-t')dt' = g * f \tag{2.2.10}$$

2.3. GREEN'S FUNCTIONS FOR INITIAL VALUE PROBLEMS

Consider the linear second-order nonhomogeneous ordinary differential equation

$$a\frac{d^2y}{dt^2} + b\frac{\mathrm{dy}}{\mathrm{dt}} + cy = f(t) \tag{2.3.1}$$

subject to the initial conditions

$$y(0) = 0;\ \frac{dy(0)}{dt} = 0 \tag{2.3.2}$$

Non-zero initial conditions can be accounted for by including appropriate homogeneous solutions. Taking Laplace transforms of both sides of (2.3.1), we have

$$\left(as^2 + bs + c\right) Y(s) = F(s) \tag{2.3.3}$$

where $Y(s)$ and $F(s)$ are Laplace transforms of $y(t)$ and $f(t)$ respectively. Equation (2.3.3) may be expressed as

$$Y(s) = F(s)Q(s) \tag{2.3.4}$$

where $Q(s) = 1/(as^2 + bs + c)$. Utilizing the convolution theorem (2.2.10), the solution may be obtained as

$$y(t) = \int_0^t f(t')q(t - t')dt' \tag{2.3.5}$$

where $q(t)$ is the inverse Laplace transform of $Q(s)$ and can be determined from tables or using partial fractions.

Let us consider the particular case of the forcing function in (2.3.1) when $f(t) = \delta(t)$. This corresponds to a unit impulse applied to the system. From Table 2.1.1, we know that $F(s) = 1.0$. From (2.3.5), $q(t)$ is the impulse response and is interpreted as the Green's function of the initial value problem. Essentially, $q(t)$ is the response at some time t due to a concentrated source of unit magnitude applied at time $t = 0$ and can be symbolically represented as

$$q(t) = G(t, 0) \tag{2.3.6}$$

Equation (2.3.5) involving convolution shows that we are interested in $q(t - t') = G(t - t', 0)$. Since the governing differential equation of (2.3.1) contains constant coefficients, the translation property implies that the response at time t due to an impulse at t' depends only on the elapsed time $t - t'$ and not on the particular values of t and t'.

$$G(t, t') = G(t - t', 0) = q(t - t') \tag{2.3.7}$$

The generalized superposition principle reflected in (2.3.5) can be expressed as

$$y(t) = \int_0^t f(t')G(t, t')dt' \tag{2.3.8}$$

The causality principle applies for such linear differential equations so that the influence of an impulse at t' is felt only for time $t > t'$. The Green's function $G(t, 0)$ is simply given as

$$G(t, 0) = \mathcal{L}^{-1}\left[\frac{1}{as^2 + bs + c}\right] \tag{2.3.9}$$

2.4. SOLUTE TRANSPORT BY DIFFUSION

The use of Laplace transforms can be motivated by examples from solute transport in porous media. We first consider the process of pure diffusion, a process that accounts for transport of solute mass resulting from random molecular movement causing solute particles to move from regions of higher to lower concentrations. This is mathematically expressed through Fick's first law for a single spatial dimension (x) as

$$J_{diff} = -D_m \frac{\partial c}{\partial x} \tag{2.4.1}$$

Equation (2.4.1) states that the diffusional mass flux $\left(J_{diff}\right)$ is proportional to the gradient of the concentration c, and the molecular diffusion coefficient (D_m) is the constant of proportionality. Fick's second law expresses the conservation of mass for solute in the fluid phase

$$\frac{\partial c}{\partial t} = -\frac{\partial}{\partial x}\left(J_{diff}\right) = D_m \frac{\partial^2 c}{\partial x^2} \tag{2.4.2}$$

Equation (2.4.2) has the same form as the one arising in heat conduction in solids.

The molecular (self) diffusion coefficient in the gas phase $D_m(g)$ is derived from kinetic theory and ideal gas law (Bird et al., 1960)

$$D_m(g) = \frac{2}{3pd^2}\sqrt{\frac{(KT)^3}{\pi^3 m}} \tag{2.4.3}$$

In (2.4.3), p is absolute pressure, d is the molecular diameter, K is Boltzmann's constant, T is the absolute temperature and m is the mass per molecule ($m = M/N$, where M is the molecular weight and N is Avogadro's number). For liquids, the hydrodynamic theory is used to obtain the Stokes-Einstein equation for predicting the diffusion coefficient $D_m(l)$

$$D_m(l) = \frac{KT}{3\pi\mu d} \tag{2.4.4}$$

Here, μ is the dynamic viscosity of the liquid, and d is the molecular diameter of the diffusing substance.

Fick's first and second laws are applied to describe diffusion-controlled transport through porous media with some modifications. First, an effective diffusion coefficient, D_s is utilized to account for the complicated pore structure. Fick's first law is restated as

$$J_{diff} = -\eta D_s \frac{\partial c_r}{\partial x} \tag{2.4.5}$$

where η is the porosity, and $c_r(x.t)$ is the resident solute concentration in the liquid phase expressed as mass of soute per unit volume of solution. The effective diffusion coefficient in soil, D_s is smaller than the diffusion coefficient in a free liquid because of tortuosity effects. It is not uncommon to define tortuosity as

$$\tau = D_s/D_m \tag{2.4.6}$$

to account for the fact that the x coordinate in (2.4.5) measures linear distance while the path taken by the solute particle could be much larger. Substituting this modified Fick's law (2.4.5) in the continuity equation (2.4.2) which for porous media has the form

$$\frac{\partial(\eta c_r)}{\partial t} + \frac{\partial}{\partial x}(J_{diff}) = 0 \tag{2.4.7}$$

yields

$$\frac{\partial c_r}{\partial t} = D_s \frac{\partial^2 c_r}{\partial x^2} \tag{2.4.8}$$

where D_s is the effective diffusion coefficient. We consider (2.4.7) under the following conditions that reflect diffusion from a constant source.

$$c_r(x, 0) = 0 \tag{2.4.9a}$$

$$c_r(\infty, t) = 0 \tag{2.4.9b}$$

$$c_r(0, t > 0) = c_0 \tag{2.4.9c}$$

Defining $\hat{c}_r(x; s)$ as the Laplace transform of $c_r(x, t)$, i.e.

$$\hat{c}_r(x; s) = \int_0^\infty e^{-st} c_r(x, t) dt \tag{2.4.10}$$

and taking Laplace transform of (2.4.8), we obtain

$$\frac{d^2 \hat{c}_r}{dx^2} - \lambda^2 \hat{c}_r = 0 \tag{2.4.11}$$

where $\lambda = \sqrt{s/D_s}$. From (2.4.9), we have

$$\hat{c}_r(\infty; s) = 0 \; ; \; \hat{c}_r(0; s) = \frac{c_0}{s}. \tag{2.4.12}$$

Equation (2.4.11) is a second order differential equation with constant coefficients and has the general solution

$$\hat{c}_r(x; s) = Ae^{-\lambda x} + Be^{\lambda x} \tag{2.4.13}$$

where A and B are constants (i.e. independent of x) to be determined from the end conditions of (2.4.11). Since $\lambda > 0$, the condition for $x \to \infty$ requires that $B = 0$. The condition for $x = 0$ yields $A = c_o/s$ so that

$$\hat{c}_r(x; s) = \frac{c_0}{s} \exp(-\lambda x) \tag{2.4.14}$$

The inverse Laplace transform yields

$$c_r(x, t) = c_0 \; erfc\left[\frac{x}{2\sqrt{D_s t}}\right] \tag{2.4.15}$$

where the complementary error function is defined as

$$erfc(z) = 1 - \frac{2}{\sqrt{\pi}} \int_0^z e^{-\xi^2} d\xi = \frac{2}{\sqrt{\pi}} \int_z^\infty e^{-\xi^2} d\xi \tag{2.4.16}$$

The solution given by (2.4.15) also suggests that a self-similar scaled variable $x/\sqrt{t}$ would have converted the partial differential equation in (2.4.7) to an ordinary differential equation in the similarity variable.

The solute flux may be evaluated from (2.4.5) as

$$J_{diff} = -\eta D_s \frac{\partial c_r}{\partial x} = \frac{\eta D_s c_0}{\sqrt{\pi D_s t}} \exp\left(-\frac{x^2}{4D_s t}\right) \tag{2.4.17}$$

Of particular interest is the total mass flux that enters the porous medium at $x = 0$. This may be evaluated as

$$\int_0^{\mathrm{t}} J_{diff}(0, \tau) d\tau = \frac{2\eta D_s c_0}{\sqrt{\pi D_s}} \, \mathrm{t}^{1/2} \tag{2.4.18}$$

2.5. ADVECTIVE – DISPERSIVE SOLUTE TRANSPORT MODEL

In this section, we consider the case of solute transport in the presence of bulk movement of fluid along with mixing processes that account for diffusive transport as described in the previous section.

Advection refers to the transport of chemical species associated with average bulk movement of the fluid. Given our inability to describe the extremely complicated pore geometry in any detail, advective transport is essentially a representation of average behavior. The transport processes that are associated with deviations from this average behavior are characterized by mechanical dispersion. Deviations from average bulk movement may occur due to different pore velocities, velocity variations within a single pore tube, and from tortuosity effects. The process of molecular diffusion is always present, except that its influence is much smaller when compared to mechanical dispersion. The processes of mechanical dispersion and molecular diffusion are often combined together into hydrodynamic dispersion represented through the coefficient D.

In this section, we restrict our attention to the transport of a conservative solute (also called as an ideal tracer). Such a tracer moves through the porous medium without any physical, chemical or biological interactions with the porous matrix, nor does it undergo any transformations. In the absence of any sources or sinks, the transport equation for a conservative species in a one-dimensional flow field is given by

$$\frac{\partial c_b}{\partial t} + q \frac{\partial c_r}{\partial x} = \frac{\partial}{\partial x}\left[\eta D \frac{\partial c_r}{\partial x}\right] \tag{2.5.1}$$

where η is the saturated water content, c_b is the bulk resident concentration, which for a conservative solute is given as

$$c_b = \eta c_r \tag{2.5.2}$$

Note that c_b is expressed as mass of solute per unit bulk volume of soil. Equation (2.5.2) is valid if the solute resides in the liquid phase alone. The expression for the total resident concentration would need to be modified if solute mass was to be present in the solid (absorbed) phase and vapor (volatized) phase. Jury and Roth (1990) provide a detailed description of flux and resident concentrations along with the use of Laplace transform applications.

The Darcian flux q in (2.5.1) is related to the seepage velocity (also called as effective or pore water velocity) V as

$$q = \eta V \tag{2.5.3}$$

Strictly speaking, the porosity appearing in (2.5.1) and (2.5.3) is the effective areal porosity or kinematic porosity, while the one appearing in (2.5.2) is the volumetric porosity. The volumetric and effective areal porosities are commonly assumed to be the same for natural soils with random pore structure, resulting in the following transport equation

$$\frac{\partial c_r}{\partial t} + V\frac{\partial c_r}{\partial x} = \frac{\partial}{\partial x}\left[D\frac{\partial c_r}{\partial x}\right] \tag{2.5.4}$$

Equations (2.5.1) and (2.5.4) are often called as the *advection-dispersion equation* (ADE) in solute transport applications. While some empirical equations have been proposed for estimating the dispersion coefficient, it is often evaluated experimentally from saturated column experiments where a chemical tracer moves through a column under known conditions at the inlet end, and the effluent concentration is measured as a function of time. Analytical solutions of (2.5.4) under the appropriate boundary conditions are fit to the experimental data to find the parameter values that provide the best agreement between the theory and the observed data. This aspect was briefly described in Section 1.9.

Before proceeding further, it is important to distinguish between different types of concentrations that appear in advection-dispersion models of solute transport. When thinking in terms of inflow and outflow across a cross-section of a soil column, we use flux concentrations c_f . For one-dimensional flows, c_f is defined as the ratio of solute mass flux q_s crossing the plane to the volumetric water flux, q, so that

$$c_f = q_s/q \tag{2.5.5}$$

Thus in column experiments, the effluent concentration is the flux concentration (Figure 2.5.1). On the other hand, the resident concentration c_r measures the instantaneous mass density of solute in solution within the porous medium, and is defined as the mass of solute per unit volume of solution. If a column experiment is interrupted, and liquid concentrations are measured at various sections of the soil column, the measurements would yield resident concentrations. For now, we assume that

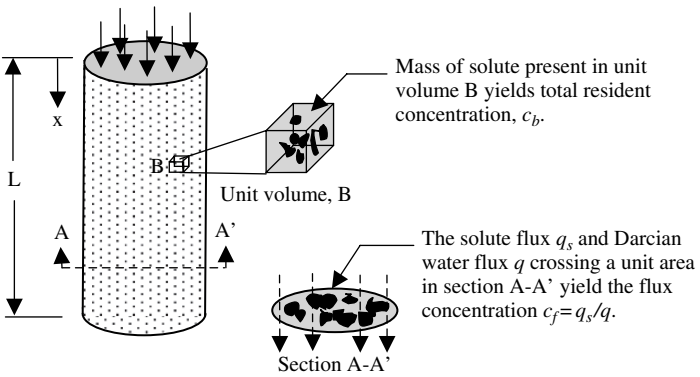

Figure 2.5.1. An illustration of flux and resident concentrations. The dark regions represent solid soil particles

the solute resides only in the liquid solution phase, even though it could exist in the solid phase (absorption) or gas phase (volatilization).

The one-dimensional mass conservation equation for a solute with no sources and sinks may be expressed as

$$\frac{\partial c_b}{\partial t} + \frac{\partial q_s}{\partial x} = \frac{\partial c_b}{\partial t} + q\frac{\partial c_f}{\partial x} = 0 \tag{2.5.6}$$

The boundary conditions for a semi-infinite soil column can be expressed as

$$c_b(x, 0) = c_{b,0}(x) \tag{2.5.7}$$

$$c_f(0, t) = c_{f,0}(t) \tag{2.5.8}$$

The flux and resident concentrations can be related by integrating (2.5.6). Thus

$$c_b(x, t) - c_{b,0}(x) = -q\frac{\partial}{\partial x}\left[\int_0^t c_f(x, \tau)d\tau\right] \tag{2.5.9}$$

or conversely,

$$c_f(x, t) - c_{f,0}(t) = -\frac{1}{q}\frac{\partial}{\partial t}\int_0^x c_b(x', t)dx' \tag{2.5.10}$$

It is also a straightforward matter to relate the Laplace transforms of the two concentrations as

$$\hat{c}_b(x; s) = \frac{c_{b,0}(x)}{s} - \frac{q}{s}\frac{d\hat{c}_f(x; s)}{dx} \tag{2.5.11}$$

$$\hat{c}_f(x; s) = \hat{c}_{f,0}(s) - \frac{s}{q}\int_0^x \hat{c}_b(x'; s)dx' + \frac{1}{q}\int_0^x c_{b,0}(x')dx' \tag{2.5.12}$$

These expressions show that a series of fairly detailed experiments are required to link the two concentrations since enough points in space and time are needed to evaluate the integrals in an accurate fashion. In most instances, we use mathematical models allowing for some form of analytical relationship that can be fit to data. As mentioned earlier, the advection-dispersion model is popular. The solute mass flux (mass/area/time) is expressed in terms of resident concentrations as

$$q_s = -\eta D \frac{\partial c_r}{\partial x} + q c_r \tag{2.5.13}$$

where both the hydrodynamic dispersion and advection modes of transport are represented. The solute mass conservation equation without sources or sinks (see also equation (2.5.6)) is

$$\frac{\partial(\eta c_r)}{\partial t} + \frac{\partial q_s}{\partial x} = 0 \tag{2.5.14}$$

Combining (2.5.13) and (2.5.14) leads to

$$\frac{\partial c_r}{\partial t} = D \frac{\partial^2 c_r}{\partial x^2} - V \frac{\partial c_r}{\partial x} \tag{2.5.15}$$

where $V = q/\eta$. Note that we continue to use the saturated water content, even though the mathematics would remain unaltered for any constant water content $\theta < \eta$. Parker and van Genuchten (1984) show that the governing equation for the flux concentration has the same form as (2.5.15), i.e.

$$\frac{\partial c_f}{\partial t} = D \frac{\partial^2 c_f}{\partial x^2} - V \frac{\partial c_f}{\partial x} \tag{2.5.16}$$

The boundary conditions in terms of flux concentrations are slightly simpler for Laplace transform operations.

$$c_f(x, 0) = 0 \tag{2.5.17}$$

$$c_f(0, t) = G\delta(t) \tag{2.5.18}$$

$$c_f(\infty, t) = 0 \tag{2.5.19}$$

These conditions correspond to a soil column that is initially free of solute. At the inlet boundary ($x = 0$), a mass M of solute is applied instantaneously at $t = 0$. The Darcian flux q is kept constant. Following Kreft and Zuber (1978), the quantity G in (2.5.18) is $M/(qA)$ where A is the cross-section area of the soil column (see Figure 2.5.1) perpendicular to the flow direction. The value of G is chosen as unity for convenience, and the total solute mass inside an infinitely long soil column should sum to unity. Taking Laplace transforms of both sides of (2.5.16) yields

$$s\,\hat{c}_f(x; s) - c_f(x, 0) = D \frac{d^2 \hat{c}_f(x; s)}{dx^2} - V \frac{d\hat{c}_f(x; s)}{dx} \tag{2.5.20}$$

Substituting the initial condition of (2.5.17), we obtain

$$D\frac{d^2\hat{c}_f(x;s)}{dx^2} - V\frac{d\hat{c}_f}{dx} - s\,\hat{c}_f = 0 \tag{2.5.21}$$

Laplace transforms of the boundary conditions yield

$$\hat{c}_f(0;s) = 1 \tag{2.5.22}$$

$$\hat{c}_f(\infty;s) = 0 \tag{2.5.23}$$

The general solution to the second-order differential equation (2.5.21) may be expressed as

$$\hat{c}_f(x;s) = \alpha\exp\left[\frac{Vx}{2D}(1-\xi)\right] + \beta\exp\left[\frac{Vx}{2D}(1+\xi)\right] \tag{2.5.24}$$

where,

$$\xi = \left(1+\frac{4sD}{V^2}\right)^{1/2} \tag{2.5.25}$$

The constants α and β are chosen so as to satisfy the conditions of (2.5.22) and (2.5.23). Thus $\beta = 0$ ensures that the solution bounded, and $\alpha = 1.0$. Consequently,

$$\hat{c}_f(x;s) = \exp\left[\frac{Vx}{2D}(1-\xi)\right] \tag{2.5.26}$$

Using appropriate tables (for example Table 2.1.1) we have the solution as

$$c_f(x,t) = \frac{x}{2\sqrt{\pi D t^3}}\exp\left[-\frac{(x-Vt)^2}{4Dt}\right] \tag{2.5.27}$$

The solution in (2.5.27) is often referred to as the *Fickian* pdf and was one of the models in Section 1.9. There are two important aspects to this solution. Because of the chosen boundary condition (2.5.18), the expression for flux concentration may be thought of as a probability function, where we substitute probability mass for solute mass. Secondly (2.5.27) also serves as the Green's function for this problem, following the logic used in the previous section. Thus if some arbitrary input $c_{f,0}(t)$ is imposed at $x = 0$, the solution is expressed through convolution as

$$c_f(x,t) = \int_0^t c_{f,0}(t-\tau)\frac{x}{2\sqrt{\pi D\tau^3}}\exp\left[-\frac{(x-V\tau)^2}{4D\tau}\right]d\tau \tag{2.5.28}$$

We are now in a position to evaluate the bulk resident concentration solution for the advection dispersion model. Combining (2.5.11) and (2.5.26) we obtain the following expression for the Laplace transform of the resident concentration

$$\hat{c}_b(x;s) = -\frac{q}{s}\frac{d\hat{c}_f}{dx} = \frac{2\eta}{1+\xi}\ \exp\left[\frac{Vx}{2D}(1-\xi)\right] \tag{2.5.29}$$

The inverse transform yields

$$c_b(x,t) = \frac{\eta V}{\sqrt{\pi D t}}\exp\left[-\frac{(x-Vt)^2}{4Dt}\right] - \frac{\eta V^2}{2D}\exp\left(\frac{Vx}{D}\right) erfc\left(\frac{x+Vt}{\sqrt{4Dt}}\right) \tag{2.5.30}$$

The resident concentration in the liquid phase $c_r(x.t)$ can be obtained from (2.5.30) and (2.5.2).

2.6. ROLE OF BOUNDARY CONDITIONS

The importance of clearly identifying flux and resident concentrations, and the imposition of physically meaningful boundary and initial conditions has been emphasized in numerous studies (for e.g., Kreft and Zuber, 1978; Parker and van Genuchten, 1984). Here we examine how the nature of the solution of the advection-dispersion equation is influenced by different kinds of boundary conditions. Only a few simple cases are described here, and readers are referred to van Genuchten and Alves (1982) for a more complete list of solutions. We write the governing equation as

$$\frac{\partial c}{\partial t} + V\frac{\partial c}{\partial x} = D\frac{\partial^2 c}{\partial x^2} \tag{2.6.1}$$

where D expresses the combined effects of molecular diffusion and mechanical dispersion. In (2.6.1), $c(x,t)$ could represent flux or resident concentrations. In this section, we merely examine the various mathematical solutions to different boundary conditions. Consider the soil column to be of length L along the direction of average water movement.

Specification of any particular boundary condition at the outlet $x = L$ for solute movement is difficult. It is customary to mathematically impose the boundary condition at $x = \infty$, and examine the solution at $x = L$. The evaluation of $c(L,t)$ in this manner allows solute efflux by both advection and dispersion mechanisms.

For a semi-infinite soil column, a simple inlet condition at $x = 0$ is to impose a Dirichlet (first type) boundary condition of a constant prescribed value for the resident concentration of the form

$$c(0,t) = c_0 \tag{2.6.2}$$

where c_0 would be solute concentration in the source reservoir at the inlet end. Ogata and Banks (1961) provide the solution for this case as

$$c(x,t) = \frac{c_0}{2}\left\{erfc\left(\frac{x-Vt}{\sqrt{4Dt}}\right) + \exp\left(\frac{xV}{D}\right) erfc\left(\frac{x+Vt}{\sqrt{4Dt}}\right)\right\} \tag{2.6.3}$$

It should be noted that the contribution of the second term on the right hand side of (2.6.3) is negligible when xV/D is large (e.g. for $xV/D > 500$, the error is less than 3%).

Consider a case of an infinite column ($-\infty < x < \infty$) where solute mass is continuously injected in the column at a location $x = 0$. Here again, we interpret $c(x,t)$ as a resident concentration and impose

$$\int_{-\infty}^{\infty} \eta c(x,t)dx = qc_0 t \tag{2.6.4}$$

In this case even though there is a constant advective field in the positive x direction, dispersion causes some spreading of solute mass in both positive and negative directions. Sauty (1980) presented the solution for this case as

$$c(x,t) = \frac{c_0}{2}\left\{erfc\left(\frac{x-Vt}{\sqrt{4Dt}}\right) - \exp\left(\frac{xV}{D}\right) erfc\left(\frac{x+Vt}{\sqrt{4Dt}}\right)\right\} \tag{2.6.5}$$

One should note that (2.6.3) and (2.6.5) provide the same solution for large xV/D.

The condition of a well-mixed reservoir at the upstream end is represented by a Cauchy (or third type) boundary condition for the resident concentration $c(x,t)$

$$qc_0 = \left[qc - \eta D\frac{\partial c}{\partial x}\right]|_{x=0} \tag{2.6.6}$$

Thus solute flux at the upstream end enters the column by pore advection alone. Lindstrom et al. (1967) provide a solution to this case as

$$\begin{aligned} c(x,t) = \frac{c_0}{2}\Bigg\{&erfc\left(\frac{x-Vt}{\sqrt{4Dt}}\right) + \sqrt{\frac{4V^2t}{\pi D}}\exp\left[-\frac{(x-Vt)^2}{4Dt}\right] \\ &- \left(1 + \frac{Vx}{D} + \frac{V^2t}{D}\right)\exp\left(\frac{Vx}{D}\right) erfc\left(\frac{x+Vt}{\sqrt{4Dt}}\right)\Bigg\} \end{aligned} \tag{2.6.7}$$

It is clear that the only variables appearing in the equations are $c(x,t)$, c_0, x, t, V and D. The quantity $c(x,t)/c_0$ appears as the scaled concentration with respect to the source. For a column of length L, the effluent concentrations are obtained by setting $x = L$ in the above solutions. Rearranging these variables leads to the *Peclet number*

$$P = \frac{VL}{D} \tag{2.6.8}$$

The Peclet number plays an important role in our understanding of the model solution. Indeed, selecting the following dimensionless variables

$$X = x/L;\ T = \frac{tV}{L} \tag{2.6.9}$$

the transport equation becomes

$$\frac{\partial c}{\partial T} + \frac{\partial c}{\partial x} = \frac{1}{P}\frac{\partial^2 c}{\partial X^2} \tag{2.6.10}$$

The Peclet number is a measure of the relative importance of advection versus dispersion as transport processes. Equation (2.6.8) suggests that the Peclet number may be interpreted as the ratio of travel time due to dispersion and travel time due to advection. For large Peclet numbers, advection is the dominating mechanism. In the limit as $P \to \infty$, we have a hyperbolic partial differential equation

$$\frac{\partial c}{\partial T} + \frac{\partial c}{\partial x} = 0 \tag{2.6.11}$$

describing purely advective transport. In the other limit, for diffusion dominated process, we obtain the parabolic differential equation

$$\frac{\partial c}{\partial T} = \frac{1}{P}\frac{\partial^2 c}{\partial x^2} \tag{2.6.12}$$

The column length was chosen as the length scale when defining the Peclet number in (2.6.8). Depending on the application, other length properties may be more appropriate as the length scaling parameter.

Figure 2.6.1 shows the values of relative concentrations as a function of time for some typical parameter values. The shapes of the curves are quite similar to each other, with the similarity increasing with increasing Peclet number. As $P \to \infty$, the ADE model approaches a piston-flow model, and dispersion effects are negligible.

Column studies seem to indicate that the extent of spreading seems to be scaled in terms of the velocity and length of the soil column. The Peclet number appears to remain constant, and the dispersion is therefore linearly dependent on V.

$$\frac{D}{V} = \frac{L}{P} = \alpha_L \tag{2.6.13}$$

The quantity α_L is called *longitudinal dispersivity* and is interpreted as the characteristic length of the soil determining dispersion effects. In laboratory column experiments, α_L values range from 0.01 to 0.1 cm. Some models for dispersion account for both diffusion and mechanical dispersion

$$D = \tau D_m + \alpha_L V \tag{2.6.14}$$

where τ is a tortuosity coefficient and D_m is the molecular diffusion coefficient. In this form, Bear (1979) refers to D as the *hydrodynamic dispersion coefficient.*

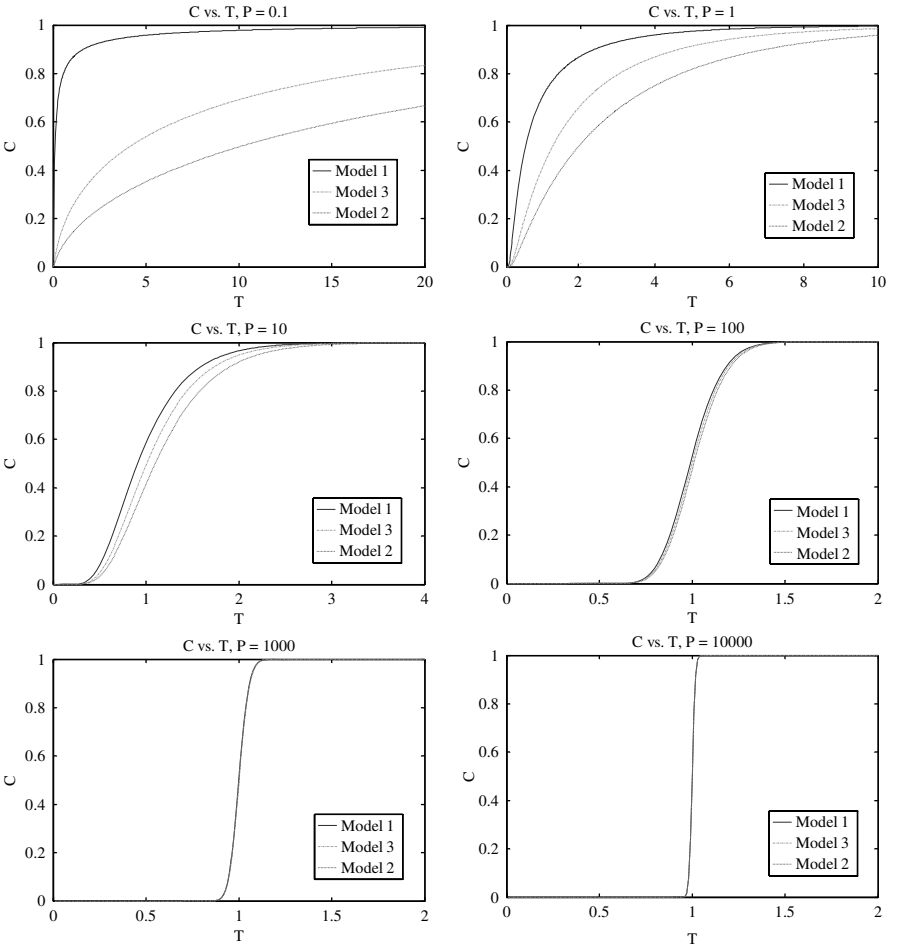

Figure 2.6.1. Plot of dimensionless concentration ($C = c/c_0$) versus dimensionless time ($T = tV/L$) for dimensionless distance $X = 1$ ($X = x/L$). In the figure, models 1, 2, and 3 refer to equations (2.6.3), (2.6.5), and (2.6.7), respectively

2.7. THE MOBILE – IMMOBILE WATER MODEL

The results of the advective-dispersive model generally tend to have a symmetric Gaussian shape as V/D increases. However, many experimental studies, both in saturated and unsaturated soils, yield very non-symmetric shapes for resident and flux concentrations. Many breakthrough curves exhibit significant tailing behavior with low concentrations persisting for a long time in the effluent solution. These asymmetrical concentration profiles were attributed to the presence of stagnant or immobile water in dead-end or blind pores. Further, aggregated soils have rapidly-conducting pores that are primarily responsible for bulk water movement, but a

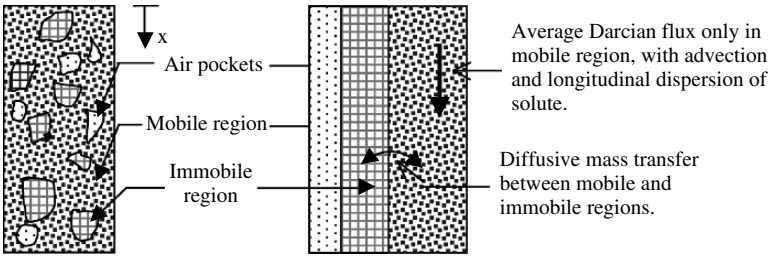

Figure 2.7.1. A conceptual sketch for the MIM model

significant portion of the total pore space is locked up within the aggregates where the pores are small and not conducive to advective transport. Solute movement in and out of the immobile water regions is conceptualized as occurring by diffusion alone. The *physical nonequilibrium model* was proposed by van Genuchten (1974) and extended further in van Genuchten and Wierenga (1976). A simpler version called the *mobile-immobile* (MIM) model is considered first.

For solute movement with a diffusion-controlled mechanism for mass transfer between mobile and immobile water zones, the soil void space is conceptualized as having three different regions (Figure 2.7.1):

(i) Air Space (assumed to have no solute vapor mass).

(ii) *Mobile* or *dynamic* water region in the inter-aggregate region where advective water movement occurs along with advection and longitudinal dispersion of solute mass. The *mobile water content* is θ_m and the resident solute concentration is $c_{m,r}$.

(iii) *Immobile* (dead or stagnant) *water region* in the intra-aggregate pores, from where solute can only move by diffusion in response to concentration difference between mobile and immobile regions. The *immobile water content* is denoted by θ_{im}, and the resident solute concentration is denoted by $c_{im,r}$.

The total water content $\theta = \theta_m + \theta_{im}$. If the soil is saturated, then $\theta = \eta$ the porosity, else $\theta < \eta$. Based on these definitions, the bulk resident concentration is

$$c_b = \theta_m c_{mr} + \theta_{im} c_{im,r} \tag{2.7.1}$$

and the solute mass flux is given by

$$q_s = q c_{m,r} - \theta_m D_m \frac{\partial c_{m,r}}{\partial x} \tag{2.7.2}$$

where D_m is the hydrodynamic dispersion coefficient in the mobile water region. From the continuity equation (2.5.6) we obtain

$$\theta_m \frac{\partial c_{m,r}}{\partial t} + \theta_{im} \frac{\partial c_{im,r}}{\partial t} = \theta_m D_m \frac{\partial^2 c_{m,r}}{\partial x^2} - q \frac{\partial c_{m,r}}{\partial x} \tag{2.7.3}$$

We have two unknowns $c_{m,r}(x,t)$ and $c_{im,r}(x,t)$. A second equation is obtained by assuming a diffusion-controlled rate law to describe mass transfer of solutes from mobile to immobile regions (Coats and Smith, 1956).

$$\theta_{im}\frac{\partial c_{im,r}}{\partial t} = \alpha\left(c_{m,r} - c_{im,r}\right) \tag{2.7.4}$$

Equation (2.7.4) suggests that when the rate of mass transfer as described by α tends to infinite, then mass transfer from mobile to immobile regions and vice-versa occurs instantaneously, so that changes in $c_{m,r}$ are followed by an immediate adjustment in $c_{im,r}$, and these two concentrations are said to be in equilibrium. An appropriate set of end conditions is

$$c_{m,r}(x,0) = 0\ ;\ c_{im,r}(x,0) = 0\ ;\ c_{m,f}(\infty,t) = 0\ ;\ c_{m,f}(0,t) = G\delta(t) \tag{2.7.5}$$

where $c_{m,f}(x,t)$ refers to the flux concentration of solute in the mobile water region. As indicated in (2.5.18), the quantity G is taken as unity. The mobile flux and resident concentrations are related as

$$c_{m,f}(x,t) = \frac{q_s}{q} = c_{m,r} - \frac{D_m}{V_m}\frac{\partial c_{m,r}}{\partial x} \tag{2.7.6}$$

where $V_m = q/\theta_m$ is the average seepage velocity of water in the mobile region. Notice that the solute in the immobile region cannot exit the control volume except by diffusing into the mobile region. Therefore, $c_{m,f}(x,t)$ represents the total flux concentration.

Defining the Laplace transforms of the mobile and immobile concentrations as

$$\hat{c}_{m,r}(x;s) = \int_0^\infty e^{-st}c_{m,r}(x,t)dt,\ \ \hat{c}_{im,r}(x;s) = \int_0^\infty e^{-st}c_{im,r}(x.t)dt \tag{2.7.7}$$

we obtain from (2.7.3), (2.7.4), and (2.7.5)

$$s\theta_m\hat{c}_{m,r} + s\theta_{i,m}\hat{c}_{im,r} = \theta_m D_m\frac{\partial^2\hat{c}_{m,r}}{\partial x^2} - q\frac{\partial\hat{c}_{m,r}}{\partial x} \tag{2.7.8}$$

$$s\theta_{i,m}\hat{c}_{im,r} = \alpha\left(\hat{c}_{m,r} - \hat{c}_{im,r}\right) \tag{2.7.9}$$

Eliminating $\hat{c}_{im,r}$ from these equations, one obtains

$$\theta_m D_m\frac{\partial^2\hat{c}_{m,r}}{\partial x^2} - q\frac{\partial\hat{c}_{m,r}}{\partial x} - g(s)\theta_m\hat{c}_{m,r} = 0 \tag{2.7.10}$$

where

$$g(s) = s + \frac{s\alpha\theta_{im}}{\theta_m(\alpha + s\theta_{im})} \tag{2.7.11}$$

From (2.7.6), we obtain

$$\hat{c}_{m,f}(x,s) = \hat{c}_{m,r}(x,s) - \frac{D_m}{V_m}\frac{\partial\left[\hat{c}_{m,r}(x;s)\right]}{\partial x} \tag{2.7.12}$$

One can see that $\hat{c}_{m,r}$ and $\partial\hat{c}_{m,r}/\partial x$ satisfy (2.7.10), and so does $\hat{c}_{m,f}(x;s)$ from linearity. Hence

$$\theta_m D_m \frac{\partial^2 \hat{c}_{f,m}}{\partial x^2} - q\frac{\partial \hat{c}_{f,m}}{\partial x} - g(s)\theta_m \hat{c}_{m,f} = 0 \tag{2.7.13}$$

with end conditions of (2.7.5). The general solution to (2.7.13) is expressed as

$$\hat{c}_{m,f} = \alpha \exp\left[\frac{V_m x}{2D_m}(1-\xi)\right] + \beta \exp\left[\frac{V_m x}{2D_m}(1+\xi)\right] \tag{2.7.14}$$

where ξ is now defined as

$$\xi = \left[1 + \frac{4g(s)D_m}{V_m^2}\right]^{1/2} \tag{2.7.15}$$

and

$$\hat{c}_{m,f}(0;s) = 1.0 \tag{2.7.16}$$

Therefore, $\alpha = 1$, $\beta = 0$ and (2.7.14) simplifies to

$$\hat{c}_{m,f}(x;s) = \exp\left[\frac{V_m x}{2D_m}(1-\xi)\right] \tag{2.7.17}$$

From (2.5.11), we have

$$\hat{c}_b(x;s) = \frac{1}{s}\frac{2\theta_m g(s)}{(1+\xi)}\exp\left[\frac{V_m x}{2D_m}(1-\xi)\right] \tag{2.7.18}$$

2.8. THE PHYSICAL NONEQUILIBRIUM MODEL

The model of van Genuchten and Wierenga (1976) includes further sophistication by considering that some solutes interact with the soil particles and a certain mass of the solute is said to reside in the solid phase. In the physical nonequilibrium (PNE) model, the soil is conceptualized as being partitioned into five regions-two

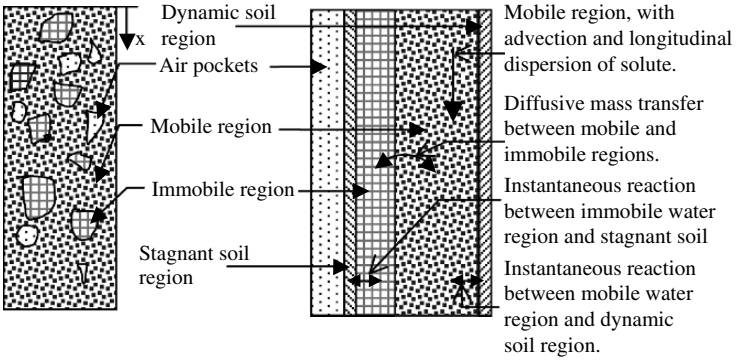

Figure 2.8.1. A conceptual sketch of the PNE model

additional regions have to be included than those for the MIM model. The additional regions (Figure 2.8.1) to be considered for solid phase concentrations are:

- A dynamic (or active) soil region that is in close enough contact with the mobile water region so that the solute concentration in the solid phase, (S_m =mass of solute/mass of dry soil), is assumed to be in equilibrium with the solute concentration in the mobile phase $C_{m,r}$. The fraction of the total soil comprising the dynamic soil region is denoted as f.
- A stagnant soil region that is not in immediate contact with mobile liquid, and is primarily associated with immobile water pockets. The solute concentration associated with this solid phase is expressed as $S_{i,m}$ (=mass of solute associated with unit mass of dry soil). The stagnant soild fraction is $(1-f)$. Defining the bulk density of the soil as ρ (mass of soil/bulk volume of soil), we have

$$c_b(x,t) = \theta_m c_{m,r} + \theta_{im} c_{im,r} + f\rho S_m + (1-f)\rho S_{im} \tag{2.8.1}$$

Note that the solid phase concentrations are always immobile and do not contribute directly to any solute flux. The solute flux is again given by (2.7.2), and combining with (2.8.1) yields

$$\theta_m \frac{\partial c_{m,r}}{\partial t} + \theta_{im} \frac{\partial c_{im,r}}{\partial t} + f\rho \frac{\partial S_m}{\partial t} + (1-f)\rho \frac{\partial S_{im}}{\partial t} = \theta_m D_m \frac{\partial^2 c_{m,r}}{\partial x^2} - q \frac{\partial c_{m,r}}{\partial x} \tag{2.8.2}$$

To relate the solid and liquid phase concentrations, van Genuchten and Wierenga (1976) assumed instantaneous adsorption described by the Freundlich isotherm

$$s_m = kC_{m,r}^n \; ; \; s_{im} = kC_{im,r}^n \tag{2.8.3}$$

where k is a proportionality constant. Hence

$$\frac{\partial S_m}{\partial t} = knC_{m,r}^{n-1}\frac{\partial c_{im,r}}{\partial t}\ ;\ \frac{\partial S_{im}}{\partial t} = knC_{im,r}^{n-1}\frac{\partial c_{im,r}}{\partial t} \tag{2.8.4}$$

Furthermore, solute mass transfer from mobile to immobile water regions is assumed to occur by a diffusion mechanism, and a transfer equation of the following form is proposed

$$\theta_{im}\frac{\partial c_{im,r}}{\partial t} + (1-f)\rho\frac{\partial S_{im}}{\partial t} = \alpha\left[c_{m,r} - c_{im,r}\right] \tag{2.8.5}$$

For linear isotherms, $n = 1$ in (2.8.3) and (2.8.4), and k is called a *distribution coefficient*. Substituting (2.8.4) with $n = 1$ in (2.8.2) and (2.8.5), respectively, yields

$$[\theta_m + f\rho k]\frac{\partial c_{m,r}}{\partial t} + [\theta_{im} + (1-f)\rho k]\frac{\partial c_{im,r}}{\partial t} = \theta_m D_m\frac{\partial^2 c_{m,r}}{\partial x^2} - q\frac{\partial c_{m,r}}{\partial x} \tag{2.8.6}$$

$$[\theta_{im} + (1-f)\rho k]\frac{\partial c_{im,r}}{\partial t} = \alpha\left[c_{m,r} - c_{im,r}\right] \tag{2.8.7}$$

For simplicity, the same boundary condition as in (2.7.5) would be applicable. The flux concentration $C_{m,f}(x, t)$ has the same definition as (2.7.6) as do the definitions of the Laplace transforms in (2.7.7). Taking transforms of (2.8.6) and (2.8.7), we obtain

$$s[\theta_m + f\rho k]\hat{c}_{m,r} + s[\theta_{im} + (1-f)\rho k]\hat{c}_{im,r} = \theta_m D_m\frac{\partial^2 \hat{c}_{m,r}}{\partial x^2} - q\frac{\partial \hat{c}_{m,r}}{\partial x} \tag{2.8.8}$$

$$s[\theta_{im} + (1-f)\rho k]\hat{c}_{im,r} = \alpha\left[\hat{c}_{m,r} - \hat{c}_{im,r}\right] \tag{2.8.9}$$

Solving for $\hat{c}_{im,r}$ from (2.8.9) and substituting in (2.8.8) yields

$$\theta_m D_m\frac{\partial^2 \hat{c}_{m,r}}{\partial x^2} - q\frac{\partial \hat{c}_{m,r}}{\partial x} - \theta_m g(s)\hat{c}_{m,r} = 0 \tag{2.8.10}$$

with

$$g(s) = s\left[1 + \frac{f\rho k}{\theta_m}\right] + \frac{s[\theta_{im} + (1-f)\rho k]\,\alpha/\theta_m}{s[\theta_{im} + (1-f)\rho k] + \alpha} \tag{2.8.11}$$

As in the previous section, the Laplace transform of the flux concentration $\hat{c}_{f,m}$ also satisfies the same differential equation (2.8.10) so that

$$\theta_m D_m\frac{\partial^2 \hat{c}_{m,f}}{\partial x^2} - q\frac{\partial \hat{c}_{m,f}}{\partial x} - \theta_m g(s)\hat{c}_{m,f} = 0 \tag{2.8.12}$$

subject to $\hat{c}_{m,f}(0; s) = 1$. The analysis follows along similar lines with the new definition of $g(s)$ in (2.8.11). Otherwise, the expressions for $\hat{c}_{m,f}(x; s)$ and $\hat{c}_b(x; s)$ have the same form as in (2.7.17) and (2.7.18), respectively. Analytical solutions for $c_{m,r}(x, t)$ and $c_{im,r}(x, t)$ were derived by van Genuchten and Wierenga (1976).

2.9. THE CHEMICAL NONEQUILIBRIUM MODEL

A somewhat different conceptualization of the soil containing both equilibrium and kinetic adsorption sites was proposed by several researchers (Selim et al., 1976; Cameron and Klute, 1977; Hoffman and Rolston, 1980) and has been described by Nkedi-Kizza et al. (1984) as a model involving surface reaction rate laws. The soil surface area is assumed to comprise of two different kinds of adsorption sites: type 1 sites where adsorption is achieved instantaneously, and type 2 sites with time-dependant kinetic sorption. This model is often termed as the *chemical nonequilibrium* (CNE) model. The water content θ is not partitioned into mobile and immobile fractions in this model, and the resident liquid concentration is $C_r(x, t)$

The solid phase concentrations $S_1(x, t)$ and $S_2(x, t)$ are the mass of solute per weight of soil at type 1 and type 2 sites, respectively. At equilibrium, these concentrations are related to the liquid phase resident concentration as

$$S_1 = K_1 c = K_D F c_r \tag{2.9.1}$$

$$S_2 = K_2 c = K_D (1 - F) c_r \tag{2.9.2}$$

where K_1, K_2, and K_D are distribution coefficients, and F is the fraction of soil sites (type 1) where adsorption is assumed to occur instantaneously. For type 1 sites, we have

$$\frac{\partial S_1}{\partial t} = F K_D \frac{\partial c_r}{\partial t} \tag{2.9.3}$$

while for type 2 sites, adsorption process is described by a linear first-order equation

$$\frac{\partial S_2}{\partial t} = \alpha_2 \left[(1 - F) K_D c_r - S_2 \right] \tag{2.9.4}$$

with α_2 representing a first-order kinetic rate coefficient. The bulk resident concentration is

$$c_b(x, t) = \theta c_r + \rho \left[S_1 + S_2 \right] \tag{2.9.5}$$

where θ is the water content (= porosity η under saturated conditions). The solute flux is

$$q_s = -D\theta \frac{\partial c_r}{\partial x} + q c_r \tag{2.9.6}$$

From the continuity equation (2.5.6), we have

$$\frac{\partial}{\partial t} \left[\theta c_r + \rho (S_1 + S_2) \right] = \theta D \frac{\partial^2 c_r}{\partial x^2} - q \frac{\partial c_r}{\partial x} \tag{2.9.7}$$

and substituting (2.9.3) and (2.9.4), we obtain

$$[\theta+\rho FK_D]\frac{\partial c_r}{\partial t}+\rho\frac{\partial S_2}{\partial t}=\theta D\frac{\partial^2 c_r}{\partial x^2}-q\frac{\partial c_r}{\partial x} \tag{2.9.8}$$

Equation (2.9.8) and (2.9.4) are the two governing partial differential equations. The flux concentration is

$$c_f(x,t)=\frac{q_s}{q}=-\frac{D}{V}\frac{\partial c_r}{\partial x}+Vc_r \tag{2.9.9}$$

where $V=q/\theta$. The end conditions are

$$c_r(x,0)=S_1(x,0)=S_2(x,0)=0\ ;\ c_f(\infty,t)=0\ ;\ c_f(0,t)=\delta(t) \tag{2.9.10}$$

Defining Laplace transforms of the concentrations as

$$\hat{c}_r(x,s)=\int_0^\infty e^{-st}c_r(x,t)dt\ ;\ \hat{S}_2(x,s)=\int_0^\infty e^{-st}S_2(x,t)dt \tag{2.9.11}$$

and taking transforms of (2.9.8) and (2.9.4) yields

$$s[\theta+\rho FK_D]\hat{C}_r+s\rho\hat{S}_2=\theta D\frac{\partial^2\hat{c}_r}{\partial x^2}-q\frac{\partial\hat{c}_r}{\partial x} \tag{2.9.12}$$

$$s\hat{S}_2=\alpha_2\left[\left((1-F)K_D\hat{c}_r-\hat{S}_2\right)\right] \tag{2.9.13}$$

Eliminating $\hat{S}_2$ from (2.9.13) and substituting in (2.9.12) yields

$$\theta D\frac{\partial^2\hat{c}_r}{\partial x^2}-q\frac{\partial\hat{c}_r}{\partial x}-\theta g(s)\hat{c}_r=0 \tag{2.9.14}$$

with $g(s)$ now defined as

$$g(s)=s\left[1+\frac{\rho FK_D}{\theta}\right]+\frac{s\rho\alpha_2(1-F)K_D}{\theta(s+\alpha_2)} \tag{2.9.15}$$

From (2.9.9) we note that

$$\hat{c}_f(x;s)=-\frac{D}{V}\frac{\partial\hat{c}_r}{\partial x}+V\hat{c}_r \tag{2.9.16}$$

and $\hat{c}_f$ also satisfies (2.9.14)

$$\theta D\frac{\partial^2\hat{c}_f}{\partial x^2}-q\frac{\partial\hat{c}_f}{\partial x}-\theta g(s)\hat{c}_f=0 \tag{2.9.17}$$

Following the same steps as in the previous sections, the expression for $\hat{c}_f(x;s)$ and $\hat{c}_b(x;s)$ have the same form as in (2.7.17) and (2.7.18) respectively with $g(s)$ now defined as in (2.9.15). Haggerty and Gorelick (1995) further expand on this model by allowing for multiple mass transfer rates at different sorption sites. The PNE and CNE models will be revisited in Chapter 5.

2.10. NONEQUILIBRIUM SORPTION BY DIFFUSION INTO SPHERICAL GRAINS

Several researchers (Rosen, 1952; Rao et al, 1980; Valocchi, 1985, Cunningham and Roberts, 1998) have conceptualized that nonequilibrium sorption in soils can be represented by solute diffusion into spherical grains. The tailing behavior in breakthrough curves is attributed to the slow approach to equilibrium from diffusion of the solute into the porous spherical aggregates that are assumed to be filled with stagnant water. As nonequilibrium is manifested by diffusion into spherical grains, Cunningham and Roberts (1998) refer to this as the DSG model (see Figure 2.10.1)

Solute mass is presumed to exist in the liquid phase with a resident concentration of $c_r(x, t)$ and in the solid phase with a concentration described by $S(x, t)$. Using definitions of previous sections,

$$c_b = \theta c_r(x, t) + \rho S(x, t) \tag{2.10.1}$$

$$q_s = -\theta D \frac{\partial c_r}{\partial x} + q c_r \tag{2.10.2}$$

and the governing equation is

$$\theta \frac{\partial c_r(x, t)}{\partial t} + \rho \frac{\partial S(x, t)}{\partial t} = \theta D \frac{\partial^2 c_r(x, t)}{\partial x^2} - q \frac{\partial c_r(x, t)}{\partial x} \tag{2.10.3}$$

To relate the solid and liquid phase concentrations, it is assumed that the soil contains spherical aggregates of radius a. The solute concentration within the aggregate at any spatial location x is described by $c_a(x, r, t)$ where r denotes radial distance from the center of the aggregate. The mathematical model for diffusion into spherical grains is represented by the following equations.

$$S(x, t) = k_d \frac{3}{a^3} \int_0^a r^2 c_a(x, r, t) dr \tag{2.10.4}$$

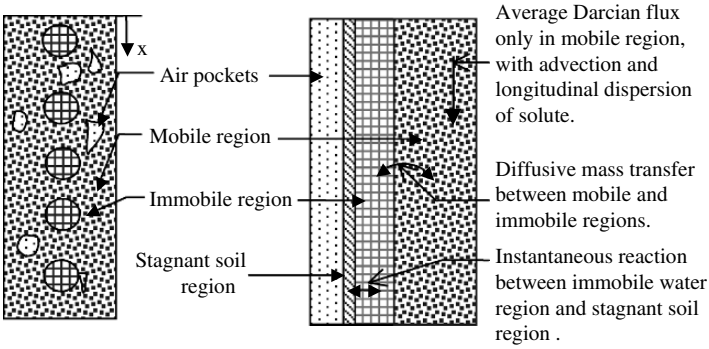

Figure 2.10.1. A conceptualization of the DSG model

where k_d is the distribution coefficient relating the solid phase concentration to the average liquid-phase concentration within the grain. Further, the governing equation for diffusion into a spherical aggregate is

$$\frac{\partial c_a(x,r,t)}{\partial t} = D_a \frac{1}{r^2}\frac{\partial}{\partial r}\left[r^2 \frac{\partial c_a(x,r,t)}{\partial r}\right] \tag{2.10.5}$$

under the end conditions

$$c_a(x, r=a, t) = c_r(x,t) \tag{2.10.6}$$

$$\lim_{r\to 0}[rc_a(x,r,t)] = 0 \tag{2.10.7}$$

In (2.10.5), D_a is the diffusion coefficient in the liquid phase within the grain. The end conditions for (2.10.3) are the same as in (2.7.5).

Taking Laplace transforms of (2.10.3) and (2.10.4) yields

$$s\theta\hat{c}_r + s\rho\hat{S} = \theta D\frac{\partial^2 \hat{c}_r}{\partial x^2} - q\frac{\partial \hat{c}_r}{\partial x} \tag{2.10.8}$$

$$\hat{S} = k_d \frac{3}{a^3}\int_0^a r^2 \hat{c}_a dr \tag{2.10.9}$$

Taking the Laplace transform of (2.10.5) and then integrating with respect to r within the limits of $[0, a]$, we have

$$\int_0^a r^2 \hat{c}_a dr = \frac{D_a}{s} a^2 \frac{\partial \hat{c}_a}{\partial r}\,|_{r=a} \tag{2.10.10}$$

To evaluate (2.10.10), we take the Laplace transform of (2.10.5), and make the substitution

$$z = r\sqrt{s/D_a} \tag{2.10.11}$$

so that the governing equation for $\hat{c}_a$ is given as

$$z^2\frac{\partial^2 \hat{c}_a}{\partial z^2} + 2z\frac{\partial \hat{c}_a}{\partial z} - z^2\hat{c}_a = 0 \tag{2.10.12}$$

Equation (2.10.12) admits solutions in terms of modified spherical Bessel functions (Abramowitz and Stegun, 1964)

$$\hat{c}_a(z, x; s) = A\sqrt{\frac{\pi}{2z}} I_{1/2}(z) + B\sqrt{\frac{\pi}{2z}} K_{1/2}(z) \tag{2.10.13}$$

We note that as $z \to 0$, $I_{1/2}(z) \to 1.0$, $K_{1/2} \to \infty$, so that from (2.10.7), $B = 0$. From (2.10.6), we observe that the second constant in (2.10.13) is evaluated as

$$A = \frac{\hat{C}_r(x; s)}{\sqrt{\frac{\pi}{2z}} I_{1/2}(z')} \tag{2.10.14}$$

Further, using the mathematical identity

$$I_{1/2}(z) = \sqrt{\frac{2}{\pi z}} \sinh z \tag{2.10.15}$$

the solution for $\hat{c}_a$ is obtained as

$$\hat{c}_a(z, r; s) = \frac{\hat{c}_r(x; s)\frac{\sinh z}{z}}{\frac{\sinh z'}{z'}} \tag{2.10.16}$$

with

$$z' = a\sqrt{s/D_a} \tag{2.10.17}$$

From (2.10.9), (2.10.10), and (2.10.16), we obtain after simplification

$$\frac{\hat{S}}{\hat{c}_r} = W(s) = 3k_d \left[\frac{\coth \sqrt{st_d}}{\sqrt{st_d}} - \frac{1}{st_d} \right] \tag{2.10.18}$$

where t_d is the time-scale suggested by Crank (1975)

$$t_d = a^2/D_a \tag{2.10.19}$$

Substituting (2.10.18) into (2.10.8) results in the equation

$$\theta D \frac{\partial^2 c_r(x; s)}{\partial x^2} - q \frac{\partial \hat{c}_r(x; s)}{\partial x} - \theta g(s) \hat{c}_r(x; s) = 0 \tag{2.10.20}$$

with $g(s)$ now defined as

$$g(s) = s + \frac{s\rho W(s)}{\theta} \tag{2.10.21}$$

Note that (2.10.20) is also the governing equation for the Laplace transform of the flux concentration. The quantities $\hat{c}_f(x; s)$ and $\hat{c}_b(x; s)$ are given as in (2.7.17) and (2.7.18), respectively, with $g(s)$ now defined in (2.10.21). To account for nonuniform grain-size distribution, Cunningham and Roberts (1998) consider a distribution of diffusion travel time scale t_d to examine the behavior of travel times through a column.

Apart from the simple advection dispersion equation, different conceptualizations result in different models such as the MIM, PNE, CNE, and DSG models. From measurements of effluent flux concentrations, it is not possible to uniquely determine which model is the appropriate choice. Given the number of model parameters, it is likely that these and other models fit the experimental observations reasonably well. Moreover, some of these models, notably the PNE and CNE models, have been shown to have similar responses by Nkedi-Kizza et al. (1984). Therefore, the choice of a particular model is based on what the user thinks best describes the experimental conditions, and which model is capable of explaining the observations most satisfactorily.

CHAPTER 3

FOURIER TRANSFORMS FOR SOLUTE TRANSPORT MODELS

The concept of Fourier transforms was introduced in Chapter 1 (Section 1.3) in the context of characteristic functions. We pursue Fourier transforms further in this chapter as a tool for analyzing linear partial differential equations in infinite and semi-infinite domains, thereby focusing on cases where the boundaries are far away and their influence is expected to be negligible in the region of interest.

3.1. SOLUTE TRANSPORT BY DIFFUSION

To motivate the discussion on Fourier transforms, let us consider the equation for diffusive transport of a conservative solute in the absence of sources and sinks (see also Section 2.4)

$$\frac{\partial c}{\partial t} = D\frac{\partial^2 c}{\partial x^2} \tag{3.1.1}$$

for $-\infty < x < \infty$, under the initial condition

$$c(x, 0) = c_0(x) \tag{3.1.2}$$

At this stage, we think of *c(x,t)* as a resident concentration of a solute and D as a diffusion coefficient. We first look at the mathematical aspects of the solution, and later in Section 3.3 discuss how to apply the solution of this equation to diffusive transport in porous media. While it is not often stated explicitly, $c(-\infty, t) = c(\infty, t) = 0$. Similarly, it is expected that $C_0(x)$ at $x \pm \infty$ is also zero. This would imply that we have 'imposed' Dirichlet boundary conditions.

We will pursue the method of *separation of variables* initially. It is assumed that the solution $c(x, t)$ can be factored into two parts: one that is a function of x alone, and other that is a function of t alone,

$$c(x, t) = \varphi(x)h(t) \tag{3.1.3}$$

Substituting (3.1.3) in (3.1.1) yields

$$\frac{1}{Dh}\frac{dh}{dt} = \frac{1}{\varphi}\frac{d^2\varphi}{dx^2} = -\lambda \tag{3.1.4}$$

where λ is a constant arising from the fact that a function of t can uniformly equal a function of x only if they are both equal to a constant. Separation of variables has now yielded two ordinary differential equations

$$\frac{dh}{dt} = -\lambda Dh \tag{3.1.5}$$

$$\frac{d^2\varphi}{dx^2} = -\lambda\varphi \tag{3.1.6}$$

Note that λ in (3.1.4) to (3.1.6) is as yet undetermined. The relevant values of λ are called *eigenvalues*. The problem now needs to be approached with some caution as a 'naive' application of the boundary conditions at $x = \pm\infty$ to (3.1.6) would not yield meaningful results. At this stage, we simply require that the solution be bounded at $x = \pm\infty$.

We first consider the following *eigenvalue problem*

$$\frac{d^2\varphi}{dx^2} + \lambda\varphi = 0 \tag{3.1.7}$$

$$|\varphi(\pm\infty)| < \infty \tag{3.1.8}$$

If $\lambda < 0$, then the general solution will be expressed as

$$\varphi(x) = \alpha e^{+\sqrt{\lambda}x} + \beta e^{-\sqrt{\lambda}x} \tag{3.1.9}$$

and it would be impossible to satisfy (3.1.8) at $x =$ both $+\infty$ and $-\infty$. It must be concluded that λ cannot be less than zero (i.e. no negative eigenvalues). If $\lambda \geq 0$, then the general solution is

$$\varphi(x) = \alpha \cos\sqrt{\lambda}\, x + \beta\, \sin\sqrt{\lambda}\, x \tag{3.1.10}$$

which is bounded for all x. Thus all eigenvalues are positive ($\lambda \geq 0$), and the *eigenfunctions* are sines and cosines. If $\lambda = 0$, then the corresponding eigenfunction is a constant. Since all continuous values of λ are possible, we have a continuous spectrum of $\lambda \geq 0$.

Equation (3.1.5) can be solved to yield

$$h(t) = Ae^{-\lambda Dt} \tag{3.1.11}$$

where A is constant (i.e. not a function of time). For linear problems, we use the principle of superposition and integrate (instead of a discrete sum) over the continuous spectrum of λ values to obtain

$$c(x,t) = \int_0^\infty \left[c_1(\lambda)\cos\sqrt{\lambda}x\; e^{-\lambda Dt} + c_2(\lambda)\sin\sqrt{\lambda}x e^{-\lambda Dt}\right] d\lambda \tag{3.1.12}$$

where $c_1(\lambda)$ and $c_2(\lambda)$ are arbitrary functions of λ. It is customary to make the substitution $\lambda = \omega^2$ for simplicity of notation so that

$$c(x,t) = \int_0^\infty \left[A(\omega)\cos\omega x \; e^{-D\omega^2 t} + B(\omega)\sin\omega x \; e^{-D\omega^2 t} \right] d\omega \tag{3.1.13}$$

where $A(\omega) = c_1(\omega^2)2\omega$ and $B(\omega) = c_2(\omega^2)2\omega$ are also arbitrary functions of ω and must be determined by the initial condition (3.1.2).

$$c_0(x) = \int_0^\infty [A(\omega) \;\cos\; \omega x + B(\omega) \;\sin\omega\; x]\, d\omega \tag{3.1.14}$$

The spatial eigenfunctions $\cos\omega x$ and $\sin\omega x$ can be replaced by the complex exponentials $e^{j\omega x}$ and $e^{-j\omega x}$, for all positive ω. It is more expedient to instead consider $e^{-j\omega x}$ as the spatial eigenfunction and let ω range from $-\infty$ to $+\infty$ (i.e. both positive and negative values). Thus the solution may be conveniently expressed as

$$c(x,t) = \int_{-\infty}^{\infty} c_0(\omega) e^{-j\omega x} e^{-D\omega^2 t} \; d\omega \tag{3.1.15}$$

The initial condition to be satisfied is

$$c_0(x) = \int_{-\infty}^{\infty} c_0(\omega) e^{-j\omega x} d\omega \tag{3.1.16}$$

which allows us to determine the form of the $c_0(\omega)$ function.

Let us consider the *discrete Fourier series representation* of a function, in this case the initial condition on an interval $-L \le x < L$

$$c_0(x) \cong \frac{a_0}{2} + \sum_{n=1}^{\infty} \left(a_n \cos\frac{n\pi x}{L} + b_n \sin\frac{n\pi x}{L} \right) \tag{3.1.17}$$

where the *Fourier coefficients* are determined from orthogonality of the eigenfunctions as

$$a_n = \frac{1}{L}\int_{-L}^{L} c_0(x)\cos\frac{n\pi x}{L} dx \tag{3.1.18}$$

$$b_n = \frac{1}{L}\int_{-L}^{L} c_0(x)\sin\frac{n\pi x}{L} dx \tag{3.1.19}$$

Using Euler's formulas $\left(\cos\theta = \frac{e^{j\theta}+e^{-j\theta}}{2},\ \sin\theta = \frac{e^{j\theta}-e^{-j\theta}}{2i}\right)$, equation (3.1.17) can be written as

$$c_0(x) \cong \frac{a_0}{2} + \frac{1}{2}\sum_{n=1}^{\infty} (a_n - jb_n) \; e^{jn\pi x/L} + \frac{1}{2}\sum_{n=1}^{\infty} \; (a_n + jb_n)\, e^{-jn\pi x/L} \tag{3.1.20}$$

In the first summation, we change the dummy summation index from n to $-n$ so that

$$c_0(x) \cong \frac{a_0}{2} + \frac{1}{2}\sum_{n=-1}^{-\infty}\left[a_{(-n)} - jb_{(-n)}\right] e^{-jn\pi x/L} + \frac{1}{2}\sum_{n=1}^{\infty}\left[a_n + jb_n\right] e^{-jn\pi x/L} \tag{3.1.21}$$

From (3.1.18) and (3.1.19), we find $a_{(-n)} = a_n$ and $b_{(-n)} = -b_n$. Further, defining $c_n = \frac{a_n + jb_n}{2}$, we have

$$c_0(x) = \sum_{n=-\infty}^{\infty} c_n e^{-jn\pi x/L} \tag{3.1.22}$$

This is commonly referred to as the *complex form of the Fourier series*, with the *complex Fourier coefficients* determined from orthogonality as

$$c_n = \frac{1}{2L}\int_{-L}^{L} c_0(x) e^{jn\pi x/L} dx \tag{3.1.23}$$

3.2. FOURIER TRANSFORM PAIR

Substituting (3.1.23) into (3.1.22), one obtains

$$c_0(x) = \sum_{n=-\infty}^{\infty}\left[\frac{1}{2L}\int_{-L}^{L} c_0(x') e^{jn\pi x'/L} dx'\right] e^{-jn\pi x/L} \tag{3.2.1}$$

In keeping with the original problem definition over infinite domain, we consider setting L to ∞. For periodic functions over $-L \le x < L$, the wave numbers ω (= number of waves in a distance of 2π) are the infinite set of discrete values

$$\omega_n = 2\pi\frac{n}{2L} \tag{3.2.2}$$

The constant spacing between successive wave numbers is

$$\Delta\omega = \frac{\pi}{L} \tag{3.2.3}$$

Consequently, from (3.2.1), we obtain

$$c_0(x) = \sum_{n=-\infty}^{\infty}\left[\frac{\Delta\omega}{2\pi}\int_{-L}^{L} c_0(x') e^{j\omega x'} dx'\right] e^{-j\omega x} \tag{3.2.4}$$

As $L \to \infty$ $\Delta\omega \to \mathrm{d}\omega$, the wave numbers (and the eigenvalues) approach a continuum. The function $c_0(x)$ can be represented by an integral, instead of the infinite sum, as

$$c_0(x) = \frac{1}{2\pi}\int_{-\infty}^{\infty}\left[\int_{-\infty}^{\infty} c_0(x') e^{j\omega x'} dx'\right] e^{-j\omega x} d\omega \tag{3.2.5}$$

Table 3.2.1. Partial list of some Fourier transform pairs

$f(x) = \int_{-\infty}^{\infty} F(\omega) e^{-j\omega x} d\omega$	$F(\omega) = \frac{1}{2\pi} \int_{-\infty}^{\infty} f(x) e^{j\omega x} dx$
$e^{-\alpha x^2}$	$\frac{1}{\sqrt{4\pi\alpha}} e^{-\omega^2/4\alpha}$
$\sqrt{\frac{\pi}{\beta}} e^{-x^2/4\beta}$	$e^{-\beta\omega^2}$
$\frac{\partial f}{\partial t}$	$\frac{\partial F}{\partial t}$
$\frac{\partial f}{\partial x}$	$-j\omega F(\omega)$
$\frac{\partial^2 f}{\partial x^2}$	$(-j\omega)^2 F(\omega)$
$\frac{1}{2\pi} \int_{-\infty}^{\infty} f(w) g(x-w) dw$	$F(\omega) G(\omega)$
$\delta(x - x_0)$	$\frac{1}{2\pi} e^{j\omega x_0}$
$f(x - \beta)$	$e^{j\omega\beta} F(\omega)$
$x f(x)$	$-j \frac{dF}{d\omega}$
$\frac{2\alpha}{x^2 + \alpha^2}$	$e^{-\lvert\omega\rvert\alpha}$
$f(x) = \begin{cases} 0 & \lvert x\rvert > a \\ 1 & \lvert x\rvert < a \end{cases}$	$\frac{1}{\pi} \frac{\sin a\omega}{\omega}$

Based on this, the Fourier transform of a function $f(x)$ is defined as

$$F(\omega) = \frac{1}{2\pi} \int_{-\infty}^{\infty} f(x') e^{j\omega x'} dx' \tag{3.2.6}$$

and the inverse Fourier transform as

$$f(x) = \int_{-\infty}^{\infty} F(\omega) e^{-j\omega x} d\omega \tag{3.2.7}$$

The functions $f(x)$ and $F(\omega)$ are called a Fourier transform pair. A brief table of Fourier transform pairs is included in Table 3.2.1.

3.3. FOURIER TRANSFORM OF THE DIFFUSION EQUATION

With this introduction, we are now in a position to use Fourier transform techniques. The previous sections showed that the solution to (3.1.1) could be expressed as (see 3.1.15)

$$c(x, t) = \int_{-\infty}^{\infty} c_0(\omega)\ e^{-j\omega x} e^{-D\omega^2 t} d\omega \tag{3.3.1}$$

with the initial condition of (3.1.2) satisfied by

$$c_0(x) = \int_{-\infty}^{\infty} c_0(\omega)\ e^{-j\omega x} d\omega \tag{3.3.2}$$

Equation (3.3.2) is the Fourier transformation representation of the initial distribution of solute concentration, where $c_0(\omega)$ is the Fourier transform of $c_0(x)$. As such, (3.3.1) can be expressed as

$$c(x,t) = \int_{-\infty}^{\infty} \left[\frac{1}{2\pi} \int_{-\infty}^{\infty} c_0(x') e^{j\omega x'} dx' \right] e^{-j\omega x} e^{-D\omega^2 t} d\omega \tag{3.3.3}$$

Changing the order of integration, (3.3.3) can be expressed in the following way to express the influence of the initial condition clearly

$$c(x,t) = \frac{1}{2\pi} \int_{-\infty}^{\infty} c_0(x') \left[\int_{-\infty}^{\infty} e^{-D\omega^2 t} e^{-j\omega(x-x')} d\omega \right] dx' \tag{3.3.4}$$

From (3.3.4), one can clearly identify how the solution is obtained as convolution of the *influence function* (also called Green's function) with the initial condition. We define the function

$$g(x) = \int_{-\infty}^{\infty} e^{-D\omega^2 t} e^{-j\omega x} d\omega \tag{3.3.5}$$

Table 3.2.1 shows that the above integral is

$$g(x) = \sqrt{\frac{\pi}{Dt}} e^{-x^2/4Dt} \tag{3.3.6}$$

and the solution for concentration as a function of space and time coordinates is

$$c(x,t) = \int_{-\infty}^{\infty} c_0(x') \frac{1}{\sqrt{4\pi Dt}} e^{-(x-x')^2/4Dt} dx' \tag{3.3.7}$$

which brings out the dependence of the solution on the initial condition. The Green's function can now be defined as

$$G(x,t\,;x',0) = \frac{1}{\sqrt{4\pi Dt}} e^{-(x-x')^2/4Dt} \tag{3.3.8}$$

This function expresses the influence of the initial concentration at x' on the solution at a spatial location x and some time t. The influence function is a maximum at $x = x'$, (i.e. at the source) and the influence decreases as the separation $|x - x'|$ increases. Similarly, as $t \to 0$, the influence function approaches a spike,

$$\lim_{t \to 0} \frac{1}{\sqrt{4\pi Dt}} e^{-(x-x')^2/4Dt} = \delta(x - x') \tag{3.3.9}$$

For application to diffusive transport in porous media, consider the release of mass M of contaminant per unit area perpendicular to flow instantaneously at $x = x_0$

and at time $t = 0$ without any loss of generality. Then defining c_b as the bulk concentration, the initial condition is expressed as

$$c_b(x, 0) = M\delta(x - x_0) \tag{3.3.10}$$

so that

$$\int_{-\infty}^{\infty} c_b(x, 0)dx = M \tag{3.3.11}$$

The governing differential equation (3.1.1) is usually written in terms of the resident concentration in the liquid phase $c_r (= c_b/\eta$, where η is porosity), so that

$$c_r(x, 0) = \frac{M}{\eta}\delta(x - x_0) \tag{3.3.12}$$

Using (3.3.7), we obtain

$$\begin{aligned} c_r(x, t) &= \int_{-\infty}^{\infty} \frac{M}{\eta}\delta(x' - x_0)\frac{1}{\sqrt{4\pi Dt}}\exp\left[-\frac{(x - x')^2}{4Dt}\right]dx' \\ &= \frac{M}{\eta\sqrt{4\pi Dt}}\exp\left[-\frac{(x - x_0)^2}{4Dt}\right] \end{aligned} \tag{3.3.13}$$

As expected, it can be shown that

$$\int_{-\infty}^{\infty} \eta c_r(x, t)dx = M \tag{3.3.14}$$

The similarity in functional form between (3.3.13) and the normal pdf (1.1.12) is useful. If we think of the distance coordinate x as the random variable, and $\eta c_r/M$ as a probability density function that evolves in time, then we conclude that the center of solute mass is located at the mean location x_0, and that the spread of the solute mass about this mean location is indicated by the variance σ^2 that changes with time

$$\sigma^2 = 2Dt \tag{3.3.15}$$

3.4. FOURIER TRANSFORMS OF DERIVATIVES

The discussion this far was motivated by the need to understand the basic concept of Fourier transforms. However, in practice, it is often simpler to apply Fourier transforms directly to linear partial differential equations without having to resort to the process of separation of variables. By definition, the Fourier transform of $c(x, t)$ is

$$\mathcal{F}[c(x, t)] = \tilde{c}(\omega; t) = \frac{1}{2\pi}\int_{-\infty}^{\infty} c(x, t)e^{j\omega x}dx \tag{3.4.1}$$

Note that unlike Laplace transforms in the previous chapter, the Fourier transform involves integration of the space variable with t remaining fixed in this application.

The Fourier transform of the time derivative is

$$\mathcal{F}\left[\frac{\partial c}{\partial t}\right] = \frac{1}{2\pi}\int_{-\infty}^{\infty}\frac{\partial c}{\partial t}e^{j\omega x}dx = \frac{\partial}{\partial t}\left[\frac{1}{2\pi}\int_{-\infty}^{\infty}ce^{j\omega x}dx\right] = \frac{\partial \tilde{c}}{\partial t} \tag{3.4.2}$$

Fourier transforms of spatial derivatives are obtained as

$$\mathcal{F}\left[\frac{\partial c}{\partial x}\right] = \frac{1}{2\pi}\int_{-\infty}^{\infty}\frac{\partial c}{\partial x}e^{j\omega x}dx = \frac{ce^{j\omega x}}{2\pi}\Big|_{-\infty}^{\infty} - \frac{j\omega}{2\pi}\int_{-\infty}^{\infty}ce^{j\omega x}dx \tag{3.4.3}$$

Assuming that $c \to 0$ as $x \to \pm\infty$, we note that

$$\mathcal{F}\left[\frac{\partial c}{\partial x}\right] = -j\omega\ \mathcal{F}[c] = (-j\omega)\ \tilde{c}(\omega, t) \tag{3.4.4}$$

In a similar manner, one can show that

$$\mathcal{F}\left[\frac{\partial^2 c}{\partial x^2}\right] = (-j\omega)^2\ \tilde{c}(\omega, t) \tag{3.4.5}$$

and, in general

$$\mathcal{F}\left[\frac{\partial^n c}{\partial x^n}\right] = (-j\omega)^n\ \tilde{c}(\omega, t) \tag{3.4.6}$$

In an analogous fashion to Laplace transforms, Fourier transforms are useful for converting partial differential equations to ordinary differential equations. For instance, taking Fourier transforms of both sides of (3.1.1), we have

$$\frac{\partial}{\partial t}\tilde{c}(\omega, t) = -D\omega^2\ \tilde{c}(\omega, t) \tag{3.4.7}$$

whose general solution is

$$\tilde{c}(\omega; t) = Ae^{-D\omega^2 t} \tag{3.4.8}$$

where the integration of (3.4.7) was carried out in time for a fixed ω. The quantity A in the right hand side of (3.4.8) is therefore, in general, a function of ω. To determine $A(\omega)$ one must apply Fourier transform to the initial conditions of (3.1.2), so that

$$A(\omega) = \frac{1}{2\pi}\int_{-\infty}^{\infty}c_0(x)e^{j\omega x}dx \tag{3.4.9}$$

It is convenient to introduce the idea of convolution for Fourier transforms at this stage. From (3.4.8), we note that $\tilde{c}(\omega, t)$ is a product of two functions of $\omega : A(\omega)$

and $e^{-D\omega^2 t}$, both of which, in turn, are transforms of other functions of x. From (3.4.9) we know $A(\omega)$ to be the Fourier transform of the initial solute distribution $c_0(x)$. From Table 3.2.1, $e^{-D\omega^2 t}$ is the transform of $\sqrt{\frac{\pi}{Dt}}e^{-x^2/4Dt}$. The product of transforms of two functions arises frequently in linear problems of solute transport.

Consider two functions $f(x)$ and $g(x)$ whose Fourier transforms are $F(\omega)$ and $G(\omega)$ respectively. The two Fourier transform pairs are mathematically expressed as

$$F(\omega) = \frac{1}{2\pi}\int_{-\infty}^{\infty} f(x)\ e^{j\omega x}dx;\ \ f(x) = \int_{-\infty}^{\infty} F(\omega)\ e^{-j\omega x}d\omega$$
$$G(\omega) = \frac{1}{2\pi}\int_{-\infty}^{\infty} g(x)\ e^{j\omega x}dx;\ \ g(x) = \int_{-\infty}^{\infty} G(\omega)\ e^{-j\omega x}d\omega \tag{3.4.10}$$

Our immediate goal is to determine the inverse Fourier transform of $H(\omega) = F(\omega)\ G(\omega)$. We may write this as

$$h(x) = \mathcal{F}^{-1}[H(\omega)] = \int_{-\infty}^{\infty} F(\omega)G(\omega)e^{-j\omega x}d\omega \tag{3.4.11}$$

After eliminating $F(\omega)$ or $G(\omega)$ and interchanging the order of integration, one obtains

$$h(x) = \frac{1}{2\pi}\int_{-\infty}^{\infty} g(x')f(x-x')\ dx' \tag{3.4.12}$$

which is the convolution of the two functions $g(x)$ and $f(x)$ and is denoted by $f^*g = g^*f$. Applying the convolution equation to (3.4.8), we find that

$$c(x,t) = \frac{1}{2\pi}\int_{-\infty}^{\infty} c_0(x')\sqrt{\frac{\pi}{Dt}}\ e^{-(x-x')/4Dt}dx' \tag{3.4.13}$$

as expected from the analysis involving separation of variables.

3.5. FOURIER SINE AND COSINE TRANSFORMS

The Fourier series is versatile enough to be applicable to semi-infinite domains with suitable modifications. We consider the following partial differential equation and end conditions describing solute movement by pure diffusion

$$\frac{\partial c}{\partial t} = D\frac{\partial^2 c}{\partial x^2},\ \ x > 0 \tag{3.5.1}$$
$$c(0,t) = 0 \tag{3.5.2}$$
$$c(x,0) = c_0(x),\ \ x > 0 \tag{3.5.3}$$

Note the difference in the end conditions from those considered in the previous chapter (2.4.9). Using separation of variables, we express $c(x,t)$ as

$$c(x,t) = \phi(x)\ h(t) \tag{3.5.4}$$

which leads to the two ordinary differential equations

$$\frac{dh}{dt} = -\lambda D h \tag{3.5.5}$$

$$\frac{d^2\phi}{dx^2} = -\lambda \phi \tag{3.5.6}$$

Now, the boundary conditions needed to determine the eigenvalues and eigenfunctions for the spatial part are

$$\phi(0) = 0\,;\ \lim_{x\to\infty} |\phi\ (x)| < \infty \tag{3.5.7}$$

Nontrivial solutions are only available for $\lambda > 0$, and the general solution is

$$\phi(x) = c_1 \sin\sqrt{\lambda}\ x = c_1 \sin\ \omega x \tag{3.5.8}$$

Solution to (3.5.5) yields

$$h(t) = Ae^{-\lambda D t} = Ae^{-\omega^2 D t} \tag{3.5.9}$$

and the solution for the concentration has the form

$$c(x,t) = \int_0^\infty A(\omega) \sin\omega x\ e^{-D\omega^2 t} d\omega \tag{3.5.10}$$

where we have used superposition in a continuous sense to accommodate the continuous spectrum of eigenvalues. The initial condition is satisfied by setting

$$c_0(x) = \int_0^\infty A(\omega)\ \sin\omega x\ dw \tag{3.5.11}$$

The determination of $A(\omega)$ from (3.5.11) motivates us to define sine and cosine transforms as well. In the previous sections, we have already defined the complete Fourier transform.

Following (3.5.11), we first consider the *Fourier sine transform*. Let us imagine that $c_0(x)$ is an odd function without loss of any generality as (3.5.3) defines $c_0(x)$ only for $x > 0$, and we can choose its behavior for $x < 0$ purely for mathematical reasons and attribute no physical significance to this choice. Thus, if $f(x)$ is an odd function, then its Fourier transform is

$$\begin{aligned} F(\omega) &= \frac{1}{2\pi}\int_{-\infty}^{\infty} f(x)\ e^{j\omega x}\ dx \\ &= \frac{1}{2\pi}\ \int_{-\infty}^{\infty} f(x)\ [\cos\omega x + j\sin\omega x]\ dx \\ &= \frac{2j}{2\pi}\ \int_0^\infty f(x)\sin\omega x\ dx \end{aligned} \tag{3.5.12}$$

since $\cos \omega\ x$ is an even function while $\sin \omega x$ is an odd function. Correspondingly,

$$\begin{aligned} f(x) &= \int_{-\infty}^{\infty} F(\omega)\ e^{-j\omega x}\ d\omega \\ &= \int_{-\infty}^{\infty} F(\omega)\ [\cos \omega x - j \sin \omega x]\ dx \\ &= -2j \int_{0}^{\infty} F(\omega) \sin \omega x\ d\omega \end{aligned} \tag{3.5.13}$$

In actuality the product of the coefficients in front of the integrals (3.5.12) and (3.5.13) should be $2/\pi$. For an odd function $f(x)$, the *Fourier sine transform pair* are defined as

$$F(\omega) = \mathcal{S}[f(x)] = \frac{2}{\pi} \int_{0}^{\infty} f(x) \sin \omega x\ dx \tag{3.5.14}$$

$$f(x) = \mathcal{S}^{-1}[F(\omega)] = \int_{0}^{\infty} F(\omega) \sin \omega x\ d\omega \tag{3.5.15}$$

Note that the Fourier sine transformation of $f(x)$ at $x = 0$ is always obtained as zero.

The same procedure may be adopted to derive the *Fourier cosine transform pair* when $f(x)$ is an even function

$$F(\omega) = \mathcal{C}[f(x)] = \frac{2}{\pi} \int_{0}^{\infty} f(x) \cos \omega x\ dx \tag{3.5.16}$$

$$f(x) = \mathcal{C}^{-1}[F(\omega)] = \int_{0}^{\infty} F(\omega) \cos \omega x\ d\omega \tag{3.5.17}$$

Brief tables of sine and cosine transforms and their inverse transforms are provided in Tables 3.5.1 and 3.5.2.

Table 3.5.1. Fourier sine transforms

$f(x) = \int_0^\infty F(\omega) \sin \omega x\ d\omega$	$\mathcal{S}[f(x)] = \frac{2}{\pi} \int_0^\infty f(x) \sin \omega x\ dx$
$\frac{df}{dx}$	$-\omega C[f(x)]$
$\frac{d^2 f}{dx^2}$	$\frac{2}{\pi} \omega f(0) - \omega^2 F(\omega)$
$\frac{x}{x^2 + \beta^2}$	$e^{-\omega\beta}$
$e^{-\varepsilon x}$	$\frac{2}{\pi} \cdot \frac{\omega}{\varepsilon^2 + \omega^2}$
1	$\frac{2}{\pi} \cdot \frac{1}{\omega}$
$\frac{1}{\pi} \int_0^\infty f(\tilde{x}) [g(x - \tilde{x}) - g(x + \tilde{x})] d\tilde{x}$ $= \frac{1}{\pi} \int_0^\infty g(\tilde{x}) [f(x + \tilde{x}) - f(\tilde{x} - x)] d\tilde{x}$	$\mathcal{S}[f(x)] \mathcal{C}[g(x)]$

Table 3.5.2. Fourier cosine transforms

$f(x) = \int_0^\infty F(\omega)\cos\ \omega x\ d\omega$	$\mathcal{C}[f(x)] = \frac{2}{\pi}\int_0^\infty f(x)\cos\ \omega x\ dx$
$\frac{df}{dx}$	$-\frac{2}{\pi}f(0) + \omega S[f(x)]$
$\frac{d^2 f}{dx^2}$	$\frac{2}{\pi}\omega f(0) - \omega^2 F(\omega)$
$\frac{\beta}{x^2+\beta^2}$	$e^{-\omega\beta}$
$e^{-\varepsilon x}$	$\frac{2}{\pi}\cdot\frac{\varepsilon}{\varepsilon^2+\omega^2}$
$e^{-\alpha x^2}$	$2\frac{1}{\sqrt{4\pi\alpha}}e^{-\omega^2/4\alpha}$
$\frac{1}{\pi}\int_0^\infty g(\tilde{x})[f(x-\tilde{x})+f(x+\tilde{x})]d\tilde{x}$	$F(\omega)G(\omega)$

To apply Fourier sine or cosine transforms to partial differential equations, we need to deal with derivatives. The transforms of the concentration function $c(x, t)$ are

$$\mathcal{S}[c(x,t)] = \frac{2}{\pi}\int_0^\infty c(x,t)\ \sin\omega x\ dx = \bar{\mathcal{S}}(\omega; t) \tag{3.5.18}$$

$$\mathcal{C}[c(x,t)] = \frac{2}{\pi}\int_0^\infty c(x,t)\ \cos\omega x\ dx = \bar{\mathcal{C}}(\omega; t) \tag{3.5.19}$$

Transforms of temporal derivatives are straightforward.

$$\mathcal{S}\left[\frac{\partial c}{\partial t}\right] = \frac{2}{\pi}\int_0^\infty \frac{\partial c}{\partial t}\sin\omega x\ dx = \frac{\partial}{\partial t}\left[\frac{2}{\pi}\int_0^\infty c(x,t)\sin\omega x\ dx\right] = \frac{\partial\bar{\mathcal{S}}(\omega;t)}{\partial t} \tag{3.5.20}$$

$$\mathcal{C}\left[\frac{\partial c}{\partial t}\right] = \frac{2}{\pi}\int_0^\infty \frac{\partial c}{\partial t}\cos\omega x\ dx = \frac{\partial}{\partial t}\left[\frac{2}{\pi}\int_0^\infty c(x,t)\cos\omega x\ dx\right] = \frac{\partial\bar{\mathcal{C}}(\omega;t)}{\partial t} \tag{3.5.21}$$

Integration by parts yields the following for transforms of first spatial derivatives.

$$\mathcal{S}\left[\frac{\partial c}{\partial x}\right] = \frac{2}{\pi}\int_0^\infty \frac{\partial c}{\partial x}\sin\omega x\ dx = \frac{2}{\pi}c(x,t)\sin\omega x\,|_0^\infty - \omega\frac{2}{\pi}\int_0^\infty c(x,t)\cos\omega x\ dx \tag{3.5.22}$$

$$\mathcal{C}\left[\frac{\partial c}{\partial x}\right] = \frac{2}{\pi}\int_0^\infty \frac{\partial c}{\partial x}\cos\omega x\ dx = \frac{2}{\pi}c(x,t)\cos\omega x\,|_0^\infty + \omega\frac{2}{\pi}\int_0^\infty c(x,t)\sin\omega x\ dx \tag{3.5.23}$$

Thus the formulae for the transforms of the derivatives are

$$\mathcal{S}\left[\frac{\partial c}{\partial x}\right] = -\omega\ \bar{\mathcal{C}}(\omega; t) \tag{3.5.24}$$

$$\mathcal{C}\left[\frac{\partial c}{\partial x}\right] = -\frac{2}{\pi}c\ (0,t) + \omega\ \bar{\mathcal{S}}(\omega; t) \tag{3.5.25}$$

where we have assumed that $c(x, t) \to 0$ as $x \to \infty$. Thus sine or cosine transforms of first spatial derivative always involve the other transform, making them generally unsuitable for partial differential equations containing the first and second spatial derivatives. As an example, one should not directly apply these transforms to advection-dispersion problems because the advective term involves the first spatial derivative.

Transforms of second spatial derivatives take the form

$$\mathcal{S}\left[\frac{\partial^2 c}{\partial x^2}\right] = -\omega\ \mathcal{C}\left[\frac{\partial c}{\partial x}\right] = \frac{2}{\pi}\omega\ \mathrm{c}(0, t) - \omega^2\ \bar{\mathcal{S}}(\omega; t) \tag{3.5.26}$$

$$\mathcal{C}\left[\frac{\partial^2 c}{\partial x^2}\right] = -\frac{2}{\pi}\frac{\partial c}{\partial x}\,|_{x=0} + \omega\ \mathcal{S}\left[\frac{\partial \mathrm{c}}{\partial \mathrm{x}}\right] = -\frac{2}{\pi}\frac{\partial c}{\partial x}\,|_{x=0} - \omega^2\ \bar{\mathcal{C}}(\omega; t) \tag{3.5.27}$$

Equations (3.5.26) and (3.5.27) suggest which transform should be used in a given problem. In order to use the Fourier sine transform for solving solute transport equations involving pure diffusion on semi-infinite domain $(x \geq 0)$, $c(0, t)$ should be specified. On the other hand, if $\partial c/\partial x$ at $x = 0$ is specified for such problems, the Fourier cosine transformation should be utilized.

We now return to the problem posed in (3.5.1), (3.5.2), and (3.5.3). The boundary condition (3.5.2) suggests the use of Fourier sine transforms, so that we have

$$\frac{\partial \bar{S}(\omega; t)}{\partial t} = -\omega^2 D\bar{\mathcal{S}}(\omega; t) \tag{3.5.28}$$

and the initial condition (3.5.3) yields (see also (3.5.11))

$$\bar{\mathcal{S}}(\omega; 0) = \frac{2}{\pi}\int_0^\infty c_0(x)\sin\omega x\ dx = g(\omega) \tag{3.5.29}$$

The solution for $\bar{\mathcal{S}}(\omega; t)$ is

$$\bar{\mathcal{S}}(\omega; t) = g(\omega)e^{-D\omega^2 t} \tag{3.5.30}$$

and from the inverse transformation, the solution is

$$c(x, t) = \int_0^\infty g(\omega)e^{-D\omega^2 t}\sin\omega x\ d\omega \tag{3.5.31}$$

While it is possible to obtain $c(x, t)$ from (3.5.31) after some simplification, a more direct approach is suggested by (3.5.30) and the use of the convolution formula presented in Tables 3.5.1 and 3.5.2. From (3.5.29) we have

$$g(\omega) = \mathcal{S}[c_0(x)] \tag{3.5.32}$$

and from Table 3.5.2, we observe that

$$\mathcal{C}^{-1}\left[e^{-D\omega^2 t}\right] = \frac{\sqrt{\pi}}{\sqrt{4Dt}}\exp\left(-\frac{x^2}{4Dt}\right) \tag{3.5.33}$$

Combining (3.5.30), (3.5.32), and (3.5.33) along with the convolution result for sine transformations which states

$$\mathcal{S}^{-1}\{\mathcal{S}[g(x)]\,\mathcal{C}[f(x)]\} = \frac{1}{\pi}\int_0^\infty g(x')\,[f(x-x') - f(x+x')]dx' \tag{3.5.34}$$

we obtain the solution for $c(x, t)$ as

$$c(x,t) = \frac{1}{\sqrt{4\pi Dt}}\int_0^\infty c_0(x')\left\{\exp\left[-\frac{(x-x')^2}{4Dt}\right] - \exp\left[-\frac{(x+x')^2}{4Dt}\right]\right\}dx' \tag{3.5.35}$$

from which the corresponding Green's function or influence function can be identified. If the entire solute mass is to be conserved in the region $0 < x < \infty$, then (3.5.2) should be changed to

$$\frac{\partial c(0,t)}{\partial x} = 0 \tag{3.5.36}$$

Fourier cosine transforms are suggested for this problem, and after a similar analysis the solution is obtained as

$$c(x,t) = \frac{1}{\sqrt{4\pi Dt}}\int_0^\infty c_0(x')\left\{\exp\left[-\frac{(x-x')^2}{4Dt}\right] + \exp\left[-\frac{(x+x')^2}{4Dt}\right]\right\}dx' \tag{3.5.37}$$

3.6. FOURIER TRANSFORM SOLUTION FOR ADVECTION-DISPERSION EQUATION OVER AN INFINITE DOMAIN

We now turn our attention to Fourier transforms of the advection-dispersion equation in one-dimension

$$\frac{\partial c}{\partial t} + V\frac{\partial c}{\partial x} = D\frac{\partial^2 c}{\partial x^2}, \quad -\infty < x < \infty \tag{3.6.1}$$

$$c(x,0) = c_0(x) \tag{3.6.2}$$

Taking Fourier transforms of (3.6.1), using results of Section 3.4, we obtain

$$\frac{\partial \tilde{c}}{\partial t} - V(j\omega)\tilde{c} = (-j\omega)^2 D\tilde{c} \tag{3.6.3}$$

The solution to this ordinary differential equation is

$$\tilde{c}(\omega; t) = A(\omega)e^{j\omega Vt}e^{-D\omega^2 t} \tag{3.6.4}$$

where $A(\omega)$ is obtained from the Fourier transform of the initial condition as

$$A(\omega) = \frac{1}{2\pi}\int_{-\infty}^{\infty} c_0(x)e^{-j\omega x}dx \tag{3.6.5}$$

The inverse Fourier transform of (3.6.4) can be obtained in a series of steps. First, as seen earlier from Table 3.2.1, the inverse Fourier transform of the last exponential in (3.6.4) is

$$\mathcal{F}^{-1}\left[e^{-D\omega^2 t}\right] = \sqrt{\frac{\pi}{Dt}} e^{-x^2/4Dt} \tag{3.6.6}$$

Applying the shift theorem listed in Table 3.2.1, we find that

$$\mathcal{F}^{-1}\left[e^{j\omega Vt} e^{-D\omega^2 t}\right] = \sqrt{\frac{\pi}{Dt}} e^{-(x-Vt)^2/4Dt} \tag{3.6.7}$$

We can now apply the convolution theorem to the right hand side of (3.6.4) to find the inverse Fourier transform of $\tilde{c}(\omega, t)$. The inverse Fourier transform of $A(\omega)$ is $c_0(x)$ from (3.6.5), while the inverse Fourier transform of the second function $e^{j\omega Vt} e^{-D\omega^2}$ is given in (3.6.7). Consequently, applying (3.4.12) we obtain the solution as

$$c(x, t) = \frac{1}{2\pi} \int_{-\infty}^{\infty} c_0(x') \sqrt{\frac{\pi}{Dt}} e^{-(x-Vt-x')^2/4Dt} dx' \tag{3.6.8}$$

We can identify the Green's function for this problem from (3.6.8) as

$$G(x, t|x', 0) = \frac{1}{\sqrt{4\pi Dt}} \exp\left[-\frac{(x - Vt - x')^2}{4Dt}\right] \tag{3.6.9}$$

The Green's function shows the contribution to the solute concentration at (x, t) due to a unit concentration 'mass' at $(x', 0)$.

3.7. FOURIER SINE TRANSFORM FOR ADVECTION–DISPERSION EQUATION OVER SEMI-INFINITE DOMAINS

In this section, we consider the ADE model

$$\frac{\partial c}{\partial t} = D\frac{\partial^2 c}{\partial x^2} - V\frac{\partial c}{\partial x}, \quad x > 0 \tag{3.7.1}$$

where $c(x, t)$ is the resident concentration under the following end conditions

$$c(0, t) = 0 \tag{3.7.2}$$

$$c(x, 0) = f(x) \tag{3.7.3}$$

Since the domain is semi-infinite, Fourier sine transform is suggested, but the advection term poses problems. One way around this is to utilize the transformation

$$c(x, t) = \exp\left[\left(x - \frac{Vt}{2}\right)\frac{V}{2D}\right] y(x, t) \tag{3.7.4}$$

to define a new dependant variable $y(x, t)$. Equations (3.7.1) to (3.7.3) now convert to

$$\frac{\partial y}{\partial t} = D\frac{\partial^2 y}{\partial x^2} \tag{3.7.5}$$

$$y(0, t) = 0$$

$$y(x, 0) = f(x)\exp\left[-\frac{xV}{2D}\right] \tag{3.7.6}$$

This problem in $y(x, t)$ has been discussed earlier in Section 3.5 (see (3.5.35)) and the solution is

$$y(x, t) = \frac{1}{\sqrt{4\pi Dt}}\int_0^\infty f(x')\exp\left(-\frac{Vx'}{2D}\right)\left\{\exp\left[-\frac{(x-x')^2}{4Dt}\right] - \exp\left[-\frac{(x+x')^2}{4Dt}\right]\right\}dx \tag{3.7.7}$$

Combining this expression for $y(x, t)$ with (3.7.4) yields the desired solution. In particular, if $c_0(x) = f(x) = \frac{M}{\eta}\delta(x - x'')$, $x'' > 0$, then the solution is

$$c(x, t) = \frac{M}{\eta}\frac{\exp\left[\left(x - x'' - \frac{Vt}{2}\right)\left(\frac{V}{2D}\right)\right]}{\sqrt{4\pi Dt}}\left\{\exp\left[-\frac{(x-x'')^2}{4Dt}\right] - \exp\left[-\frac{(x+x'')^2}{4Dt}\right]\right\} \tag{3.7.8}$$

3.8. FOURIER TRANSFORMS IN HIGHER DIMENSIONS

The focus throughout this book is on one-dimensional cases. We briefly discuss higher dimensional cases to illustrate the extension of one-dimensional concepts. To motivate the discussion, consider three-dimensional solute transport in a uniform steady flow field. The governing partial differential equation for the concentration $c(x, y, z, t)$ is

$$\frac{\partial c}{\partial t} + V_x\frac{\partial c}{\partial x} + V_y\frac{\partial c}{\partial y} + V_z\frac{\partial c}{\partial z} = D_{xx}\frac{\partial^2 c}{\partial x^2} + D_{yy}\frac{\partial^2 c}{\partial y^2} + D_{zz}\frac{\partial^2 c}{\partial z^2} \tag{3.8.1}$$

where V_x, V_y and V_z are the seepage velocities in the x, y, and z directions, while D_{xx}, D_{yy}, and D_{zz} are the hydrodynamic dispersion components. In reality, dispersion is a tensor, and (3.8.1) is applicable for special cases. We treat the problem in an infinite domain $(-\infty < x, y, z < \infty)$ under the initial condition

$$c(x, y, z, 0) = c_0(x, y, z) \tag{3.8.2}$$

As always, we assume that all functions decay sufficiently fast as $x, y, z \to \pm\infty$. We first define Fourier transform pairs in higher dimensions for a function $f(x, y, z)$ as

$$\begin{aligned}\mathcal{F}[f(x,y,z)] &= \tilde{f}(\omega_1,\omega_2,\omega_3)\\ &= \frac{1}{(2\pi)^3}\int_{-\infty}^{\infty}\int_{-\infty}^{\infty}\int_{-\infty}^{\infty} f(x,y,z)e^{j\omega_1 x}e^{j\omega_2 y}e^{j\omega_3 z}dx\ dy\ dz\end{aligned} \tag{3.8.3}$$

$$\begin{aligned}\mathcal{F}^{-1}[\tilde{f}(\omega_1,\omega_2,\omega_3)] &= f(x,y,z)\\ &= \int_{-\infty}^{\infty}\int_{-\infty}^{\infty}\int_{-\infty}^{\infty} \tilde{f}(\omega_1,\omega_2,\omega_3)e^{-j\omega_1 x}e^{-j\omega_2 y}e^{-j\omega_3 z}d\omega_1\ d\omega_2 d\omega_3\end{aligned} \tag{3.8.4}$$

In higher dimensional problems, a more compact notation may be adopted. In one-dimensional problems, we refer to the transform variable as wave number. We define a position vector

$$\mathbf{r} = x\hat{\mathbf{i}} + y\hat{\mathbf{j}} + z\hat{\mathbf{k}} \tag{3.8.5}$$

where $\hat{\mathbf{i}}$, $\hat{\mathbf{j}}$, and $\hat{\mathbf{k}}$ are unit vectors in the three orthogonal x, y, and z directions. Similarly, we can define a wave vector as

$$\boldsymbol{\omega} = \omega_1\hat{\mathbf{i}} + \omega_2\hat{\mathbf{j}} + \omega_3\hat{\mathbf{k}} \tag{3.8.6}$$

Therefore we may write

$$e^{j(\omega_1 x+\omega_2 y+\omega_3 z)} = e^{j\boldsymbol{\omega}\bullet\mathbf{r}} \tag{3.8.7}$$

Physical interpretation of the wave vector in three dimensions is more difficult, even though it is an extension of the one-dimensional case. The real part of $e^{j\boldsymbol{\omega}\bullet\mathbf{r}} = \cos(\omega_1 x + \omega_2 y + \omega_3 z)$. The waves in three-dimensional space have their crests located at $\omega_1 x+\omega_2 y+\omega_3 z = n(2\pi)$ for integer n. The wave direction is the direction normal to the crests and is given by

$$\nabla(\omega_1 x + \omega_2 y + \omega_3 z = \omega_1\hat{\mathbf{i}} + \omega_2\hat{\mathbf{j}} + \omega_3\hat{\mathbf{k}} = \boldsymbol{\omega},$$

implying that the wave number vector is in the direction of the wave. The magnitude of the wave vector

$$|\boldsymbol{\omega}| = \left(\omega_1^2 + \omega_2^2 + \omega_3^2\right)^{1/2} \tag{3.8.8}$$

is the number of waves in a distance 2π along the wave direction.

The Fourier transform pair for a function are

$$\tilde{f}(\boldsymbol{\omega}) = \frac{1}{(2\pi)^3}\int_{-\infty}^{\infty}\int_{-\infty}^{\infty}\int_{-\infty}^{\infty} f(\mathbf{r})e^{j\boldsymbol{\omega}.\mathbf{r}}d\boldsymbol{r} \tag{3.8.9}$$

$$\tilde{f}(\boldsymbol{r}) = \int_{-\infty}^{\infty}\int_{-\infty}^{\infty}\int_{-\infty}^{\infty} \tilde{f}(\boldsymbol{\omega})e^{j\boldsymbol{\omega}.\mathbf{r}}d\boldsymbol{\omega} \tag{3.8.10}$$

where $\tilde{f}(\boldsymbol{r}) = f(x, y, z), \tilde{f}(\boldsymbol{\omega}) = \tilde{f}(\omega_1, \omega_2, \omega_3)$, $d\boldsymbol{r} = dx\ dy\ dz$ and $d\omega = d\omega_1\ d\omega_2\ d\omega_3$. If we denote the triple Fourier transform of $c(x, y, z, t)$ as $\tilde{c}(\omega_1, \omega_2, \omega_3; t)$, then the transforms of the derivatives are obtained as

$$\boldsymbol{\mathcal{F}}\left[\frac{\partial c}{\partial t}\right] = \frac{\partial}{\partial t}\tilde{c} \tag{3.8.11}$$

$$\boldsymbol{\mathcal{F}}\left[\frac{\partial^n c}{\partial x^n}\right] = (-j\omega_1)^n\,\tilde{c} \tag{3.8.12}$$

$$\boldsymbol{\mathcal{F}}\left[\frac{\partial^n c}{\partial y^n}\right] = (-j\omega_2)^n\,\tilde{c} \tag{3.8.13}$$

$$\boldsymbol{\mathcal{F}}\left[\frac{\partial^n c}{\partial z^n}\right] = (-j\omega_3)^n\,\tilde{c} \tag{3.8.14}$$

$$\boldsymbol{\mathcal{F}}\left[\nabla^2 c\right] = -\omega^2\tilde{c} \tag{3.8.15}$$

In (3.8.15), $\omega^2 = \omega_1^2 + \omega_2^2 + \omega_3^2$. Applying Fourier transforms to (3.8.1) yields

$$\frac{d\tilde{c}}{dt} - j(\omega_1 V_x + \omega_2 V_y + \omega_3 V_z)\tilde{c} = -\left(\omega_1^2 D_{xx} + \omega_2^2 D_{yy} + \omega_3^2 D_{zz}\right)\tilde{c} \tag{3.8.16}$$

The solution to this ordinary differential in time is

$$\begin{aligned}\tilde{c}(\omega_1, \omega_2, \omega_3; t) = A(\omega_1, \omega_2, \omega_3)e^{j\omega_1 V_x t}e^{-D_{xx}\omega_1^2 t}\\ e^{j\omega_2 V_y t}e^{-D_{yy}\omega_2^2 t}e^{j\omega_3 V_z t}e^{-D_{zz}\omega^2 t}\end{aligned} \tag{3.8.17}$$

where the integration constant is

$$A(\omega_1, \omega_2, \omega_3) = \frac{1}{(2\pi)^3}\int_{-\infty}^{\infty}\int_{-\infty}^{\infty}\int_{-\infty}^{\infty} C_0(x, y, z)e^{j\omega_1 x}e^{j\omega_2 y}e^{j\omega_3 z}dx\ dy\ dz \tag{3.8.18}$$

The convolution theorem holds for multi-dimensional Fourier transforms as well. Thus, if $F(\boldsymbol{\omega})$ and $G(\boldsymbol{\omega})$ are Fourier transforms of $f(\mathbf{r})$ and $g(\mathbf{r})$, respectively, and $H(\boldsymbol{\omega}) = F(\boldsymbol{\omega})\ G(\boldsymbol{\omega})$, then

$$h(\boldsymbol{r}) = \frac{1}{(2\pi)^3}\int_{-\infty}^{\infty}\int_{-\infty}^{\infty}\int_{-\infty}^{\infty} f(\boldsymbol{r}')g(\boldsymbol{r} - \boldsymbol{r}')d\boldsymbol{r}' \tag{3.8.19}$$

By successive applications of the shift and convolution theorems, the inverse multi-dimensional Fourier transform of (3.8.17) is given as

$$c(x, y, z, t) = \int_{-\infty}^{\infty}\int_{-\infty}^{\infty}\int_{-\infty}^{\infty} c_0(x, y, z)\frac{1}{\sqrt{4\pi D_{xx}t}}\exp\left[-\frac{(x - V_x t - x')^2}{4D_{xx}t}\right]\cdot$$
$$\frac{1}{\sqrt{4\pi D_{yy}t}}\exp\left[-\frac{(y - V_y t - y')^2}{4D_{yy}t}\right]\cdot$$
$$\frac{1}{\sqrt{4\pi D_{zz}t}}\exp\left[-\frac{(z - V_z t - z')^2}{4D_{zz}t}\right]dx'\,dy'\,dz' \qquad (3.8.20)$$

Equation (3.8.20) immediately helps us identify the Green's function (or influence function) for the three dimensional advective-dispersive solute transport model. Further, comparison with (3.6.8) and (3.6.9) shows that the three-dimensional Green's function is the product of one-dimensional Green's function in each of the three dimensions. In notational form

$$G(x, y, z, t|x', y', z', 0) = G(x, t|x', 0)\ G(y, t|y', 0)\ G(z, t|z', 0) \qquad (3.8.21)$$

Leij et al. (2000) present solutions to multi-dimensional transport problems under different boundary conditions using Green's functions.

CHAPTER 4

TRANSFER FUNCTION APPROACHES

4.1. RESIDENCE TIME DISTRIBUTIONS

In many problems of interest to modelers, the goal is to relate system output to inputs. In some applications of solute transport through porous media, for example, one is often interested in the effluent concentration out of a soil column as a function of time for a given influent concentration. This can be very conveniently accomplished by the *residence time distribution* (RTD) theory originally proposed by Danckwerts (1953). The concept of RTDs is not restricted to soil columns alone and can be used in a wide variety of flow and solute transport problems. Provided that the process or system being modeled can be treated in a linear fashion, the RTD theory provides a way of characterizing the system without having to know explicitly about the inner mechanics of the system in any detail. In the context of solute moving through a soil column, this would imply that the exact path taken by each solute particle along with the local velocities do not need to be characterized in a detailed manner.

Consider that a conservative solute of mass M is released instantaneously at time $t = 0$ from a source location. The influent flux concentration is mathematically $c_{in}(t) = \frac{M}{Q_{in}(t)}\delta(t)$, where $Q_{in}(t)$ is the volumetric flowrate at the inflow end, and $\delta(t)$ is the Dirac-delta function. If the effluent flux concentration (mass per unit volume of liquid) is described by $c_f(t)$, from mass continuity we require that

$$\int_0^\infty c_{in}(t)dt = M = \int_0^\infty Q_{out}(t)\, c_f(t)\; dt \tag{4.1.1}$$

where $Q_{out}(t)$ is the volumetric flow rate at the outlet. For cases of steady flows, the inflow and outflow rates are a constant, Q. If, after appropriate normalization, the effluent concentration function is treated as a probability density function, then the machinery of random variables can be applied to these problems. We first define

$$f_T(t) = \frac{Q}{M}c(t) \tag{4.1.2}$$

In this example, since all the solute particles were introduced instantaneously at $t = 0$, $f_T(t)$ is a representation of how long solute particles stay within the soil

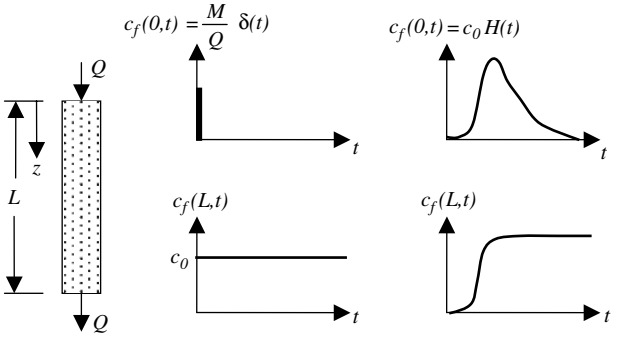

Figure 4.1.1. Schematic of inflow and outflow flux concentrations for a soil column for a delta function and a Heaviside function as inputs

column (system). Indeed, if T is a random variable denoting the travel time from the source to the receptor location (i.e. the residence time in the system), then $f_T(t)$ may be viewed as the pdf of travel times (see Figure 4.1.1). On the other hand, if the inlet concentration is held at a constant value c_0 (i.e. $c_{in}(t) = c_o H(t)$, where $H(t)$ is the Heaviside step function), then the effluent curve can be thought of as cumulative distribution function after normalization.

$$F_T(t) = \frac{c(t)}{c_o} = \int_0^t f_T(\tau) d\tau \tag{4.1.3}$$

Since the effluent concentration function under a Dirac input can be thought of as a probability density function, the center of mass of the effluent curve under instantaneous injection of solute at the inlet is the expected value of the travel time, i.e.

$$E[T] = \int_0^\infty t\ f_T(t)\, dt = \int_0^\infty [1 - F(t)]\ dt \tag{4.1.4}$$

This conceptualization allows us to define the displaced pore volume V_p as

$$V_p = QE[T] \tag{4.1.5}$$

If the velocity field is transient, then the travel time pdf would need to be conditioned on the inlet time – the time at which the solute particle entered the system. The above definitions are valid for steady flows.

4.2. MODELS OF SOLUTE TRANSPORT

The question of the actual form of $f_T(t)$ can be addressed in two ways. The first method would be to conduct experiments with measured inputs and outputs, and $f_T(t)$ would be determined from experimental observations. The second approach

is to use conceptual models where the physical processes are represented by mathematical equations, and the travel time pdfs are obtained from mathematical considerations. The simplest mathematical model, for instance, is one where we assume that solute particles at the inlet end experience pure translation over a flow path of length L under a constant velocity V. The travel time pdf

$$f_T(t) = \delta(t - L/V) \tag{4.2.1}$$

is a generalized pdf. Consequently, one can visualize the travel time as a random variable T, and the travel time moments can then be defined as

$$E[T^n] = \int_0^\infty t^n \ \delta(t - L/V) \ dt = \left(\frac{L}{V}\right)^n \tag{4.2.2}$$

This implies that $E[T] = L/V$ and the variance is 0. In this model note that all particles experience the same travel time $= L/V$, and hence the zero variance.

Let our process model be given by the one-dimensional advection-dispersion equation (ADE) which is popular for representing movement of a conservative solute in a soil column under steady flow condition.

$$\frac{\partial c}{\partial t} = D\frac{\partial^2 c}{\partial x^2} - V\frac{\partial c}{\partial x} \tag{4.2.3}$$

where $c(x, t)$ is the flux-averaged concentration, V is the average pore water velocity, and D is the coefficient of hydrodynamic dispersion encompassing the effects of both molecular diffusion and mechanical dispersion resulting from the complex pore structure. The end conditions for (4.2.3) are

$$c(x, 0) = 0 \tag{4.2.4a}$$

$$c(0, t) = \frac{M}{Q}\delta(t) \tag{4.2.4b}$$

$$c(\infty, t) = 0 \tag{4.2.4c}$$

where M is the mass of solute applied instantaneously, and Q is the constant volumetric flowrate. The ratio $\frac{M}{Q}$ is assumed as unity. In Section (2.5), the impulse-response function (or the travel time pdf) was found for $x = L$ (see (2.5.27)) as

$$f_T(L; t) = \frac{L}{2\sqrt{\pi D t^3}} \ \exp\left[-\frac{(L - Vt)^2}{4Dt}\right] \tag{4.2.5}$$

Note that the travel distance $x = L$ appears as a parameter in the travel time pdf using the ADE model. From linear system theory, we state that (4.2.5) contains the same information as embodied in the governing differential equation (4.2.3) and the corresponding boundary conditions. The travel time moments for this model are

$$E[T^n] = \int_0^\infty t^n \cdot \frac{L}{2\sqrt{\pi D t^3}} \ \exp\left[-\frac{(L - Vt)^2}{4Dt}\right] dt \tag{4.2.6}$$

These are more easily derived from the moment generating property of the Laplace transform.

The Laplace transform of $c(x, t)$ in (4.2.3) for this case was obtained as (2.5.26)

$$\mathcal{L}[c\ (L; s)] = \hat{c}(L; s) = \exp\left[\frac{VL}{2D}\left(1 - \sqrt{1 + \frac{4sD}{V^2}}\right)\right] \tag{4.2.7}$$

$$E[T] = -\frac{d\hat{c}(L; s)}{ds}\,|_{s=0} = \frac{L}{V} \tag{4.2.8}$$

$$E\left[T^2\right] = \frac{d^2\hat{c}(L; s)}{ds^2}\,|_{s=0} = \frac{2DL}{V^3} - \frac{L^2}{V^2} \tag{4.2.9}$$

and consequently

$$Var[T] = \frac{2DL}{V^3} \tag{4.2.10}$$

Clearly, the mean of the travel time is the same in both the pure translation model (also called as piston flow model) as seen from (4.2.2) and the advection-dispersion equation (ADE). However, the variance for the ADE model increases linearly with distance as in (4.2.10). The process of dispersion contributes to the smearing of the solute front as expressed through D, but does not contribute to mean advection.

Mathematical models like the ADE can be postulated in terms of representation of physical processes, but they cannot be 'validated' as true models very easily. It may take several experiments to categorically verify a mathematical model. Note that one can 'postulate' any pdf as the impulse response function $f_T(t)$ of which (4.2.1) and (4.2.5) are two examples. One does not know *a-priori*, the true response of a physical system.

While a strict validation test may not be feasible, there are certain conditions that we would like the chosen travel time pdf to satisfy. For instance, can the travel time pdf $f_T(t)$ that was obtained under a certain set of flow conditions be used to develop the impulse response function if these conditions are changed? This is a difficult question to answer. The initial temptation is to answer yes to this question for the model of (4.2.5) because it is expressed in terms of physical parameters. However, this presupposes that the ADE model of (4.2.3) is a true representation of solute movement in soils.

For simplicity, let us assume that the only condition we want to change is the pore water velocity$V$, and that this change leaves all other parameters unchanged. We may denote the travel time pdf obtained under a velocity of V_1 as $f_{T_1}(t)$. We want to know if it is possible to derive the travel time pdf $f_{T_2}(t)$when the velocity is V_2. Let us first consider (4.2.1). Clearly, if the constant flow velocity is V_2, then

$$f_{T_2}(t) = \delta(t - L/V_2) \tag{4.2.11}$$

Note that in this case, since the velocities are constant and the process is essentially deterministic as indicated by the zero variance, we note that the two travel time random variables T_1 and T_2 are related to each other (for a constant travel distance L) as

$$T_2 = \frac{V_1}{V_2} T_1 \tag{4.2.12}$$

Then the cumulative distribution functions are related to each other as

$$F_{T_2}(t) = P[T_2 \leq t] \; = F_{T_1}\left(\frac{V_2}{V_1} t\right) \tag{4.2.13}$$

because V_1, V_2, and t are all greater than zero. Also, we have the pdf of travel time when the velocity is V_2 as

$$f_{T_2}(t) \; = \frac{V_2}{V_1} \cdot f_{T_1}\left(\frac{V_2}{V_1} t\right) \tag{4.2.14}$$

Equations (4.2.13) or (4.2.14) are useful since we can, in principle, deal with all velocities by knowing the pdf corresponding to a single velocity. From (4.2.12), it is evident that with the choice of $Vt = I$ as the independent variable, the pdf would be invariant. Here, I is the cumulative amount of water that enters the soil by time t.

Let us examine the travel time pdf given by (4.2.5) to see if this form would satisfy (4.2.13) or (4.2.14). If travel times denoted by T_2 and T_1 are related then $f_{T_2}(t_2)dt_2 = f_{T_1}(t_1)dt$, we obtain that the dispersion coefficient must satisfy the condition

$$D = \lambda V \tag{4.2.15}$$

where λ is a constant called dispersivity. Similarly, several other travel time pdfs can be examined to see if they satisfy (4.2.13) and (4.2.14), and if so under what constraints on their distribution parameters.

One can also devise a more difficult test for a model of the travel time density function. Both the models considered so far (4.2.1) and (4.2.5) can be used to predict the solute behavior at a particular distance L. Indeed, the model parameters would be estimated from an experiment. It would be useful to see if one could use these travel pdfs to estimate the travel time pdf at some other distance for the same velocity. This question can be partially addressed by examining the moments of any model. From (4.2.8) and (4.2.10), we observe that the mean and variance of travel time increase linearly with travel distance x (or L) for the ADE model.

For the purely advective model of (4.2.1), we know that the mean increases with distance, but the variance is zero. The problem can be made more interesting by assuming that (4.2.1) describes solute behavior along a single path (or stream

tube) with a constant velocity V. If the soil porous medium is considered to be a collection of such stream tubes, with the velocities following a distribution denoted by $f_V(v)$, then the travel time through each stream tube for a distance L is simply $T = L/V$s so that the n-th moment of the travel time is

$$E[T^n] = E[(L/V)^n] = \int_0^\infty \left(\frac{L}{V}\right)^n f_V(v)\ dv \tag{4.2.16}$$

Therefore,

$$E[T] = L\ E\left[\frac{1}{V}\right] \tag{4.2.17}$$

$$Var\ [T] = L^2 \cdot Var\left[\frac{1}{V}\right] \tag{4.2.18}$$

Note that the model considered here assumes that there is no interaction (or mixing) of solute parcels from one stream tube to the other. This is different from the conceptualization of the ADE model (4.2.5) where the process of dispersion allows complete mixing to occur so that concentration gradients in the transverse direction (i.e. between stream tubes) are 'smoothed out'.

We define the pdf of the travel time to a distance L as $f_T(L, t)$. Assuming a uniform and steady velocity field, we expect that

$$\int_0^t f_T\ (L_1, \tau)\, dt = \int_0^{tL_0/L_1} f_T(L_0, \tau)\ d\tau \tag{4.2.19}$$

In other words, the probability that the travel time over a distance L_1, will be less than or equal to t, is the same as the probability that the travel time to a distance L_0 will be less than or equal to tL_0/L_1. Therefore

$$F_T(L_1, t) = F_T\left(L_0, \frac{tL_0}{L_1}\right) \tag{4.2.20}$$

$$f_T(L_1, t) = \frac{L_0}{L_1} f_T\left(L_0, \frac{tL_0}{L_1}\right) \tag{4.2.21}$$

If a model for travel time pdf obeys (4.2.21), then the n-th moment for travel time to depth L_1 is

$$E_{L_1}[T^n] = \int_0^\infty t^n f_T(L_1, t)\ dt = \left(\frac{L_1}{L_0}\right)^n E_{L_0}[T^n] \tag{4.2.22}$$

Say, we have measurements at a reference location L_0, and we want to predict the travel time moments at another distance $L_1 \neq L_0$. From (4.2.22),

$$E_{L_1}[T] = \frac{L_1}{L_0} E_{L_0}[T] \tag{4.2.23}$$

implying that the mean of the travel time increases with distance in a manner similar to the ADE model. However, the behavior of the variance is quite different.

$$E_{L_1}[T^2] = \left(\frac{L_1}{L_0}\right)^2 E_{L_0}[T^2] \Rightarrow Var_{L_1}[T] = \left(\frac{L_1}{L_0}\right)^2 Var_{L_0}(T) \tag{4.2.24}$$

Thus, for travel time pdfs that obey (4.2.20) or (4.2.21), we find that the variance of the travel time increases as the square of the distance unlike the linear increase in variance with distance for the ADE model as shown in (4.2.10). Travel time pdfs that exhibit an increase in variance with the square of the travel distance have been generally labeled as stochastic convective models (Simmons, 1982). This increased variance is a direct consequence of the fact that stochastic convective models do not allow for mixing among stream tubes.

In particular, velocities are often treated as being distributed in a log-normal fashion such that $Y = \ln\ V$ is normally distributed with mean μ_y and variance σ_y^2 so that from (1.1.14)

$$f_V(v) = \frac{1}{\sqrt{2\pi}\ \sigma_v t} \exp\left[-\frac{\left(\ln V - \mu_y\right)^2}{2\sigma_y^2}\right] \tag{4.2.25}$$

At this point, it is useful to consider that if we define a random variable $Z = aV^b$, then Z is log-normally distributed with,

$$E[\ln Z] = \ln a + bE[\ln\ V] = \ln a + b\mu_Y \tag{4.2.26}$$

$$Var[\ln Z] = b^2 \cdot Var[\ln V] = b^2\sigma_y^2 \tag{4.2.27}$$

Thus if we now define $T = L/V$ (i.e. $Z = T$ with $a = L, b = -1$), then

$$E\left[\ln T\right] = \ln L - \mu_y \tag{4.2.28}$$

$$Var\ [\ln\ T] = \sigma_y^2 \tag{4.2.29}$$

Now, since T is log-normally distributed, from (1.2.10) and (1.2.11) we obtain

$$E[T] = L\exp(-\mu_y)[\exp(\sigma_y^2)]^{1/2} \tag{4.2.30}$$

$$Var\ [T] = L^2 \exp\ (-2\mu_y) \cdot \exp(\sigma_y^2)[\exp(\sigma_y^2) - 1] \tag{4.2.31}$$

4.3. DEPTH MOMENTS OF THE ADVECTION-DISPERSION EQUATION

In Chapter 2 the ideas of flux and resident concentrations were presented in conjunction with solute transport through soil columns. We shall pursue the idea of moments and travel times for such models here. The impulse-response function for a delta-function (instantaneous) flux input of solute is the flux averaged

concentration measured at a distance along the column and is denoted as $f_f(x, t)$. It is also the probability distribution of travel times of solute particles as they move from $x = 0$ at the inlet to a specified distance x along the soil column. Thus $f_f(x, t)$ is also the temporal behavior of effluent concentrations at a fixed location x for the appropriate delta input at $x = 0$.

In keeping with the notion of spatial Green's functions, one may also be interested in the spatial distribution of resident concentration at a fixed time in response to a delta input at $x = 0$. The resident concentration $f_r(x, t)$ could be interpreted as the probability distribution of travel distances of solute particles at a fixed time t assuming that they were all released at $t = 0$. The two pdfs can be related as

$$\int_0^t f_f(x, t')\,\mathrm{d}t' = \int_x^\infty f_r(x', t)\,\mathrm{d}x' \tag{4.3.1}$$

The left hand side of (4.3.1) is the fraction of the initial solute mass that has moved past a distance x by time t. The right hand side is the fraction of the input solute mass that exists within distances greater than x from the source, assuming that the soil volume is initially free of solute. Simmons (1986a,b) and Dagan and Nguyen (1989) differentiated (4.3.1) with respect to x and t to obtain

$$\frac{\partial f_f}{\partial x} + \frac{\partial f_r}{\partial t} = 0 \tag{4.3.2}$$

Equation (4.3.2) can be used to relate the two pdfs. It is customary to measure the flux concentration from the effluent of column experiments, so that the resident pdf may be obtained as

$$f_r(x, t) = -\frac{\partial}{\partial x} \int_0^t f_f(x, \tau)\, d\tau \tag{4.3.3}$$

From results of Chapter 2, (see (2.5.11)) the Laplace transforms of the two pdfs are related as

$$\hat{f}_r(x; s) = -\frac{1}{s} \frac{\partial \hat{f}_f(x; s)}{\partial x} \tag{4.3.4}$$

The depth moments (we will deal with the more general spatial moments in Chapter 6 for infinite domains) may be defined in this context as (Jury and Roth, 1990)

$$X_n(t) = E[x^n] = \int_0^\infty x^n f_r(x, t)\, dx \tag{4.3.5}$$

Laplace transforms of (4.3.5) yields

$$\hat{X}_n = \int_0^\infty x^n \hat{f}_r(x; s)\, dx \tag{4.3.6}$$

From (2.5.29), the transform of the resident concentration yields

$$\hat{f}_r(x;s) = \frac{2}{V(1+\xi)} \exp\left[\frac{\mathrm{V}x}{2\mathrm{D}}(1-\xi)\right] \tag{4.3.7}$$

where $\xi = \left[1 + \frac{4sD}{V^2}\right]^{1/2}$, $\hat{f}_r(x;s) = \hat{c}_b(x;s)/q$, and $V = \frac{q}{\eta}$ is the seepage velocity. From (4.3.6) and (4.3.7), we obtain after some algebra (see Jury and Roth, 1990)

$$\hat{X}_n = \frac{n!}{s} \left[\frac{2\mathrm{D}}{\mathrm{V}(\xi - 1)}\right]^n \tag{4.3.8}$$

The lower order depth moments are evaluated successively. For instance

$$\hat{X}_0 = \frac{1}{s} \Rightarrow X_o = 1 \tag{4.3.9}$$

as would be expected since $f_r(x,t)$ is a probability density function.

$$\hat{X}_1 = \frac{2D}{Vs(\xi - 1)} \tag{4.3.10a}$$

$$X_1 = \sqrt{\frac{Dt}{\pi}} \exp\left[-\frac{V^2}{4D}t\right] + \frac{D}{2V}\left\{\left(1 + \frac{V^2}{D}t\right) erfc\left(-\frac{V\sqrt{t}}{2\sqrt{D}}\right) - erfc\left(\frac{V\sqrt{t}}{2\sqrt{D}}\right)\right\} \tag{4.3.10b}$$

$$\hat{X}_2 = \frac{2}{s}\left[\frac{2D}{V(\xi - 1)}\right]^2 \tag{4.3.11a}$$

$$X_2 = \left(\frac{2D}{V} + Vt\right)\sqrt{\frac{Dt}{\pi}} \exp\left(-\frac{V^2}{4D}t\right) + \left(\frac{D}{V}\right)^2 \left\{erfc\left(\frac{V\sqrt{t}}{2\sqrt{D}}\right) + \left[\frac{1}{2}\frac{V^4t^2}{D^2} + \frac{2V^2t}{D} - 1\right] erfc\left(-\frac{V\sqrt{t}}{2\sqrt{D}}\right)\right\} \tag{4.3.11b}$$

where (4.3.10b) and (4.3.11b) are obtained after inversion of the respective Laplace transforms. The expressions for the moments can be simplified for large t as

$$X_1 \cong \frac{D}{V} + Vt \tag{4.3.12}$$

$$X_2 \cong V^2t^2 + 4Dt - \frac{2D^2}{V^2} \tag{4.3.13}$$

Note that expressions for the depth moments were derived for a semi-finite domain, where no solute is allowed to diffuse/disperse into the region $x < 0$. Treating the resident flux concentration as a pdf, the first two moments can be used to calculate the variance as $X_2 - X_1^2$. This quantity would indicate the spread of the concentration distribution about its center of mass or mean location X_1. A detailed treatment of depth moments is available in Jury and Roth (1990).

In order to bring out the role of the boundary condition more clearly, let us consider the advective-dispersive transport model in an infinite domain. The governing partial differential equation for the resident concentration for unit cross-sectional area perpendicular to the flow direction is

$$\frac{\partial c_r}{\partial t} + V\frac{\partial c_r}{\partial x} = D\frac{\partial^2 c_r}{\partial x^2}. \tag{4.3.14}$$

with the initial condition

$$c_r(x, 0) = {}^{M}\!/_{\eta}\,\delta(x) \tag{4.3.15}$$

Note that in accordance with (3.3.12), the quantity M/η has been chosen as unity to make $c_r(x, t)$ be a pdf in x. The definitions of depth moments now are

$$X_n'(t) = \int_{-\infty}^{\infty} x^n c_r(x, t)\, dx \tag{4.3.16}$$

The domain is now infinite unlike the previous case, and solute is allowed to diffuse into the region $x < 0$. While it is possible to use transform methods (to be discussed in Chapter 6), we adopt a different approach here. Multiplying 4.3.14 by x^n and integrating over the spatial domain, we obtain

$$\frac{dX_n'}{dt} - nV\ X_{n-1}' - n(n-1)DX_{n-2}' = 0 \tag{4.3.17}$$

where we have used integration by parts and further required that the resident concentration and its derivatives equal zero for $x = \pm\infty$. From the initial condition of (4.3.15), we have

$$X_0'(t = 0) = 1.0,\ \ X_n'(t = 0) = 0 \text{ for } n \geq 1 \tag{4.3.18}$$

The expressions for the first few moments are obtained easily as

$$X_0' = 1.0 \tag{4.3.19}$$

$$X_1' = Vt \tag{4.3.20}$$

$$X_2' = V^2t^2 + 2Dt \tag{4.3.21}$$

Expressions (4.3.20) and (4.3.21) may be compared to (4.3.10b) and (4.3.11b) respectively, or to the large time results in (4.3.12) and (4.3.13).

The variance of resident concentration distribution in the infinite domain model is obtained as

$$\sigma^2 = X_2' - X_1'^2 = 2Dt \tag{4.3.22}$$

This coincides with Einstein's result, and many models define effective dispersion as

$$D_{eff} = \frac{1}{2}\frac{d(\sigma^2)}{dt} \tag{4.3.23}$$

Similarly, the effective resident velocity is often expressed as

$$V_{r,eff} = \frac{dX_1'}{dt} \tag{4.3.24}$$

4.4. DEPTH-MOMENTS FOR STOCHASTIC-CONVECTIVE MODELS

In Section 4.2, we introduced the concept of stochastic-convective models that are not 'process-based.' Equation (4.2.21) is a characteristic of the flux pdf of stochastic-convective models. Using (4.2.21) and (4.3.3), the resident pdf of such models is obtained as

$$f_r(x,t) = -\frac{\partial}{\partial x}\int_0^t f_f(x,t')\,dt' = -\frac{\partial}{\partial x}\int_0^t \frac{x_1}{x} f_f\left(x_1, \frac{tx_1}{x}\right)\,dt \tag{4.4.1}$$

Substituting $y = \frac{tx_1}{x}$, $dy = \frac{x_1}{x}dt$ and using Leibnitz rule, we obtain

$$f_r(x,t) = -\frac{\partial}{\partial x}\int_0^{\frac{tx_1}{x}} f_f(x_1,y)dy = \frac{tx_1}{x^2} f_f\left(x_1, \frac{tx_1}{x}\right) \tag{4.4.2}$$

For example, if the flux pdf is described by a lognormal model as

$$f_f(x,t) = \frac{1}{\sqrt{2\pi}\,\sigma_1 \mathrm{t}} \exp\left\{-\frac{\left[\ln(t) - \mu_{x_1}\right]^2}{2\sigma_1^2}\right\} \tag{4.4.3}$$

then the corresponding resident pdf from (4.4.2) is (Jury, 1982)

$$f_r(x,t) = \frac{1}{\sqrt{2\pi}\,\sigma_1 \mathrm{x}} \exp\left\{-\frac{\left[\ln(tx_1/x) - \mu_{x_1}^2\right]^2}{2\sigma_1^2}\right\} \tag{4.4.4}$$

In equations (4.4.1) to (4.4.4), we have used x_1 as the reference depth. Thus the model parameters μ_{x_1} and σ_1^2 are determined from effluent flux concentrations at a distance of x_1.

Note that these models are deemed as being purely convective in nature as they are primarily based on 'fitting' a distribution to observed data. Consequently, they

do not allow for dispersion in the negative x direction and the domain should be defined as a semi-infinite one. The pdfs for such models as in (4.4.3) or (4.4.4) are zero at the origin not because of any boundary condition but because of the nature of the function chosen for the stochastic-convective model.

The depth moments for stochastic-connective models are given as

$$\begin{aligned} X_n(t) &= \int_0^\infty x^n f_r(x,t)\, dx = \int_0^\infty x^n \frac{tx_1}{x^2} f_f\left(x_1, \frac{tx_1}{x}\right) dx \\ &= (tx_1)^n \int_0^\infty (t')^{-n} f_f(x_1, t')\, dt' \\ &= (tx_1)^n \cdot E_{x_1}[t^{-n}] \end{aligned} \tag{4.4.5}$$

where the final expectation is over the random travel times to a distance x_1.

From (4.3.24), we obtain the Lagrangian velocity from the resident pdf as

$$V_{r,eff} = \frac{dX_1(t)}{dt} = x_1 E\left[\frac{1}{t}\right] \tag{4.4.6}$$

Another expression for effective velocity is obtained from flux pdf as

$$V_{f,eff} = \left\{\frac{d}{dx} E_{x_1}[t]\right\}^{-1} = \frac{x_1}{E_{x_1}[t]} \tag{4.4.7}$$

and is referred to as the Eulerian velocity (Simmons, 1986). The Lagrangian and Eulerian velocities are the same for the piston flow model of (4.2.1).

4.5. TRANSFER FUNCTIONS FOR LAYERED SOILS

We briefly consider the case of solute transport in soils with two layers, with flow perpendicular to the layering. This problem has been studied by researchers (Jury and Roth, 1990; Leij and Dane, 1991; Jury and Utermann, 1992), and Figure 4.5.1 shows a definition sketch. The discussion can be extended to multiple layers along similar lines.

The soil properties in the two layers could be quite different, so that the travel times T_1 and T_2 within the two layers maybe treated as two different random variables. We assume that the Darcian flux through the two layers is constant. If each of the layers were considered as individual soil columns, then the travel time flux pdfs through each layer could be represented as $f_{T_1}(x,t)$ and $f_{T_2}(x,t)$ respectively.

Let a delta pulse of solute be added to the soil surface at $x = 0$. Then the flux-averaged effluent concentration measured at the bottom is the travel time pdf $f_T(x,t)$of the combined system. The total travel time may be thought of as

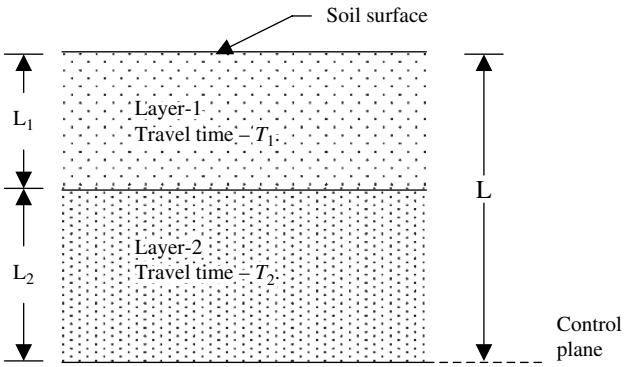

Figure 4.5.1. Schematic for the two-layer problem

a random variable $T = T_1 + T_2$ the sum of travel times within each layer. Thus, from convolution for sum of random variables, the travel time flux pdf is

$$f_T(x,t) = \int_0^t \int_0^{t-t_2} \delta(t - t_1 - t_2) f_{T_1,T_2}(t_1, t_2) dt_1,\ dt_2 \tag{4.5.1}$$

where $f_{T_1,T_2}(t_1, t_2)$ is the joint pdf of T_1 and T_2. If the travel times through the two layers are independent and then

$$f_{T_1,T_2}(t_1, t_2) = f_{T_1}(t_1) f_{T_2}(t_2) \tag{4.5.2}$$

and

$$f_T(L,t) = \int_0^t f_1(L_1, t_1)\ f_2(L_2, t - t_1) dt_1 \tag{4.5.3}$$

where L is the sum of the lengths of the two columns L_1 and L_2.

On the other hand, assumption of perfect correlation between the travel times of the two soil layers implies that knowledge of one perfectly determines the other in a deterministic fashion as

$$T_2 = g(T_1) \tag{4.5.4}$$

The joint pdf of the travel times T_1 and T_2 may be expressed as

$$f_{T_1,T_2}(t_1, t_2) = f_{T_1}(L_1, t_1)\ \delta[t_2 - g(t_1)] \tag{4.5.5}$$

If we assume that the travel times are perfectly correlated in a positive way, then it is customary to equate the two cumulative distribution functions

$$F_{T_1}(t_1;\ L_1) = F_{T_2}(t_2; L_2) \tag{4.5.6}$$

Let us consider a soil that has N distinct layers of thickness ΔL each in the vertical direction. Assuming that the layers are statistically homogeneous implies that the random travel times within each layer are identically distributed. We assume that the advection dispersion equation governs solute movement in each layer. If T_i is a random variable denoting the travel time in the i-th layer, then from (4.2.8) and (4.2.10), we have

$$E[T_i] = \Delta L/V \tag{4.5.7}$$

$$Var[T_i] = 2D \cdot \Delta L/V^3 \tag{4.5.8}$$

If we define $T\left(=\sum_{i=1}^{N} T_i\right)$ as the travel time through all the N layers, then

$$E[T] = L/V = N \cdot E[T_i] \tag{4.5.9}$$

$$Var[T] = \frac{2D \cdot L}{V^3} = N \text{ Var}[T_i] \tag{4.5.10}$$

Thus the mean and variance of the travel times are essentially the sums of the means and variances of travel time of individual layers, respectively. Equation (4.5.10) implies that the correlation between travel times of any two layers T_i and T_j is zero for $i \neq j$.

If the travel times within all layers were perfectly correlated, then $E[T] = NE[T_i]$ as in (4.5.9). However,

$$Var[T] = Var\left[\sum_{i=1}^{N} T_i\right] = N^2 \; Var \; [T_i] \tag{4.5.11}$$

Comparing with (4.2.24), we conclude that stochastic advective models are those that exhibit perfect correlation between travel times of different layers. In general, if the travel time pdf within each layer is described by $f_f(\Delta l, t)$, then the travel time pdf through all the N layers is given by

$$f_f(L, t) = \int_0^\infty \ldots\ldots \int_0^\infty \delta\left(t - \sum_{j=1}^{N} t_j\right) f(t_1, t_2, t_N) \; \mathrm{dt}_1, dt_2 \ldots . dt_N \tag{4.5.12}$$

where t_j is travel time through the j-th soil layer, $L = N\,\Delta l$, and $f(t_1, \mathrm{t}_2, \ldots . t_N)$ is the joint pdf of the travel times $T_1, T_2, \ldots, T_N$. If the correlation between travel times T_i and T_j is represented by ρ_{ij}, then $E[T]$ is given by (4.5.9), and

$$Var \; [T] = Var \; [T_i] \; \sum_{i=1}^{N} \sum_{j=1}^{N} \rho_{ij} \tag{4.5.13}$$

assuming that travel times for all layers are identically distributed. Equation (4.5.11) is a particular case of (4.5.13).

4.6. STOCHASTIC STREAM TUBE MODELS

A special class of models have been developed by first using a 'simple' local scale model, and then performing an 'averaging' operation over such independent, non-interacting local scale (stream tube) models to describe large-scale behavior (see Ginn, 2002, for a detailed presentation). In solute transport applications, the soil is approximated by a series of non-interacting stream tubes. The movement of solute through each of these tubes (i.e., at the local scale) is represented by a simple model, such as those of (4.2.1), (4.2.5), or (4.4.3). The model parameters (such as V, D, μ, σ, etc.) are assumed to be constant within each streamtube but may be correlated random variables in terms of their variations from tube to tube. If $\lambda_1, \lambda_2, \ldots, \lambda_k$ are the k parameters in the local-scale model, then their combined behavior is described by their joint probability density function. For simplicity, it is assumed that all the tubes experience the same initial and boundary conditions.

At the local scale, let $C_l\ (x,\ t;\ \lambda_1,\ \lambda_2, \ldots, \lambda_k)$ denote the local concentration as a function of distance and time within a single stream tube. Indeed, the behavior of $C_l(x, t)$ in each tube in this fashion may be treated as a single realization among the ensemble of realizations available from all the stream tubes. The mean or ensemble average concentration is

$$C(x,t) = \int_{-\infty}^{\infty} \ldots . \int_{-\infty}^{\infty} C_l(x,t;\lambda_1,\lambda_2,\ldots,\lambda_k) f(\lambda_1,\ \lambda_2,\ldots,\lambda_k) d\lambda_1\ d\lambda_2\ \ldots\ d\lambda_k \tag{4.6.1}$$

where $f(\lambda_1,\ \lambda_2, \ldots, \lambda_k)$ is the joint density function of all the parameters.

For instance, say the local scale model is described by the piston flow model of (4.2.1), i.e. the local flux concentration is

$$C_{l,f}\ (x,t;V) = G\delta(t - x/V) \tag{4.6.2}$$

where G, defined in (2.5.18), is chosen as unity. Here the only model parameter is the velocity V whose pdf is $f_V(v)$. The ensemble averaged flux concentration is

$$C_f(x,t) = \int_0^{\infty} \delta(t - x/V) f_v(v) dv = \frac{x}{t^2} f_V\left(\frac{x}{t}\right) \tag{4.6.3}$$

where V takes on only non-negative values. In fact, if the local flux concentration is the response due to a delta function within a stream tube, then $C_f(x, t)$ is the impulse-response function or the travel time flux pdf for the soil $f_f(x, t)$. Therefore, the n-th travel time moment to a distance x becomes

$$E_x[t^n; V] = \int_0^{\infty} t^n f_f(x,t)\, dt \tag{4.6.4}$$

Applying this to the piston flow model of (4.6.3), we obtain

$$E_x[t^n; V] = \int_0^{\infty} t^n \cdot \delta(t - x/V)\, dt = \left(\frac{x}{V}\right)^n \tag{4.6.5}$$

The average of the n-th moment is

$$E_x[t^n] = E_V\left[\left(\frac{x}{V}\right)^n\right] = x^n \cdot E_V\left[\frac{1}{V^n}\right] \tag{4.6.6}$$

implying that

$$E_x[t] = xE_V[1/V] \tag{4.6.7}$$

$$E_x[t^2] = x^2 E_V[\frac{1}{V^2}] \tag{4.6.8}$$

The effective (Eulerian) quantities in terms of the flux pdfs are defined as (Valocchi, 1985)

$$V_{f,eff} = \frac{x}{E_x[t]} \tag{4.6.9}$$

$$D_{f,eff} = \frac{E_x[t^2] - E_x^2[t]}{2E_x[t]}\, V_{f,eff}^2 \tag{4.6.10}$$

Since V is often treated as a log-normally distributed random variable as in (4.2.25), with $Y = \ln V$ being normally distributed with mean μ_y and variance σ_y^2, we obtain

$$V_{f,eff} = \frac{1}{\exp[-\mu_y + \sigma_y^2/2]} \tag{4.6.11}$$

$$D_{f,eff} = \frac{x}{2}\exp\left(\mu_y - \frac{3}{2}{\sigma_y}^2\right)\left[\exp\left(2{\sigma_y}^2\right) - \exp\left({\sigma_y}^2\right)\right] \tag{4.6.12}$$

Now, given the flux pdf (4.6.3) for streamtube model, the resident pdf is given as

$$f_r(x,t) = -\frac{\partial}{\partial x}\int_0^t \frac{x}{t^2} f_V(x/t)\ dt = \frac{\partial}{\partial x}\int_\infty^{x/t} f_V(y)\ dy = \frac{1}{t} f_V(x/t) \tag{4.6.13}$$

where we have again used Leibnitz rule. The n-th depth moment of the resident pdf is therefore

$$X_n = \int_0^\infty \frac{x^n}{t} f_V(x/t)\, dx = t^n \int_0^\infty y^n f_V(y) dy = t^n E_V[V^n] \tag{4.6.14}$$

where we have used the substitution $y = x/t$. The effective Eulerian quantities are

$$V_{r,eff} = E_r[V] \tag{4.6.15}$$

If V is log-normally distributed, this yields

$$V_{r,eff} = \exp\left[\mu_y + \sigma_y^2/2\right] \tag{4.6.16}$$

which can be compared to (4.6.11). Similarly, defining $D_{r,eff}$ from (4.3.23), we have

$$D_{r,eff} = \frac{1}{2}\frac{d}{dt}\left(X_2 - X_1^2\right) = t \cdot \exp\left(2\mu_y + \sigma_y^2\right)\left[\exp\left(\sigma_y^2\right) - 1\right] \tag{4.6.17}$$

which, in turn, can be compared to (4.6.12).

4.7. A STOCHASTIC STREAM TUBE MODEL FOR CONTAMINANT DISSOLUTION AND TRANSPORT WITH DEGRADATION

As discussed in the previous section, stream-tube modeling technique is one of the simpler methods that allow for a stochastic description of the field scale solute transport using various local models of choice. Here, a simplified version of Berglund's (1997) stream-tube model is proposed for modeling nonaqueous phase liquid (NAPL) transport in porous media. With the proposed model, the effects of (1) heterogeneity of the flow field, (2) distribution of the contaminant source, and (3) rate of degradation are examined. Details are available in Chan and Govindaraju (2006) from where this section has been abstracted.

4.7.1 Local Model

A simple one-dimensional stream-tube model is considered in this study (see Figure 4.7.1). In this conceptualization, the heterogeneous flow field is represented by a collection of stream tubes with constant area, A. Within each tube, the velocity is assumed to be steady and uniform and is given by v. (Later, in Section 10.6, this assumption is relaxed and properties are allowed to vary along a stream tube). A log-normal distribution of the velocities is used, i.e. $\ln V \sim N(\mu, \sigma^2)$ where v is one realization of the random variable V. A source of NAPL mass M_0 is located at the source zone ($x = 0$) in each tube. The distribution of this solute mass is assumed to be uniform such that $M_0 \sim$Uniform (0, $M_{\max}$). It is also assumed that random variables V and M_0 are independent. The rate of depletion of the mass m at the source zone is given by

$$\frac{dm}{dt} = -Av\theta c_s \tag{4.7.1}$$

where c_s is the solubility limit, and θ is the water content. The dissolution of the solute mass is assumed to be instantaneous, and no degradation occurs at the source. Integrating (4.7.1) and equating m to 0, the life duration of the source in each tube is

$$\tau = \frac{b}{v} \text{ where } b = \frac{M_0}{A\theta c_s} \tag{4.7.2}$$

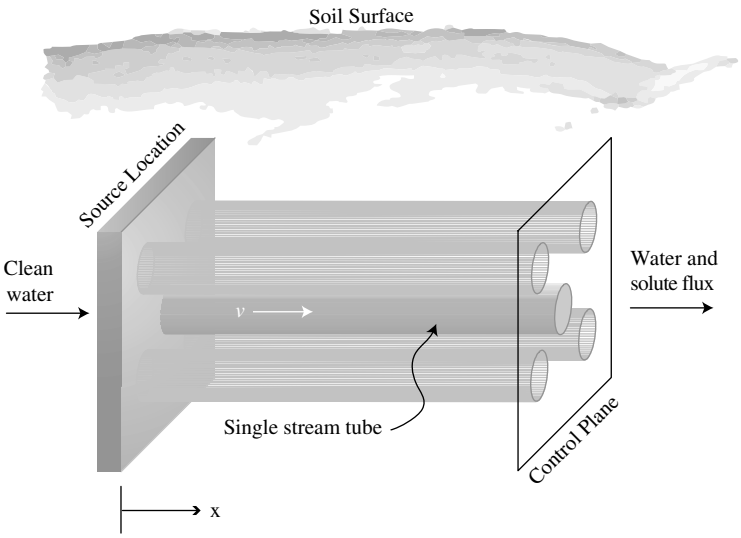

Figure 4.7.1. Schematic of the conceptualized stream-tube model (adapted from Chan and Govindaraju, 2006, with permission from Elsevier)

Since M_0 is a random variable, b is also a random variable with uniform distribution, i.e. $B \sim \text{Uniform}(0, b_{max})$ where $b_{\max} = M_{\max} \big/ A\theta c_s$. Assuming advective transport with first-order degradation of the dissolved NAPL, the local model for each tube can be written as

$$c_l(x,t) = \begin{cases} 0, & 0 < t \le \dfrac{x}{v} \\ c_s \exp\left(-\lambda \dfrac{x}{v}\right), & \dfrac{x}{v} < t \le \dfrac{x+b}{v} \\ 0, & t > \dfrac{x}{v} + \tau \end{cases} \tag{4.7.3}$$

where λ is the first-order degradation rate constant. The following dimensionless parameters are introduced:

$$\begin{aligned} V^* &= \frac{v}{v_{ref}}; \quad & B^* &= \frac{b}{b_{max}}; \quad & C^* &= \frac{c}{c_s}; \\ X^* &= \frac{x}{b_{max}}; \quad & T^* &= \frac{t v_{ref}}{b_{max}}; \quad & \lambda^* &= \frac{\lambda b_{max}}{v_{ref}} \end{aligned} \tag{4.7.4}$$

where $v_{ref} = \exp(\mu)$ is the geometric mean of V. As a result, $\ln V^*$ is normally distributed with zero mean and variance σ^2, and B^* is uniformly distributed between

0 and 1. With this non-dimensional form, the number of parameters of the model is reduced to only two $-\sigma^2$ and λ^*. Substituting (4.7.4) into (4.7.3), we have

$$C_l^*(X^*, T^*) = \begin{cases} 0, & 0 < T^* \le \dfrac{X^*}{V^*} \\ \exp\left(-\lambda^* \dfrac{X^*}{V^*}\right), & \dfrac{X^*}{V^*} < T^* \le \dfrac{X^*+B^*}{V^*} \\ 0, & T^* > \dfrac{X^*+B^*}{V^*} \end{cases} \tag{4.7.5}$$

To obtain the averaged flux concentration past a control plane (CP) at (X^*, T^*) as shown in Figure 4.7.1, the local concentrations in the stream tubes are averaged over the random quantities of V and M_0; thus, we have

$$\left\langle C_f^*(X^*, T^*) \right\rangle = \iint\limits_{V^* B^*} C_1^*(X^*, T^*) f_{B^*} f_{V^*} dB^* dV^* \tag{4.7.6}$$

where f_{B^*} and f_{V^*} are the probability density functions of random variables B^* and V^* respectively, and $\langle \cdot \rangle$ stands for the expected value. Substituting in (4.7.5), the double integral of (4.7.6) can be integrated over the appropriate region to obtain:

$$\begin{aligned} \langle C_l^*(X^*, T^*) \rangle &= \int_{\frac{X^*}{T^*}}^{\frac{X^*+1}{T^*}} \int_{V^*T^*-X^*}^{1} \exp\left(-\lambda^* \frac{X^*}{V^*}\right) f_{B^*} f_{V^*} dB^* dV^* \\ &= \int_{\frac{X^*}{T^*}}^{\frac{X^*+1}{T^*}} (1 - V^*T^* + X^*) \exp\left(-\lambda^* \frac{X^*}{V^*}\right) f_{V^*} dV^* \end{aligned} \tag{4.7.7}$$

If a function $P(z, n; X^*)$ is defined as

$$P(z, n; X^*) = \int_0^z (V^*)^n \exp\left(-\frac{\lambda^*}{V^*} X^*\right) f_{V^*} dV^* \tag{4.7.8}$$

then (4.7.1) can be written as

$$\begin{aligned} \left\langle C_f^*(X^*, T^*) \right\rangle = (1 + X^*) &\left[P\left(\frac{X^*+1}{T^*}, 0\right) - P\left(\frac{X^*}{T^*}, 0\right) \right] \\ - T^* &\left[P\left(\frac{X^*+1}{T^*}, 1\right) - P\left(\frac{X^*}{T^*}, 1\right) \right] \end{aligned} \tag{4.7.9}$$

Equation (4.7.8) contains an exponential function due to degradation in the local model. One can perhaps expand the exponential into an infinite series so that

$$P(z, n; X^*) = \sum_{k=0}^{\infty} \frac{(-\lambda^* X^*)^k}{k!} G(z, n-k) \tag{4.7.10}$$

where (see Govindaraju et al., 2001; Jawitz, 2004)

$$G(z,n) = \int_0^z (V^*)^n f_{V^*} dV^* = \exp\frac{n^2\sigma^2}{2}\left[1 - \frac{1}{2}\mathrm{erfc}\left(\frac{\ln z}{\sqrt{2}\sigma} - \frac{n\sigma}{\sqrt{2}}\right)\right] \tag{4.7.11}$$

and $\mathrm{erfc}(\cdot)$ is the complementary error function. Convergence of infinite series as in (4.7.10) is not guaranteed, but a numerical evaluation of $P(z, n; X^*)$ in (4.7.8) is possible with relative ease.

The averaged flux concentration given in (4.7.9) can be used to generate solute breakthrough curves (BTC) at a specified distance away from the source zone. The BTCs at three locations ($X^* = 0.2$, 1.0, and 2.5) are plotted in Figure 4.7.2 for different values of dimensionless degradation parameter, λ^*. Without degradation, the total mass of the solute is conserved. Variability in the velocities causes a widening spread of the BTC as distance increases. The peak concentration decreases as a result. With degradation, the solute decays over time; the area under the BTC decreases over distance. We note that as X^* increases, the curves tend to be more Gaussian-shaped, and the influence of the source variability decreases. The effect of the variation in velocities on the shape of the BTC can be observed in Figure 4.7.3. For small σ, the triangular-shaped curve is a result of the uniform distribution of the solute mass at the source zone. As σ increases, the tailing of the BTC becomes more substantial.

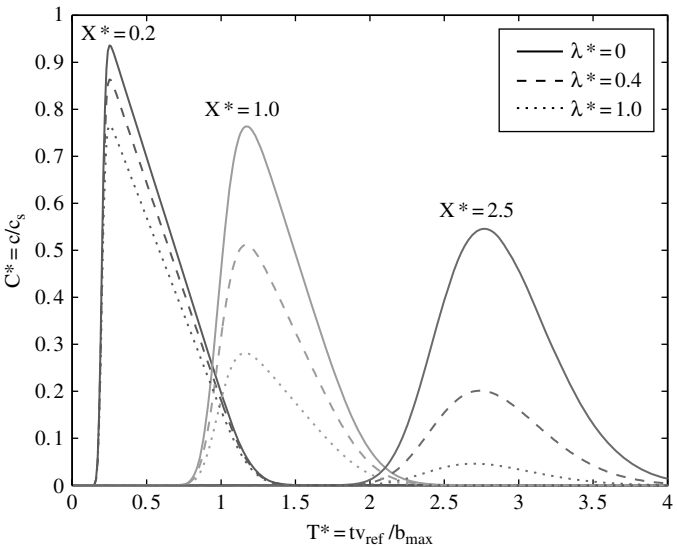

Figure 4.7.2. Solute breakthrough curves at $X^* = 0.2, 1.0$, and 2.5 with varying degradation rate λ^* (adapted from Chan and Govindaraju, 2006, with permission from Elsevier)

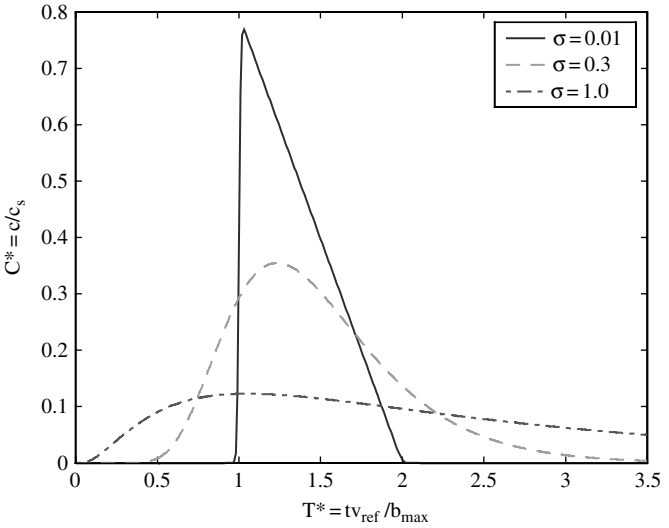

Figure 4.7.3. Influence of velocities variations (σ) on the breakthrough curve (adapted from Chan and Govindaraju, 2006, with permission from Elsevier)

One way to characterize the BTCs shown in Figures 4.7.2 and 4.7.3 is through the use of moments. The moments of travel time to the dimensionless distance X^* are defined as

$$m_n = \int_0^\infty (T^*)^n \langle C_f^*(X^*, T^*)\rangle dT^* \tag{4.7.12}$$

Normalized temporal moments are defined as

$$m_n' = \frac{m_n}{m_0} \tag{4.7.13}$$

Instead of directly integrating (4.7.12), we first take the expectation of $(T^*)^n$ using the local model, which gives

$$\begin{aligned}\langle (T^*)^n; V^*, B^*\rangle &= \int_0^\infty (T^*)^n C_l^*(X^*, T^*) dT^* \\ &= \frac{1}{n+1} \exp\left(-\lambda^* \frac{X^*}{V^*}\right)\left[\left(\frac{X^*+B^*}{V^*}\right)^{n+1} - \left(\frac{X^*}{V^*}\right)^{n+1}\right]\end{aligned} \tag{4.7.14}$$

The ensemble average of the travel time moments is then obtained as

$$m_n = \int_0^\infty \int_0^1 \frac{1}{n+1} \exp\left(-\lambda^* \frac{X^*}{V^*}\right)\left[\left(\frac{X^*+B^*}{V^*}\right)^{n+1} - \left(\frac{X^*}{V^*}\right)^{n+1}\right] f_{B^*} f_{V^*} dB^* dV^* \tag{4.7.15}$$

Specifically, for $n = 0$, 1, and 2, we have

$$\begin{aligned} m_0 &= \frac{1}{2} P(\infty, -1; \lambda^*, X^*); \\ m_1 &= \frac{1}{2}\left(X^* + \frac{1}{3}\right) P(\infty, -2; \lambda^*, X^*); \\ m_2 &= \frac{1}{3}\left(\frac{3(X^*)^2}{2} + X^* + \frac{1}{4}\right) P(\infty, -3; \lambda^*, X^*) \end{aligned} \tag{4.7.16}$$

As defined in (4.7.13), the normalized first and second moments are

$$\begin{aligned} m_1'(X^*) &= \left(X^* + \frac{1}{3}\right) \frac{P(\infty, -2; \lambda^*, X^*)}{P(\infty, -1; \lambda^*, X^*)}; \\ m_2'(X^*) &= \left((X^*)^2 + \frac{2X^*}{3} + \frac{1}{6}\right) \frac{P(\infty, -3; \lambda^*, X^*)}{P(\infty, -1; \lambda^*, X^*)} \end{aligned} \tag{4.7.17}$$

Since the NAPL source is not a delta input in our model, the moments obtained in (4.7.17) must be corrected for the finite input pulse (see Section 5.3 for a detailed discussion). The normalized moments of the input pulse are derived as follows:

$$m_1'(X^* = 0) = \frac{1}{3} \exp\left(\frac{3\sigma^2}{2}\right), \quad m_2'(X^* = 0) = \frac{1}{6} \exp\left(4\sigma^2\right) \tag{4.7.18}$$

Subtracting (4.7.18) from (4.7.17), the corrected normalized travel time moments are

$$\begin{aligned} m_{1,c}' &= m_1' - \frac{1}{3} \exp\left(\frac{3\sigma^2}{2}\right); \\ m_{2,c}' &= m_2' - \frac{1}{6} \exp\left(4\sigma^2\right) \end{aligned} \tag{4.7.19}$$

In this construct, it should be noted that m_0 is not the same as the total solute mass which is given by $P(\infty, 0; X^*)$. As expected, m_0 is constant with no degradation (see Figure 4.7.4a). With degradation, m_0 decreases exponentially and approaches zero asymptotically. Increase in the variance of velocities (σ) raises m_0 for no degradation (Figure 4.7.4b) because the spread of the BTC is increased resulting in an increase in the area under the curve. The same holds true for cases with degradation at locations closer to the source. Moving away from the source, however, results in smaller m_0 for larger σ because more of the slower moving solute is allowed time to decay.

The first moment, m_1, measures the average travel time of the solute from the source to the CP. Without degradation, m_1 increases proportionally with the distance due to advection (see Figure 4.7.5). With degradation, however, m_1 increases and peaks at a certain distance, and eventually approaches zero asymptotically. This is due to the fact that only solute in the higher-velocity tubes can reach the CP before

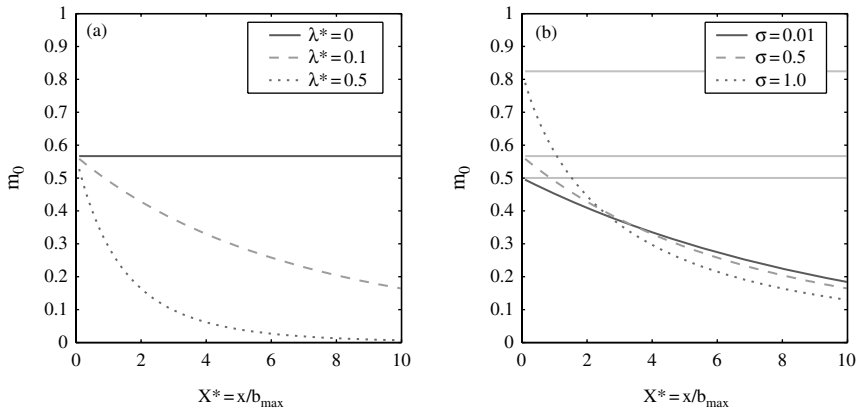

Figure 4.7.4. Zeroth moments (a) for $\sigma = 0.5$ with varying degradation rates; (b) for $\lambda^* = 0.1$ with varying σ (adapted from Chan and Govindaraju, 2006, with permission from Elsevier)

being degraded; therefore, the corresponding travel time is smaller. In Figure 4.7.5b, as σ increases, the larger spread of velocities increases the number of slower tubes and hence biases towards higher travel times.

The spread of the BTC is described by the second moment, m_2. Without degradation, m_2 increases indefinitely as distance increases (see Figure 4.7.6). Variability in velocities and the distribution of solute mass at the source zone both contribute to m_2. Degradation, on the other hand, brings m_2 down and eventually to zero as the plume disappears over a long distance. As expected, increase in σ leads to an increase in m_2.

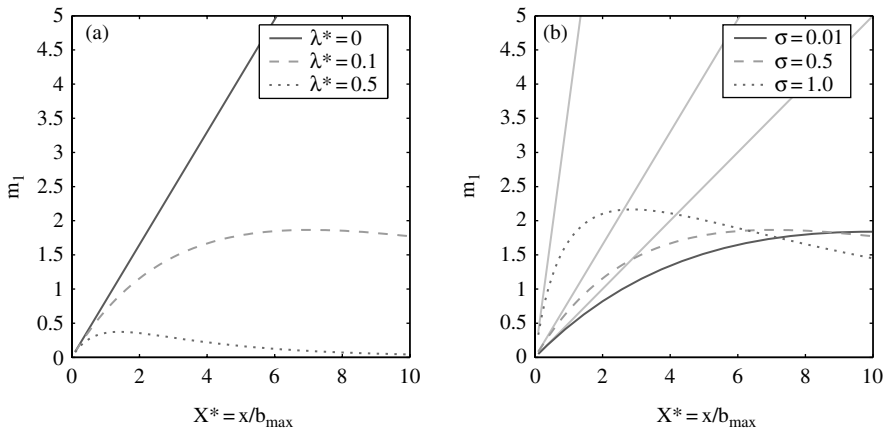

Figure 4.7.5. First moments (a) for $\sigma = 0.5$ with varying degradation rates; (b) for $\lambda^* = 0.1$ with varying σ (adapted from Chan and Govindaraju, 2006, with permission from Elsevier)

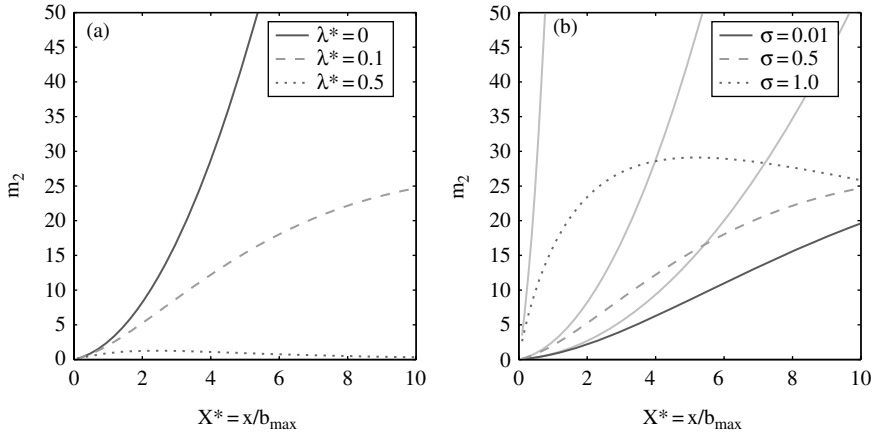

Figure 4.7.6. Second moments (a) for $\sigma = 0.5$ with varying degradation rates; (b) for $\lambda^* = 0.1$ with varying σ (adapted from Chan and Govindaraju (2006) with permission from Elsevier)

Using the definitions in (4.6.9) and (4.6.10), the effective Eulerian velocity is

$$V_{eff} = \frac{P(\infty, -1; \lambda^*, X^*)}{P(\infty, -2; \lambda^*, X^*)} \tag{4.7.20}$$

and the effective dispersion is

$$D_{eff} = \left[\left(\frac{X^* - 1}{2}\right)\frac{P(\infty, -3; \lambda^*, X^*)}{P(\infty, -2; \lambda^*, X^*)} - \left(\frac{X^*}{2}\right)\frac{P(\infty, -2; \lambda^*, X^*)}{P(\infty, -1; \lambda^*, X^*)}\right] V_{eff}^2 \tag{4.7.21}$$

For the proposed model, the effective velocity increases with distance in the presence of degradation as shown in Figure 4.7.7. The effective model is defined with only the advective and dispersive terms. Degradation lowers concentration over time; as a result, the net effect is an increase in the effective velocity. As discussed earlier, increase in σ lowers the effective velocity and such effect is shown in Figure 4.7.7b.

Degradation causes a slight increase in the effective dispersion, probably as an 'enhanced' effect on top of the dispersion resulted from heterogeneity of velocities and the initial uniform distribution of the solute mass at the source zone. It is also interesting to note that if σ is small, the effect degradation has on dispersion is negligible (as shown in Figure 4.7.8). The effective dispersion seems to be of a constant value for $\sigma = 0.01$. The little dispersion is due to the distribution of the source rather than the variability in velocities. Chan and Govindaraju (2006) employed a different definition of effective parameters to incorporate the effect of degradation.

With the proposed model, we can derive the mass fraction of solute remaining at the source zone, f_s, from (4.7.1), and in terms of the dimensionless parameters in (4.7.4) we have

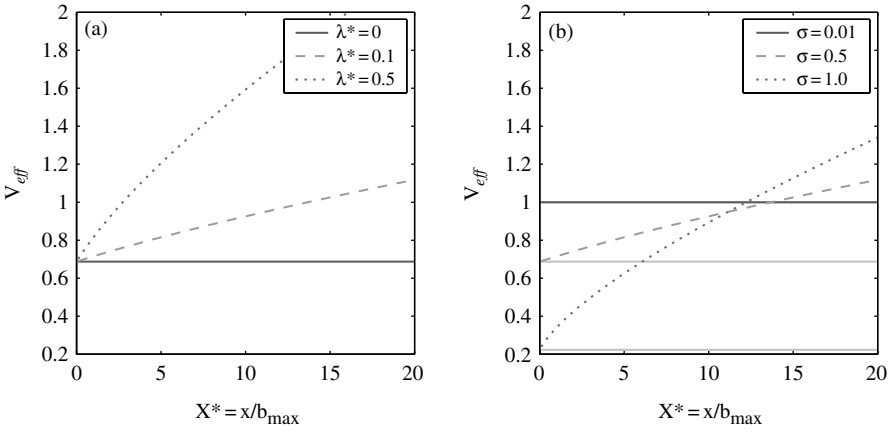

Figure 4.7.7. Effective velocity (a) for $\sigma = 0.5$ with varying degradation rates; (b) for $\lambda^* = 0.1$ with varying σ (adapted from Chan and Govindaraju (2006) with permission from Elsevier)

$$f_s = 1 - \frac{V^* T^*}{B^*} \tag{4.7.22}$$

The ensemble average of f_s over random quantities of V^* and B^*, is

$$\begin{aligned} \langle f_s \rangle &= \int_0^{\frac{1}{T^*}} \int_{V^*T^*}^{1} \left(1 - \frac{V^* T^*}{B^*}\right) f_{B^*} f_{V^*} dB^* dV^* \\ &= \int_0^{\frac{1}{T^*}} \left[1 - V^* T^* + V^* T^* \ln(V^* T^*)\right] f_{v^*} dV^* \end{aligned} \tag{4.7.23}$$

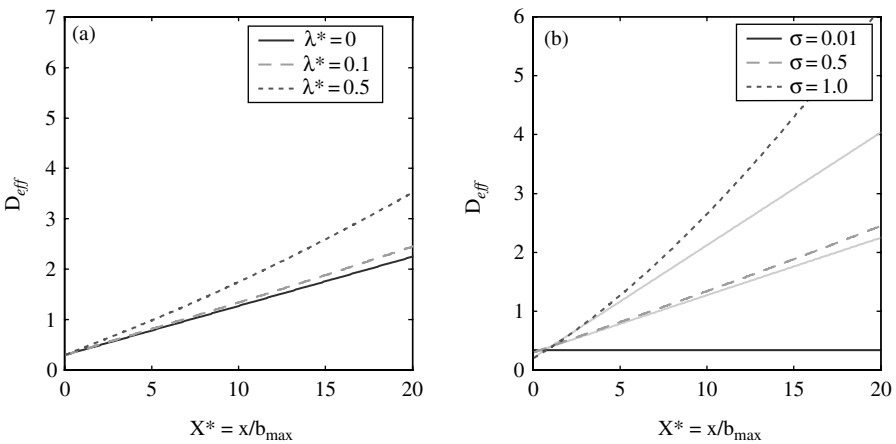

Figure 4.7.8. Effective dispersion (a) for $\sigma = 0.5$ with varying degradation rates; (b) for $\lambda^* = 0.1$ with varying σ (adapted from Chan and Govindaraju (2006) with permission from Elsevier)

Figure 4.7.9a shows the mass fraction of the immobile solute at the source zone. Over time, the mass dissolves and f_s approaches zero asymptotically. The long tail exhibited by larger σ indicates that a small fraction of solute remains at the source and continues to contribute to the dissolved plume. This is evident in Figure 4.7.9b where the BTCs at $X^* = 1$ are plotted. The BTC of $\sigma = 1.0$ have a substantially long tail, which means that it will take a long time to clean up. From the enlarged portion of the tail region, one can see that the concentration is still quite far from the fictitious limit of $C^* = 0.01$ for $T^* \gg 5$. Several studies (Rao and Jawitz, 2003; Jawitz et al., 2005) state that source zone remediation can significantly reduce the mass contaminant flux. For the cases where the velocity variability is high,

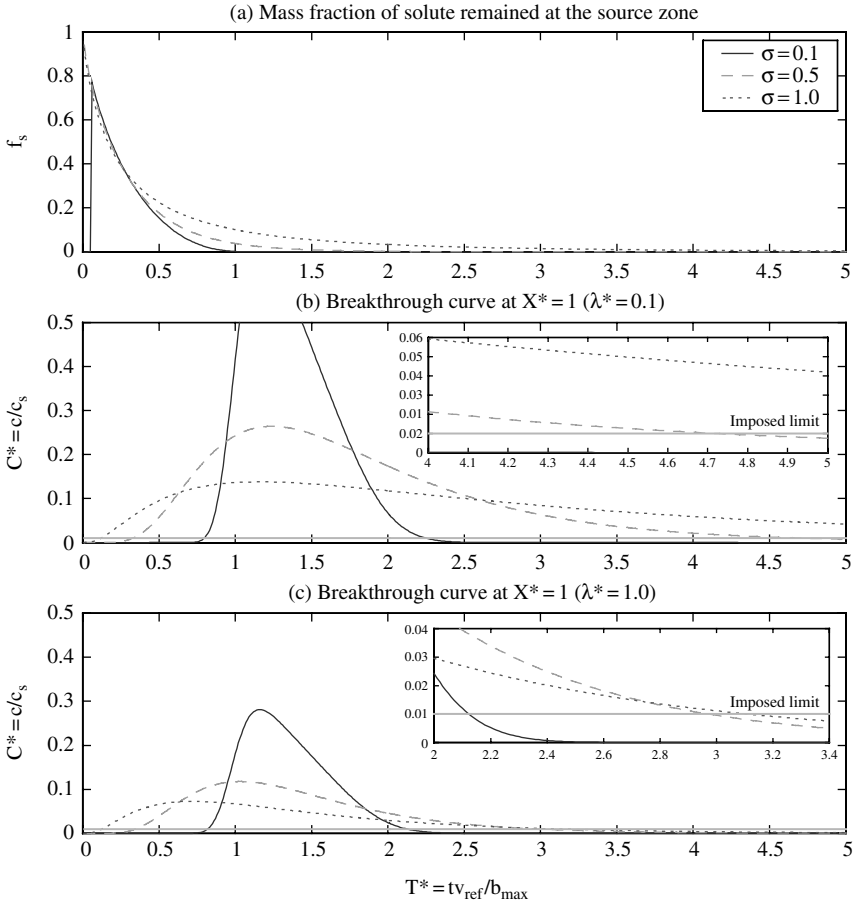

Figure 4.7.9. (a) Mass fraction of the solute remained at the source zone; (b) Breakthrough curve at $X^* = 1$ for $\lambda^* = 0.1$; (c) Breakthrough curve at $X^* = 1$ for $\lambda^* = 1.0$ (adapted from Chan and Govindaraju (2006) with permission from Elsevier)

lower contaminant mass reductions are needed to achieve equivalent reductions in mass flux. The presence of NAPL in the smaller velocity tubes continues to supply tailing concentration that often exceeds regulatory limit. If degradation can be enhanced, such as in the case shown in Figure 4.7.9c, the tailing concentration can then be brought down below the imposed limit, and cleanup time will be significantly reduced.

CHAPTER 5

TEMPORAL MOMENT ANALYSIS FOR SOLUTE TRANSPORT IN POROUS MEDIA

In Chapters 2 and 4, temporal moment analysis was shown to be useful for describing solute breakthrough curves (BTC) measured in a solute transport experiment. Typically, such a transport experiment consists of applying solutes as a finite pulse or as a Dirac input followed by the application of a solute-free background solution. Although strictly finite pulse inputs are not commonly observed in an agricultural field, the practice of fertigation may be treated as finite pulse-type input. A Dirac input refers to the application of input as an impulse, i.e., the entire amount of input is applied instantaneously. Thus, the quick broadcast of fertilizers on agricultural fields may be viewed as a Dirac input. Breakthrough curves resulting from such boundary conditions are usually bell-shaped and closely match a probability distribution function (pdf). As a result, the statistical properties of the measured BTC can be used to assess solute transport processes in soil.

As discussed in Chapter 1, a probability distribution is well characterized by its measures of central tendencies such as mean, variance, skewness, and other higher-order measures. These measures are related to moments of the pdf. Thus, the moments of a solute BTC can be related to the total mass moving through the soil pores (zero-th moment), the mean position (first moment), or the degree of mixing of the solute mass within the porous medium (second moment). In this fashion, the temporal (or time) moments of a solute BTC provide time-averaged responses of solute behavior in soil.

In this chapter, a comprehensive analysis of temporal moments is presented for examining solute transport data. We have assumed simple cases of steady, one-dimensional water transport through homogeneous soil profiles. For a comprehensive treatment, time moment expressions for the general bi-continuum transport model are developed and moments for simpler transport models are derived from these general moment expressions. Although the theoretical treatment in this chapter is restricted to one-dimensional solute transport, it is possible to apply moment analysis to three-dimensional transport scenarios.

5.1. MODEL DESCRIPTIONS AND GOVERNING DIFFERENTIAL EQUATIONS

Mass conservation equations of solute transport relate the rate of change of solute concentration within a representative volume element to the divergence of the solute flux and changes in solute concentrations resulting from other transformation processes involving decay or production of solute within the representative elementary volume (REV)

$$\frac{\partial c_b}{\partial t} + \frac{\partial q_s}{\partial x} = \phi\,(x, t, c_b, \ldots) \tag{5.1.1}$$

where c_b is the resident concentration in bulk volume of soil (ML^{-3}), q_s is the solute flux due to the combined effects of molecular diffusion, hydrodynamic dispersion and advection ($ML^{-2}T^{-1}$), ϕ is the source or sink term ($ML^{-3}T^{-1}$), x is distance (L), and t is time (T). Equation (5.1.1) is a general advection-dispersion equation (ADE) from which models describing specific processes are derived. Some examples were provided in equations (2.4.7) and (2.5.4). As another example, consideration of one-dimensional and steady water flow, uniform soil profile, linear equilibrium sorption, and first-order degradation in the soil solution phase yields the simple ADE representing *local equilibrium assumption* (LEA):

$$R\frac{\partial c}{\partial t} = D\frac{\partial^2 c}{\partial x^2} - V\frac{\partial c}{\partial x} - \gamma c \tag{5.1.2}$$

where $R = 1 + \rho\, k_d/\theta$ is the dimensionless retardation factor, ρ is the dry soil bulk density (ML^3), k_d is the distribution coefficient for linear sorption ($M^{-1}L^{-3}$), D is the dispersion coefficient (L^2T^{-1}), V is the pore water velocity (LT^{-1}), and γ is the first-order degradation rate coefficient in the soil solution phase (T^{-1}).

The LEA-based ADE is a simplistic representation of solute transport and often fails to capture the commonly observed rate-limited mass transfer processes in soil. For instance, many hydrophobic organic compounds such as pesticides, polycyclic aromatic hydrocarbons (PAHs) and other emerging contaminants tend to show a slower rate of mass transfer through soil relative to non-reactive solutes. Such mass transfer limitations result in a skewed BTC and cannot be described by the LEA-based ADE, and require use of kinetic or nonequilibrium models. In addition to the inherent chemical nature of solute and sorbent, the physical soil pore structure also yields nonequilibrium-like behavior, specifically in structured soils. A general class of models describing such behavior is the bi-continuum transport models. This category of models describes the rate-limited mass transfer processes arising either because of physical or chemical limitations to mass transfer. Some of these models (MIM, PNE, CNE, and DSG) are briefly discussed in Chapter 2.

In the bi-continuum modeling approach, it is assumed that solutes move at two different rates in two distinctly different pore regimes in soil: the mobile pore water region and the immobile pore water region. Linear, equilibrium sorption is assumed in each region and mass transfer from the mobile to the immobile region is modeled

as a first-order kinetic process (van Genuchten, 1974). Thus, solute transport through such dual-porosity soil pores is modeled with a physical nonequilibrium (PNE) model (van Genuchten and Wagenet, 1989) as described in Section 2.8. Assuming steady-state water flow, the general form of the advection-dispersion equation for the PNE model may be written as

$$(\theta_m + f\,\rho k_d)\,\frac{\partial c_m}{\partial t} = \theta_m D_m \frac{\partial^2 c_m}{\partial x^2} - q\frac{\partial c_m}{\partial x} - \alpha(c_m - c_{im}) - (\theta_m \gamma_{l,m} + f\,\rho k_d \gamma_{s,m})c_m \tag{5.1.3}$$

$$[\theta_{im} + (1-f)\rho k_d]\,\frac{\partial c_{im}}{\partial t} = \alpha(c_m - c_{im}) - \left[\theta_{im}\gamma_{l,m} + (1-f)\rho k_d \gamma_{s,im}\right] c_{im} \tag{5.1.4}$$

where c is the volume-averaged concentration (ML^{-3}); θ is the volumetric water content (L^3L^{-3}); f is the fraction of sorption sites that equilibrate with the mobile liquid phase; ρ is the dry soil bulk density (ML^{-3}); k_d is the distribution coefficient for linear sorption ($M^{-1}L^3$); D is the dispersion coefficient (L^2T^{-1}); q is the steady-state volumetric water flux density (LT^{-1}); α is the first-order kinetic rate constant (T^{-1}); γ is the degradation rate constant (T^{-1}); x is distance (L); t is time (T); the subscripts m and im represent the mobile and the immobile liquid region, respectively; and the subscripts l and s refer to the liquid and the solid phase, respectively.

Similar to the two distinct pore domains in the PNE model, the soil solids or more precisely, the sorption sites in the solid phase are viewed as two distinct types in a chemical nonequilibrium (CNE) model. For example, the two-site CNE model (Section 2.9) assumes the presence of equilibrium and kinetic sorption sites in the solid matrix. Linear, equilibrium sorption occurs in the equilibrium sorption sites, and a first-order kinetic sorption occurs in the kinetic sorption sites (Selim et al., 1977). Assuming steady-state water flow, the general form of advection-dispersion equation for the CNE model may be written as

$$\left(1 + \frac{f\rho k_d}{\theta}\right)\frac{\partial c}{\partial t} = D\frac{\partial^2 c}{\partial x^2} - V\frac{\partial c}{\partial x} - \frac{\alpha\rho}{\theta}\left[(1-f)k_d c - s_k\right] - \gamma_l c - \frac{f\rho k_d \gamma_{s,e} c}{\theta} \tag{5.1.5}$$

$$\frac{\partial s_k}{\partial t} = \alpha\left[(1-f)k_d c - s_k\right] - \gamma_{s,k} s_k \tag{5.1.6}$$

where the subscripts e and k refer to the equilibrium and kinetic sorption sites, respectively; and s_k is the concentration in the sorbed phase (MM^{-1}). Detailed development of these two transport models is presented by van Genuchten and Wagenet (1989). Nkedi-Kizza et al. (1984) showed that both the PNE and the CNE models can be represented by a single transport equation in dimensionless form by choosing different dimensionless quantities (Table 5.1.1),

$$\beta\, R\frac{\partial C_1}{\partial T} = \frac{1}{P}\frac{\partial^2 C_1}{\partial Z^2} - \frac{\partial C_1}{\partial Z} - \omega\,(C_1 - C_2) - \gamma_1 C_1 \tag{5.1.7}$$

Table 5.1.1. Dimensionless Parameters for the Physical and Chemical Nonequilibrium Models of van Genuchten and Wagenet (1989) (adapted from Das et al., 2002, with permission from ASCE Press)

Parameter	CNE model	PNE model
T	Vt/L	Vt/L
Z	x/L	x/L
R	$1+\rho k_d/\theta$	$1+\rho k_d/\theta$
P	VL/D	$V_m L/D_m$
β	$(\theta+f\rho k_d)/(\theta+\rho k_d)$	$(\theta_m+f\rho k_d)/(\theta+\rho k_d)$
ω	$\alpha(1-\beta)RL/V$	$\alpha L/\theta V$
γ_1	$\left(\theta\gamma_l+f\rho k_d\gamma_{s,e}\right)L/\theta V$	$\left(\theta_m\gamma_{l,m}+f\rho k_d\gamma_{s,m}\right)L/\theta V$
γ_2	$(1-f)\rho k_d\gamma_{s,k}L/\theta V$	$\left[\theta_{im}\gamma_{l,im}+(1-f)\rho k_d\gamma_{s,im}\right]L/\theta V$
C_1	c/c_0	c_m/c_0
C_2	$s_2/[(1-f)k_d c_0]$	c_{im}/c_0

$$(1-\beta)R\frac{\partial C_2}{\partial T}=\omega(C_1-C_2)-\gamma_2 C_2 \tag{5.1.8}$$

where C_1 and C_2 are dimensionless concentrations; P is the column Peclet number; T and Z are dimensionless time and length, respectively; R is the retardation factor; β is the fraction of equilibrium sorption sites; ω is the Damkohler number; and γ_1 and γ_2 are dimensionless degradation rate constants.

Equations (5.1.7) and (5.1.8) serve as a general system of nonequilibrium transport equations with degradation and will be referred to as the nonequilibrium transport (NE) model. For solutes obeying local equilibrium assumption (LEA), these two equations can also be reduced to an equilibrium transport model. For example, under equilibrium (single-domain) transport condition, equation (5.1.8) vanishes for $\beta=1$ and $\omega=0$, and equation (5.1.7) reduces to

$$R\frac{\partial C_1}{\partial T}=\frac{1}{P}\frac{\partial^2 C_1}{\partial Z^2}-\frac{\partial C_1}{\partial Z}-\gamma_1 C_1 \tag{5.1.9}$$

with $f=1$ substituted in the definition for γ_1 in Table 5.1.1. Note that this equation is the dimensionless form of Equation (5.1.2).

Although analytical solutions to the above set of equations for different initial and boundary conditions are available (Toride et al., 1993), we are interested in deriving moment expressions for effectively describing measured solute BTCs. We have stated earlier that a pulse-type or a Dirac input boundary (concentration at $x=0$) condition is required to apply the MOM. Both of these boundary conditions can also be compactly represented by

$$C_1(0,T)=f(T) \tag{5.1.10}$$

For a pulse of finite duration, $f(T)=H(T)-H(T+\Delta T)$ where $H(T)$ is the unit step function. For a Dirac delta input, $f(T)=\delta(T)$ (Valocchi, 1985). Both of these input boundary conditions are similar and a simple translation of moments accounting for

the duration of input (pulse) application may be performed to derive moment expressions for pulse-type boundary condition from moments for the Dirac-type boundary condition as shown in Section 5.3. The choice of the top (or input) boundary condition is also dependent on the way the solute is introduced into soil. Equation (5.1.10) is a first-type boundary condition and is used to model flux-type concentration observed in transport experiments. For representing a resident concentration, often a mixed boundary condition

$$\left(C_1 - \frac{1}{P}\frac{\mathrm{d}C_1}{\mathrm{d}Z}\right)\Bigg|_{Z\to 0} = f(T) \tag{5.1.11}$$

is required. For the outflow boundary condition (concentration at $x = L$), it is convenient to assume a zero concentration gradient far away from $x = L$:

$$\left.\frac{\partial C_1}{\partial Z}\right|_{Z\to\infty} = 0 \tag{5.1.12}$$

for deriving moment expressions. Similarly, an initially solute-free soil as an initial condition

$$C_1(Z, 0) = C_2(Z, 0) = 0 \tag{5.1.13}$$

is convenient for deriving moment expressions. For cases with uniformly distributed solute in soil at $t = 0$, a simple linear translation for initial solute concentration can be made and then the rest of the moment expressions can be adopted.

5.2. TEMPORAL MOMENT DEFINITIONS

In Chapter 1, the theory of moments and moment generating functions in relation to probability distributions is presented. Direct relationships exist between the probability $P(X)$ of a pdf and concentration c of a chemical moving through a porous medium. For example, consider one dimensional flow of water and solute through a finite soil column of length L and cross sectional area A. Assuming steady-state water flow and employing transfer function concepts, it is possible to show that the solute concentrations at the inlet boundary ($x = 0$) and outlet boundary ($x = L$) are related through the expression

$$c(L, t) = \int_0^t c(0, \tau_{in}) f\,(L, t - \tau_{in} | \tau_{in})\, d\tau_{in} \tag{5.2.1}$$

where $f(L, t{-}\tau_{in}|\tau_{in})$ is the probability density function for solute travel time, and the quantity τ_{in} is the lifetime of a solute molecule introduced into the soil column at time τ_{in}. When the total mass of solute M is instantaneously applied to a unit cross sectional area at the inlet boundary ($x = 0$) in the presence of a steady water flow, a Dirac delta type boundary condition (Valocchi, 1985),

$$c(0, t) = \frac{M}{\theta L}\delta(t) \tag{5.2.2}$$

can be substituted into Equation (5.2.1) and the resulting expression can be simplified to

$$f(L,t) = \frac{c(L,t)}{\int_0^\infty c(L,\tau)d\tau} = \frac{Qc(L,t)}{\int_0^\infty Qc(L,\tau)d\tau} \tag{5.2.3}$$

Here, θ is the volumetric water content ($L^3\ L^{-3}$), and x and t are length (L) and time (T), respectively. We have explicitly shown the volumetric water flux, Q ($L^3\ T^{-1}$), in Equation (5.2.3) to indicate that the relative solute concentration or the relative solute mass can be treated as a solute travel time pdf if the solute is applied instantaneously to the inlet boundary with a steady stream of water.

Once the probabilistic nature of solute concentrations is established, the statistical properties of moments illustrated in Chapter 1 may be applied to study solute transport simply by replacing X with a time variable and $P(X)$ with relative concentration. As before, absolute time moments are defined as

$$\mu_n = \int_0^\infty T^n C(Z,T)dT \tag{5.2.4}$$

where μ_n is the absolute temporal (time) moment of order n. For convenience, we have used dimensionless length variable Z and dimensionless time variable T in addition to relative concentration C in Equation (5.2.3). In principle, the relative concentration C equals the probability density f shown in Equation (5.2.3) and is defined as the ratio between concentrations measured in effluent at a given time and the cumulative concentration recovered in effluent during a leaching experiment. For a nondegrading solute, the cumulative concentration recovered in the effluent equals the total amount of solute added [$= M/(\theta L)$] to a soil column with the steady stream of input solution in an experiment if the experiment is run for long enough time such that all the solute molecules applied are eluted out of soil column.

In addition to the absolute moments defined in Equation (5.2.4), two other quantities, the normalized absolute moment

$$\mu_n^* = \frac{\mu_n}{\mu_0} \tag{5.2.5}$$

and the central moments

$$m_n = \frac{1}{\mu_0}\int_0^\infty (T-\mu_1^*)^n\ C(Z,T)dT \qquad n \geq 2 \tag{5.2.6}$$

are also frequently used to characterize solute BTCs. The central moments and normalized absolute moments are related through the well-known formula (Kendall and Stuart, 1977):

$$m_n = \sum_{r=0}^{n} \binom{n}{r} \mu_{n-r}^* (-\mu_1^*)^r \qquad n \geq 2 \tag{5.2.7}$$

Table 5.2.1. Expressions for central moments of order 2 to 10 (from Das et. al., 2002, with permission from ASCE in press)

$$m_2 = \mu_2^* - \mu_1^{*^2}$$
$$m_3 = \mu_3^* - 3\mu_2^*\mu_1^* + 2\mu_1^{*^3}$$
$$m_4 = \mu_4^* - 4\mu_3^*\mu_1^* + 6\mu_2^*\mu_1^{*^2} - 3\mu_1^{*^4}$$
$$m_5 = \mu_5^* - 5\mu_4^*\mu_1^* + 10\mu_3^*\mu_1^{*^2} - 10\mu_2^*\mu_1^{*^3} + 4\mu_1^{*^5}$$
$$m_6 = \mu_6^* - 6\mu_5^*\mu_1^* + 15\mu_4^*\mu_1^{*^2} - 20\mu_3^*\mu_1^{*^3} + 15\mu_2^*\mu_1^{*^4} - 5\mu_1^{*^6}$$
$$m_7 = \mu_7^* - 7\mu_6^*\mu_1^* + 21\mu_5^*\mu_1^{*^2} - 35\mu_4^*\mu_1^{*^3} + 35\mu_3^*\mu_1^{*^4} - 21\mu_2^*\mu_1^{*^5} + 6\mu_1^{*^7}$$
$$m_8 = \mu_8^* - 8\mu_7^*\mu_1^* + 28\mu_6^*\mu_1^{*^2} - 56\mu_5^*\mu_1^{*^3} + 70\mu_4^*\mu_1^{*^4} - 56\mu_3^*\mu_1^{*^5} + 28\mu_2^*\mu_1^{*^6} - 7\mu_1^{*^8}$$
$$m_9 = \mu_9^* - 9\mu_8^*\mu_1^* + 36\mu_7^*\mu_1^{*^2} - 84\mu_6^*\mu_1^{*^3} + 126\mu_5^*\mu_1^{*^4} - 126\mu_4^*\mu_1^{*^5} + 84\mu_3^*\mu_1^{*^6} - 36\mu_2^*\mu_1^{*^7} + 8\mu_1^{*^9}$$
$$m_{10} = \mu_{10}^* - 10\mu_9^*\mu_1^* + 45\mu_8^*\mu_1^{*^2} - 120\mu_7^*\mu_1^{*^3} + 210\mu_6^*\mu_1^{*^4} - 250\mu_5^*\mu_1^{*^5} + 210\mu_4^*\mu_1^{*^6} - 120\mu_3^*\mu_1^{*^7} + 45\mu_2^*\mu_1^{*^8} - 9\mu_1^{*^{10}}$$

Higher-order central moments are easily derived from Equation (5.2.7) when expressions for normalized absolute moments are known. Expanded expressions for the first few central moments are shown in Table 5.2.1.

We noted earlier that moments describe the central tendency of probability distributions. Of n possible moments, the first four ($n = 0, 1, 2, 3$) are frequently used to describe the central tendency of a distribution. These first four moments correspond to the total mass density, arithmetic mean, variance, and skewness of the distribution, respectively. For solute transport in a finite soil column, the zeroth absolute time moment, μ_0, of the effluent breakthrough curve (BTC) is a measure of the total mass eluted from the soil column during the leaching event (Skopp, 1985). The first absolute time moment, μ_1, of the BTC is a measure of the average time solute molecules spend inside the column (Skopp, 1985). The second absolute time moment, μ_2, is a measure of the variance of the BTC. Variance in this case describes solute spreading in the soil column, a process attributed to diffusion, hydrodynamic dispersion, time variation of the input concentration, kinetic sorption (Valocchi, 1989), and macrodispersion (Gelhar and Axness, 1983; Dagan, 1986). The third absolute time moment, μ_3, is a measure of the skewness of the concentration distribution. Skewness in this case describes the asymmetry of the solute distribution (Skopp, 1985), a process attributed to the deviation of the flow process from flow ideality. Concentration distributions resemble a symmetric Gaussian distribution under ideal flow conditions in long columns.

5.3. ARIS'S METHOD OF MOMENT ANALYSIS

Theoretical time moments are easily computed using the method developed by Aris (1958). From the definition of the Laplace transform

$$\hat{C}_1(Z; s) = \int_0^\infty e^{-sT} C_1(Z, T) dT \tag{5.3.1}$$

we can show that

$$\int_0^\infty T^n C_1(Z,T)e^{-sT}\,dT = (-1)^n \frac{\mathrm{d}^n}{\mathrm{d}s^n}\left[\int_0^\infty C_1(Z,T)e^{-sT}\,\mathrm{d}T\right] \tag{5.3.2}$$

where $\hat{C}_1(Z;s)$ is the Laplace transform of $C_1(Z,T)$ and s is the transformation variable (T^{-1}). Setting $s=0$ in Equation (5.3.2) yields

$$\int_0^\infty T^n C_1(Z,T)dT = (-1)^n \underset{s\to 0}{\mathrm{Lim}}\left\{\frac{\mathrm{d}^n}{\mathrm{d}s^n}\left[\hat{C}_1(Z;s)\right]\right\} \tag{5.3.3}$$

Substituting (5.3.2) into (5.3.3) yields a specific computational formula for the absolute time moment

$$\mu_n = (-1)^n \underset{s\to 0}{\mathrm{Lim}}\left\{\frac{\mathrm{d}^n}{\mathrm{d}s^n}\left[\hat{C}_1(Z;s)\right]\right\} \tag{5.3.4}$$

Equation (5.3.4) can be solved for μ_n when an expression for $\hat{C}_1(Z;s)$ is available.

The Laplace transforms of Equations (5.1.7) and (5.1.8) result in an ordinary differential equation (ODE). The solution of the ODE and the use of boundary and initial data yield the Laplace-domain solution for $\hat{C}_1(Z;s)$:

$$\hat{C}_1(Z,s) = \hat{f}(s)\exp\left[Z\lambda(s)\right] \tag{5.3.5}$$

where $\lambda(s)$ is given by

$$\lambda(s) = \frac{P}{2} - \left\{\frac{P^2}{4} + P\left[\frac{\omega sR(1-\beta)+\omega\gamma_2}{sR(1-\beta)+\gamma_2+\omega} + \gamma_1 + sR\beta\right]\right\}^{1/2} \tag{5.3.6}$$

and $\hat{f}(s)$ is derived by taking the Laplace transform of $f(T)$. For a Dirac delta type input condition, $\hat{f}(s)=1.0$. For this case, Equation (5.3.5) is directly substituted into Equation (5.3.4) and the results can be combined with Equation (5.2.5) and Equation (5.2.7) to yield specific expressions for time moments. Expressions for the first five time moments for $Z=1$ are:

$$m_0 = \mu_0 = \exp\left(\frac{P-\eta}{2}\right) \tag{5.3.7}$$

$$m_1 = \mu_1^* = \frac{\xi_1}{\eta} \tag{5.3.8}$$

$$m_2 = \frac{\xi_2}{\eta} + \frac{2m_1^2}{\eta} \tag{5.3.9}$$

$$m_3 = \frac{\xi_3}{\eta} + \frac{6m_1m_2}{\eta} \tag{5.3.10}$$

$$m_4 = \frac{\xi_4}{\eta} + \frac{6m_2^2}{\eta} + \frac{8m_1m_3}{\eta} \tag{5.3.11}$$

where the parameters η and ξ are defined in Table 5.3.1 for different sorption and degradation scenarios. Note that two additional symbols m_0 and m_1 have been introduced in Equation (5.3.7) and (5.3.8) for notational simplicity, although m was earlier defined with subscript $n > 1$. The recursive formula

$$m_n = \frac{Z}{\eta}\left[\xi_n + \frac{1}{Z^2}\sum_{i=1}^{n-1}\frac{n!}{i!(n-i)!}m_i m_{n-i}\right]; \qquad n = 2, 3, \ldots \tag{5.3.12}$$

can be used to develop similar expressions for higher-order moments.

Time moment expressions derived in this section are valid when a measured solute BTC may be viewed as a residence time distribution (RTD) function. The RTD characterizes the distribution of travel times (or residence times) for pure tracer molecules during transport through soil column. Experimentally, if molecules of a solute are simultaneously introduced at the inlet end of a soil column during steady water flow [an input boundary condition approximating a Dirac delta function, $\delta(T)$], the RTD would describe how long each of the molecules stay inside the soil column. Thus, when a pure tracer is applied at the inlet boundary of soil column as $\delta(T)$, the effluent concentration distribution may be viewed as a RTD. In the above derivations, we have estimated moments assuming a Dirac delta-type input boundary condition. Therefore, the requirement for the RTD assumption is inherently met.

For generalized transfer functions such as for a finite pulse-type input boundary condition, Valocchi (1985) showed that moment expressions can easily be derived using a simple linear translation with the moments of the input conditions:

$$\mu_1^* = \mu_1^*(L) = \mu_1^*(0) \tag{5.3.13}$$

$$m_n = m_n(L) - m_n(0) \tag{5.3.14}$$

where the arguments in the parentheses indicate moment expressions evaluated at $Z = L$ and $Z = 0$, respectively. Note that the moments indicated in the right-hand

Table 5.3.1. Parameters η and ξ for four different limiting cases of reaction and transformation processes (Das et. al., 2002)

Parameter	Nonequilibrium sorption and first-order degradation [ND]	Equilibrium sorption and first-order degradation [ED]	Nonequilibrium sorption and no degradation [N]	Equilibrium sorption and no degradation [E]
η	$\left[P^2 + 4P\left(\frac{\omega\gamma_2}{\omega+\gamma_2} + \gamma_1\right)\right]^{1/2}$	$(P^2 + 4P\gamma)^{1/2}$	P	P
ξ_1	$P\beta R + \frac{\omega^2 P[(1-\beta)R]}{(\omega+\gamma_2)^2}$	PR	PR	PR
ξ_n	$\frac{n!\omega^2 P[(1-\beta)R]^n}{(\omega+\gamma_2)^{n+1}}$	0	$\frac{n!P[(1-\beta)R]^n}{\omega^{n-1}}$	0

side of these two equations represent moments for the pulse-type boundary condition while those in the left-hand side represent moments for the resulting RTD. It may also be noted that the second term on the right-hand side of these two equations is zero for the Dirac delta-type input condition showing that Equation (5.3.13) and (5.3.14) is the trivial case when a BTC conforms to the RTD. Figure 5.3.1 further illustrates this concept using the first normalized moment as an example.

Three quantities viz., mean travel time (t_r), mean breakthrough time (t_{br}), and the first normalized moment are shown in this figure for the Dirac delta- (Figure 5.3.1A) and finite pulse-type (Figure 5.3.1B) input conditions. Mean breakthrough time is defined as the duration from time = 0 till the time when the center of the solute

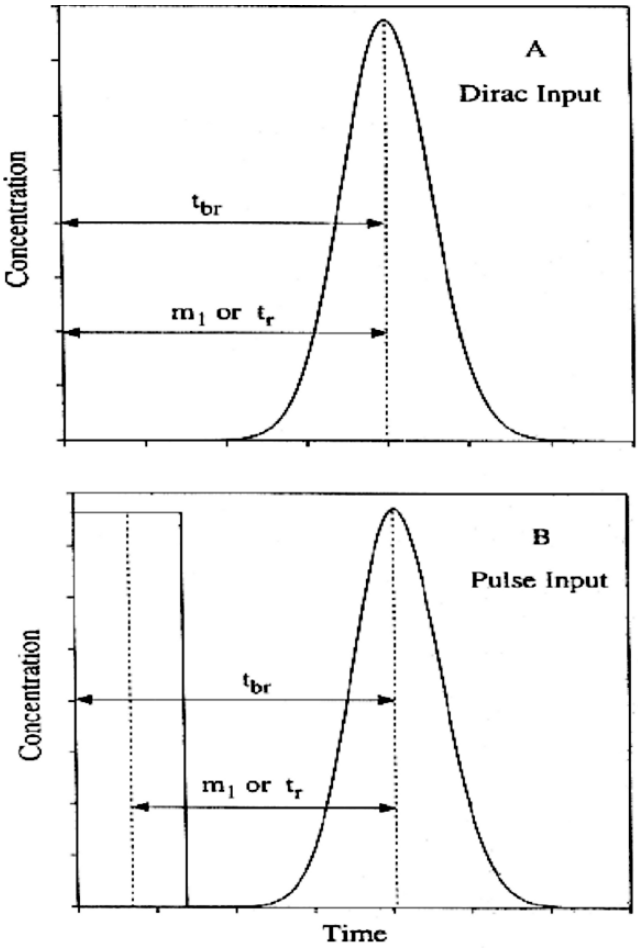

Figure 5.3.1. Relationship among mean travel time, mean breakthrough time, and the first normalized first moment of a breakthrough curve

mass exits the outflow end of soil column irrespective of the method of solute application. Mean travel time is defined as the average time taken for the solute to travel from the inlet end to the outflow end. Observe that $t_r = t_{br} = m_1$ for the Dirac input conditions. For the pulse-type input condition, $t_r = m_1$ while t_{br} is shown to be larger than t_r by the quantity equal to half of the pulse width. Indeed, half the pulse width is the first normalized moment of the finite pulse-type input condition, and t_{br} in Figure 5.3.1B is the first term in the right-hand side of Equation (5.3.13).

Moment formulas presented above are valid if time and length variables are expressed as dimensionless quantities; for real time and real length scales, moments may be obtained by using the following transformation,

$$m_n^r = \left(\frac{L}{V}\right)^n m_n \tag{5.3.15}$$

where m_n^r represents time moments for real time and length scales.

Equation (5.3.12) applies only when solute is applied as Dirichlet-type input (Equation 5.1.10) or, in other words, the concentration is viewed as a flux-averaged quantity as discussed in Chapter 2 (Parker and van Genuchten, 1984). Although the governing differential equations are written in terms of resident concentrations, the effluent concentration is measured as a flux-averaged concentration (Parker and van Genuchten, 1984). Because in many laboratory-scale leaching experiments, flux-averaged concentration is of primary interest, we have chosen to discuss moments for flux type concentrations. To generate moment formulas for volume-averaged or resident concentrations (Kreft and Zuber, 1978), the steps discussed above should be repeated with the mixed-type boundary condition shown in Equation (5.1.11). Alternatively, the following relationship can be employed directly to obtain moments for the volume-averaged or resident concentrations,

$$\mu_n^v = \sum_{k=0}^{n} \frac{n!}{k!(n-k)!} V_{n-k} \mu_k^f \tag{5.3.16}$$

where μ_n^v and μ_n^f are the absolute time moments for volume-averaged and flux-averaged concentrations, respectively, and V_n is given by:

$$V_n = (-1)^n \operatorname*{Lim}_{s\to 0} \left\{ \frac{\mathrm{d}^n}{\mathrm{d}s^n} \left[\frac{P}{P - \lambda(s)} \right] \right\} \tag{5.3.17}$$

and $\lambda(s)$ is given by Equation (5.3.6). Expressions for first few moments are as follows:

$$m_0^v = \frac{\mu_0^v}{T_0} = \frac{2P}{P+\eta} \exp\left(\frac{P-\eta}{2}\right) = \frac{2P}{P+\eta} m_0^f \tag{5.3.18}$$

$$m_1^v = \left(1 + \frac{2P}{P+\eta}\right) m_1^f \tag{5.3.19}$$

$$m_2^v = \left(1 + \frac{2P}{P+\eta}\right) m_2^f + \left(\frac{2m_1^f}{P+\eta}\right)^2 \tag{5.3.20}$$

$$m_3^v = \left(1 + \frac{2P}{P+\eta}\right) m_2^f + 3\left(\frac{2}{P+\eta}\right)^2 m_1^f\, m_2^f + 2\left(\frac{2m_1^f}{P+\eta}\right)^3 \tag{5.3.21}$$

where η is defined as before. The superscripts v and f have been used to distinguish moments for volume-averaged and flux-averaged concentrations, respectively. Note that the specific moment expressions for volume-averaged concentrations are increasingly complex.

5.4. COMPUTING TIME MOMENTS FROM EXPERIMENTAL DATA

In this section, we outline the steps for estimating time moments from measured BTCs. Example calculations on four sets of laboratory-scale leaching data covering both saturated (Das, 1996) and unsaturated flow conditions are discussed. This topic was briefly considered in Section 1.9 in the context of parameter estimation.

5.4.1 Experimental Data

For the saturated flow experiment, a uniformly packed soil column (length = 30 cm, internal diameter = 6.03 cm) was saturated with 0.001 M $CaSO_4$ solution over a period of three days. Steady-state flow rate was maintained by controlling q and θ. The resulting pore water velocity ($V = q/\theta$) was 1.403 cm h^{-1}. After steady-state flow was established, a tracer solution containing 2.59×10^3 Bq mL^{-1} tritiated water and 7.40×10^2 Bq mL^{-1} ^{14}C-labeled atrazine (3.77 mg L^{-1}) was leached through the soil column for a period of 25 h. Then the input solution was switched back to the 0.001 M $CaSO_4$ solution. The experiment was continued until the ^{14}C concentration in the effluent was below 5.0 Bq mL^{-1}. The effluent concentration (flux-averaged) was measured using scintillation spectrometry.

For the unsaturated flow experiment, a uniformly packed soil column (length = 10.9 cm, internal diameter = 15.3 cm) was connected to a vacuum chamber to maintain a constant matric potential of –15 kPa at the column's bottom boundary. A constant flow rate was maintained by applying a steady stream of solution containing 0.125 dS m^{-1} KCl. The resulting θ was 0.36 $cm^3\, cm^{-3}$ (degree of saturation = 77%) and the pore water velocity ($V = q/\theta$) was 1.207 cm h^{-1}. After steady-state flow was established, a tracer solution containing 1.69 dS m^{-1} KCl solution was leached through the soil column for a period of 11.25 h. Then the input solution was switched back to the 0.125 dS m^{-1} KCl solution. The effluent concentration (flux-averaged) was measured using an EC meter. The volume-averaged concentration was also measured by monitoring the bulk electrical conductivity (Wraith et al., 1993; Risler et al., 1996; Wraith and Das, 1998) with a time-domain

reflectometry (TDR) probe inserted horizontally at 6.9 cm measured from the top of the soil.

5.4.2 Computing Moments from Observed Data

Experimental time moments are conveniently estimated from BTCs expressed in terms of dimensionless time T and dimensionless depth Z. Equation (5.2.4) is evaluated in a numerical integration technique such as the trapezoidal rule to estimate absolute experimental time moments. The absolute moments are then substituted into Equation (5.2.5) and (5.2.6) to estimate normalized moments and central moments, respectively. The resulting moment values can be transformed to moments for dimensionalized variables using Equation (5.3.15). Moments can also be modified according to Equation (5.3.13) and (5.3.14) to account for the input pulse width if necessary. Note that the necessity to use Equation (5.3.13) and (5.3.14) arises only when the experimental and the theoretical moments for a given experimental condition are matched. We shall provide an example of matching experimental moments with theoretical moments when we present examples of parameter estimation (see also Section 1.9). When reporting moments, it should be indicated whether or not moments are corrected for the pulse width.

Two different integration schemes are reported for estimating experimental moments from measured BTCs (Haas, 1996): the trapezoidal rule,

$$\mu_n = \frac{\sum_{i=2}^{m} 0.5\,(T_i^n C_i + T_{i-1}^n C_{i-1})\,(T_i - T_{i-1})}{\sum_{i=2}^{m} 0.5\,(C_i + C_{i-1})\,(T_i - T_{i-1})} \tag{5.4.1}$$

and the inertia method,

$$\mu_n = \frac{\sum_{i=2}^{m} \left(\frac{T_i + T_{i-1}}{2}\right)^n \left(\frac{C_i + C_{i-1}}{2}\right)(T_i - T_{i-1})}{\sum_{i=2}^{m} \left(\frac{C_i + C_{i-1}}{2}\right)(T_i - T_{i-1})} \tag{5.4.2}$$

where m is the total number of data points, and T_i and C_i are the i^{th} time and concentration observations, respectively. The trapezoidal rule is a commonly used (Misra and Mishra, 1977; Jacobsen et al., 1992) and is an unbiased (Haas, 1996) integration scheme for estimating moments from experimental data. Using synthetic data sets, Haas (1996) showed that the inertia method is more biased than the trapezoidal method. Recently, Das et al. (2005) used these two integration schemes to estimate moments for 85 BTCs collected from repacked and undisturbed soil columns and from field-scale leaching experiments. Their results show that the difference in the estimated moments by these two methods slightly increases with the order of the moments, but the differences are not significant. Das et al. (2005) concluded that either of these methods may be used for estimating moments from

experimental data as long as high resolution (close proximity) solute concentration histories are available. For the example datasets, the simpler inertia method has been used to compute moments as was done by Jacobsen et al. (1992). Note that computer subroutines are also available to estimate moments from observed data sets (Press et al., 1989).

Table 5.4.1 lists results of moment calculations for the tritiated water, atrazine and KCl BTCs shown in Figure 5.4.1. The pulse widths and the mass recovery fraction (= ratio of the total mass recovered in the effluent to the total mass applied to the inlet end of the column) are listed for each BTC in the table. Because the BTCs in Figure 5.4.1 are presented in dimensionless form, the moments in Table 5.4.1 must be transformed using Equation (5.3.15) to obtain moments for dimensionalized BTCs. The absolute moments are obtained by using (5.4.1) and the BTCs, and have not been corrected for the pulse width. The central moments have been corrected for the pulse width using Equation (5.3.13) and Equation (5.3.14). Once corrected for the pulse width, these moments represent measures of central tendency of the RTD and thus are independent of the input conditions.

Tritiated water and KCl are conservative tracers. Thus, mass recoveries for these solutes are very close to 100%. Incomplete recovery for atrazine is indicative of the mass loss inside the soil column and may be caused by degradation or immobilization of atrazine in soil. The first time moment represents the mean travel time of the solutes through the soil column. Larger m_1 for atrazine than tritiated water and KCl indicates that atrazine is retarded while moving through soil. Similarly, larger m_2 and m_3 for atrazine suggest that atrazine is more dispersed and more kinetically sorbed in soil compared to tritiated water and KCl. For all our example data sets, the magnitudes of moments increase with their order. This is a particularly undesirable characteristic (Govindaraju et al., 1996) with moments as the error for estimating moments also increases with their order. However, for

Table 5.4.1. Pulse duration, absolute moments, percent mass recovery, and central moments for example data sets (from Das et. al., 2002, with permission from ASCE Press)

	Tritiated water flux-averaged	Atrazine flux-averaged	KCl flux-averaged	KCl resident
Pulse width (PV)	1.169E+0	1.169E+0	1.245E+0	1.197E+0
μ_0	1.184E+0	1.006E+0	1.241E+0	1.967E+0
μ_1	1.817E+0	3.956E+0	2.004E+0	3.738E+0
μ_2	2.945E+0	1.815E+1	3.624E+0	8.239E+0
μ_3	5.006E+0	9.914E+1	7.214E+0	2.052E+1
μ_4	8.853E+0	6.422E+2	1.562E+1	5.726E+1
Mass recovery (%)	1.013E+2	8.609E+1	9.963E+1	9.999E+2
m_1	9.503E−1	3.347E+0	9.928E−1	9.166E−1
m_2	1.880E−2	2.462E+0	1.819E−1	2.550E−1
m_3	2.800E−3	7.375E+0	9.047E−2	2.759E−1
m_4	1.404E-2	4.448E+1	2.901E−1	1.272E+0

Note: Moments were estimated from BTCs plotted as relative concentration versus pore volume

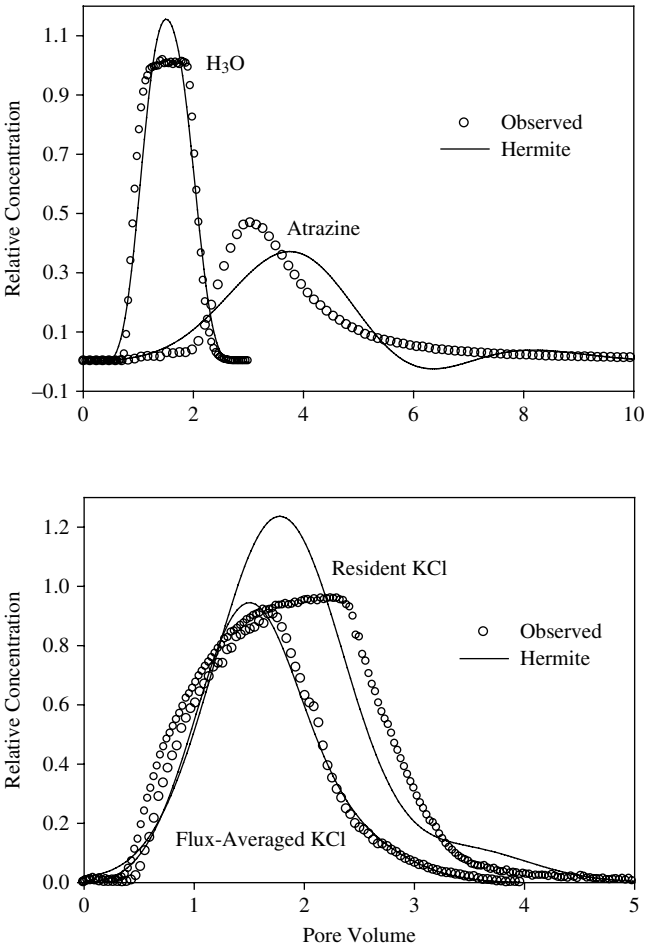

Figure 5.4.1. Observed (circles) and constructed (lines) BTCs for (a) tritiated water and atrazine and (b) resident and flux-averaged KCl concentrations (adapted from Das et al., 2002, with permission from ASCE Press)

most practical applications of MOM, we only need the first few moments (Skopp, 1985). For example, for conservative tracers, only first and second moments are used to estimate parameters such as the pore water velocity and the dispersion coefficient (Aris, 1958). Similarly, Kucera (1965) and Kubin (1965) used the first five moments to construct the chromatographic elution curves, (see Chapter 12).

5.4.3 Estimation Errors

In this section we investigate sources of error that produce uncertainty in estimating moments from the example data sets.

Figure 5.4.2 was constructed by adding randomly generated positive and negative errors to the observed atrazine BTC (Figure 5.4.1). The maximum magnitude of their absolute values was changed during each simulation and the moments were reconstructed. The open circles in the top panel show the generated data for a maximum relative random error of 45%. The solid line represents the true data set. In the bottom panel, the percent error in absolute moments for first five order are shown as a function of maximum percent random error in the observed data. Obviously, the effect of random error on the observed concentration data is very

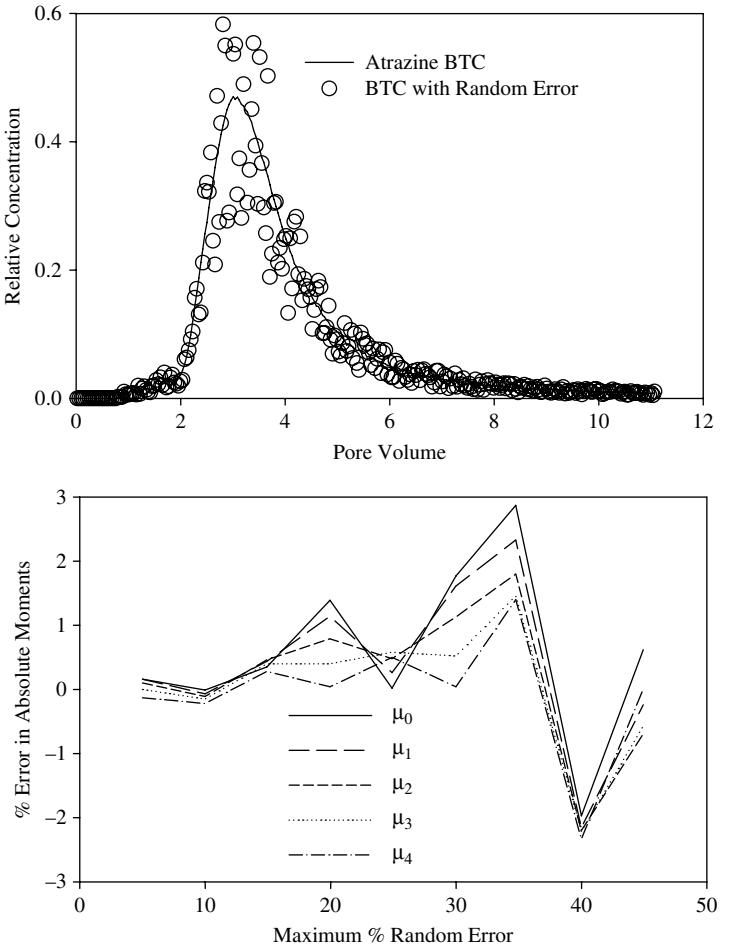

Figure 5.4.2. Top panel (a) shows the observed atrazine BTC (line) and the BTC (circles) generated by adding a maximum random error of 45%. Bottom panel (b) shows the percent error in the first five absolute moments as a function of maximum percent random error (adapted from Das et al., 2002, with permission from ASCE Press)

small. Note that moments are essentially weighted averages of the BTC and random errors tend to cancel out.

In Figure 5.4.3, the effect of a large time interval between successive concentration measurements in a leaching experiment on moment calculations is investigated. The open circles in the top panel show the generated data obtained by deleting 20 data points between each successive concentration measurement. The solid line represents the true data set. Again, the bottom panel clearly shows that errors arising from large time intervals between successive measurements are under 10% for

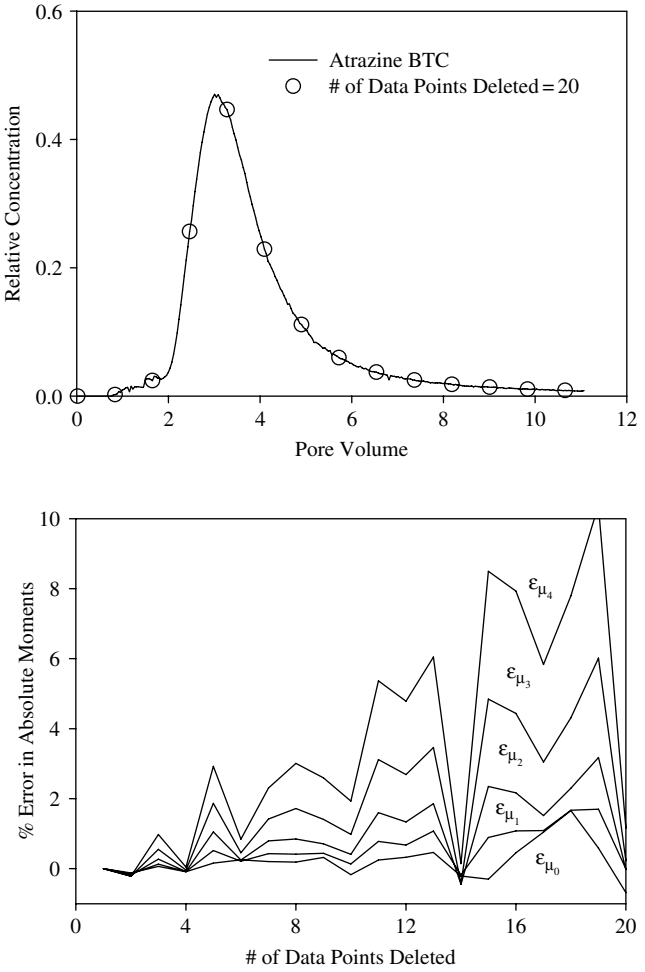

Figure 5.4.3. Top panel (a) shows the observed atrazine BTC (line) and the BTC (circles) generated by deleting 20 data points between two successive observations. Bottom panel (b) shows the percent error in the first five absolute moments as a function of the number of data points deleted between two successive observations (adapted from Das et al., 2002, with permission from ASCE Press)

the first five moments. This is encouraging because in many field-scale leaching data sets, smooth BTCs with measurements at close time intervals are rarely obtained.

The third source of error is the truncation error that results from not representing the tail of the BTC, and can be a major source of inaccuracy when estimating moments. In Figure 5.4.4, the effect of truncation error is shown. On the top panel, the time when the atrazine BTC was truncated are indicated. Truncation of the BTC results in a reduction in mass recovery. On the bottom panel, the truncation error

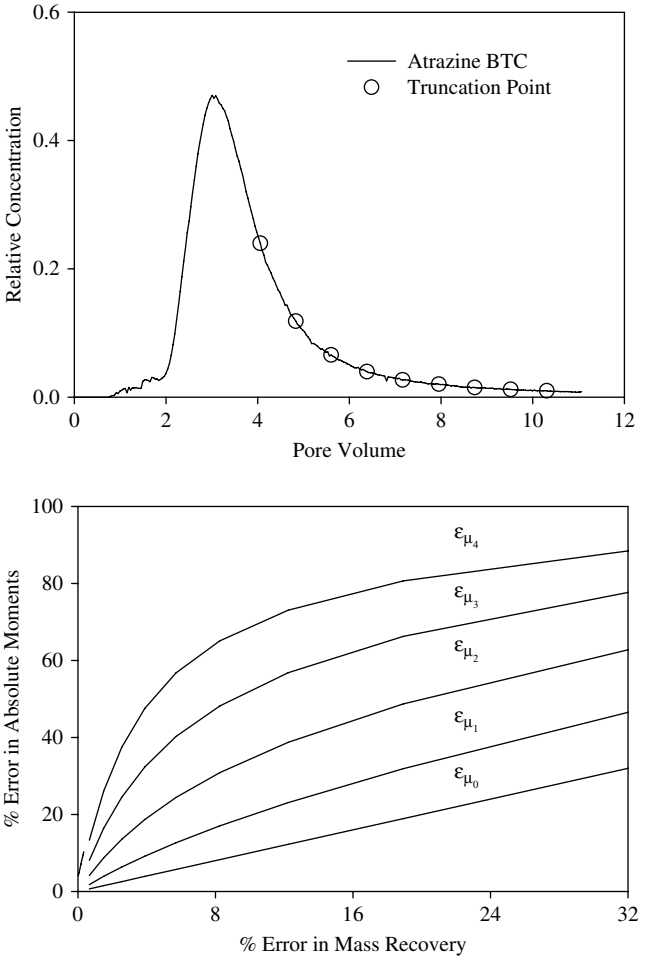

Figure 5.4.4. Top panel (a) shows the observed atrazine BTC (line) and the position of the truncation (circles). Bottom panel (b) shows the percent error in the first five absolute moments as a function of percent error in mass recovery (adapted from Das et al., 2002, with permission from ASCE Press)

is shown as a function of the percent error in mass recovery. These figures clearly show that an incomplete BTC significantly affects moment calculations.

These results suggest that although moment calculations are straightforward, the integration of Equation (5.2.4) is sensitive to the lack of high resolution BTC data especially along the tails. An examination of Equation (5.2.4) reveals that unequal weights are placed on the frontal and tail ends of the BTCs during moment calculations (Fahim and Wakao, 1982). Measured concentration values at these observation points, on the other hand, may not be very reliable because these concentrations are low and may be near the detection limit of the measuring device. To accurately estimate moments from observed BTCs, modified methods have been proposed. These methods include the weighted moment method and transfer function fitting method (Østergaard and Michelsen, 1969), Fourier analysis (Gangwal et al., 1971), and time-domain analysis (Clements, 1969). Fahim and Wakao (1982) examined these four methods with experimental data sets and concluded that the time-domain analysis is most reliable in estimating moments, followed by the Fourier analysis, the transfer function fitting, and the weighted moment method. We observed an additional problem in the weighted moment method where the moments are estimated by multiplying an exponentially decaying function e^{-pT}, to the argument of the integral in Equation (5.2.4):

$$\mu_n = \int_0^\infty T^n C(z, T) e^{-pT} dT \tag{5.4.3}$$

This technique is flawed because the suggested modification is equivalent to including a first-order production process in the governing differential equation. The effects of mass recovery error are further discussed under in 5.5.1.

5.5. APPLICATIONS OF THE METHOD OF MOMENTS

In the previous sections, explicit time moment formulas were presented for the n^{th} central moment for a selected set of initial and boundary conditions. In this section, we discuss the following applications of the method of moments: estimating transport parameters from experimental data, obtaining effective properties, and gaining physical insight by analyzing moment indices (Valocchi, 1985).

5.5.1 Estimating Parameters of the Transport Equation

Parameter estimation has been a major application of the MOM in Soil Science and related disciplines. The technique is based on equating experimental moments estimated from observed BTCs with the theoretical moments derived from an assumed transport model. While matching experimental moments with theoretical moments, pulse width correction is an important step as most laboratory-scale leaching experiments are conducted with a pulse type top boundary condition. It should be noted that the theoretical moment expressions are already corrected for the pulse width in Equation (5.3.13) and (5.3.14). Experimental moments

from Equation (5.2.4), (5.2.5), and (5.2.6) should also be corrected for the pulse width before they are equated with the theoretical moment expressions shown in Equation (5.3.12).

After correctly matching experimental moments with theoretical moments, the resulting identities are either rearranged to express transport parameters in terms of experimental moments or solved in an iterative scheme to estimate transport parameters. Aris (1958) first showed that the pore water velocity and the dispersion coefficient for a conservative, non-reactive tracer can be estimated by rearranging the first and the second central moments

$$V = \frac{L}{m_1}, \text{ and } D = \frac{m_2 V_{eff}^3}{2R^2 L} \tag{5.5.1}$$

of a BTC plotted as concentration vs. time assuming Dirac delta-type input condition. Bischoff (1960) extended this technique to account for the pulse width. Equation (5.5.1) is useful only when solute transport is one-dimensional, the flow domain is homogeneous, and the *local equilibrium assumption* (LEA) is valid. For heterogeneous media or for solutes whose fates are influenced by additional processes, a greater number of parameters are involved, and other schemes must be followed to estimate desired parameters from the moments. For example, for solutes showing nonequilibrium sorption, the retardation factor R is estimated from the first moment ($m_1 = R$ when $\gamma_1 = \gamma_2 = 0$ in Equation (5.3.8)) of a BTC plotted in terms of pore volume and relative concentration. Peclet number may be obtained from the second central moment of the BTC for a conservative, non-reactive tracer using Equation (5.5.1). The two nonequilibrium parameters β and ω may be estimated by substituting $\gamma_1 = \gamma_2 = 0$ into Equation (5.3.9) and Equation (5.3.10) and rearranging the resulting expressions:

$$\beta = 1 - \frac{3\left(m_2 P - 2R^2\right)^2}{2RP\left(m_3 P - 6m_2 R\right)} \tag{5.5.2}$$

$$\omega = \frac{2(1-\beta)^2 R^2 P}{m_2 P - 2R^2} \tag{5.5.3}$$

An iterative scheme is needed to estimate V and D from a conservative tracer BTC for a volume-averaged (resident) concentration distribution in a homogeneous soil profile because the expressions for the first and the second moments (Leij and Dane, 1991),

$$m_1 = \frac{D}{V^2} + \frac{L}{V} \tag{5.5.4}$$

$$m_2 = \frac{3D^2}{V^4} + \frac{2DL}{V^3} \tag{5.5.5}$$

for this case involve both V and D (Risler et al., 1996). Similarly, to estimate parameters for degrading solutes, iterative schemes are required because no explicit

expressions as shown in Equation (5.5.1) to (5.5.3) can be derived. The presence of degradation confounds parameter estimation further, and an alternative approach has been proposed to estimate degradation rate constant from the measured BTC data following the work of Misra and Mishra (1977). Misra and Mishra (1977) considered the first moment of a BTC as the mean decay time ($\bar{t}$) for degrading solutes in a first order rate expression. They defined the mass recovery fraction (MRF) as

$$MRF = \exp\left(-\gamma_{eff}\bar{t}\right) \tag{5.5.6}$$

to estimate the effective denitrification rate constant (γ_{eff}) for nitrogenous fertilizers. The technique has been extended to estimate sequential transformation of ammoniacal fertilizers under field soil conditions (Mishra and Misra, 1990). Das and Kluitenberg (1996) detected a computational error in using Equation (5.5.6) and derived the mean degradation time as

$$\bar{t} = \frac{2}{\dfrac{1}{\left(m_1/R\right)} + \dfrac{1}{\left(L/V\right)}} \tag{5.5.7}$$

to accurately estimate first-order rate constants for solutes which obey LEA. For kinetically sorbed solutes, a modified expression for $\bar{t}$ must be used (Das and Kluitenberg, 1996).

5.5.1.1 Estimated parameters for the example data sets

Transport parameters were estimated for the example data sets (Figure 5.4.1) using the MOM and a popular parameter estimation program, CXTFIT2 (Toride et al., 1995). The optimization program CXTFIT2 performs calculations in terms of dimensionless variables (Toride et al., 1995) to reduce the problem of uniqueness among parameter values. Thus, only the dimensionless parameters P, R, β, and ω were optimized using CXTFIT2. Once P was optimized, $D\,(=VL/P)$ was estimated from the known values of column length L and pore water velocity V. The pore water velocity was determined from the measured flux density and water content and was found to be $1.403\,\text{cm h}^{-1}$ for the saturated flow experiment and $1.207\,\text{cm h}^{-1}$ for the unsaturated flow experiment. To match the mode of calculation with CXTFIT2, the MOM was employed in terms of dimensionless variables. The estimated parameters were close to each other (Table 5.5.1). An interesting observation is that V cannot be estimated by the MOM if the BTC is plotted with concentration as a function of pore volume. Real time and concentration data are needed to estimate V. The estimated values for V for the saturated and unsaturated flow experiments were $1.476\,\text{cm h}^{-1}$ and $1.215\,\text{cm h}^{-1}$, respectively. These two values are similar to the true pore water velocity for these experiments.

The example data sets represent leaching scenarios with uniformly repacked soil columns in the laboratory. Jacobsen et al. (1992) estimated both equilibrium

Table 5.5.1. Solute Transport Parameters Estimated by the Method of Moments and CXTFIT2 Using the Example Data Sets (adapted from Das et al., 2002, with permission from ASCE Press)

	Parameters	MOM	CXTFIT2
Flux-averaged KCl	R	0.993	0.991
	D (cm^2h^{-1})	1.214	1.220
Resident KCl	R	0.917	0.912
	D(cm^2h^{-1})	1.263	1.043
Tritiated water	R	0.950	0.944
	D(cm^2h^{-1})	0.438	0.377
Atrazine	R	3.347	3.821
	β	0.676	0.640
	ω	1.058	0.935

and nonequilibrium transport parameters for chloride and tritiated water in undisturbed soil monolith lysimeters. Reasonably good agreement between parameters obtained with the MOM and the conventional least-squares optimization method was observed. Jury and Sposito (1985) compared parameters estimated by the MOM with the least-squares and the maximum likelihood optimization methods for field scale studies.

Close agreement among estimated parameters via the MOM or the least-squares optimization method (CXTFIT2) is predicated on high resolution leaching data being available. In addition, the success of the MOM for parameter estimation also depends on *a priori* knowledge of appropriate transport processes occurring under a given transport scenario. These two requirements should also be met for other parameter estimation techniques such as least-squares optimization.

5.5.1.2 *Effects of mass recovery error on estimating transport parameters for nonreactive solutes*

A common observation with the MOM as a parameter estimation tool is that even for simple flow geometries it often yields parameters that are substantially different from those estimated with the least-squares optimization (LSO) method. For example, Jacobsen et al. (1992) showed that the curve-fitted dispersion coefficients (D) were always lower than those obtained by the MOM, whereas Kamra et al. (2001) reported both higher and lower values for D estimated with the least-squares optimization relative to the MOM method. Das et al. (2005) estimated the percent deviations between the MOM- and LSO-estimated D values to range from 5 to 255% in Jacobsen et al. (1992) and from – 21 to 53% in Kamra et al. (2001). Explanations for such discrepancies include: 1) equal weighting is given to all observed points in the concentration response curve in the LSO method, while the MOM is biased towards concentrations which appear at later times (for BTCs) or deeper soil layers (for CPs) (Fahim and Wakao, 1982; Jury and Sposito, 1985); 2) uncertainty (scatter) in the individual data points in a BTC or CP and lack of high frequency (small sampling interval) measurements for many experimental BTCs; 3) missing tails and extended tailing of BTCs or CPs preclude accurate

estimation of moments; 4) while the least-squares method provides equal flexibility for all model parameters, the dependence of higher-order moments on lower-order moments leads to propagation of error during parameter estimation; and 5) incorrect model assumption while using the LSO approach may lead to unrealistic model parameters.

Each of the above possibilities leads to a common problem of the error in mass balance. Figure 5.4.4 clearly shows the mass balance error can lead to large errors in estimated moments. It is expected that erroneous moment estimates would lead to inaccurate estimates for transport parameters. Figure 5.5.1 shows that this problem becomes worse with the estimation of parameters requiring higher-order moments. This figure was constructed using 85 BTCs from three different sources encompassing repacked and undisturbed soil columns under laboratory conditions and the field-scale leaching experiments. These authors also theoretically demonstrated that the error in mass balance can lead to very large errors in estimated parameters specifically those that are derived from higher-order moments. They observed that a mass recovery of 91% (9% error in mass recovery) resulted in errors of 138% and 57% in D values estimated by the MOM for the truncated BTCs of the repacked and undisturbed soil columns, respectively. Corresponding errors in estimated D values

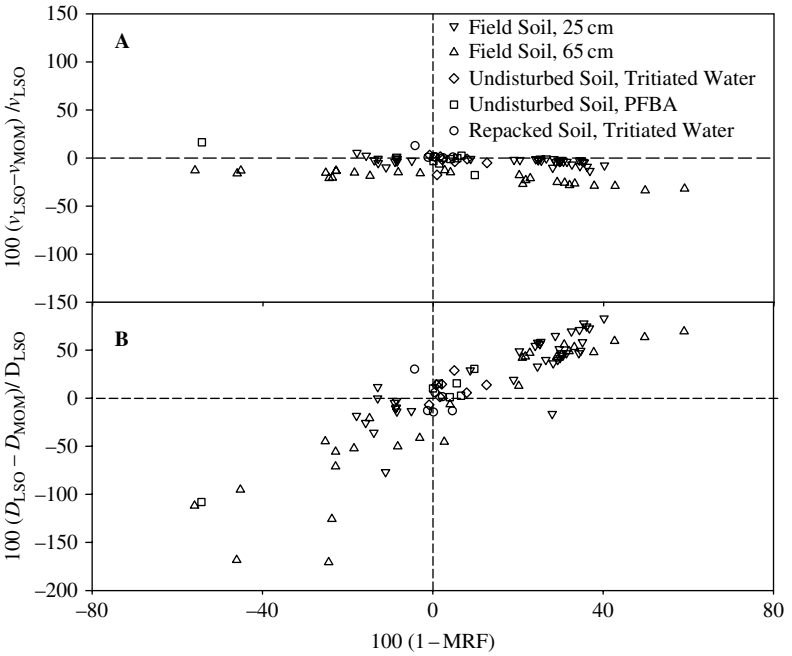

Figure 5.5.1. Impact of the mass recovery fraction (MRF) on the relative difference in (A) pore water velocity (v) and (B) dispersion coefficient (D) estimated by the least-squares optimization (LSO) and the method of moment (MOM) approaches for 85 measured solute breakthrough curves. The subscripts indicate the estimation method (LSO or MOM) for the respective parameters

were below 5% for the LSO approach. The difference in estimated errors (138% vs. 57%) using two different experimental conditions for the same value of mass recovery error suggests that the experimental conditions influence the magnitude of errors for a particular parameter estimate and, therefore, it is not possible to identify an unequivocal acceptable limit for the mass recovery that would correspond to an allowable error in the parameter estimate in any transport experiment. However, considering that the errors in D estimates were <5% in the LSO approach for a mass recovery of <10%, we suggest that 10% error in mass recovery may be allowable in a laboratory-scale transport experiment if the parameters are estimated using the LSO approach. However, where the MOM is applied, 100% mass balance should be ensured.

5.5.2 Effective Parameters

Moments are measures of overall average properties of solute plumes and thus integrate the effects of various processes. Moments thus provide a means to quantify the impact of processes upon the rate of plume migration and spreading, thereby enabling the determination of effective transport processes. To illustrate, we consider a simplified transport problem that is 'equivalent' to the problem at hand. In particular, we consider a nonreactive solute that travels through a medium with constant 'effective' velocity and dispersion coefficient.

$$\frac{\partial c}{\partial t} = D_{eff}\frac{\partial^2 c}{\partial x^2} - V_{eff}\frac{\partial c}{\partial x} \tag{5.5.8}$$

In dimensionless form, the above equation is

$$\frac{\partial C}{\partial T_{eff}} = \frac{1}{P_{eff}}\frac{\partial^2 C}{\partial Z^2} - \frac{\partial C}{\partial Z} \tag{5.5.9}$$

where the dimensionless parameters are defined as: $Z = x/L$, $P_{eff} = V_{eff}L/D_{eff}$, and $T_{eff} = V_{eff}t/L$. By setting the zeroth, first and second temporal moments of Equation (5.5.9) equal to those of Equation (5.1.7) and (5.1.8), we can relate the effective velocity and dispersion coefficient to physically meaningful parameters of the original problem. This approach is prevalent in the literature, especially for spatial moments, and some representative work with time moments includes Valocchi (1985), Goltz and Roberts (1987), and Espinoza and Valocchi (1998).

Using the formulae presented in Valocchi (1985), the effective parameters are given by

$$\frac{V_{eff}}{V} = \frac{\theta_m}{\theta}\frac{L}{m_1};\ \frac{1}{P_{eff}} = \frac{D_{eff}}{V_{eff}L} = \frac{1}{2}\frac{\theta}{\theta_m}\left(\frac{V_{eff}}{V}\right)\frac{m_2}{m_1} \tag{5.5.10}$$

where the central moments m_1 and m_2 are defined in Equation (5.3.8), (5.3.9), and Table 5.3.1. For the case of no degradation with nonequilibrium sorption (see Table 5.3.1), we find that

$$V_{eff} = \frac{V}{R}\frac{\theta_m}{\theta} \tag{5.5.11}$$

$$\frac{1}{P_{eff}} = \frac{(1-\beta)^2}{\omega} + \frac{1}{P}; D_{eff} = \frac{D}{R}\frac{\theta_m}{\theta} + \frac{(1-\beta)\,V^2\theta_m}{\alpha P^2\theta} \tag{5.5.12}$$

Equation (5.5.11) is the definition of the retarded velocity, and (5.5.12) demonstrates the well-known fact that nonequilibrium sorption enhances the spreading of solute profiles.

5.5.3 Nonequilibrium Indices

To examine the validity of LEA and effects of flow processes on sorption nonequilibrium, Valocchi (1985) defined nonequilibrium indices in terms of time moments:

$$\varepsilon_n = \frac{m_n^K - m_n^E}{m_n^E} \tag{5.5.13}$$

The terms m_n^K and m_n^E in Equation (5.5.13) represent the n^{th} central moments for the ADE with kinetic and equilibrium sorption, respectively. In addition to providing a quantitative measure for the degree of nonequilibrium under a given transport and reaction scenario, nonequilibrium indices provided insight into the transport processes. Valocchi (1985) observed that the center of mass for a nondegrading solute plume is not affected by sorption nonequilibrium. This means that regardless of the presence or absence of nonequilibrium sorption, the solutes would have the same average life time within the soil column. The expression for ε_2,

$$\varepsilon_2 = \frac{P}{\omega}(1-\beta)^2 \tag{5.5.14}$$

and other higher order nonequilibrium indices further revealed that the column Peclet number and retardation factor influence sorption nonequilibrium, in addition to the nonequilibrium parameters β and ω. These observations partly explained why symmetric BTCs are obtained in slow flow velocity experiments despite the presence of nonequilibrium sorption; slow velocity yields a smaller column Peclet number and a larger ω both of which reduce ε_2. Flow properties characterized by high Peclet number can accentuate the effects of sorption nonequilibrium. Considering a Gaussian distribution for solute concentration, Valocchi (1985) also defined highest possible degrees of nonequilibrium under a given transport and reaction scenario. The derivations presented by Das (1996) and Das and Kluitenberg (1996) confirmed that the first moment depends on nonequilibrium parameters if degradation is a component process.

Inclusion of degradation leads to four different cases (see Table 5.3.1): nonequilibrium sorption and degradation (ND), equilibrium sorption and degradation (ED), nonequilibrium sorption and no degradation (N), and equilibrium sorption and no degradation (E). For all values of R, P, β, and ω, Das (1996) showed:

$$m_0(ND) < m_0(ED) < m_0(N) = m_0(E) \tag{5.5.15}$$

$$m_1(ND) < m_1(ED) < m_1(N) = m_1(E) \tag{5.5.16}$$

$$m_2(ED) < m_2(E) < m_2(N); m_2(ND) < m_2(N) \tag{5.5.17}$$

These equations show that the magnitude of moments can change depending on the processes occurring in a leaching scenario. Valocchi (1985) considered cases of N and E. Therefore, the nonequilibrium indices for the zeroth and the first moments both were zero in his analysis. However, when degradation occurs (cases ND and ED), the zeroth and the first moments for the equilibrium and nonequilibrium sorption models are not equal [see Equation (5.5.15) and Equation (5.5.16)]. The zeroth moment is the total mass transported across any location, or out of the lower boundary. In other words, it is the total mass recovered at any location in the direction of flow. The first moment is the solute travel time. Degradation changes both of these moments. Thus, nonequilibrium sorption changes both the solute mass recovery and the solute travel time, if degradation is present. This is true even when kinetic sorption is completely absent in a leaching scenario (cases ED and E). Thus, the conclusions of Valocchi (1985) and Harvey and Gorelick (1995) cannot be extended to cases where degradation is present.

The inclusion of degradation requires that we redefine the nonequilibrium index. Valocchi's (1985) definition of nonequilibrium indices in Equation (5.5.13) is essentially a normalized difference between the n^{th} time moments of the N and D cases. Along similar lines, the following three different indices are developed to bring out the influence of degradation and nonequilibrium effects:

$$\varepsilon_n^D = \frac{m_n^{ND} - m_n^{ED}}{m_n^{ED}} \tag{5.5.18}$$

$$\varepsilon_n^N = \frac{m_n^{ND} - m_n^{N}}{m_n^{N}} \tag{5.5.19}$$

$$\varepsilon_n^E = \frac{m_n^{ED} - m_n^{E}}{m_n^{E}} \tag{5.5.20}$$

The superscripts in these equations are used to distinguish the new moment indices [Equation (5.5.18) to Equation (5.5.20)] from the nonequilibrium indices of Valocchi (1985).

The index defined in Equation (5.5.18) may be treated as the nonequilibrium index in the presence of degradation because it illustrates the effects of nonequilibrium sorption (or transport) on overall solute transport behavior for degrading solutes. Note that for the limiting case where degradation is assumed to be absent,

Equation (5.5.18) will be identical to Equation (5.5.13). For analyzing the nature of these indices, Equation (5.3.7) and (5.3.12) were substituted into Equation (5.5.18) to yield ε_n^D for the respective time moments. For example, the expressions for ε_0^D and ε_1^D are given by

$$\varepsilon_0^D = \exp\left\{\frac{ZP}{2}\left(1+\frac{4\gamma}{P}\right)^{0.5} - \frac{ZP}{2}\left[1+\frac{4\gamma_1}{P}\left(1+\frac{\gamma_2/\gamma_1}{1+\gamma_2/\omega}\right)\right]^{0.5}\right\} - 1 \tag{5.5.19}$$

$$\varepsilon_1^D = \left[\beta + \frac{(1-\beta)}{(1+\gamma_2/\omega)^2}\right]\left(1+4\frac{\gamma_1}{P}\right)^{0.5}\left[1+\frac{4\gamma_1}{P}\left(1+\frac{\gamma_2/\gamma_1}{1+\gamma_2/w}\right)\right]^{-0.5} - 1 \tag{5.5.20}$$

The expressions for higher-order nonequilibrium indices continue to grow in complexity with increasing order. Thus, only graphical illustrations of these indices are summarized using the following four transport scenarios (Table 5.5.2).

Figure 5.5.2 shows the first four nonequilibrium indices γ_n^D as a function of degradation rate constants (for n ranging from 0 to 3). For simplicity, it was assumed that the degradation rate constant in all phases are equal, i.e., $\gamma = \gamma_1 = \gamma_2$. Because both ND and ED include degradation, these figures show nonequilibrium effects in the presence of degradation. As γ increases, the resulting influence is different for different n values. In Figures 5.5.2a and 5.5.2b for zeroth and first moments, respectively, the indices increase in magnitude, implying a departure from equilibrium conditions. The negative values in these figures imply that degradation leads to a decrease in mass and a decrease in travel time. This was also observed by Das and Kluitenberg (1996), who concluded that in the absence of kinetic sorption, the interaction between degradation and dispersion tends to reduce solute travel time. The curves for Cases I and III are almost identical in Figures 5.5.2a and 5.5.2b and the curves for Cases II and IV are similar. This implies that the results are more sensitive to changes in β and ω than they are to changes in P and R. Smaller values of β and ω result in the zeroth-index being closer to zero and the first-index being larger in magnitude. Larger zeroth index with larger γ implies less mass is recovered with nonequilibrium sorption than with equilibrium sorption. This is because nonequilibrium tends to increase residence time and thus provides

Table 5.5.2. Dimensionless parameters P, R, β, ω, and γ for four different cases

Case	P	R	β	ω	$\gamma = \gamma_1 = \gamma_2$
I	60	4	0.3	0.3	0.5
II	60	4	0.6	0.6	0.5
III	20	2	0.3	0.3	0.5
IV	20	2	0.6	0.6	0.5

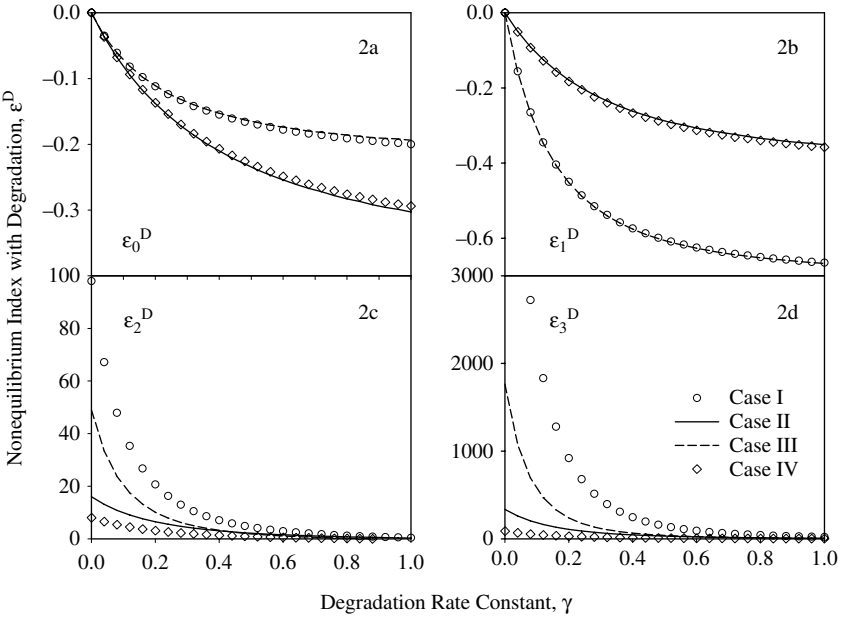

Figure 5.5.2. Moment indices ε_n^D for examining the effects of nonequilibrium sorption on degradation during transport for degrading solutes using (a) zeroth moment, $n = 0$; (b) first moment, $n = 1$; (c) second moment, $n = 2$; and (d) third moment, $n = 3$. Parameters used for generating these four plots correspond to four cases shown in Table 5.5.2

more opportunity for degradation. The reduction in the first moment in the presence of nonequilibrium is a result of reduced tailing due to degradation.

The cases shown in Table 5.5.2 do not allow for independent evaluation of P and R or β and ω, because they increase or decrease as pairs. Simulations show that as P, β, and ω increase, both ε_1^D and ε_2^D approach zero, indicating that an equilibrium condition is favored. These results have been discussed already by Valocchi (1985) for $\gamma = 0$. The effect of the column Peclet number on ε_1^D appears to be less important compared with the effects of β and ω. These results clearly demonstrate that degradation alters the magnitude of nonequilibrium indices. Thus, if a solute is known to degrade, then degradation must be considered while studying the validity of local equilibrium assumptions for given set of experimental conditions.

The index presented in Equation (5.5.19) describes the effects of degradation on nonequilibrium transport because both the cases of ND and N include nonequilibrium transport. This index differs from the previous one in that we specifically look at degradation effects under nonequilibrium conditions. Indices close to zero imply that degradation effects are not important, whereas larger indices indicate that degradation effects are more pronounced. The first four indices for this case are presented in Figure 5.5.3.

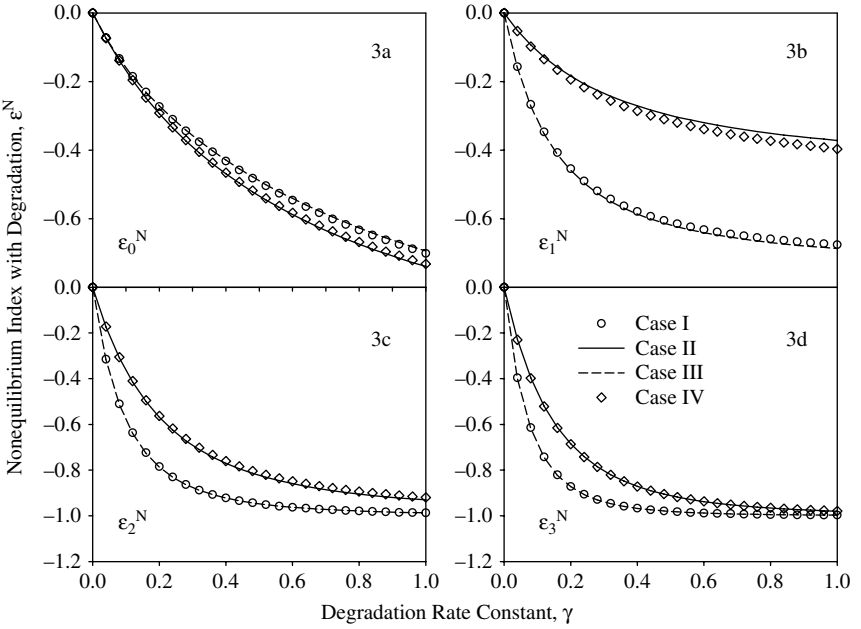

Figure 5.5.3. Moment indices ε_n^N for examining the effects of degradation on nonequilibrium sorption and transport processes using (a) zeroth moment, $n = 0$; (b) first moment, $n = 1$; (c) second moment, $n = 2$; and (d) third moment, $n = 3$. Parameters used for generating these four plots correspond to four cases shown in Table 5.5.2

For all the results shown in Figure 5.5.3a–d, increasing γ increases the influence of degradation as the indices keep growing in magnitude. All the indices have negative values, implying that degradation tends to reduce the moments. The results for Cases I and III are similar, and the indices for Case II and IV yield identical results, indicating that degradation influences the moments more strongly for changes in β and ω than changes in P and R. Thus, indices would be more useful for detecting changes in β and ω. Results for the zeroth index in Figure 5.5.3a show that increasing β and ω causes ε_0^N to be larger in magnitude, implying that degradation effects are more important. The reverse is true for the results in Figure 5.5.3b for the index ε_1^N corresponding to the first moments, where smaller values of β and ω cause degradation effects to be manifested more strongly. Lowering P and R values seems to accentuate the effect of degradation on this index, even though the results are less sensitive to changes in these parameters. Figures 5.5.3c and 5.5.3d show results for $n = 2$ and 3, respectively. The trend in the results is the same as in Figure 5.5.3b, except that the results show hardly any sensitivity to changes in P and R.

The index presented in Equation (5.5.20) describes the effects of degradation during ideal (equilibrium) transport conditions because both the cases of ED and E do not include nonequilibrium transport. Graphical illustrations in Figure 5.5.4a-d

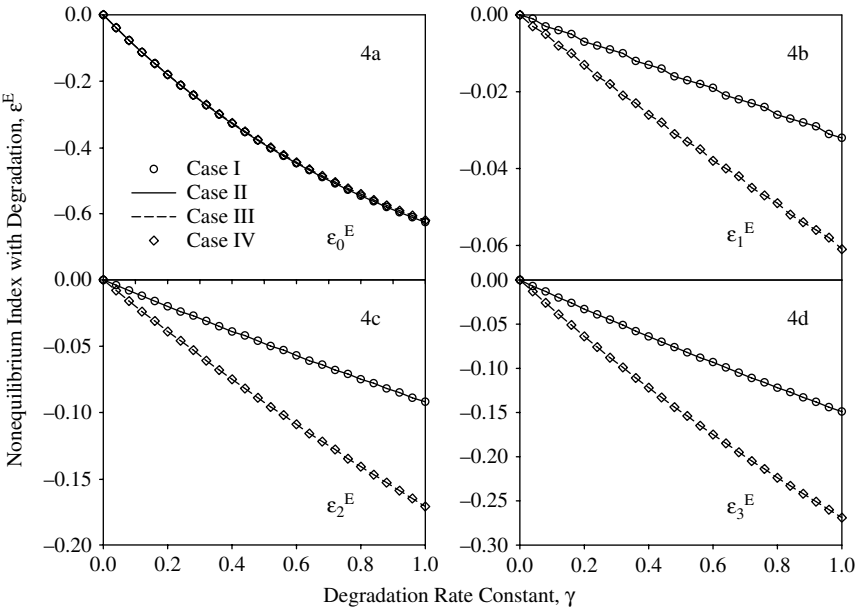

Figure 5.5.4. Moment indices ε_n^E for examining the effects of degradation on equilibrium sorption and transport using (a) zeroth moment, $n = 0$; (b) first moment, $n = 1$; (c) second moment, $n = 2$; and (d) third moment, $n = 3$. Parameters used for generating these four plots correspond to four cases shown in Table 5.5.2

show that with increasing degradation this index increases in magnitude and is negative, similar to the results in Figures 5.5.3a-d for nonequilibrium conditions.

In Figure 5.5.4a, the curves for all four indices are identical, implying that the zeroth index is primarily controlled by the magnitude of γ. The curves split up for Figures 5.5.4b-d, with the results being identical for Cases I and II, and also for Cases III and IV. In this instance, β and ω have no role to play. Lower P and R values lead to larger magnitudes for this index, implying that degradations effects are manifested more strongly for these cases. The three indices in equations Equation (5.5.18) through Equation (5.5.20) show that degradation has a significant role to play in determining the relative nature of the moments. If these indices are interpreted as representing the relative roles of component processes, the presence of degradation may enhance or suppress the roles of some of these processes. Chan and Govindaraju (2006) discuss the implications of determining effective parameters when degradation is present.

5.6. SUMMARY

In this chapter, we have presented a comprehensive analysis of time moments for the commonly used bi-continuum transport model. General and specific expressions for moments have been presented for pulse-type and Dirac-type input condi-

tions and for both resident and flux-averaged concentrations. Numerical methods for computing moments from four example datasets are also presented as a part of example exercises and different sources of errors are also discussed. A major emphasis in this chapter is laid on the discussion of the degradation process and its influence on sorption and transport processes. Several anthropogenic chemicals undergo degradation and therefore, their transport behavior must consider degradation as a major process. It should be further emphasized that the nature of degradation process should also be considered while analyzing solute transport data. The current analysis does not include sequential decay or similar chain reactions nor does it consider processes not described by the first-order kinetics.

5.7. APPENDIX: SAMPLE BTC DATA

Sample datasets for four different breakthrough curves. PV is the pore volume and Rel. Conc. is the relative concentration.

Appendix 5.7. Sample datasets for four different breakthrough curves. PV is the pore volume and Rel. Conc. is the relative concentration

Tritiated water		Atrazine		Flux-averaged KCl		Resident KCl	
PV	Rel. Conc.	PV	Rel. Conc.	PV	Rel. Conc.	PV	Rel. Conc.
0.020	0.000	0.020	0.0000	0.000	0.0000	0.000	0.0000
0.060	0.000	0.060	0.0000	0.021	0.0045	0.029	0.0082
0.099	0.000	0.099	0.0000	0.062	0.0070	0.058	0.0108
0.138	0.000	0.138	0.0000	0.104	0.0064	0.087	0.0147
0.177	0.000	0.177	0.0000	0.145	0.0026	0.117	0.0098
0.217	0.000	0.217	0.0000	0.187	0.0006	0.146	0.0137
0.256	0.000	0.256	0.0000	0.228	0.0013	0.175	0.0082
0.295	0.000	0.295	0.0000	0.270	0.0006	0.204	0.0108
0.334	0.000	0.334	0.0000	0.311	0.0006	0.233	0.0085
0.372	0.000	0.372	0.0000	0.353	0.0000	0.262	0.0088
0.411	0.000	0.411	0.0000	0.394	0.0013	0.291	0.0098
0.450	0.000	0.450	0.0000	0.436	0.0058	0.321	0.0124
0.487	0.000	0.487	0.0000	0.477	0.0211	0.350	0.0166
0.524	0.000	0.524	0.0000	0.519	0.0518	0.379	0.0261
0.563	0.000	0.563	0.0000	0.560	0.1054	0.408	0.0463
0.602	0.000	0.602	0.0000	0.602	0.1502	0.437	0.0711
0.640	0.000	0.640	0.0000	0.643	0.2141	0.466	0.1097
0.680	0.002	0.680	0.0000	0.685	0.2875	0.495	0.1443
0.719	0.003	0.719	0.0000	0.726	0.3342	0.525	0.1929
0.758	0.024	0.758	0.0000	0.768	0.3840	0.554	0.2389
0.798	0.089	0.798	0.0017	0.809	0.4249	0.583	0.2817
0.837	0.203	0.837	0.0024	0.851	0.4594	0.612	0.3163
0.877	0.338	0.877	0.0032	0.893	0.5176	0.641	0.3551
0.955	0.580	0.955	0.0058	0.976	0.5847	0.699	0.4275

(Continued)

Appendix 5.7. (Continued)

Tritiated water		Atrazine		Flux-averaged KCl		Resident KCl	
PV	Rel. Conc.	PV	Rel. Conc.	PV	Rel. Conc.	PV	Rel. Conc.
0.993	0.690	0.993	0.0095	1.017	0.6038	0.729	0.4563
1.032	0.780	1.032	0.0107	1.059	0.6422	0.758	0.4820
1.071	0.854	1.071	0.0129	1.100	0.6677	0.787	0.5020
1.110	0.907	1.110	0.0137	1.142	0.6933	0.816	0.5248
1.150	0.945	1.150	0.0069	1.183	0.7252	0.845	0.5476
1.187	0.962	1.187	0.0151	1.225	0.7380	0.874	0.5689
1.224	0.984	1.224	0.0113	1.266	0.7380	0.903	0.5930
1.264	0.990	1.264	0.0142	1.308	0.7827	0.933	0.6201
1.303	0.993	1.303	0.0145	1.349	0.7891	0.962	0.6351
1.342	0.995	1.342	0.0148	1.391	0.8275	0.991	0.6540
1.380	0.995	1.380	0.0143	1.432	0.8339	1.020	0.6740
1.418	1.012	1.418	0.0136	1.474	0.8466	1.049	0.6945
1.456	1.017	1.456	0.0136	1.515	0.8530	1.078	0.7115
1.495	1.003	1.495	0.0246	1.557	0.8594	1.108	0.7285
1.534	1.005	1.534	0.0272	1.598	0.8786	1.137	0.7425
1.573	1.003	1.573	0.0271	1.640	0.8722	1.166	0.7572
1.612	1.008	1.612	0.0260	1.681	0.9042	1.195	0.7722
1.651	1.000	1.651	0.0243	1.723	0.9042	1.224	0.7882
1.690	1.009	1.690	0.0307	1.764	0.8914	1.253	0.8006
1.730	1.003	1.730	0.0305	1.806	0.8594	1.282	0.8202
1.768	1.000	1.768	0.0281	1.847	0.8211	1.312	0.8254
1.804	1.011	1.804	0.0283	1.889	0.7700	1.341	0.8430
1.840	1.008	1.840	0.0260	1.930	0.7252	1.370	0.8473
1.878	1.005	1.878	0.0276	1.972	0.6869	1.399	0.8561
1.918	0.991	1.918	0.0297	2.013	0.6294	1.428	0.8662
1.957	0.929	1.957	0.0321	2.055	0.6038	1.457	0.8740
1.996	0.823	1.996	0.0367	2.096	0.5911	1.486	0.8851
2.036	0.698	2.036	0.0441	2.138	0.5374	1.516	0.8910
2.075	0.576	2.075	0.0529	2.179	0.4594	1.545	0.8991
2.114	0.468	2.114	0.0653	2.221	0.3917	1.574	0.9037
2.154	0.364	2.154	0.0819	2.262	0.3502	1.603	0.9080
2.193	0.272	2.193	0.0989	2.304	0.3125	1.632	0.9210
2.231	0.200	2.231	0.1198	2.345	0.2831	1.661	0.9168
2.269	0.140	2.269	0.1423	2.387	0.2473	1.690	0.9200
2.308	0.094	2.308	0.1647	2.428	0.2275	1.720	0.9226
2.347	0.063	2.347	0.1877	2.470	0.1974	1.749	0.9337
2.386	0.042	2.386	0.2121	2.511	0.1827	1.778	0.9341
2.425	0.028	2.425	0.2328	2.553	0.1751	1.807	0.9350
2.464	0.019	2.464	0.2565	2.594	0.1617	1.836	0.9399
2.502	0.013	2.502	0.2742	2.636	0.1412	1.865	0.9350
2.541	0.009	2.541	0.2970	2.678	0.1284	1.894	0.9370
2.579	0.005	2.579	0.3187	2.719	0.1278	1.924	0.9442
2.618	0.004	2.618	0.3379	2.761	0.1188	1.953	0.9390
2.658	0.002	2.658	0.3598	2.802	0.1067	1.982	0.9478
2.697	0.001	2.697	0.3794	2.844	0.1003	2.011	0.9517
2.735	0.000	2.735	0.3956	2.885	0.0875	2.040	0.9533
2.773	0.000	2.773	0.4116	2.927	0.0786	2.069	0.9491

2.812	0.000	2.812	0.4259	2.968	0.0722	2.098	0.9563
2.851	0.000	2.851	0.4396	3.010	0.0665	2.128	0.9488
2.890	0.000	2.890	0.4503	3.051	0.0581	2.157	0.9579
2.929	0.000	2.929	0.4586	3.093	0.0562	2.186	0.9533
2.968	0.000	2.968	0.4651	3.134	0.0466	2.215	0.9556
3.007	0.000	3.007	0.4703	3.176	0.0415	2.244	0.9585
		3.046	0.4662	3.217	0.0383	2.273	0.9572
		3.085	0.4697	3.259	0.0332	2.302	0.9582
		3.124	0.4649	3.300	0.0307	2.332	0.9520
		3.163	0.4584	3.342	0.0300	2.361	0.9497
		3.201	0.4560	3.383	0.0262	2.390	0.9364
		3.240	0.4499	3.425	0.0243	2.419	0.9279
		3.279	0.4464	3.466	0.0198	2.448	0.8972
		3.318	0.4374	3.508	0.0173	2.477	0.8332
		3.356	0.4307	3.549	0.0179	2.506	0.8267
		3.395	0.4189	3.591	0.0109	2.536	0.7679
		3.434	0.4089	3.632	0.0083	2.565	0.7448
		3.474	0.3992	3.674	0.0083	2.594	0.7030
		3.513	0.3878	3.715	0.0064	2.623	0.6674
		3.552	0.3755	3.757	0.0032	2.652	0.6420
		3.591	0.3681	3.798	0.0026	2.681	0.6044
		3.630	0.3559	3.840	0.0000	2.710	0.5744
		3.668	0.3469	3.881	0.0006	2.740	0.5503
		3.708	0.3328	3.923	0.0006	2.769	0.5307
		3.747	0.3200	3.964	0.0000	2.798	0.5023
		3.786	0.3104			2.827	0.4683
		3.824	0.2991			2.856	0.4442
		3.861	0.2895			2.885	0.4158
		3.900	0.2784			2.915	0.3894
		3.940	0.2670			2.944	0.3626
		3.979	0.2580			2.973	0.3378
		4.018	0.2483			3.002	0.3172
		4.057	0.2400			3.031	0.2905
		4.095	0.2290			3.060	0.2670
		4.134	0.2219			3.089	0.2480
		4.173	0.2103			3.119	0.2265
		4.212	0.2060			3.148	0.2056
		4.251	0.1992			3.177	0.1997
		4.289	0.1940			3.206	0.1841
		4.328	0.1864			3.235	0.1622
		4.367	0.1807			3.264	0.1456
		4.405	0.1739			3.293	0.1299
		4.444	0.1673			3.323	0.1165
		4.482	0.1634			3.352	0.1074
		4.520	0.1568			3.381	0.0963
		4.559	0.1507			3.410	0.0871
		4.598	0.1438			3.439	0.0800
		4.637	0.1434			3.468	0.0754
		4.676	0.1363			3.497	0.0705
		4.715	0.1297			3.527	0.0604

(Continued)

Appendix 5.7. (Continued)

Tritiated water	Atrazine		Flux-averaged KCl	Resident KCl	
	4.753	0.1271		3.556	0.0574
	4.792	0.1226		3.585	0.0539
	4.831	0.1185		3.614	0.0529
	4.868	0.1132		3.643	0.0545
	4.906	0.1115		3.672	0.0473
	4.944	0.1072		3.701	0.0421
	4.982	0.1049		3.731	0.0460
	5.021	0.1021		3.760	0.0379
	5.060	0.0969		3.789	0.0343
	5.099	0.0939		3.818	0.0343
	5.138	0.0898		3.847	0.0398
	5.177	0.0834		3.876	0.0307
	5.216	0.0837		3.905	0.0320
	5.255	0.0821		3.935	0.0307
	5.294	0.0801		3.964	0.0238
	5.333	0.0776		3.993	0.0287
	5.372	0.0747		4.022	0.0264
	5.411	0.0754		4.051	0.0264
	5.449	0.0725		4.080	0.0193
	5.488	0.0700		4.109	0.0228
	5.526	0.0709		4.139	0.0222
	5.563	0.0646		4.168	0.0228
	5.602	0.0657		4.197	0.0222
	5.641	0.0636		4.226	0.0183
	5.681	0.0623		4.255	0.0255
	5.721	0.0599		4.284	0.0199
	5.761	0.0584		4.313	0.0147
	5.799	0.0577		4.343	0.0137
	5.838	0.0565		4.372	0.0157
	5.877	0.0548		4.401	0.0124
	5.917	0.0541		4.430	0.0202
	5.957	0.0516		4.459	0.0153
	5.996	0.0510		4.488	0.0111
	6.035	0.0489		4.517	0.0222
	6.073	0.0476		4.547	0.0193
	6.110	0.0458		4.576	0.0134
	6.147	0.0456		4.605	0.0140
	6.185	0.0464		4.634	0.0114
	6.224	0.0439		4.663	0.0114
	6.263	0.0427		4.692	0.0095
	6.302	0.0432		4.721	0.0127
	6.342	0.0412		4.751	0.0078
	6.382	0.0399		4.780	0.0065
	6.422	0.0383		4.809	0.0088
	6.461	0.0381		4.838	0.0114
	6.501	0.0378		4.867	0.0082
	6.539	0.0373		4.896	0.0117
	6.578	0.0360		4.926	0.0062

6.617	0.0349	4.955	0.0124
6.656	0.0345	4.984	0.0039
6.695	0.0340	5.013	0.0072
6.733	0.0337	5.042	0.0091
6.770	0.0328	5.071	0.0072
6.810	0.0256	5.100	0.0078
6.852	0.0320	5.130	0.0042
6.890	0.0310	5.159	0.0062
6.929	0.0307	5.188	0.0072
6.968	0.0299	5.217	0.0026
7.007	0.0303	5.246	0.0055
7.046	0.0287	5.275	0.0114
7.085	0.0294	5.304	0.0029
7.125	0.0273	5.334	0.0036
7.164	0.0268	5.363	0.0042
7.208	0.0271	5.392	0.0016
7.249	0.0268	5.421	0.0108
7.286	0.0266	5.450	0.0091
7.327	0.0252	5.479	0.0052
7.367	0.0250	5.508	0.0033
7.407	0.0242	5.538	0.0046
7.446	0.0239	5.567	0.0049
7.486	0.0232	5.596	0.0055
7.525	0.0231	5.625	0.0075
7.564	0.0239	5.654	0.0059
7.603	0.0226	5.683	0.0026
7.642	0.0226	5.712	0.0023
7.680	0.0215	5.742	0.0039
7.719	0.0207	5.771	0.0036
7.758	0.0212	5.800	0.0075
7.797	0.0205	5.829	0.0033
7.835	0.0206	5.858	0.0020
7.874	0.0204	5.887	0.0055
7.912	0.0210	5.916	0.0020
7.951	0.0202	5.946	0.0010
7.990	0.0197	5.975	0.0020
8.029	0.0200	6.004	0.0013
8.068	0.0195	6.033	0.0000
8.107	0.0189	6.062	0.0039
8.146	0.0189	6.091	0.0003
8.185	0.0183	6.120	0.0029
8.223	0.0176	6.150	0.0046
8.262	0.0183	6.179	0.0078
8.301	0.0176	6.208	0.0033
8.341	0.0174	6.237	0.0007
8.381	0.0166	6.266	0.0036
8.420	0.0162		
8.460	0.0158		
8.499	0.0155		
8.538	0.0156		

(Continued)

Appendix 5.7. (Continued)

Tritiated water	Atrazine		Flux-averaged KCl	Resident KCl
	8.578	0.0154		
	8.617	0.0158		
	8.656	0.0145		
	8.695	0.0152		
	8.735	0.0150		
	8.774	0.0147		
	8.813	0.0140		
	8.852	0.0144		
	8.889	0.0144		
	8.927	0.0147		
	8.967	0.0143		
	9.008	0.0139		
	9.048	0.0137		
	9.087	0.0139		
	9.127	0.0140		
	9.166	0.0128		
	9.204	0.0132		
	9.244	0.0131		
	9.282	0.0133		
	9.321	0.0125		
	9.360	0.0118		
	9.398	0.0122		
	9.436	0.0127		
	9.476	0.0122		
	9.520	0.0121		
	9.562	0.0117		
	9.601	0.0118		
	9.640	0.0114		
	9.680	0.0110		
	9.719	0.0110		
	9.758	0.0113		
	9.797	0.0112		
	9.836	0.0108		
	9.875	0.0104		
	9.914	0.0106		
	9.953	0.0110		
	9.992	0.0101		
	10.031	0.0109		
	10.071	0.0102		
	10.111	0.0099		
	10.151	0.0103		
	10.190	0.0099		
	10.230	0.0101		
	10.268	0.0102		
	10.307	0.0099		
	10.346	0.0090		
	10.385	0.0100		
	10.424	0.0091		
	10.462	0.0086		

10.500	0.0090
10.538	0.0092
10.576	0.0089
10.615	0.0084
10.655	0.0089
10.694	0.0086
10.733	0.0087
10.772	0.0087
10.812	0.0086
10.851	0.0080
10.890	0.0081
10.929	0.0082
10.968	0.0076
11.007	0.0079
11.040	0.0080
11.067	0.0085

CHAPTER 6

SPATIAL MOMENT ANALYSIS FOR SOLUTE TRANSPORT IN POROUS MEDIA

6.1. INTRODUCTION

The specification of a transport model is based on our conceptualization of the porous medium and on the several processes that act to transform the contaminant as it moves from source to receptor locations. Several popular models of solute transport in porous media were described in Chapter 2. Among these, two popular models are the physical nonequilibrium model (PNE) and the chemical nonequilibrium model (CNE). These models have been utilized for simulating solute breakthrough responses obtained from laboratory-scale leaching experiments (van Genuchten and Wagenet, 1989; Gamerdinger et al., 1990; Gaber et al., 1995). Chapter 5 dealt with temporal moments based on flux concentrations across a control plane. In this chapter, we consider spatial moments that are computed using snap-shots of the concentration distribution at specific times. Spatial moments can be used to describe different attributes of a solute plume such as total mass of solute present, the distance traveled by the center of the mass of solute plume, and the degree of mixing of solute within the porous medium.

Spatial moment analysis was introduced by Aris (1956) to study the dispersion of a solute in a fluid flowing through a tube. Later, Marle et al. (1967) and Guven et al. (1984) used spatial moments to analyze transport of nonreactive solutes for steady horizontal flow in a perfectly stratified aquifer. The aim of these investigations was to derive expressions for the effective velocity and dispersion coefficient governing the transport of the depth-averaged solute plume in terms of the vertical distribution of the Darcy scale seepage velocity vector and hydrodynamic dispersion tensor. Aris' (1956) spatial moment analysis was extended by Horn (1971) to account for solutes that undergo partitioning reactions between two or more phases. Horn (1971) developed a mathematical technique to compute asymptotic moments at large times with respect to global coordinates of the solute concentration averaged over a local domain. Therefore, in the context of solute transport through stratified aquifers with adsorption, Horn's technique yields the spatial moments of the combined depth-averaged concentrations in both the aqueous (mobile) and adsorbed (immobile)

phases. For pollution assessment and remediation studies, it is important to know the distribution of the mobile phase contaminant plume separately from that of the immobile phase.

Spatial concentration data from field experiments tend to be sparse. Thus, the application of a classical parameter estimation method of solving the governing advection-dispersion equation and fitting the parameters may lead to problems of identifiability and non-uniqueness. Average statistical properties tend to be better behaved, and spatial moment analysis offers an alternative method of parameter estimation.

A large scale field experiment on natural gradient transport of solutes in groundwater was conducted at a site in Borden, Ontario. During the field study, a solution containing two inorganic/nonreactive tracers and five volatile halogenated organic compounds was introduced into the aquifer as a pulse input. Freyberg (1986) provided detailed descriptions of the methodology used to interpret the data based on advection and dispersion of nonreactive tracers at the Borden site. This analysis focused on the zero-th, first, and second spatial moments of the concentration distribution. These moments define integrated measures of the dissolved mass, mean solute velocity and the dispersion of the plume. Roberts et al. (1986) described the sorption, retardation and transformation of organic solutes at the Borden site, and Sudicky (1986) discussed spatial variability of aquifer hydraulic conductivity and its relationship to the mean motion of the solute mass. Another large scale natural gradient tracer test was conducted to examine the movement and spreading of reactive and nonreactive tracers in a sand and gravel aquifer in Cape Cod, Massachusetts (LeBlanc et al., 1991). One of the objectives of the Cape Cod study was to test the theoretical studies of Dagan (1982) and Gelhar and Axness (1983). In this study, a pulse solution containing both reactive and nonreactive tracers was introduced into the aquifer. The statistical properties of the spatial variations in aquifer hydraulic conductivity were determined to compute the dispersivity. The predicted results were then compared with the dispersivity calculated from spatial moment analysis of the solute concentrations. Results of spatial moment analysis of nonreactive solute (bromide) transport at the Cape Cod site were presented by Garabedian et al. (1991).

Goltz and Roberts (1987) used a modified form of Aris' method to study spatial moments using the three-dimensional form of the advective-dispersive solute transport equation, with solute diffusion into regions of immobile water. Valocchi (1988) used spatial moment analysis to derive analytical expressions for the temporal evolution of the lower order spatial moments of the depth-averaged concentrations. These expressions, which explicitly show the contribution of kinetics to overall plume spreading, were then utilized to assess the validity of the local equilibrium assumption. Valocchi (1989) examined the impact of adsorption kinetics upon the spatial moments of the depth-averaged contaminant plume using the generalized spatial moment analysis earlier used by Horn (1971) and Brenner (1980). These studies demonstrate the relevance of spatial moment analysis for analyzing experimental results.

Since the studies of Aris (1958), Kubin (1965) and Kucera (1965), method of moments (MOM) has become a standard technique for estimating parameters in equations that describe solute movement through porous media (Ostergaard and Michelsen, 1969; Turner, 1972; Villermaux, 1981; Fahim and Wakao, 1982, Shapiro and Brenner, 1988). Understanding and predicting the movement of various contaminants and nutrients through soil becomes complicated when chemical and biological transformations occur in addition to advection and dispersion processes. Spatial moments may be useful in such instances as well for parameter estimation.

Despite the popularity of spatial moment analysis for studying fate and transport of contaminants, few studies account for rate-limited sorption and degradation when the contaminant is present both in mobile and immobile phases. In this chapter, we focus on spatial moment analysis of several solute transport models.

6.2. SPATIAL MOMENTS

When dealing with spatial moments, the averaging operation occurs in the spatial domain and spatial moments evolve in time. Spatial moments serve as physically meaningful descriptors of overall solute plume behavior. For example, the zero-th order spatial moment yields the total aqueous phase mass contained in the plume, the first moment yields the mean location of the center of the mass of the plume, and the second moment relates to spreading of the plume about its mean position (Freyberg, 1986). Higher order moments describe other properties of the plume. Mathematically the one-dimensional n-th spatial moment of the concentration distribution $c(x, t)$ is expressed as:

$$m_n = \int_{-\infty}^{\infty} x^n c(x, t) dx \tag{6.2.1}$$

The Fourier transform of the function $c(x, t)$ is defined as:

$$\mathcal{F}[c(x, t)] = \tilde{c}(\omega; t) = \int_{-\infty}^{\infty} e^{-j\omega x} c(x, t) dx \tag{6.2.2}$$

from which one obtains:

$$\mathcal{F}[x^n c(x, t)] = \int_{-\infty}^{\infty} e^{-j\omega x} x^n c(x, t) dx = j^n \frac{d^n \tilde{c}(\omega; t)}{d\omega^n} \tag{6.2.3}$$

In equations (6.2.2) and (6.2.3), ω is the Fourier transform variable. Using the property of the Fourier transform, and taking the limit as $\omega \to 0$:

$$\int_{-\infty}^{\infty} x^n c(x, t) dx = j^n \lim_{\omega \to 0} \frac{d^n \tilde{c}(\omega; t)}{d\omega^n} \tag{6.2.4}$$

Comparing with the definition of the n-th spatial moment in (6.2.1)

$$m_n = j^n \lim_{\omega \to 0} \frac{d^n \tilde{c}(\omega; t)}{d\omega^n} \tag{6.2.5}$$

This is the one-dimensional spatial analog to Aris' temporal moments. The method of spatial moments is quite useful as it allows the calculation of moments in the Fourier domain, eliminating the need for complicated inversions of the transformed concentration variables. Spatial moments can also be extended to two and three-dimensional cases (Goltz and Roberts, 1987).

The choice of the model determines the expressions for these spatial moments in terms of model parameters. The first central moment of the mobile phase represents the location of the center of the mobile mass and is expressed as:

$$X(t) = \frac{m_1(t)}{m_0(t)} \tag{6.2.6}$$

where m_0 is the total mass of solute in the soil, m_1 is the first moment, and X is the location of center of mass. In equation (6.2.6) the explicit dependence of moments on time is indicated. The large scale effective velocity of the solute plume can be defined as (Goltz and Roberts, 1987):

$$V_{eff} = \frac{d}{dt}\{X(t)\} = \frac{d}{dt}\left\{\frac{m_1(t)}{m_0(t)}\right\} \tag{6.2.7}$$

The second spatial moment relates to the dispersion characteristics of the solute as it moves through soil. Defining variance as,

$$\sigma^2 = \frac{m_2}{m_0} - \left(\frac{m_1}{m_0}\right)^2 \tag{6.2.8}$$

the effective dispersion coefficient may be obtained as:

$$D_{eff} = \frac{1}{2}\frac{d}{dt}(\sigma^2) \tag{6.2.9}$$

Several investigators (Brenner and Adler, 1982; Guven et al., 1984) have discussed the significance of the long-time, asymptotic values of effective velocity and the effective dispersion coefficient.

6.3. SPATIAL MOMENTS TO DESCRIBE SOLUTE PLUME BEHAVIOR

To motivate the discussion on spatial moments, we start with a simple case of three-dimensional solute movement of a contaminant in a flow field. Under simplifying assumptions, solute mass conservation may be expressed as (Charbeneau, 2000)

$$\frac{\partial c_b}{\partial t} + \nabla \boldsymbol{q}_s = -\gamma c_b \tag{6.3.1}$$

where c_b is the bulk resident solute concentration defined in Chapter 2, $\boldsymbol{q}_s$ is the solute flux vector, and γ is a first-order degradation rate constant. We assume that

the solute is not present in the solid and vapor phases, so that the resident liquid concentration is defined as

$$c_{l,r} = c_b/\eta \tag{6.3.2}$$

where η is the porosity and is taken to be uniform.

For simplicity, the initial condition is chosen to be a mass of solute M added as bulk concentration instantaneously at the origin, so that

$$c_b(x, y, z, t = 0) = M\delta(x)\ \delta(\mathrm{y})\ \delta(\mathrm{z}) \tag{6.3.3}$$

This initial condition was presented in a one-dimensional case in (3.3.10).

The vectorial solute flux $\boldsymbol{q}_s$ in (6.3.1) has three components, and can be represented in the x-direction as (see also equation (2.5.13))

$$q_{s,x} = -\eta\ \mathrm{D}_{xx}\frac{\partial c_{l,r}}{\partial x} + q_x c_{l,r} \tag{6.3.4}$$

where q_x is the Darcian water flux in the x-direction. The expressions for solute flux in the y and z directions have the same form as equation (6.3.4).

The three dimensional spatial moments for the bulk and liquid resident concentrations can be defined as

$$M(t)_{jkn} = \int_{-\infty}^{\infty}\int_{-\infty}^{\infty}\int_{-\infty}^{\infty} x^j y^k z^n c_b(x, y, z, t)\ dx\ dy\ dz \tag{6.3.5a}$$

$$M'(t)_{jkn} = \int_{-\infty}^{\infty}\int_{-\infty}^{\infty}\int_{-\infty}^{\infty} x^j y^k z^n c_{l,r}(x, y, z, t)\ dx\ dy\ dz \tag{6.3.5b}$$

Using Fourier transforms in three dimensions and Aris' method, it is possible to develop expressions for moments (see Goltz and Roberts, 1987). Alternatively, one can directly integrate equation (6.3.1) as

$$\int_{\mathbf{\Omega}} x^j y^k z^n \left[\frac{\partial c_b}{\partial t} + \nabla \mathbf{q}_s + \gamma_{c_b}\right] d\,\mathbf{\Omega} = 0 \tag{6.3.6}$$

where $\mathbf{\Omega}$ represents the spatial domain, with $\mathbf{\Gamma}$ denoting its boundary. Using Green's theorem, and denoting by $\boldsymbol{r}$ the outward printing normal at the boundary of the region, one obtains from (6.3.1)

$$\frac{d\ M_{jkn}}{dt} + \int_{\mathbf{\Gamma}} x^j y^k z^n \boldsymbol{q}_s \cdot \boldsymbol{r}\mathbf{d}\mathbf{\Gamma} - \int_{\mathbf{\Omega}} j x^{j-1} y^k z^n q_{s,x} \cdot d\mathbf{\Omega}$$

$$- \int_{\mathbf{\Omega}} k x^j y^{k-1} z^n q_{s,y}\ d\Omega - \int_{\mathbf{\Omega}} n x^j y^k z^{n-1} q_{s,z}\ d\Omega\ + \gamma\ M_{jkn} = 0 \tag{6.3.7}$$

Substituting expressions for solute fluxes (6.3.4) into (6.3.7) and simplifying yields the following equation

$$\frac{d\ M_{jkn}}{dt} + \gamma M_{jkn} = j\ q_x\ M'_{j-1,k,n} + j(j-1)\ D_{xx}\ \eta\ M'_{j-2,k,n} + kq_y\ M'_{j,k-1,n} + k(k-1)D_{yy}\eta M'_{j,k-2,n} + nq_z\ M'_{j,k,n-1} + n(n-1)\ \mathrm{D}_{zz}\eta\ M'_{j,k,n-2} \tag{6.3.8}$$

Note that the equation for M_{jkn} involves moments of lower orders in the right hand side of (6.3.8). We observe from (6.3.2) and (6.3.5) that

$$M'_{j,k,n} = M_{j,k,n}/\eta \tag{6.3.9}$$

Furthermore, from (6.3.3) we have the initial condition

$$M_{j,k,n}(t=0) = \begin{cases} M, & j=k=n=0 \\ 0, & \text{otherwise} \end{cases} \tag{6.3.10}$$

We are now in a position to evaluate the spatial moments for this problem. Setting $j=k=n=0$ in (6.3.8) we obtain

$$\frac{d}{dt}\left(M_{0,0,0}\right) + \gamma\ M_{0,0,0} = 0\ ;\ \mathrm{M}_{0,0,0}(0) = M \tag{6.3.11}$$

for which the solution is

$$M_{0,0,0}(t) = M_0\ \mathrm{e}^{-\gamma t} \tag{6.3.12}$$

This is a result that we expect. It states that the total solute mass (in the plume ($M_{0,0,0}$) decays exponentially with time at the rate of γ. Similarly, setting $j=\ 1,\ k=\ 0,\ n=0$ in (6.3.8)

$$\frac{dM_{1,0,0}}{dt} + \gamma\ M_{1,0,0} = \frac{q_x M_{0,0,0}}{\eta};\ M_{1,0,0}(0) = 0 \tag{6.3.13}$$

from which

$$\mathrm{M}_{1,0,0}(t) = M\ V_x\ te^{-\gamma t} \tag{6.3.14}$$

where $V_x(=q_x/\eta)$ is the pore water velocity in the x direction. For $j=2,\ k=0,$ $n=0$, we obtain

$$\frac{dM_{2,0,0}}{dt} + \gamma M_{2,0,0} = 2\cdot\frac{q_x}{\eta}M_{1,0,0} + 2D_{xx}M_{0,0,0}\ ;\ \mathrm{M}_{2,0,0}\ (0) = 0 \tag{6.3.15}$$

The solution for this equation yields

$$M_{2,0,0}(t) = 2M\ \mathrm{e}^{-\gamma t}\left[\frac{V_x^2 t^2}{2} + D_{xx} t\right] \tag{6.3.16}$$

Using the definitions for effective properties in equations (6.2.7) and (6.2.9), we have

$$V_{eff,x} = \frac{d}{dt}\left(\frac{M_{1,0,0}}{M_{0,0,0}}\right) = V_x \tag{6.3.17a}$$

$$D_{eff,x} = \frac{d}{dt}\left[\frac{M_{2,0,0}}{M_{0,0,0}} - \left(\frac{M_{1,0,0}}{M_{0,0,0}}\right)^2\right] = D_{xx} \tag{6.3.17b}$$

6.4. SPATIAL MOMENTS FOR THE PNE MODEL

Consider the non-dimensional form of the PNE model described in Chapter 5. The governing equations are

$$\beta R\frac{\partial C_1}{\partial T} = \frac{1}{P}\frac{\partial C_1}{\partial Z^2} - \frac{\partial C_1}{\partial Z} - \bar{\alpha}\,(C_1 - C_2) - \gamma_1 C_1 \tag{6.4.1}$$

$$(1-\beta)R\frac{\partial C_2}{\partial T} = \bar{\alpha}\,(C_1 - C_2) - \gamma_2 C_2 \tag{6.4.2}$$

under the initial condition

$$C_1\,(Z, 0) = M \cdot \delta(Z) \tag{6.4.3}$$

Here C_1 and C_2 refer to non-dimensional values of resident liquid phase concentrations association with mobile and immobile water regions, respectively. Using a slight variation of the Fourier transforms discussed in Chapter 3, we define as Goltz and Roberts (1987).

$$\tilde{C}_1\,(\omega; T) = \int_{-\infty}^{\infty} e^{-j\omega Z} C_1(Z, T)\ dZ \tag{6.4.4}$$

$$\tilde{C}_2\,(\omega; T) = \int_{-\infty}^{\infty} e^{-j\omega Z} C_2(Z, T)\ dZ \tag{6.4.5}$$

Defining spatial moments as

$$m_k(T) = \int_{-\infty}^{\infty} Z^k\ C_1(Z, T)\ dZ \tag{6.4.6}$$

$$n_k(T) = \int_{-\infty}^{\infty} Z^k\ C_2(Z, T)\ dZ \tag{6.4.7}$$

and using the analog of Aris (1958) method to spatial moments, we obtain

$$m_k = j^k \lim_{\omega \to 0} \frac{\mathrm{d}^k \tilde{C}_1(\omega; T)}{d\omega^k} \tag{6.4.8}$$

$$n_k = j^k \lim_{\omega \to 0} \frac{\mathrm{d}^k \tilde{C}_2(\omega; T)}{d\omega^k} \tag{6.4.9}$$

Using (6.4.4) and (6.4.5) in the governing equations (6.4.1) and (6.4.2), we obtain the transformed equations as

$$\beta R \frac{d\tilde{C}_1}{dT} = \frac{1}{p} j^2 \omega^2 \tilde{C}_1 - j\omega \tilde{C}_1 - \bar{\alpha}\left(\tilde{C}_1 - \tilde{C}_2\right) - \gamma_1 \tilde{C}_1 \tag{6.4.10}$$

$$(1-\beta) R \frac{d\tilde{C}_2}{dT} = \alpha\left(\tilde{C}_1 - \tilde{C}_2\right) - \gamma_2 \tilde{C}_2 \tag{6.4.11}$$

and furthermore,

$$\tilde{C}_1(T=0) = M \; ; \; \tilde{C}_2(T=0) = 0 \tag{6.4.12}$$

Note that (6.4.10) and (6.4.11) constitute a system of first-order linear differential equations. Solving for $\tilde{C}_1$ and $\tilde{C}_2$ and then using (6.4.8) would yield expressions for successively higher order moments. However, the resulting algebra can be quite tedious, and only the procedure is indicated here. Equations (6.4.10) and (6.4.11) are written in matrix form as

$$\begin{Bmatrix} \frac{d\tilde{C}_1}{dT} \\ \frac{d\tilde{C}_2}{dT} \end{Bmatrix} = \begin{bmatrix} a_{11} & a_{12} \\ a_{21} & a_{22} \end{bmatrix} \begin{Bmatrix} \tilde{C}_1 \\ \tilde{C}_2 \end{Bmatrix} \tag{6.4.13}$$

where

$$a_{11} = \frac{j^2\omega^2/P - j\omega - \bar{\alpha} - \gamma_1}{\beta R} \tag{6.4.14a}$$

$$a_{12} = \frac{\bar{\alpha}}{\beta R} \tag{6.4.14b}$$

$$a_{21} = \frac{\bar{\alpha}}{(1-\beta)R} \tag{6.4.14c}$$

$$a_{22} = -\frac{\bar{\alpha} + \gamma_2}{(1-\beta)R} \tag{6.4.14d}$$

The eigenvalues of the square matrix [A] in (6.4.13) are

$$\lambda_{1,2} = \frac{(a_{11} + a_{22}) \pm \sqrt{(a_{11} + a_{22})^2 - 4(a_{11}a_{22} - a_{21}a_{12})}}{2} \tag{6.4.15}$$

Using the Cayley-Hamilton theorem (see for example, Bronson, 1973), we have

$$\tilde{C}_1(T) = \alpha_1 a_{11} T + \alpha_0 \tag{6.4.16}$$

$$\tilde{C}_2(T) = \alpha_1 a_{21} T \tag{6.4.17}$$

where

$$\alpha_1 = \frac{e^{\lambda_1 T} - e^{\lambda_2 T}}{(\lambda_1 - \lambda_2)\, T} \tag{6.4.18}$$

$$\alpha_0 = \frac{\lambda_1 e^{\lambda_2 T} - \lambda_2 e^{\lambda_1 T}}{(\lambda_1 - \lambda_2)} \tag{6.4.19}$$

An alternate method is based on the realization that (6.4.10) and (6.4.11) are amenable to Laplace transforms. Thus defining

$$\hat{\tilde{C}}_1 = \int_0^\infty e^{-sT} \tilde{C}_1(T) dT; \;\; \hat{\tilde{C}}_2 = \int_0^\infty e^{-sT} C_2(T) dT \tag{6.4.20}$$

and taking Laplace transforms of (6.4.10) and (6.4.11) under the initial conditions described in (6.4.12) yields

$$\hat{\tilde{C}}_1 = \frac{M\beta R}{\beta R s - \frac{1}{P} j^2 \omega^2 + j\omega + \bar{\alpha} - \frac{\bar{\alpha}^2}{(1-\beta)Rs + \bar{\alpha} + \gamma_2} + \gamma_1} \tag{6.4.21}$$

Taking the inverse Laplace transform of (6.4.21) yields an expression for $\tilde{C}_1$. Taking derivatives with respect to ω and using Aris' method yields expressions for the spatial moments. However, the resulting expressions are very complicated. A somewhat simpler method will be presented in Chapter 8 in the form of moment generating differential equations.

6.5. SPATIAL MOMENTS FOR FIRST-ORDER RATE MODEL

Goltz and Roberts (1987) considered the formulation of physical nonequilibrium model where immobile water regions exchange solute with mobile water regions according to a first-order rate law. They presented the governing differential equation for solute movement in three dimensions with Darcian flux in a single (x) direction

$$\frac{\partial C_m}{\partial t} = D_x \frac{\partial^2 C_m}{\partial x^2} + D_y \frac{\partial^2 C_m}{\partial y^2} + D_z \frac{\partial^2 C_m}{\partial x^2} - V \frac{\partial C_m}{\partial_x} - \beta \frac{\partial C_{im}}{\partial t} \tag{6.5.1}$$

$$\frac{\partial C_{im}}{\partial t} = \alpha (C_m - C_{im}) \tag{6.5.2}$$

where C_m and C_{im} are resident solute concentrations in mobile and immobile regions, V is the average seepage velocity in the x-direction, β is a parameter representing

the solute capacity ratio of the mobile region to that of the immobile region. An instantaneous point source in an infinite porous media leads to the following initial conditions.

$$C_m(x, y, z, 0) = M\ \delta(\mathrm{x})\delta(y)\ \delta(\mathrm{z}) \tag{6.5.3a}$$

$$C_{im}(x, y, z, 0) = 0 \tag{6.5.3b}$$

Concentrations far away from the region of interest are assumed to be zero. Defining spatial moments of the mobile concentrations as

$$m_{jkn} = \int_{-\infty}^{\infty}\int_{-\infty}^{\infty}\int_{-\infty}^{\infty} x^j y^k z^n C_m(x, y, z, t)\ dx\ dy\ dz \tag{6.5.4}$$

Goltz and Roberts (1987) developed expressions for some moments as

$$m_{000} = \frac{M(1+\beta A)}{1+\beta} \tag{6.5.5}$$

$$\frac{m_{100}}{m_{000}} = \frac{Vt(1+\beta^2 A)}{(1+\beta)(1+\beta A)} + \frac{2V\beta(1-A)}{\alpha(1+\beta)^2(1+\beta A)} \tag{6.5.6}$$

$$\begin{aligned}\frac{m_{200}}{m_{000}} = {} & \frac{2D_x t(1+\beta^2 A)}{(1+\beta)(1+\beta A)} + \frac{4D_x\beta(1-A)}{\alpha(1+\beta)^2(1+\beta A)} \\ & + \frac{V^2t^2(1+\beta^3 A)}{(1+\beta)^2(1+\beta A)} + \frac{6V^2\beta(\beta-1)(1-A)}{\alpha^2(1+\beta)^4(1+\beta A)} \\ & + \frac{6\beta V^2 t(1-\beta A)}{\alpha(1+\beta)^3(1+\beta A)}\end{aligned} \tag{6.5.7}$$

$$\frac{m_{020}}{m_{000}} = \frac{2D_y t(1+\beta^2 A)}{(1+\beta)(1+\beta A)} + \frac{4D_y\beta(1-A)}{\alpha(1+\beta)^2(1+\beta A)} \tag{6.5.8}$$

$$\frac{m_{002}}{m_{000}} = \frac{2D_z t(1+\beta^2 A)}{(1+\beta)(1+\beta A)} + \frac{4D_z\beta(1-A)}{\alpha(1+\beta)^2(1+\beta A)} \tag{6.5.9}$$

In the above expressions for moments, the quantity $A = \exp[-\alpha t(1+\beta)]$. Under the local equilibrium assumption, the parameter β would be set to zero in the above expressions for moments. From symmetry of the governing equations (6.5.1) and (6.5.2) it should be noted that $m_{jkn} = 0$ for k or n odd.

Using the expressions for the spatial moments, the Lagrangian effective properties can be defined. For instance

$$V_{eff,x} = \frac{d}{dt}\left[\frac{m_{100}}{m_{000}}\right] \tag{6.5.10}$$

$$D_{eff,x} = \frac{1}{2}\ \frac{d}{dt}\left\{\frac{m_{200}}{m_{000}} - \left(\frac{m_{100}}{m_{000}}\right)^2\right\} \tag{6.5.11}$$

However, the resulting expressions are too complex, and Goltz and Roberts (1987) suggest that the derivatives may be evaluated numerically and their plots studied to obtain insights into the behavior of these effective properties. Goltz and Roberts (1987) also studied the behavior of spatial (and temporal) moments for the model in (6.5.1) combined with diffusion into spherical grains as was discussed in Chapter 2. In this case, equation (6.5.2) is replaced with

$$\frac{\partial C_a}{\partial t} = \frac{D_e}{r^{\nu-1}} \frac{\partial}{\partial r} \left[r^{\nu-1} \frac{\partial C_a}{\partial r} \right] \tag{6.5.12a}$$

$$C_{im} = \frac{\nu}{b^{\nu}} \int_0^b r^{\nu-1} \, C_a dr \tag{6.5.12b}$$

where $\nu = 1, 2,$ or 3 corresponding to the geometry of the immobile regions, b is the size of the immobile region and C_a is the solute concentration within the immobile region. The moment expressions for this model tend to be much more complicated.

CHAPTER 7

MOMENT ANALYSIS FOR VOLATILE COMPOUNDS

7.1. INTRODUCTION

Organic solutes, owing to their volatility, have a significant amount of their total mass exist in vapor phase in the soil. These volatile fractions experience transport by diffusion and bulk air movement. Volatilization losses to the atmosphere can be a significant fraction of the total solute mass. Remediation methods, such as soil venting or vacuum extraction, rely on the occurrence of substantial transport in the vapor phase. In this chapter, we explore moment analysis techniques for volatile compounds.

A schematic sketch of loss pathways for compounds is shown in Figure 7.1.1. As indicated, part of the contaminant mass undergoes transformation into intermediate products called metabolites. Some solutes are susceptible to degradation losses because of chemical and or biological reactions. Both models (Jury et al., 1983, 1990; van Genuchten and Wagenet, 1989) and experimental studies (Hutzler et al., 1989; Gierke et al., 1992) have been used to investigate the fate and transport of volatile compounds. Gierke et al. (1990) developed a deterministic model for nondegradable organic chemicals that accounts for the processes of advection and dispersion in air as well as water, mass transfer between air-water and mobile-immobile water, sorption, and, diffusion in immobile water. It was believed that mass transfer at the air-water interface could be important for volatile pollutants in unsaturated soil. Based on experimental results for trichloroethene, it was concluded that both liquid dispersion and diffusion in immobile water are important when accounting for the transport of nondegradable volatile organic chemicals (VOCs).

Jury et al. (1983) presented a mathematical model that assumes linear equilibrium partitioning between vapor, liquid and adsorbed chemical phases, net first order degradation, and chemical movement to the atmosphere by volatilization loss through a stagnant air boundary layer at the top of the soil surface. In a later paper (Jury et al., 1990), a screening model was introduced to evaluate relative volatilization losses of a number of compounds under typical soil conditions. These authors used an analytical solution for 1-D transport of VOCs under the initial condition of a uniform concentration of organic chemical located at a certain depth. It was observed that volatilization losses are highly sensitive to the organic carbon

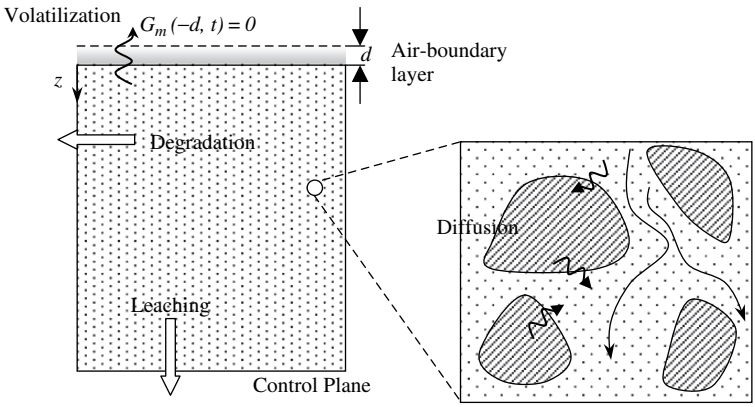

Figure 7.1.1. Schematic illustration of pollutant loss pathways in two-region soils (adapted from Hantush et al., 2002, with permission from Elsevier)

fraction and the stagnant boundary layer thickness through which the chemical escapes to the atmosphere. It has been shown that nonequilibrium sorption of moderately hydrophobic, volatile organic compounds can be attributed to intragranular diffusion (Cunningham et al., 1997a,b), and this aspect can significantly influence the fate and transport of these compounds. A one-dimensional model of vapor transport that accounts for structured porous medium and rate-limited sorption was developed by Brusseau (1991).

Hutzler et al. (1989) examined the predominant mechanisms affecting transport of VOCs at low degrees of saturation in uniform sands and at higher degrees of saturation in aggregated soils. To examine the impact of gas advection and diffusion, Gierke et al. (1992) developed a mathematical model and performed laboratory experiments to investigate the impact of various mechanisms on vapor transport. They showed that the models that are developed for predicting complete removal of contaminants by vapor extraction must account for nonequilibrium transport.

Simple models have been often used for devising rating schemes, and for developing a list of priority pesticides that have a high potential for contaminating groundwater. Such models were used for screening organic chemicals relative to their mobility in the soil (Laskowski et al., 1982; Jury et al., 1983; Meeks and Dean, 1990). Leached fraction models are also used for screening of pesticides and estimating the likelihood of ground-water contamination (Rao et al., 1985; Meeks and Dean, 1990; van der Zee and Boesten, 1991; Beltman et al., 1995; Hantush et al., 2000). Hantush et al. (2000) developed a leaching mass fraction index that lumps the effect of volatilization and lateral diffusive mass transfer into a single parameter. Mass fraction models of this kind can be integrated with relative ease into a GIS framework to produce an effective assessment tool for the management of nonpoint source pollution in watersheds (e.g., Khan and Liang, 1989; Loague et al., 1995;

Mulla et al., 1996; Shukla et al., 2000). Hantush et al. (2002) and Hantush and Govindaraju (2003) have presented moment analyses for volatile compounds.

7.2. IMMOBILE VAPOR PHASE MODEL

A box-diagram with different compartments for partial nonequilibrium model with immobile air phase is shown in Figure 7.2.1. In this section, we assume that the air phase within the soil is stagnant and does not play an active role in advection, but it is involved in solute exchange with the liquid phase. However, at the soil surface, volatilization losses are assumed to exist because of diffusion of solute from the air phase of the soil to the atmosphere across a thin boundary layer (Jury et al., 1983, 1990). Under this construct, the relative importance of solute leaching past a control plane, degradation and vapor-phase emissions to the air will be examined through moment analysis. Volatilization at the soil-air interface by diffusion across an air boundary (Jury et al., 1983; Wagenet and Rao, 1990; and Yates et al., 2000) layer will be treated as a boundary condition. The analysis of Parashar (2003) and (Parashar et al., 2007), is presented here briefly. The important model assumptions are:

- Gas-phase diffusion is generally more complex than aqueous-phase diffusion as it can occur not only by molecular diffusion but also by Knudsen diffusion and nonequimolar diffusion. However, for vadose zone systems, in absence of fine grained materials and the assumption of dilute concentration in the gas phase being valid, molecular diffusion is assumed to be the predominant form of diffusion (Brusseau, 1991).

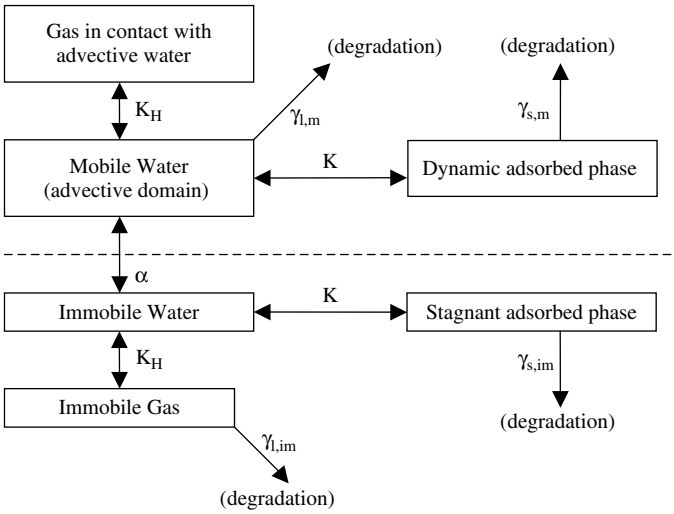

Figure 7.2.1. Conceptual diagram of the partial nonequilibrium model with immobile air phase (adapted from Parashar et al., 2007, with permission from ASCE)

- The exchange of solute between mobile and immobile regions is governed by liquid-liquid mass transfer coefficient $\alpha(T^{-1})$.
- The assumption of zero liquid flux at the surface, which is usually true for water flow, may not be valid for gas flow. As stated, it is assumed that volatilization of chemical vapor to the atmosphere occurs through a stagnant air boundary layer above which the chemical concentration is assumed to be zero (i.e., $G_m(-d, t) = 0$ in Figure 7.1.1).
- The condition of incompressibility will be assumed to hold true for both water flow and gas flow.
- Mass transfer between gas and liquid phase will be assumed to be instantaneous and governed by Henry's Law. It has been shown experimentally that in the presence of other nonideality factors, assumption of local equilibrium for gas-liquid mass transfer is reasonable (Baehr et al., 1989; Brusseau et al., 1990; Gierke et al., 1990, 1992).
- Sorption of organic chemicals by the soil will also be assumed to be instantaneous and reasonably described by a linear isotherm. It will be further assumed that vapor-phase sorption is negligible. The degradation occurring in solid and liquid phases will be modeled as a first-order process.

Solute flux q_s $(ML^{-2}T^{-1})$ is the sum of diffusion through the gaseous phase and the hydrodynamic dispersion and advection in the liquid phase. Expressing diffusion and dispersion processes by Fick's law,

$$q_s = -\theta_m D_m \frac{\partial c_m}{\partial z} - a_m D_G \frac{\partial G_m}{\partial z} + q c_m \tag{7.2.1}$$

where θ_m (L^3L^{-3}) is the volumetric water content in mobile region, a_m (L^3L^{-3}) is the volumetric air content in mobile region, D_m (L^2T^{-1}) is the liquid dispersion coefficient in soil, D_G (L^2T^{-1}) is the gaseous diffusion coefficient in soil, G_m (ML^{-3}) is the gaseous phase concentration of solute in mobile region where concentration is expressed as mass of solute per unit volume of soil air, c_m (ML^{-3}) is the concentration of solute in liquid phase in mobile region expressed as mass of solute per unit volume of soil solution, and q (LT^{-1}) is the volumetric soil water Darcian flux.

The total mass of solute present per unit bulk volume of soil c_b (ML^{-3}) can be written as the sum of masses residing in liquid, gas, and adsorbed phases as

$$c_b = \theta_m c_m + \theta_{im} c_{im} + f\rho S_m + (1-f)\rho S_{im} + a_m G_m + a_{im} G_{im} \tag{7.2.2}$$

where f is the fraction of sorption sites in mobile region, ρ (ML^{-3}) is the soil bulk density, and S (MM^{-1}) is the solid phase concentration expressed as mass of solute per unit mass of soil. The subscripts 'm' and 'im' on S represent mobile and immobile regions, respectively.

Based on the stated assumptions, equilibrium relationships can be expressed as,

$$S_m = Kc_m = f_{oc}K_{oc}c_m, \tag{7.2.3a}$$

$$S_{im} = Kc_{im} = f_{oc}K_{oc}c_{im}, \tag{7.2.3b}$$

$$G_m = K_H\ c_m, \tag{7.2.3c}$$

$$G_{im} = K_H\ c_m \tag{7.2.3d}$$

where K (L^3T^{-1}) is the distribution coefficient, f_{oc} is the soil organic carbon fraction, and K_{oc} (L^3T^{-1}) is the organic carbon coefficient. In equations (7.2.3c) and (7.2.3d) K_H is the dimensionless form of Henry's constant.

Combining (7.2.1) and (7.2.3) with mass conservation equation (5.1.1), and accounting for degradation losses leads to

$$\begin{aligned}(\theta_m + f\rho K + a_m K_H)\frac{\partial c_m}{\partial t} + \{\theta_{im} + (1-f)\rho K + a_{im}K_H\}\frac{\partial c_{im}}{\partial t}\\ = (\theta_m D_m + a_m D_G K_H)\frac{\partial^2 c_m}{\partial z^2} - q\frac{\partial c_m}{\partial z} - \left(\theta_m \gamma_{l,m} + f\rho K\gamma_{s,m}\right)c_m\\ - \left\{\theta_{im}\gamma_{l,im} + (1-f)\rho K\gamma_{s,im}\right\}c_{im}\end{aligned} \tag{7.2.4}$$

where γ [T^{-1}] is the degradation rate constant. Subscripts 'l' and 's' denote the liquid and adsorbed solid phases, respectively.

Assuming diffusional mass transfer from mobile to immobile region in the liquid phase, the rate of change of mass in the immobile zone with respect to time can be expressed as,

$$\frac{\partial}{\partial t}\{\theta_{im}c_m + (1-f)\rho S_{im} + a_{im}G_{im}\} = \alpha(c_m - c_{im}) - \left\{\theta_{im}\gamma_{l,im} + (1-f)\rho K\gamma_{s,im}\right\}c_{im} \tag{7.2.5}$$

where α (T^{-1}) is the diffusional mass transfer coefficient between mobile and immobile regions. Equations (7.2.4) and (7.2.5) constitute the set of governing differential equations that describe the fate and transport of dissolved concentrations in the mobile and immobile regions.

In most applications, the first-order rate model has been used to describe physical nonequilibrium transport with α being treated as a calibration parameter (e.g., van Genuchten and Wierenga, 1976; Li et al., 1994; Griffioen et al., 1998). Expressions relating the parameter to the geometry of the immobile water zone, by fitting to diffusion models of uniformly sized geometry (e.g., spherical, cylindrical, and finite slabs) have been developed (e.g., Parker and Valocchi, 1986; van Genuchten and Dalton, 1986). Although this conceptualization is strictly applicable to infinite slabs of the immobile-phase region, it may be generalized to other geometries (e.g., spheres, cylinders, and finite slabs) by using appropriate shape factors (Parker and Valocchi, 1986; van Genuchten and Dalton, 1986; Goltz and Roberts, 1987). In

these studies it was implicitly assumed that the diffusion time in the mobile phase is much smaller than that in the immobile phase. This assumption may not always be satisfied for highly volatile compounds, where D_m and D_{im} may be dominated by vapor-phase diffusion, and where the diffusion time in both the mobile and immobile phases may be of the same order of magnitude (Hantush et al. 2002). Hantush and Mariño (1998) describe how the mass transfer coefficient α is affected by diffusion time in both phases.

The initial concentration is assumed to be zero throughout the semi-infinite soil column. Volatilization of the chemical vapor to the atmosphere is assumed to occur by vapor diffusion through a stagnant air boundary layer of thickness d (L), above which the chemical concentration is zero. Jury et al. (1983) discuss ways of estimating values of d. A boundary layer transfer coefficient h (LT^{-1}) can be defined as the quotient of D_G and d. The liquid flux at the soil surface ($z = 0$) can be assumed to be an impulse input with total amount of mass injected being equal to M_0. Therefore, the complete set of initial and boundary conditions can be written as,

$$c_m(z, 0) = c_{im}(z, 0) = 0 \tag{7.2.6a}$$

$$c_m(\infty, t) = c_{im}(\infty, t) = 0 \tag{7.2.6b}$$

$$\text{Gas flux} : q_G = -a_m D_G \frac{\partial G_m}{\partial z} = -hG_m \tag{7.2.6c}$$

$$\text{Liquid flux} : q_L = -\theta_m D_m \frac{\partial c_m}{\partial z} + qc_m = M_0 \delta(t) \tag{7.2.6d}$$

The total flux q_s is the sum of liquid flux q_L and the gaseous flux q_G. Hence at the upper boundary ($z = 0$), q_s can be written as,

$$\begin{aligned} q_s(0, t) &= q_L(0, t) + q_G(0, t) \\ &= \left[-\theta_m D_m \frac{\partial c_m}{\partial z} - a_m D_G \frac{\partial G_m}{\partial z} + qc_m \right]_{z=0} \\ &= \left[-\left(\theta_m D_m + a_m D_G K_H\right) \frac{\partial c_m}{\partial z} + qc_m \right]_{z=0} \\ &= hK_H c_m|_{z=0} + M_0 \delta(t) \end{aligned} \tag{7.2.7}$$

The following nondimensional variables are introduced:

$$\phi = \frac{\theta_m}{\theta} = \frac{\theta_m}{\theta_m + \theta_{im}} \tag{7.2.8a}$$

$$T = \frac{V_0 t}{L} = \frac{V_m \phi t}{L} \tag{7.2.8b}$$

$$X = \frac{z}{L} \tag{7.2.8c}$$

$$C_1 = \frac{c_m}{C_0};\ C_2 = \frac{c_{im}}{C_0};\quad C_0 = \frac{M_0}{\theta_m L} \tag{7.2.8d}$$

$$\gamma_1 = \frac{L}{V_m \theta_m}\left(\theta_m \gamma_{l,m} + f\rho K \gamma_{s,m}\right) \tag{7.2.8e}$$

$$\gamma_2 = \frac{L}{V_m \theta_m}\left(\theta_{im} \gamma_{l,im} + (1-f)\,\rho K \gamma_{s,im}\right) \tag{7.2.8f}$$

$$P = \frac{V_m L}{D},\ \text{where } D = \frac{\theta_m D_m + a_m D_G K_H}{\theta_m} \tag{7.2.8g}$$

$$V_m = \frac{q}{\theta_m} \tag{7.2.8h}$$

Here, L is the distance from the source ($z = 0$) to the control plane. Retardation in the mobile region, R_m, and retardation in the immobile region, R_{im}, may be defined as

$$R_m = \frac{\theta_m + f\rho K + a_m K_H}{\theta_m} = 1 + \frac{f\rho K}{\theta_m} + \frac{a_m K_H}{\theta_m} \tag{7.2.9}$$

$$R_{im} = \frac{\theta_{im} + (1-f)\,\rho K + a_{im} K_H}{\theta_m} \cdot \frac{\phi}{1-\phi} = 1 + \frac{(1-f)\,\rho K}{\theta_{im}} + \frac{a_{im} K_H}{\theta_{im}} \tag{7.2.10}$$

A nondimensional mass transfer rate coefficient is defined as

$$\omega = \frac{\alpha L}{V_m \theta_m} \tag{7.2.11}$$

Utilizing equations (7.2.8) to (7.2.11), equations (7.2.4) and (7.2.5) may be expressed as

$$R_m \phi \frac{\partial C_1}{\partial T} = \frac{1}{P}\frac{\partial^2 C_1}{\partial X^2} - \frac{\partial C_1}{\partial X} - \omega\,(C_1 - C_2) - \gamma_1 C_1 \tag{7.2.12}$$

$$(1-\phi)\,R_{im}\frac{\partial C_2}{\partial T} = \omega\,(C_1 - C_2) - \gamma_2 C_2 \tag{7.2.13}$$

The end conditions of (7.2.6) and (7.2.7) are

$$\left[-\frac{1}{P}\frac{\partial C_1}{\partial X} + C_1\right]_{X=0} = -HC_1|_{X=0} + M_1\delta(T);\ C_1(X,0) = C_2(X,0) = 0 \tag{7.2.14}$$

with

$$H = \frac{hK_H}{\theta_m V_m}; \tag{7.2.15}$$

$$M_1 = \frac{M_0}{C_0 L \theta} \tag{7.2.16}$$

7.3. DESCRIPTION OF LOSS FRACTIONS

Following the definitions in Chapter 5, the Laplace transforms of the dimensionless concentrations are defined as

$$\hat{C}_i(X;s) = \int_0^\infty e^{-sT} C_i(X,T)dT, \qquad i = 1,2 \tag{7.3.1}$$

Taking Laplace transform of equations (7.2.12) and (7.2.13) and solving the resulting ODE using the boundary conditions of equation (7.2.14) results in the following expressions

$$\hat{C}_1(X;s) = \frac{M_1 P\ exp\left[\frac{PX}{2}\left\{1-\sqrt{1+\frac{4}{P}\left(R_m\phi s+\gamma_1+\omega-\frac{\omega^2}{(1-\phi)R_{im}s+\omega+\gamma_2}\right)}\right\}\right]}{(1+H)\,P-\left[\frac{P}{2}\left\{1-\sqrt{1+\frac{4}{P}\left(R_m\phi s+\gamma_1+\omega-\frac{\omega^2}{(1-\phi)R_{im}s+\omega+\gamma_2}\right)}\right\}\right]} \tag{7.3.2}$$

$$\hat{C}_2(X;s) = \frac{\omega\hat{C}_1(X;s)}{(1-\phi)R_m s+\omega+\gamma_2} \tag{7.3.3}$$

Based on the boundary condition (7.2.14) and assuming that mass of M_0 is instantaneously applied at the soil surface at $t = 0$, the volatilization and leaching fractions are obtained as (see Hantush et al., 2002; Parashar, 2003; Parashar et al., 2007)

$$I_v = \frac{H}{M_1}\lim_{s\to 0}\hat{C}_1(0;s) = \frac{2H}{2(1+H)+A-1} \tag{7.3.4}$$

$$I_l = \frac{1}{M_1}\lim_{s\to 0}\left[-\frac{1}{P}\frac{\partial\hat{C}_1}{\partial X}+\hat{C}_1\right]_{x=1} = \frac{(1+A)\,e^{\left\{\frac{P}{2}(1-A)\right\}}}{2(1+H)+A-1} \tag{7.3.5}$$

The fraction of M_1 lost due to degradation in the mobile and immobile regions over the entire depth ($0 \le X \le 1$) is given, respectively, by

$$I_m = \lim_{s\to 0}\frac{\gamma_1}{M_1}\int_0^1 \hat{C}_1(X;s)dX = \frac{1}{1+\varphi^*}\frac{(1+A)\left[1-e^{\left\{\frac{P}{2}(1-A)\right\}}\right]}{2H+A+1} \tag{7.3.6}$$

$$I_{im} = \frac{\gamma_2}{M_1}\lim_{s\to 0}\int_0^1 \hat{C}_2(X;s)dX = \frac{\varphi^*}{1+\varphi^*}\frac{(1+A)\left[1-e^{\left\{\frac{P}{2}(1-A)\right\}}\right]}{2H+A+1} \tag{7.3.7}$$

where

$$A = \sqrt{1 + \left\{ \frac{4\gamma_1 + \left(\frac{4\omega\gamma_2}{\omega + \gamma_2} \right)}{P} \right\}} \tag{7.3.8}$$

$$\varphi^* = \frac{\omega\gamma_2}{\gamma_l(\omega + \gamma_2)} \tag{7.3.9}$$

From overall mass balance considerations, we note that $I_v + I_l + I_m + I_{im} = 1$. Inspection of equation (7.3.4) makes it clear that volatilization losses increase rapidly with increasing H, and that as $H \to \infty$, $I_v \to 1$.

7.4. EFFECTIVE PARAMETER DEFINITIONS

As discussed in Chapter 5, moments can be used for defining effective properties. Absolute moments (μ_n) and normalized time moments (μ_n^*) are defined as

$$\mu_n = \int_0^\infty T^n C(X, T)\, dT, \quad n = 0, 1, 2, \ldots \tag{7.4.1}$$

and,

$$\mu_n^* = \frac{\mu_n}{\mu_0}, n = 1, 2, 3, \ldots \tag{7.4.2}$$

The n^{th} central moments (for $n > 1$) are defined as

$$m_n = \frac{\int_0^\infty (T - m_1)^n C(X, T) dT}{\int_0^\infty C(X, T) dT}, \quad n = 2, 3, 4 \ldots \tag{7.4.3}$$

Utilizing (5.2.7), we can express lower order central moments in terms of absolute moments as

$$m_2 = \frac{\mu_0\mu_2 - \mu_1^2}{\mu_0^2} \tag{7.4.4}$$

$$m_3 = \frac{\mu_3\mu_0^2 + 2\mu_1^3 - 3\mu_0\mu_1\mu_2}{\mu_0^3} \tag{7.4.5}$$

Equations (7.4.4) and (7.4.5) can be used to describe a concentration distribution if the input is in the form of a Dirac delta function, $\delta(t)$ for an ideal tracer (Sardin et al., 1991).

With $\hat{C}_1(X;s)$ given by (7.3.2), the absolute theoretical moments (μ_n) can be calculated by the method described in Aris (1958)

$$\mu_n = (-1)^n \lim_{s\to 0}\left\{\frac{d^n}{ds^n}\left[\hat{C}_l(X;s)\right]\right\} \tag{7.4.6}$$

After simplification, the following expressions are obtained for the lower-order absolute moments

$$\mu_0 = \exp\left\{\frac{P}{2}(1-A)\right\} \tag{7.4.7}$$

$$\mu_1 = \frac{\exp\left\{\frac{P}{2}(1-A)\right\}\left\{R_m\phi + \frac{(1-\phi)\omega^2 R_{im}}{(\omega+\gamma_2)^2}\right\}}{A} \tag{7.4.8}$$

$$\begin{aligned}\mu_2 = &\frac{\exp\left\{\frac{P}{2}(1-A)\right\}\left\{R_m\phi + \frac{(1-\phi)\omega^2 R_{im}}{(\omega+\gamma_2)^2}\right\}^2\left(A+\frac{2}{P}\right)}{A^3}\\ &+\frac{2\exp\left(\frac{P}{2}(1-A)\right)\{(1-\phi)\,\omega R_{im}\}^2}{A\,(\omega+\gamma_2)^3}\end{aligned} \tag{7.4.9}$$

In this context, we define effective parameters as those that can be used in an equilibrium model to obtain the same zeroth, first and second temporal moments that would be calculated by using an equivalent nonequilibrium model (Valocchi, 1985). However, the governing differential equation with effective parameters is defined as

$$\frac{\partial C}{\partial T} = D_{eff}\frac{\partial^2 C}{\partial X^2} - V_{eff}\frac{\partial C}{\partial X} - \gamma_{eff}C \tag{7.4.10}$$

to explicitly include the effect of degradation. It must be noted that equation (7.4.10) will lead to different definitions of effective parameters than those prescribed by Valocchi (1985). For mathematical convenience, effective parameters were developed for the simpler Drichlet boundary condition of $C(X,T) = \delta(T)$ at $X = 0$ implying that the concentrations in the model should be interpreted as flux concentrations (see Chapter 2 for a discussion on why flux and resident concentrations satisfy the same transformed equation). When degradation follows first-order kinetics, the degradation time is an adjusted convection time ($\bar{t}$) expressed as (Das and Kluitenberg, 1996)

$$\mu_0 = \exp(-\gamma_{eff}\bar{t}) \tag{7.4.11}$$

The adjustment of the convection time is required because of the simultaneous occurrence of dispersion and degradation. These two processes interact to reduce

the true convection time for the leaching event ($\bar{t} < L/V$). The effective velocity and adjusted convection time are related as (Das and Kluitenberg, 1996),

$$\bar{t} = \frac{2}{\frac{1}{m_1} + V_{eff}} \tag{7.4.12}$$

Equating the normalized moments from (7.4.10) with those obtained from (7.2.12) to (7.2.14) yields the following expressions for the effective parameters (Parashar, 2003)

$$V_{eff} = \frac{1}{m_1}\sqrt{1 + \frac{2m_2}{m_1}\left\{\frac{ln\ \mu_0}{m_1} + \frac{(ln\ \mu_0)^2\, m_2}{2m_1^3}\right\}} \tag{7.4.13}$$

$$D_{eff} = \left(\frac{m_2}{2m_1^3}\right) \tag{7.4.14}$$

$$\gamma_{eff} = -\left[\frac{ln\ \mu_0}{m_1} + \frac{(ln\ \mu_0)^2\, m_2}{2m_1^3}\right] \tag{7.4.15}$$

For illustration purposes, Table 7.4.1 shows properties for two different soils used in computations for loss fractions and effective parameters. Longitudinal dispersion coefficients were assumed to be the sum of the value of diffusion coefficient and the product of dispersivity and darcian velocity. The value of dispersivity was taken to be equal to 10% of the length of soil column. The water content (θ) and air content (a) were chosen to represent typical values encountered in the vadose zone of sandy and clayey type soils. Liquid flux values were selected to represent a small rainfall event. Boundary layer transfer coefficients were based on the recommendations of Jury et al. (1983, 1990). Table 7.4.2 shows a list of organic compounds along with their properties (adapted from Jury et al., 1990, and Spitz and Moreno, 1996)

Table 7.4.1. Values of soil properties used in the computations (from Parashar et al., 2007, with permission from ASCE)

Property	Sandy soil	Clayey soil
Porosity	0.4	0.5
Bulk density, ρ_b, (kg/m^3)	1590	1320
Mobile water content, θ_m	0.1	0.12
Air content, a	0.25	0.3
Immobile water content, q_{im}	0.05	0.08
Gas diffusion constant, D_G, (m^2/d)	0.432	0.432
Liquid dispersion constant, D_m, (m^2/d)	0.2	0.0334
Liquid flux, q, (m/d)	0.2	0.04
Boundary layer transfer coefficient, h, (m/d)	80	80
Fraction of sorption sites, f	0.5	0.5
Partition coefficient, α (d^{-1})	1.0	1.0

Table 7.4.2. Effective velocity, effective dispersion and effective degradation rate for compounds in a sandy and clayey soil

Compound	K_H	$K_{oc}(m^3/kg)$	$T_{1/2}$ (days)	Sandy soil			Clayey soil		
				With degradation		$T_{1/2}\rightarrow\infty$	With degradation		$T_{1/2}\rightarrow\infty$
				P_{eff}	γ_{eff-nd}	P_{eff}	P_{eff}	γ_{eff-nd}	P_{eff}
1,1,1-Trichloroethane	0.78	0.113	365	1.67	1.42E − 02	1.68	0.37	1.88E − 01	0.38
1,1-Dichloroethane	0.255	0.046	45	3.26	5.39E − 02	3.32	0.99	6.75E − 01	1.07
1,2-Dichloroethane	0.054	0.022	90	5.64	1.59E − 02	5.66	3.47	1.78E − 01	3.51
2,4-Dichlorophenol	0.0002	0.447	160	6.55	1.19E − 01	6.70	8.22	1.63E + 00	9.04
2-Chloronapthalene	0.015	1.15	1440	6.29	3.34E − 02	6.34	6.13	4.60E − 01	6.30
Acrolein	0.0055	0.001	300	7.73	1.87E − 03	7.73	8.01	1.35E − 02	8.01
Benzene	0.252	0.08	365	3.37	1.05E − 02	3.38	1.07	1.35E − 01	1.08
Bromoethane	0.336	0.009	30	2.72	2.98E − 02	2.75	0.80	2.89E − 01	0.83
Chlordane	0.0022	0.48	100	6.39	2.04E − 01	6.65	7.16	2.86E + 00	8.54
Chloroethane	0.505	0.025	30	2.15	5.19E − 02	2.19	0.52	6.14E − 01	0.57
Chloroethene	1.26	0.003	30	1.11	2.15E − 02	1.12	0.23	1.75E − 01	0.24
Chloroform	0.167	0.029	100	3.98	1.72E − 02	4.00	1.51	2.01E − 01	1.53
Chloromethane	0.4	0.006	120	2.47	6.40E − 03	2.47	0.70	5.75E − 02	0.71
DBCP	0.0067	0.129	1000	6.61	5.85E − 03	6.62	7.58	7.72E − 02	7.61

Dichlorodifluoromethane	15.59	0.111	10000	0.12	5.11E−04	0.12	0.02	6.70E−03	0.02
Dichloromethane	0.148	0.013	100	4.13	1.06E−02	4.14	1.68	1.09E−01	1.69
EPTC	0.0007	0.28	30	6.21	4.04E−01	6.71	6.16	6.03E+00	8.92
Ethylene Dibromide	0.029	0.044	3650	6.19	6.41E−04	6.19	4.91	7.84E−03	4.92
Heptachlor	0.013	6.81	2200	6.21	1.28E−01	6.37	5.85	1.80E+00	6.57
Hexachlorocyclohexane	0.012	2.34	725	6.22	1.34E−01	6.40	5.95	1.88E+00	6.71
Methyl Ethyl Ketone	0.0025	0.01	100	7.39	9.33E−03	7.40	8.60	9.18E−02	8.63
Methyl isobutyl Ketone	0.0063	0.022	100	6.97	1.43E−02	6.99	7.70	1.60E−01	7.76
Phorate	0.0002	0.66	82	6.26	3.40E−01	6.69	6.62	5.01E+00	9.04
Toluene	0.302	0.098	5	2.27	9.74E−01	3.09	0.98	4.86E+00	0.92
Toxaphene	0.00027	0.632	3650	6.68	7.30E−03	6.69	8.97	1.00E−01	9.02
Trichloroethylene	0.448	0.138	730	2.47	8.53E−03	2.48	0.63	1.13E−01	0.64
Trillate	0.00055	3.6	100	5.01	1.55E+00	6.66	0.41	2.14E+02	8.94
Xylene	0.29	0.295	110	3.12	1.16E−01	3.22	0.78	1.71E+00	0.95

required for the computations: Henry's coefficient (K_H), organic carbon partition coefficient (K_{oc}) and the half-life ($T_{1/2}$).

Using equations (7.3.4) to (7.3.9), loss fractions for the 28 compounds listed in Table 7.4.2 are presented in Figures 7.4.1 and 7.4.2 sandy and clayey soils, respectively. Majority of the organic compounds analyzed were found to be highly susceptible to volatilization when modeled using a nonequilibrium model with immobile air phase. For compounds having $K_H > 0.1$, the percentage of solute getting volatized was consistently seen to be above 95%. With no constraint on the duration of computation, significant leaching losses (excess of 10%) were obtained for few compounds in sandy soil. As anticipated, leaching losses were further reduced for solute transport through clayey soil owing to lower values of advective liquid flux. Losses increased with decreasing K_H and decreasing half-life period.

Figures 7.4.3 to 7.4.7 show the sensitivity of dimensionless volatilization, leaching, and degradation losses to the non-dimensional parameters H, P, ω, γ_1 and γ_2 that arise in the governing equations and boundary conditions from (7.2.12) to (7.2.16). This sensitivity analysis shows that volatilization losses will reduce down to a moderate range only in cases of very low H or $P(< 1)$. Figure 7.4.3 shows that while volatilization losses increase with H, there is a proportionate decrease in leaching and degradation losses. H is directly proportional to the boundary layer transfer coefficient h, and inversely proportional to the boundary layer thickness d

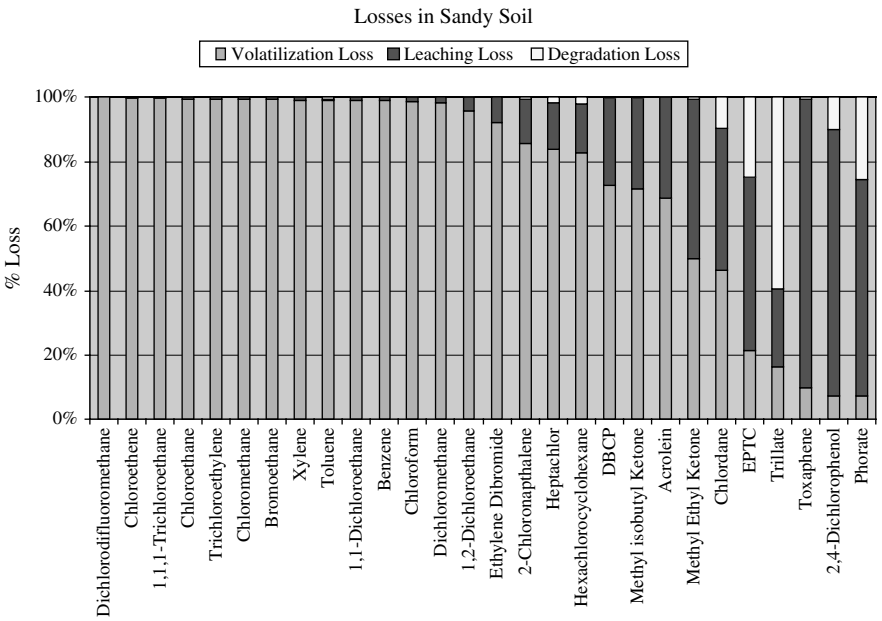

Figure 7.4.1. Volatilized, leached and degraded fractions in sandy soil (adapted from Parashar et al., 2007, with permission from ASCE)

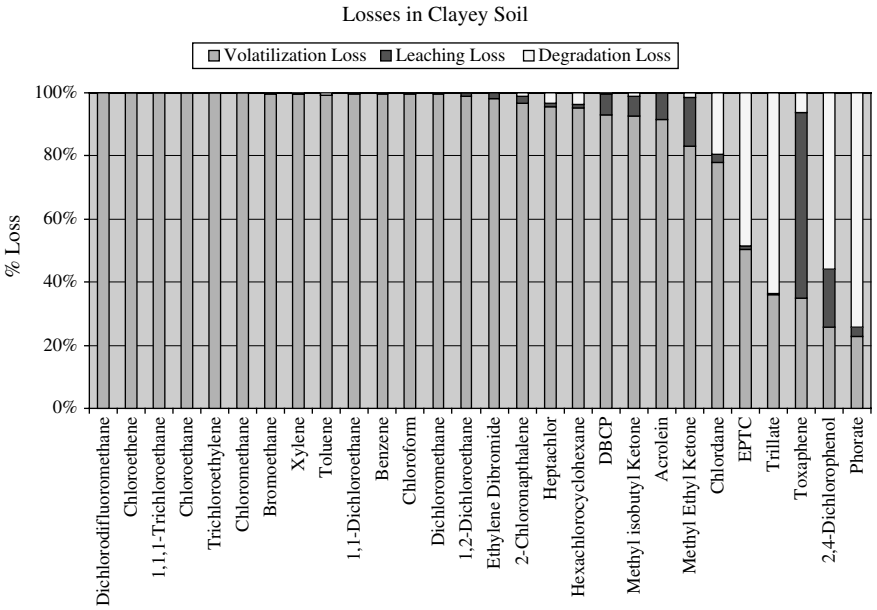

Figure 7.4.2. Volatilized, leached and degraded fractions in clayey soil (adapted from Parashar et al., 2007, with permission from ASCE)

through which volatilization is assumed to occur by vapor diffusion. In calculations, d was given a specified value of 5.4×10^{-3} m. However, d will strongly depend on the type of vegetation used as soil cover, and the value used in the simulation is characteristic of sparse vegetation.

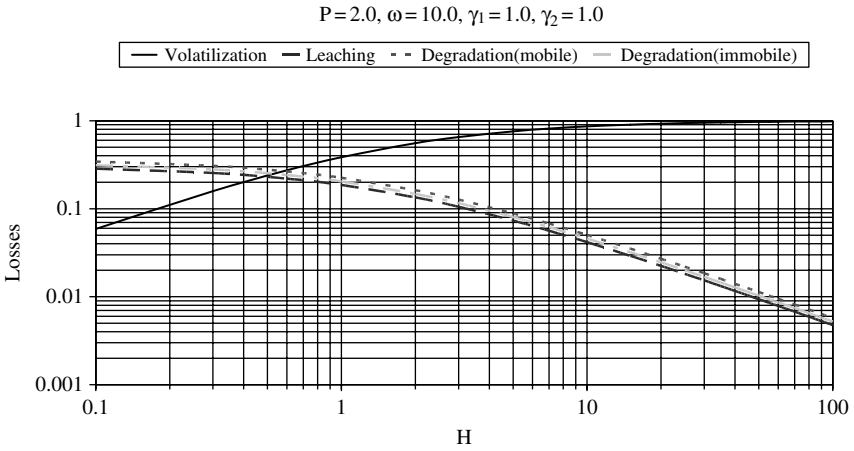

Figure 7.4.3. Sensitivity of losses with respect to H (adapted from Parashar et al., 2007, with permission from ASCE)

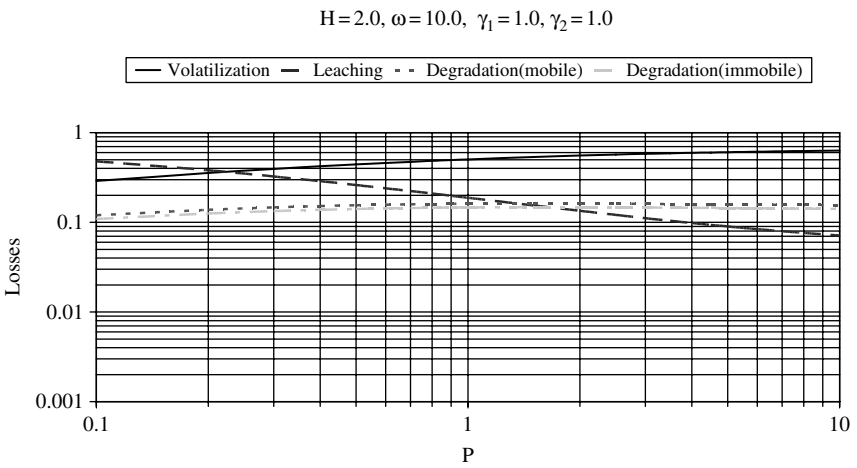

Figure 7.4.4. Sensitivity of losses with respect to P (adapted from Parashar et al., 2007, with permission from ASCE)

The remaining parameters ω, γ_1 and γ_2 have relatively milder influences on volatilization loss. The dependence of I_v, I_l, I_m, and I_{im} on ω is through the quantities A and ϕ^*. Equations (7.3.8) and (7.3.9) indicate that both A and ϕ^* are independent of ω for $\omega \gg 1$. Larger γ_1 and γ_2 values can lead to more sensitivity with respect to ω. Leaching losses showed a weak correlation with the nondimensional parameters except for the case of H and P. Figure 7.4.4 shows that dimensionless

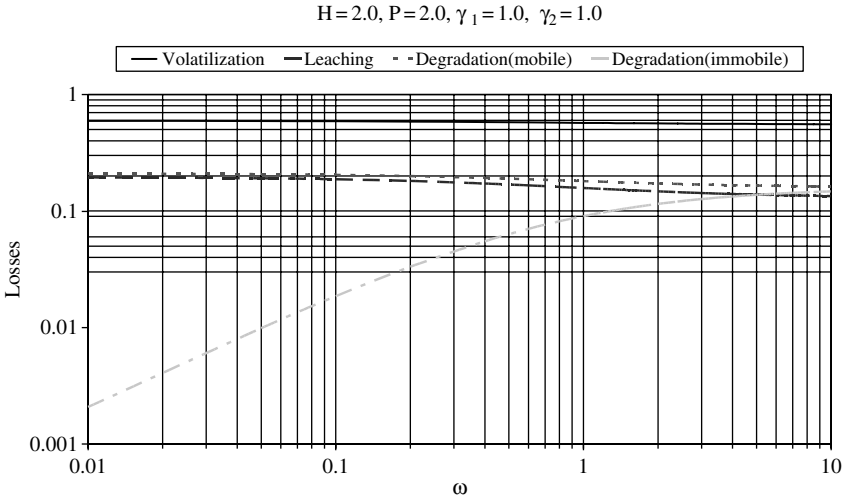

Figure 7.4.5. Sensitivity of losses with respect to ω (adapted from Parashar et al., 2007, with permission from ASCE)

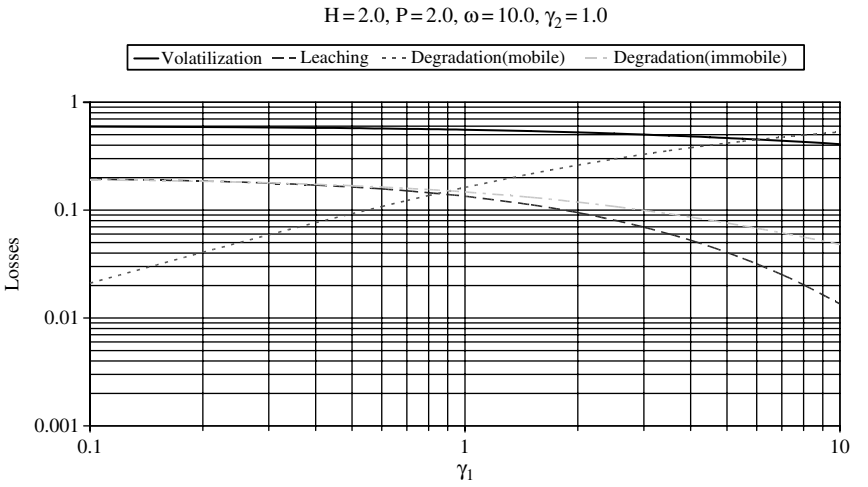

Figure 7.4.6. Sensitivity of losses with respect to γ_1 (adapted from Parashar et al., 2007, with permission from ASCE)

leaching losses increase with decreasing P. Dispersion reduces concentrations and thus reduces losses, consequently leading to more mass being available for leaching. Figure 7.4.6 shows that degradation losses increase with increasing γ_1 and correspondingly leaching and degradation in immobile regions decreases. Volatilization losses remain relatively uninfluenced. In a parallel fashion, increase in γ_2 causes degradation losses in immobile region to increase, while leaching and degradation

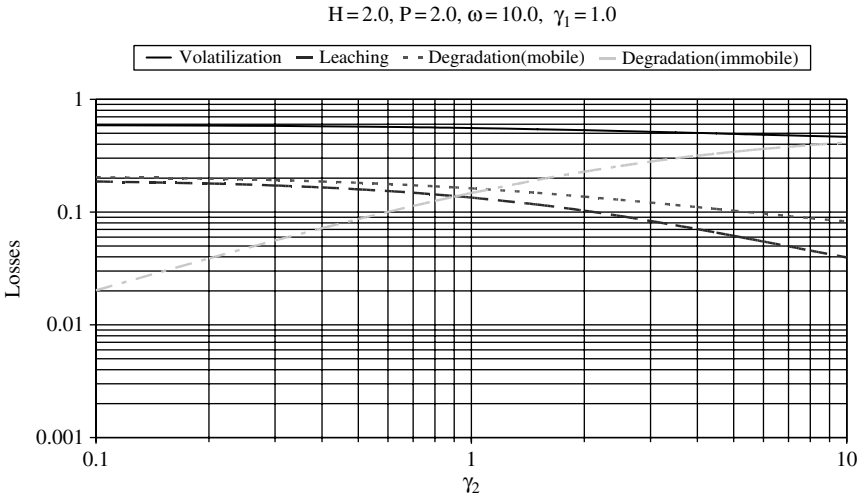

Figure 7.4.7. Sensitivity of losses with respect to γ_2 (adapted from Parashar et al., 2007, with permission from ASCE)

losses in mobile regions decrease (Figure 7.4.7). An inspection of (7.3.4) to (7.3.7) for the various losses shows that I_v is less influenced by A than I_l, I_m, and I_{im}. This is because volatilization losses occur at the soil surface boundary and are less influenced by processes occurring at deeper locations in the soil column.

Table 7.4.2 also lists effective Peclet number (P_{eff}) and effective dimensionless degradation rate (γ_{eff-nd}) computed from equations (7.4.13) to (7.4.15) for various organic compounds for the two different soil types in Table 7.4.1. These computations were done for a soil column length of 1 m. We define two non-dimensional parameters for the effective transport equation (7.4.10) as

$$P_{eff} = \frac{V_{eff} L}{D_{eff}} \tag{7.4.16}$$

$$\gamma_{eff-nd} = \frac{\gamma_{eff} L}{V_{eff}} \tag{7.4.17}$$

where P_{eff} is the effective Peclet number, while γ_{eff-nd} is the non-dimensional effective degradation rate constant. Here, P_{eff} may be interpreted in the usual way as representing the ratio of dispersive to convective travel times, with these travel times being influenced by all the processes that are encompassed in the governing equations and boundary conditions (7.2.12) to (7.2.14). The quantity γ_{eff-nd} expresses the combined effects of all loss mechanism other than leaching from the soil below the control plane. Thus, it represents effects of degradation losses within the soil column, and volatilization losses at the soil surface as well.

The results for the effective parameters in Table 7.4.2 also shows the value of P_{eff} when degradation is absent (i.e. as $T_{1/2} \to \infty$). This allows us to assess the role of degradation on the Peclet number. Degradation losses tend to not only cause advection to be enhanced but also influence solute spreading in the breakthrough curve. The Peclet number expresses the ratio of travel times by both these mechanisms. Thus small change in non-dimensional degradation may not show an immediate change in the Peclet number. The values in Table 7.4.2 show that for a large fraction of the compounds considered, the Peclet number does not change substantially when $T_{1/2} \to \infty$. We note that apart from $T_{1/2}$, K_H and K_{oc} also have a role to play in determining the loss fractions. For those compounds where the non-dimensional degradation rate γ_{eff-nd} is greater than unity, there is substantial increase in P_{eff} when $T_{1/2} \to \infty$. Examples in clayey soils are 2,4-Dichlorophenol, Chlordane, EPTC, Phorate, and others. When compared to Figure 7.4.3, these compounds are generally clustered towards the right side where, as expected, volatilization losses are generally low. Both degradation and volatilization losses contribute to the estimation of γ_{eff-nd}. This effective non-dimensional degradation is more likely to play a greater influence in clayey soils than in sandy soils when determining P_{eff}. This is clearly demonstrated in the case of Trillate in Table 7.4.2 and in Figures 7.4.2 and 7.4.3.

Hantush et al. (2002) utilized a similar model and conducted a detailed study of leached fraction, volatilization losses, and transformation (biochemical) losses for many compounds under a variety of soil types. Vapor losses at the soil-air interface, I_v,

showed relatively greater variations with P than other parameters. They state that when P increases, dispersion in the mobile phase becomes smaller relative to advection, and volatilization losses increase due to increased concentration gradients at the interface. Dispersion enhances leaching and as a result reduces concentrations at the soil surface (e.g., van der Zee and Boesten, 1991; Beltman et al., 1995; Hantush et al., 2000). Lateral dispersion produced by diffusion into stagnant-water regions and subsequent degradation is another mechanism that may reduce concentration gradient across the soil-air interface, thereby leading to decreased volatilization losses. The effect of the immobile-water phase on volatilization losses, however, appear to be less than that of dispersion. The combined effect of dispersion in the mobile water region and diffusion is to moderate volatilization losses. Hantush et al. (2002) discuss how moment analysis can be used for screening of pesticides. Hantush and Govindaraju (2003) discuss further solutions to the system (7.2.12) to (7.2.16) for different initial and boundary conditions.

7.5. MOBILE VAPOR PHASE MODEL

In this section we consider a model with mobile air phase. Traditionally, majority of transport models developed for modeling gas-phase processes were based on the assumption of homogeneous porous media properties (Johnson et al., 1987; Wilson et al., 1987, 1988; Baehr et al., 1989). In these models, it was assumed that hydraulic conductivity and sorption capacity are spatially homogeneous at the macroscopic level and that the sorption is instantaneous. It has been shown that the assumption of instantaneous sorption is not met in several instances (Buxton and Green, 1987; Smith et al., 1990).

Dual-porosity models with a macropore (gas-phase) and micropore (liquid-phase) porosity were developed (Rasmuson et al., 1990; Gierke et al., 1992). Some models (Brown and Rolston, 1980) included rate-limited sorption and were limited to homogeneous soil properties. Brusseau (1991) developed a model for gas-phase transport in a dual-porosity model that includes rate-limited sorption. We present simple mathematical expressions for effective values of transport parameters for the same set of compounds listed in Table 7.4.2 within the framework of Brusseau's model. More details are available in Parashar and Govindaraju (2006a) from where this material is abstracted.

The conceptual framework upon which the model is based is shown in Figure 7.5.1. The processes included in the model are: (1) advective-dispersive transport of the gas-phase in the advective domain, (2) equilibrium-governed partitioning to immobile water residing in the advective domain, (3) combined instantaneous and rate-limited mass transfer between water and solid phases residing in the advective domain, (4) rate-limited mass transfer between water residing in the non-advective domain and the gas phase, and (5) combined instantaneous and rate-limited mass transfer between water and solid phases residing in the non-advective domain. Model assumptions include:

- Incompressible gas flow and negligible slippage effects allowing the use of Darcy's equation for gas flow (Brusseau, 1991).

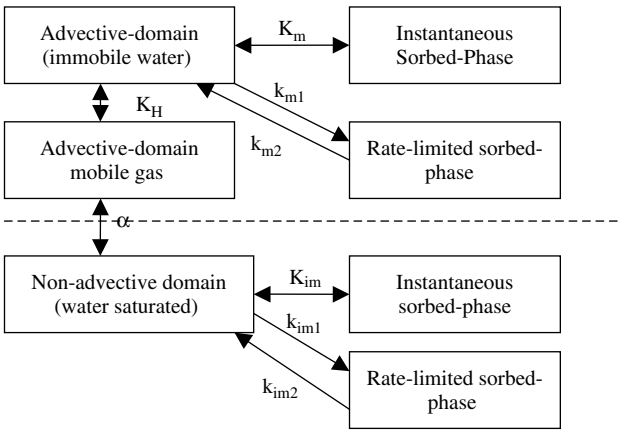

Figure 7.5.1. Conceptual diagram of the multiprocess nonequilibrium transport model by gas advection (adapted from and Parashar and Govindaraju, 2006a, with permission from Springer)

- A first-order mass transfer approach to describe mass transfer of solute between the advective and non-advective domain.
- Since the assumption of dilute concentrations is generally valid in vadose zone, except when a large source of a chemical with a high vapor pressure is present at the location, the use of Fick's law which is based on molecular diffusion is thought to be adequate.
- Mass transfer between gas and liquid phases is assumed to be instantaneous and governed by Henry's law. It has been experimentally verified that assumption of local equilibrium for gas liquid mass transfer is justified (Baehr et al., 1989; Brusseau et al., 1990; Gierke et al., 1990). However, sorption of organic chemicals by soil is often rate-limited.
- The first order bicontinumm approach (Selim et al., 1976), wherein sorption is assumed to be instantaneous for a fraction of sorbent and rate-limited for the remainder, has been used in the model. The bicontinumm approach can be used to model systems where rate-limited sorption is caused by chemical reaction or by diffusion (Brusseau and Rao, 1989).
- Lastly, it has been assumed that the vapor phase sorption is negligible.

The governing equations under the condition of steady state gas flow and water content, the water phase being assumed immobile (Brusseau, 1991), are

$$\theta_g \frac{\partial c_g}{\partial t} + \theta_{wg} \frac{\partial c_{wg}}{\partial t} + \theta_w \frac{\partial c_w}{\partial t} + f\rho \frac{\partial S_{m1}}{\partial t} + f\rho \frac{\partial S_{m2}}{\partial t} + (1-f)\rho \frac{\partial S_{im1}}{\partial t} + (1-f)\rho \frac{\partial S_{im2}}{\partial t} = \theta_g D \frac{\partial^2 c_g}{\partial x^2} - q \frac{\partial c_g}{\partial x} \tag{7.5.1}$$

$$\theta_w \frac{\partial c_w}{\partial t} + (1-f)\rho \frac{\partial S_{im1}}{\partial t} + (1-f)\rho \frac{\partial S_{im2}}{\partial t} = \alpha(c_g - K_H c_w) \tag{7.5.2}$$

$$\frac{\partial S_{m2}}{\partial t} = k_{m2}[(1-F_m)K_m c_{wg} - S_{m2}] \tag{7.5.3}$$

$$\frac{\partial S_{im,2}}{\partial t} = k_{im2}[(1-F_{im})K_{im} c_w - S_{im2}] \tag{7.5.4}$$

Here θ is the porosity and subscripts *g, wg* and *w* represent gas-filled porosity, water-filled porosity of advective domain, and water-filled porosity of nonadvective domain, respectively. In the above equations, c (ML^{-3}) is the concentration of solute and subscripts have the same meaning as before. S (MM^{-1}) is the concentration of the sorbate and the subscripts *m1, m2, im1* and *im2* stand for instantaneous sorbent associated with advective domain, rate-limited sorbent associated with advective domain, instantaneous sorbent associated with nonadvective domain, and rate-limited sorbent associated with nonadvective domain, respectively. The fraction of sorbent associated with the advective domain is represented by f, and F with subscripts m and *im* representing fraction of sorbent in the advective domain for which sorption is instantaneous, and fraction of sorbent in the nonadvective domain for which sorption is rate-limited, respectively. The quantities $D(L^2T^{-1})$, $q(LT^{-1})$, $\alpha(T^{-1})$ and K_H are global dispersion coefficient, Darcy flux, first-order rate coefficient for mass transfer between water in nonadvective domain and mobile gas phase and Henry's constant, respectively. In the above equations, $K(L^3M^{-1})$ with subscripts m and *im* represents equilibrium sorption coefficient for advective and nonadvective domains respectively, and $k(T^{-1})$ with subscripts *m2* and *im2* represents first-order reverse sorption rate constant for advective and nonadvective domains, respectively.

Equations (7.5.3) and (7.5.4) show that sorption parameters are defined by two-domain type heterogeneity (both equilibrium and rate constant). Equation 7.5.2 describes the mass balance in the non-advective domain. The coefficient α is a lumped parameter denoting mass transfer between non-advective domain water and gas phase. The following parameters were defined to nondimensionalize the governing set of equations.

$$R = 1 + \frac{\theta_{wT}}{\theta_g K_H} + \frac{\rho}{\theta_g K_H} K_p \tag{7.5.5a}$$

$$R_{m1} = 1 + \frac{\theta_{wg}}{\theta_g K_H} + \frac{f\rho}{\theta_g K_H} F_m K_m \tag{7.5.5b}$$

$$R_{m2} = \frac{f\rho}{\theta_g K_H}(1-F_m)K_m \tag{7.5.5c}$$

$$R_{im1} = \frac{\theta_w}{\theta_g K_H} + \frac{(1-f)\rho}{\theta_g K_H} F_{im} K_{im} \tag{7.5.5d}$$

$$R_{im2} = \frac{(1-f)\rho}{\theta_g K_H}(1-F_{im})K_{im} \tag{7.5.5e}$$

$$T = \frac{tV}{L};\ V = \frac{q}{\theta_g} \tag{7.5.5f}$$

$$P = VL/D \tag{7.5.5g}$$

$$X = x/L \tag{7.5.5h}$$

$$\omega = \frac{\alpha L}{V\theta_g} \tag{7.5.5i}$$

$$K_m^0 = \frac{k_{m2}L}{v}R_{m2} \tag{7.5.5j}$$

$$K_{im}^0 = \frac{k_{im2}L}{v}R_{im2} \tag{7.5.5k}$$

Total retardation factor in equation (7.5.5a) is the sum of R_{m1}, R_{m2}, R_{im1} and R_{im2}. The total water-filled porosity is denoted by $\theta_{wT}(=\theta_{wg}+\theta_w)$ in equation (7.5.5a) and $K_P(\mathrm{L^3M^{-1}})$ is the weighted sorption constant for the entire porous medium

$$K_P = fK_m + (1-f)K_{im} \tag{7.5.6}$$

Nondimensionalizing equations (7.5.1) to (7.5.4) using (7.5.5) results in

$$R_{m1}\frac{\partial C^*}{\partial T} + R_{m2}\frac{\partial S_m^*}{\partial T} + R_{im1}\frac{\partial C_w^*}{\partial T} + R_{im2}\frac{\partial S_{im}^*}{\partial T} = \frac{1}{P}\frac{\partial^2 C^*}{\partial X^2} - \frac{\partial C^*}{\partial X} \tag{7.5.7}$$

$$R_{im1}\frac{\partial C_w^*}{\partial T} + R_{im2}\frac{\partial S_{im}^*}{\partial T} = \omega(C^* - C_w^*) \tag{7.5.8}$$

$$R_{m2}\frac{\partial S_m^*}{\partial T} = K_m^0(C^* - S_m^*) \tag{7.5.9}$$

$$R_{im2}\frac{\partial S_{im}^*}{\partial T} = K_{im}^0(C_w^* - S_{im}^*) \tag{7.5.10}$$

The subscripts in equations (7.5.7) – (7.5.10) have the usual meaning as defined earlier in the text. The normalized concentrations are

$$C^* = \frac{C_g}{C_0};\ C_w^* = \frac{C_w K_H}{C_0};\ S_m^* = S_{m2}K_H/[(1-F_m)K_m C_0;$$
$$S_{im}^* = S_{im2}K_H/\left((1-F_m)\,K_{im}C_0\right) \tag{7.5.11}$$

where C_0 is the concentration of solute in the influent gas. The initial and boundary condition were defined as follows.

$$C^*(X,0) = C_{wg}^*(X,0) = C_w^*(X,0) = 0 \tag{7.5.12a}$$

$$S_m^*(X,0) = S_{im}^*(X,0) = 0 \tag{7.5.12b}$$

$$M\delta(T) = C^* - \frac{1}{P}\left.\frac{\partial C^*}{\partial X}\right|_{X=0} \tag{7.5.12c}$$

where M is set to unity for simplicity. Taking Laplace Transforms of (7.5.7) to (7.5.10) under the end condition of (7.5.12) and simplifying yields the following expressions for the normalized moments (Brusseau, 1991; Parashar and Govindaraju, 2006)

$$\mu_0 = 1 \tag{7.5.13}$$

$$\mu_1 = \left(\frac{1+P}{P}\right) R \tag{7.5.14}$$

and,

$$\mu_2 = R^2 \frac{(2+P)^2}{P^2} + \frac{2(1+P)}{P}\left[\frac{R_{m2}^2}{K_m^0} + \frac{(R_{im1}+R_{im2})^2}{\omega} + \frac{R_{im2}^2}{K_{im}^0}\right] \tag{7.5.15}$$

Consequently, the expressions for central moments are obtained as

$$m_1 = \mu_1 = \left(\frac{1+P}{P}\right) R \tag{7.5.16}$$

and,

$$m_2 = \frac{R^2}{P^2} + \frac{2(1+P)}{P}\left[\frac{R^2}{P} + \frac{R_{m2}^2}{K_m^0} + \frac{(R_{im1}+R_{im2})^2}{\omega} + \frac{R_{im2}^2}{K_{im}^0}\right] \tag{7.5.17}$$

The expressions used for effective parameters are

$$D_{eff} = \left(\frac{m_2}{2m_1^3}\right) VL \tag{7.5.18}$$

and,

$$V_{eff} = \frac{V}{m_1} \tag{7.5.19}$$

Note that these definitions of effective parameters differ from those given by Valocchi (1985) by a factor of θ_w/θ.

We consider the same set of compounds investigated in Table 7.4.2. Typical values of soil and transport properties used in the simulation are presented in Table 7.5.1. Using these values, retardation factor, Peclet number and other nondimensional variables were calculated according to their definitions given in equation (7.5.5). Substituting these values in (7.5.16) and (7.5.17), and using them with equations (7.5.18) and (7.5.19) resulted in simulated values of effective velocity and dispersion coefficients. The domain length L was chosen to be equal to unity for all computations.

Table 7.5.1. Typical values of soil properties used in the simulation (adapted from Parashar and Govindaraju, 2006a, with permission from Springer)

Property	Unit	Sandy soil	Clayey soil
Porosity, θ	–	0.4	0.5
Bulk density, ρ	kg/m^3	1590	1320
Water content (nonadvective), θ_w	–	0.1	0.12
Gas filled porosity, θg	–	0.25	0.3
Water content(advective), $\theta_w g$	–	0.05	0.08
Gas diffusion constant	m^2/d	0.432	0.432
Global dispersion constant	m^2/d	1.7	0.6
Darcy flux	m/d	50	5
Fraction of sorbent (advective), f	–	0.8	0.8
Fraction of sorbent(instantaneous), F	–	0.35	0.2
Mass transfer coeff (nonadvective water/gas)	d^{-1}	2500	100
Reverse sorption rate (K_2)	d^{-1}	250	75

The values shown in Table 7.5.2 were obtained under a set of hypothetical conditions, but do show expected trends. Most of the compounds analyzed showed small values of effective velocity or dispersion coefficient. Table 7.5.2 indicates that for the values of soil properties presented in Table 7.5.1, only a small number of compounds are transported at appreciable rates when used with soil venting techniques. It is apparent that higher values of effective parameters are generally associated with compounds having higher Henry's constant (K_H) as shown in Table 7.4.2. It is further observed that decrease in value of organic carbon partition coefficient (K_{oc}) also favors transport of chemicals under gas advection. However, the values presented can be very susceptible to changes in value of Darcy's flux and other soil and transport parameters listed in Table 7.5.1. The expressions developed here can be used to make a preliminary assessment of efficacy of soil venting for different compounds under different soil types.

A partial sensitivity analysis of moments with respect to model parameters is presented here. From equation (7.5.16), the dependence of m_1 (and therefore V_{eff}) on P and R is clear, As $P \to \infty$, $m_1 \to R$ and the effective velocity is simply the average pore water velocity retarded by R.

Figure 7.5.2 examines the dependence of m_2 on P. Clearly m_2 and D_{eff} reduce with increasing P values. However as $P \to \infty$, advection-dominated conditions will result and in the limit we will have

$$m_2 = 2\left[\frac{R_{m2}^2}{K_m^0} + \frac{(R_{im1} + R_{im2})^2}{\omega} + \frac{R_{im2}^2}{K_{im}^0}\right] \tag{7.5.20}$$

and D_{eff} can be computed from (7.5.18) as

$$D_{eff} = \frac{VL}{R^3}\left[\frac{R_{m2}^2}{K_m^0} + \frac{(R_{im1} + R_{im2})^2}{\omega} + \frac{R_{im2}^2}{K_{im}^0}\right] \tag{7.5.21}$$

Table 7.5.2. Effective velocity and effective dispersion for compounds in a sandy and clayey soil (adapted from Parashar and Govindaraju, 2006a, with permission from Springer)

	Sandy soil		Clayey soil	
Compound	V_{eff} (m/d)	D_{eff} (m^2/d)	V_{eff} (m/d)	D_{eff} (m^2/d)
1,1,1-Trichloroethane	2.15E−01	5.41E−01	2.52E−02	9.39E−02
1,1-Dichloroethane	1.72E−01	1.06E+00	2.02E−02	1.83E−01
1,2-Dichloroethane	7.62E−02	9.78E−01	8.91E−03	1.68E−01
2,4-Dichlorophenol	1.39E−05	9.01E−06	1.64E−06	1.59E−06
2-Chloronapthalene	4.07E−04	1.04E−04	4.77E−05	1.91E−05
Acrolein	1.57E−01	3.72E+01	1.74E−02	5.52E+00
Benzene	9.81E−02	3.49E−01	1.15E−02	6.04E−02
Bromoethane	1.15E+00	3.51E+01	1.33E−01	5.92E+00
Chlordane	1.43E−04	8.60E−05	1.68E−05	1.53E−05
Chloroethane	6.26E−01	7.04E+00	7.31E−02	1.20E+00
Chloroethene	1.19E+01	9.41E+02	1.34E+00	1.43E+02
Chloroform	1.79E−01	1.74E+00	2.09E−02	3.00E−01
Chloromethane	2.03E+00	9.13E+01	2.34E−01	1.52E+01
DBCP	1.62E−03	3.58E−03	1.90E−04	6.23E−04
Dichlorodifluoromethane	4.28E+00	1.05E+01	4.97E−01	1.78E+00
Dichloromethane	3.52E−01	7.57E+00	4.10E−02	1.29E+00
EPTC	7.79E−05	7.99E−05	9.14E−06	1.40E−05
Ethylene Dibromide	2.05E−02	1.32E−01	2.40E−03	2.28E−02
Heptachlor	5.95E−05	3.01E−06	6.98E−06	6.81E−07
Hexachlorocyclohexane	1.60E−04	2.08E−05	1.87E−05	4.04E−06
Methyl Ethyl Ketone	7.72E−03	2.16E−01	9.00E−04	3.67E−02
Methyl isobutyl Ketone	8.89E−03	1.14E−01	1.04E−03	1.96E−02
Phorate	9.45E−06	4.16E−06	1.11E−06	7.45E−07
Toluene	9.60E−02	2.79E−01	1.12E−02	4.84E−02
Toxaphene	1.33E−05	6.12E−06	1.56E−06	1.09E−06
Trichloroethylene	1.01E−01	2.09E−01	1.18E−02	3.64E−02
Trillate	4.76E−06	4.18E−07	5.59E−07	8.52E−08
Xylene	3.06E−02	2.98E−02	3.59E−03	5.24E−03

Figure 7.5.3 shows the sensitivity of m_2 to changes in the dimensionless mass transfer coefficient ω. Small values of ω lead to high values of m_2 and D_{eff}. This figure also allows us to examine the validity of local equilibrium assumption (LEA) which holds when the mass transfer rates from the various compartments in Figure 7.5.1 are occurring at a much faster rate than advective process of fluid flow through the pores. For the set of parameters chosen, Figure 7.5.3 indicates that LEA may be reasonably assumed for $\omega > 10$. Note that the effective velocity is not influenced by ω. However for $\omega \to \infty$ (i.e. when LEA is valid), we have

$$m_2 = \frac{R^2}{P^2} + \frac{2(1+P)}{P}\left[\frac{R^2}{P} + \frac{R_{m2}^2}{K_m^0} + \frac{R_{im2}^2}{K_{im}^0}\right] \tag{7.5.22}$$

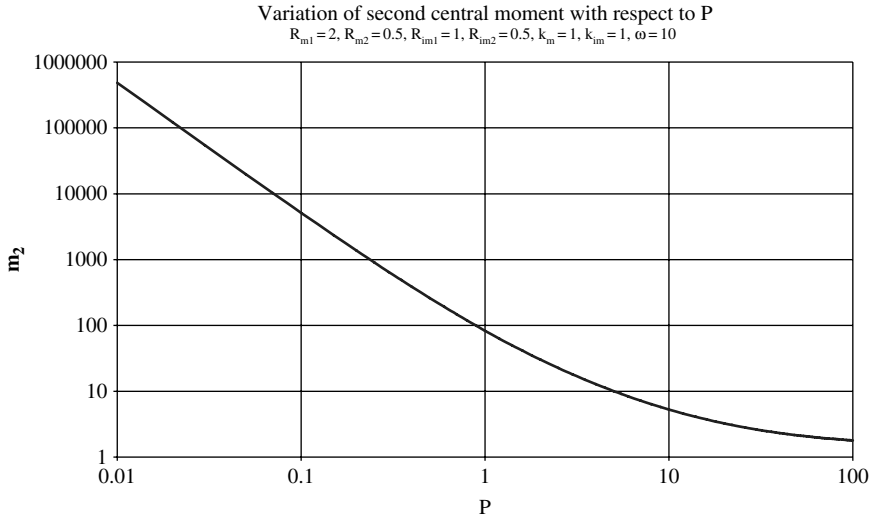

Figure 7.5.2. Sensitivity of second central moment to changes in P (adapted from Parashar and Govindaraju, 2006a, with permission from Springer. Parameters used to obtain this graph are $R_{m1} = 2$, $R_{m2} = 0.5$, $R_{im1} = 1$, $R_{im2} = 0.5$, $k_m = 1$, $k_{im} = 1$, and $\omega = 10$)

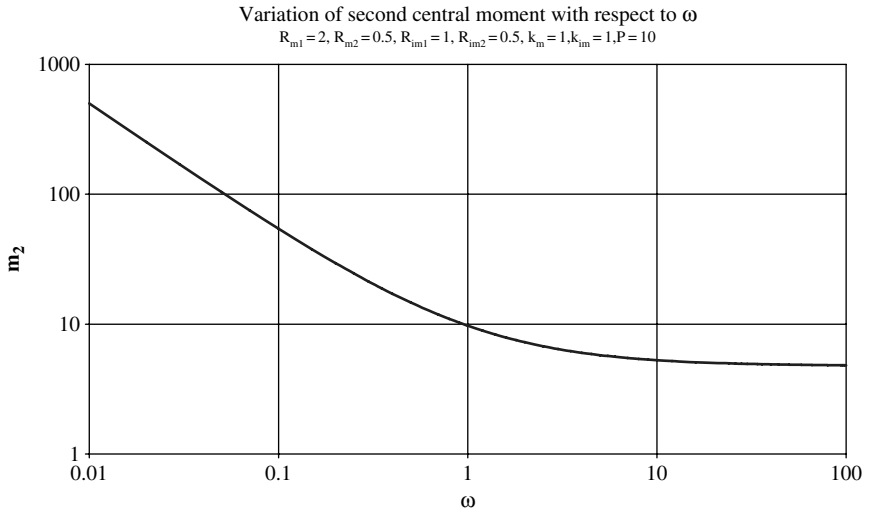

Figure 7.5.3. Sensitivity of second central moment to changes in ω (adapted from Parashar and Govindaraju, 2006a, with permission from Springer. Parameters used to obtain this graph are $R_{m1} = 2$, $R_{m2} = 0.5$, $R_{im1} = 1$, $R_{im2} = 0.5$, $k_m = 1$, $k_{im} = 1$, and $\omega = 10$)

and the effective dispersion is

$$D_{eff} = VL\left[\frac{P}{2R(1+P)^3} + \left(\frac{P}{1+P}\right)^2 \frac{1}{R^3}\left[\frac{R^2}{P} + \frac{R_{m2}^2}{K_m^0} + \frac{R_{im2}^2}{K_{im}^0}\right]\right] \tag{7.5.23}$$

For advection-dominated transport and when LEA is valid, the effective dispersion coefficient simply reduces to

$$D_{eff} = \frac{VL}{R^3}\left[\frac{R_{m2}^2}{K_m^0} + \frac{R_{im2}^2}{K_{im}^0}\right] \tag{7.5.24}$$

7.6. SPATIAL MOMENTS FOR MOBILE VAPOR PHASE MODEL

Spatial moment analysis can be conducted for equations (7.5.7) to (7.5.10) under the initial condition

$$C^*(X, 0) = A\delta(X) \tag{7.6.1}$$

with all concentrations and their derivatives vanishing at $X = \pm\infty$. Further, we can define the corresponding spatial moments

$$\mu_{1,n} = \int_{-\infty}^{\infty} X^n \; C^*(X, T) \; dX \tag{7.6.2a}$$

$$\mu_{2,n} = \int_{-\infty}^{\infty} X^n \; S_m^*(X, T) \; dX \tag{7.6.2b}$$

$$\mu_{3,n} = \int_{-\infty}^{\infty} X^n \; C_w^*(X, T) \; dX \tag{7.6.2c}$$

$$\mu_{4,n} = \int_{-\infty}^{\infty} X^n \; S_{im}^*(X, T) \; dX \tag{7.6.2d}$$

Multiplying each term in equations (7.5.7) to (7.5.10) by X^n and integrating over X, leads to the following set of differential equations

$$R_{m1}\frac{d\mu_{1,n}}{dT} + R_{m2}\frac{d\mu_{2,n}}{dT} + R_{im1}\frac{d\mu_{3,n}}{dT} + R_{im2}\frac{d\mu_{4,n}}{dT} = \frac{n(n-1)}{p}\mu_{1,n-2} + n\mu_{1,n-1} \tag{7.6.3a}$$

$$R_{im1}\frac{d\mu_{3,n}}{dT} + R_{im2}\frac{d\mu_{4,n}}{dT} = \omega\left(\mu_{1,n} - \mu_{3,n}\right) \tag{7.6.3b}$$

$$R_{m2}\frac{d\mu_{2,n}}{dT} = K_m^0\left(\mu_{1,n} - \mu_{2,n}\right) \tag{7.6.3c}$$

$$R_{im2}\frac{d\mu_{4,n}}{dT} = K_{im}^0\left(\mu_{3,n} - \mu_{4,n}\right) \tag{7.6.3d}$$

From (7.6.1), only $\mu_{1,0}(T=0)=A$, and all other moments are initially zero. Defining Laplace transforms of the spatial moments as

$$\hat{\mu}_{j,n}=\int_0^\infty e^{-sT}\mu_{j,n}(T)\,dT,\quad j=1,2,3,4,\ \ n=0,1,2\ldots \tag{7.6.4}$$

and performing Laplace transform operations on (7.6.3) leads to

$$G(s)\hat{\mu}_{1,n}-R_{m1}\mu_{1,n}(0)=\frac{n(n-1)}{p}\hat{\mu}_{1,n-2}+\hat{\mu}_{1,n-1} \tag{7.6.5}$$

where $G(s)$ is given as

$$G(s)=s\left[R_{m1}+R_{m2}A_2+R_{im1}A_3+R_{im2}A_4\right] \tag{7.6.6a}$$

$$A_2=\frac{K_m^0}{sR_{m2}+K_m^0} \tag{7.6.6b}$$

$$A_3=\frac{\omega}{sR_{im1}+\frac{sR_{im2}K_{im}^0}{sR_{im2}+K_{im}^0}+\omega} \tag{7.6.6c}$$

$$A_4=\frac{K_{im}^0A_3}{sR_{im2}+K_{im}^0} \tag{7.6.6d}$$

The expressions for the lower order moments can be obtained successively from (7.6.5) as

$$\mu_{1,0}=AR_{m1}\mathcal{L}^{-1}\left[\frac{1}{G(s)}\right] \tag{7.6.7}$$

$$\mu_{1,1}=AR_{m1}\mathcal{L}^{-1}\left[\frac{1}{G^2(s)}\right] \tag{7.6.8}$$

$$\mu_{1,2}=\frac{2AR_{m1}}{p}\mathcal{L}^{-1}\left[\frac{1}{G^2(s)}\right]+2A\ R_{m1}\mathcal{L}^{-1}\left[\frac{1}{G^3(s)}\right] \tag{7.6.9}$$

While inversion of the transform may be possible in some instances, the resulting expressions tend to be very complex, and a numerical inversion may be desirable.

CHAPTER 8

MOMENT GENERATING DIFFERENTIAL EQUATIONS

Moment generating functions were discussed in Chapter 1 in the context of probability density functions. Spatial moments were described in Chapters 3 and 6. It was found that the resulting expressions for spatial moments tend to be complicated. In this chapter, we explore the use of moment generating differential equations (MGDEs) to address this problem.

Estimation of moments via the MGDE method is convenient as it can be implemented for arbitrary boundary conditions, and for some cases of heterogeneity of parameters. Three dimensional flow and transport processes are also conveniently implemented in this approach. Moreover, existing numerical codes for solute transport processes may also be used to numerically solve temporal MGDEs as they involve the solution of the steady-state part of the transport equation. MGDEs can be generated for both spatial and temporal moments.

8.1. DEFINITIONS OF MGDEs

The concept of MGDEs can be introduced using the model of Harvey and Gorelick (1995). MGDEs are ordinary differential equations, which can be solved following standard integration techniques to obtain moments for arbitrary boundary conditions. Such differential equations are obtained by expressing a set of advection-dispersion equations with differential operators and subsequently applying Laplace and/or Fourier transform techniques.

Here, we illustrate the methodology by considering the ADEs that Harvey and Gorelick (1995) used to represent three-dimensional advective-dispersive transport with nonequilibrium sorption and no degradation.

$$\beta \frac{\partial q}{\partial t} + \frac{\partial c}{\partial t} = \boldsymbol{D} \frac{\partial^2 c}{\partial \boldsymbol{x}^2} - \boldsymbol{V} \frac{\partial c}{\partial \boldsymbol{x}} \tag{8.1.1}$$

$$\frac{\partial q}{\partial t} = \alpha (c - q) \tag{8.1.2}$$

Note that equation (8.1.1) is written in vector notation with bold faced quantities D and V representing dispersion and pore water velocity fields in three principal

directions $\boldsymbol{x}$ (x_1, x_2, x_3). Furthermore, these two equations are simplified forms of the general ADEs we have defined in Chapter 5 with equations (5.1.7) and (5.1.8).

An operator notation is used for simplicity. We define

$$\boldsymbol{L}(c) = \boldsymbol{D}\frac{\partial^2 c}{\partial \boldsymbol{x}^2} - V\frac{\partial c}{\partial \boldsymbol{x}} \tag{8.1.3}$$

such that

$$\beta\frac{\partial q}{\partial t} + \frac{\partial c}{\partial t} = \boldsymbol{L}(c) \tag{8.1.4}$$

Laplace transform of equations (8.1.4) and (8.1.2) with constant initial conditions:

$$c(\boldsymbol{x}, 0) = c_0 \qquad and \qquad q(\boldsymbol{x}, 0) = q_0 \tag{8.1.5}$$

yields

$$\boldsymbol{L}(\hat{c}) = s\hat{c} - c_0 + \beta s\hat{q} - \beta q_0 \tag{8.1.6}$$

$$s\hat{q} - q_0 = \alpha(\hat{c} - \hat{q}) \tag{8.1.7}$$

where $\hat{c}$ and $\hat{q}$ denote the Laplace transforms of c and q, respectively, as in (2.4.10). Equations (8.1.6) and (8.1.7) may further be simplified to yield a Laplace domain solution of the ADE with the operator $\boldsymbol{L}$:

$$\boldsymbol{L}(\hat{c}) = \left(s + \frac{\alpha\beta s}{s+\alpha}\right)\hat{c} + \beta q_0\left(\frac{s}{s+\alpha} - 1\right) - c_0 \tag{8.1.8}$$

Successive differentiation of equation (8.1.8) with respect to the Laplace variable s and subsequent evaluation of the resulting equations in the limit $s \to 0$ results in ordinary differential equations (ODEs) for absolute moments. This step is identical to Aris's method outlined in Chapter 5 for obtaining close-form expressions for moments. For example, setting $s = 0$ in equation (8.1.8) and using the definition for the zero-th moment $\hat{c}|_{s=0} = \mu_0$ leads to an ODE for μ_0:

$$\boldsymbol{L}(\mu_0) = -\beta q_0 - c_0 \tag{8.1.9}$$

Equation (8.1.9) is a linear, second-order ODE with constant coefficients and can easily be solved using standard integration techniques to obtain zeroth moments. Note also that equation (8.1.9) can provide solutions for zeroth moments in all three dimensions as the operator L is defined for x_1, x_2 and x_3 directions. Harvey and Gorelick (1995) used numerical methods to integrate Equation (8.1.9) in a three-dimensional flow field. They also showed that a steady-state numerical code can be used to solve for moments of all orders. If a numerical solution is sought for the temporal moments, then apart from arbitrary boundary conditions, spatial variation in $\boldsymbol{D}$ and $\boldsymbol{V}$ in (8.1.3) can be accommodated as well.

8.2. TEMPORAL MGDEs FOR SOLUTE TRANSPORT IN SOIL

To obtain temporal MGDEs for a general solute transport problem, we consider the dimensionless form of the ADE with nonequilibrium sorption and first-order degradation (equation [5.1.7] and equation [5.1.8]). For simplicity, we consider one-dimensional flow and transport processes only in one direction, i.e., vertical flow alone. The advective-dispersive differential operator for this case may be defined as,

$$\boldsymbol{L}(C_1) = \frac{1}{P}\frac{\partial^2 C_1}{\partial Z^2} - \frac{\partial C_1}{\partial Z} \tag{8.2.1}$$

such that Equation (5.1.7) becomes

$$\boldsymbol{L}(C_1) = \beta R\frac{\partial C_1}{\partial T} + \omega(C_1 - C_2) + \gamma_1 C_1 \tag{8.2.2}$$

Laplace transform of equations (8.2.2) and (5.1.8) with constant initial conditions:

$$C_1(Z,0) = C_{1,0} \quad ; \qquad C_2(Z,0) = C_{2,0} \tag{8.2.3}$$

and subsequent simplifications yield a Laplace domain solution of the ADE with the operator L:

$$\begin{aligned}\boldsymbol{L}(\hat{C}_1) = &\left(\beta Rs + \gamma_1 + \frac{\omega\left[(1-\beta)Rs + \gamma_2\right]}{(1-\beta)Rs + \omega + \gamma_2}\right)\hat{C}_1 \\ &+ \left\{\frac{-\omega(1-\beta)\mathrm{R}}{(1-\beta)Rs + \omega + \gamma_2}\right\} C_{2,0} - \beta R C_{1,0}\end{aligned} \tag{8.2.4}$$

Successive differentiation of Equation (8.2.4) with respect to the Laplace variable s and subsequent evaluation of the resulting equations in the limit $s \to 0$ results in ordinary differential equations (ODEs) for absolute moments. For example, first three ODEs for the absolute moments are:

$$\boldsymbol{L}(\mu_0) = \left[\gamma_1 + \frac{\omega\gamma_2}{\omega + \gamma_2}\right]\mu_0 - \frac{\omega(1-\beta)R}{\omega + \gamma_2} C_{2,0} - \beta R C_{1,0} \tag{8.2.5}$$

$$\boldsymbol{L}(\mu_1) = \left[\gamma_1 + \frac{\omega\gamma_2}{\omega + \gamma_2}\right]\mu_1 - \left[\frac{\beta R + \omega^2(1-\beta)R}{(\omega + \gamma_2)^2}\right]\mu_0 - \omega\left[\frac{(1-\beta)R}{\omega + \gamma_2}\right]^2 C_{2,0} \tag{8.2.6}$$

$$\begin{aligned}\boldsymbol{L}(\mu_2) = &\left(\gamma_1 + \frac{\omega\gamma_2}{\omega + \gamma_2}\right)\mu_2 - 2\left[\beta R + \frac{\omega^2(1-\beta)R}{(\omega + \gamma_2)^2}\right]\mu_1 \\ &+ \frac{-2\omega^2}{(\omega + \gamma_2)}\left[\frac{(1-\beta)R}{\omega + \gamma_2}\right]^2 \mu_0 - 2\omega\left[\frac{(1-\beta)R}{\omega + \gamma_2}\right]^3 C_{2,0}\end{aligned} \tag{8.2.7}$$

In fact, a recursive formulation for the n-th-order MGDE can be obtained as

$$\boldsymbol{L}(\mu_n) = \left[\gamma_1 + \frac{\omega\gamma_2}{\omega+\gamma_2}\right]\mu_n - n\beta R\mu_{n-1} - \frac{n!\omega^2(1-\beta)R}{(\omega+\gamma_2)^2}\sum_{i=1}^{n}\left[\frac{(1-\beta)R}{\omega+\gamma_2}\right]^{n-i}\frac{\mu_{i-1}}{(i-1)!}$$
$$- n!\omega\left[\frac{(1-\beta)R}{\omega+\gamma_2}\right]^{n+1} C_{2,0} \tag{8.2.8}$$

Equations (8.2.5) to (8.2.8) can be written in the following general form for the n-th order temporal moment generating differential equation:

$$L^*(\mu_n) = \frac{1}{P}\frac{d^2\mu_n}{dZ^2} - \frac{d\mu_n}{dZ} - g\mu_n = f_n(Z) \tag{8.2.9}$$

This is a non-homogeneous second-order differential equation with constant coefficients. The non-homogeneous term depends on the order n, while g is a constant given as

$$g = \gamma_1 + \frac{\omega\gamma_2}{\omega+\gamma_2} \tag{8.2.10}$$

In what follows, we present explicit solutions for the zero-th, first and second moments with and without degradation. Similar to the analysis of Harvey and Gorelick (1995), we consider the following end conditions.

$$C_1(-\infty, T) = C_1(\infty, T) = C_2(-\infty, T) = C_2(\infty, T) = 0 \tag{8.2.11}$$

$$C_1(0, T) = \delta(Z), \quad C_2(0, T) = 0 \tag{8.2.12}$$

where $\delta(Z)$ represents the Dirac-delta function.

8.2.1 Analysis with Degradation

We observe that the form of the advective-dispersive operator in (8.2.9) does not depend on the order n, suggesting that the analysis could be simplified by finding the appropriate Green's function, which is a solution to the problem

$$L^*(G^*(Z, a)) = \delta(Z - a) \tag{8.2.13}$$

The solution is readily obtained as

$$G^*(Z, a) = -\frac{e^{r_1(Z-a)}}{r_1 - r_2}[1 - H(Z-a)] - \frac{e^{r_2(Z-a)}}{r_1 - r_2}H(Z-a) \tag{8.2.14}$$

where $H(Z)$ is the Heaviside function, and r_1 and r_2 are the characteristic roots of the operator L^*

$$r_1 = \frac{1+\sqrt{1+4g/P}}{2/P} \; ; \; r_2 = \frac{1-\sqrt{1+4g/P}}{2/P} \tag{8.2.15}$$

The general solution (8.2.9) is now available using (8.2.14) through a convolution of the form

$$\mu_n(Z) = \int_{-\infty}^{\infty} f_n(a) G^*(Z, a) \mathrm{da} \tag{8.2.16}$$

This leads to the following explicit expressions for moments by using the appropriate non-homogeneous part $f_n(Z)$ from equations (8.2.5) to (8.2.8),

$$\mu_0(Z) = \beta R \frac{e^{r_1 z}}{r_1 - r_2}[1 - H(Z)] + \frac{\beta R e^{r_2 z}}{r_1 - r_2} H(Z) \tag{8.2.17}$$

$$\begin{aligned}\mu_1(Z) = {} & \frac{a_3 \beta R}{(r_1 - r_2)^3}[-2 + (r_1 - r_2)Z)]\, e^{r_1 z}[1 - H(Z)] \\ & + \frac{a_3 \beta R}{(r_1 - r_2)^3}[-2 - (r_1 - r_2)Z)] e^{r_2 Z} \cdot H(Z)\end{aligned} \tag{8.2.18}$$

$$\begin{aligned}\mu_2(Z) = {} & \left\{ \frac{a_2 \beta R}{(r_1 - r_2)^3}[-2 + (r_1 - r_2)Z)] \right. \\ & \left. + \frac{a_1 a_3 \beta R}{(r_1 - r_2)^5} \left[6 - 3Z\ (r_1 - r_2) + \frac{(r_1 - r_2)^2\ Z^2}{2} \right] \right\} e^{r_1 Z}[1 - H(Z)] \\ & + \left\{ \frac{a_2 \beta R}{(r_1 - r_2)^3}[-2 - (r_1 - r_2)Z] \right. \\ & \left. + \frac{a_1 a_3 \beta R}{(r_1 - r_2)^5} \left[6 + 3Z\ (r_1 - r_2) + \frac{(r_1 - r_2)^2\ Z^2}{2} \right] \right\} \cdot e^{r_2 Z}\ H(Z)\end{aligned} \tag{8.2.19}$$

where

$$a_1 = -2\beta R - \frac{2\omega^2(1 - \beta)\mathrm{R}}{(\omega + \gamma_2)^2} \tag{8.2.20}$$

$$a_2 = -\frac{2\omega^2(1 - \beta)^2\ \mathrm{R}^2}{(\omega + \gamma_2)^3} \tag{8.2.21}$$

$$a_3 = \frac{a_1}{2} \text{ and H(.) is the Heaviside step function.} \tag{8.2.22}$$

8.2.2 Analysis without Degradation

This is the case considered by Harvey and Gorelick (1995). We now seek a Green's function solution to the problem

$$L\ (G\,(Z, \mathrm{a})) = \frac{1}{P}\frac{d^2 G}{dZ^2} - \frac{dG}{dZ} = \delta(Z - a) \tag{8.2.23}$$

the solution to which is obtained as

$$G\ (Z,a) = -\frac{1}{P}e^{P(Z-a)}[1-H(Z-a)] - \frac{1}{P}\ H(Z-a) \tag{8.2.24}$$

Equations (8.2.6) and (8.2.8) without degradation have the general form

$$L(\mu_n) = f_n'\ (Z) \tag{8.2.25}$$

the solution to which is expressed through the convolution

$$\mu_n(Z) = \int_{-\infty}^{\infty} f_n'(a)\ G(Z,a)\ da \tag{8.2.26}$$

Using (8.2.24) and (8.2.26), equations for the first three moments for no degradation are explicitly obtained as

$$\mu_0(Z) = \frac{\beta R}{P}e^{PZ}[1-H(Z)] + \frac{\beta R}{P}\mathrm{H}(Z) \tag{8.2.27}$$

$$\mu_1(Z) = \frac{\beta R}{P^2}[Z-\frac{2}{P}]\ e^{PZ}\ [1-H(Z)] + \frac{\beta R}{P^2}\left[\frac{2}{p}+Z\right]H(Z) \tag{8.2.28}$$

$$\begin{aligned}\mu_2(Z) = &\left\{\frac{2\beta(1-\beta)^2R^3}{\omega P^3}[-2+PZ] + \frac{2\beta R^3}{P^5}\left[6-3PZ+\frac{P^2Z^2}{2}\right]\right\}\ e^{PZ}[1-H(Z)] \\ &+\left\{\frac{2\beta(1-\beta)^2R^3}{\omega P^3}[2+PZ] + \frac{2\beta R^3}{P^5}\left[6+3PZ+\frac{P^2Z^2}{2}\right]\right\}H(Z)\end{aligned} \tag{8.2.29}$$

This solution method can be extended to higher dimensional cases. Figure 8.2.1 shows the behavior of these moments for the cases considered in Table 5.5.2. The panels on the right correspond to those cases where degradation is set to zero. The spatial domain is infinite ($-\infty < Z \leq \infty$), and while moments can be mathematically defined for $Z < 0$, it must be cautioned that they do not have the usual interpretation in this region. It should be noted that locations $Z < 0$ do not sample the entire plume. Some solute mass does extend into the negative Z region because of dispersion, especially for small times, but moments cannot be used to define travel times, effective velocities, and effective dispersion coefficients as in equations (4.6.9) and (4.6.10).

Moments have their usual interpretation for $Z > 0$, and effective values are meaningful in this range. Using the definition of normalized moments in equation (5.2.5), we express effective properties in the same form of equations (4.7.20) and (4.7.21) as

$$V_{eff} = \frac{Z}{\mu_1^*} = \frac{Z(r_1-r_2)}{\left[\beta R + \frac{\omega^2(1-\beta)R}{(\omega+\gamma_2)^2}\right]\left(\frac{2}{r_1-r_2}+Z\right)} \tag{8.2.30}$$

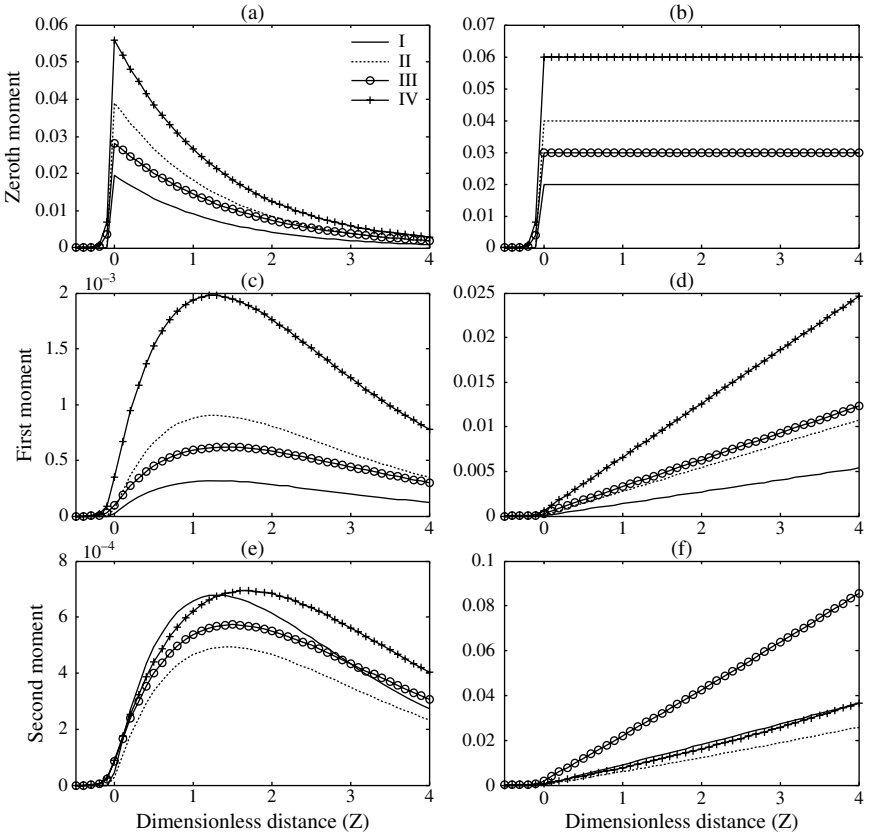

Figure 8.2.1. Absolute temporal moments for the PNE model. Cases I, II, III, and IV correspond to different parameter values described in Table 5.5.2. Panels to the right are cases for no degradation, i.e. when $\gamma_1 = \gamma_2 = 0$

$$D_{eff} = \frac{\mu_2^* - (\mu_1^*)^2}{2\mu_1^*} V_{eff}^2 \tag{8.2.31}$$

These expressions can be used to derive effective properties that are shown in Figure 8.2.2 for the cases described in Table 5.5.2. The domain $Z < 0$ is not considered. Expressions for the limiting cases of no degradation and large Z can be obtained from these expressions.

8.3. SPATIAL MGDEs FOR PNE MODEL OF SOLUTE TRANSPORT IN SOIL

In an analogous manner, applying Fourier transforms, the corresponding MGDEs for spatial moments are obtained in this section. Nahar (1998) provides detailed derivations for the results presented in this section.

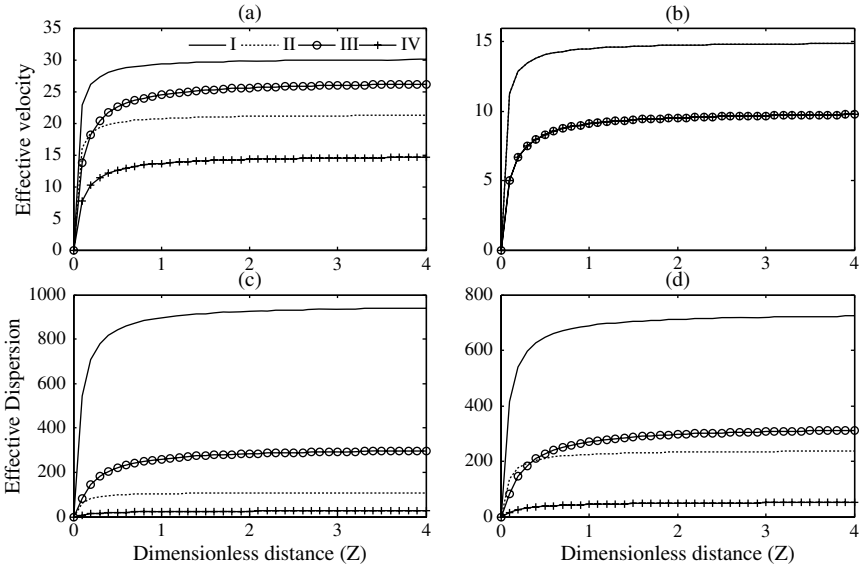

Figure 8.2.2. Effective parameters according to the definitions of Equations (8.2.30) and (8.2.31) for the PNE model. Cases I, II, III, and IV correspond to different parameter values described in Table 5.5.2. Panels to the right are cases for no degradation, i.e. when $\gamma_1 = \gamma_2 = 0$

The advection-dispersion equations for the non-dimensional PNE model were presented in equations (5.1.7) and (5.1.8) (as in van Genuchten and Wagenet, 1989). An infinite domain is assumed in this section where boundary effects do not influence the movement of the solute plume far away from the region of interest. For simplicity, the initial conditions are chosen as

$$C_1(Z,0) = M\,\delta(Z)\ ;\ \ C_2(Z,0) = 0 \tag{8.3.1}$$

This initial condition states that all the solute mass is located initially at $x = 0$ in the mobile phase, representing an instantaneous spill. Equation (8.3.1) is mathematically simple and leads to analytical solutions for several interesting cases. Moreover, solutions for more complicated initial conditions can be obtained using superposition principles, once the solution is available using Equation (8.3.1).

Applying Fourier transforms to Equations (5.1.7) and (5.1.8) results in:

$$\beta RL(\tilde{C}_1) = \frac{j^2\omega^2}{P}\tilde{C}_1 - j\omega\ \tilde{C}_1 - \bar{\alpha}(\tilde{C}_1 - \tilde{C}_2) - \gamma_1\tilde{C}_1 \tag{8.3.2}$$

$$(1-\beta)\,RL(\tilde{C}_2) = \bar{\alpha}(\tilde{C}_1 - \tilde{C}_2) - \gamma_1\tilde{C}_2 \tag{8.3.3}$$

where the operator L now has the definition:

$$L(^*) = \frac{d(^*)}{dt} \tag{8.3.4}$$

and $\tilde{C}_1$ and $\tilde{C}_2$ are the Fourier transforms defined analogous to (6.2.2) as

$$\tilde{C}_1(\omega\ ;\ T) = \int_{-\infty}^{\infty} e^{-j\omega Z}\ C_1(Z,T)\ dZ\ ; \quad \tilde{C}_2(\omega;T) = \int_{-\infty}^{\infty} e^{-j\omega Z}\ C_2(Z,T)\ dZ \tag{8.3.5}$$

Note that the Damkohler number has been labeled as $\bar{\alpha}$ in (8.3.2) and (8.3.3) to distinguish it from the transform variable ω. Using Aris' method, the spatial moments are

$$\xi_n = \int_{-\infty}^{\infty} Z^n C_1(Z,T)dZ = j^n \lim_{\omega\to 0} \frac{d^n \tilde{C}_1(\omega;T)}{d\omega^{\mathrm{n}}} \tag{8.3.6a}$$

$$\eta_n = \int_{-\infty}^{\infty} Z^n C_2(Z,T)dZ = j^n \lim_{\omega\to 0} \frac{d^n \tilde{C}_2(\omega;T)}{\mathrm{d}\omega^{\mathrm{n}}} \tag{8.3.6b}$$

From (8.3.2) and (8.3.3), we obtain for n= 0

$$L(\xi_0) = -\frac{\bar{\alpha}+\gamma_2}{(1-\beta)R} m_0 + \frac{\bar{\alpha}}{\beta R}\eta_0 \tag{8.3.7}$$

$$L(\eta_0) = -\frac{\bar{\alpha}+\gamma_2}{(1-\beta)R} \eta_0 + \frac{\bar{\alpha}}{(1-\beta)R} m_0 \tag{8.3.8}$$

and for higher orders ($n > 1$):

$$L(\xi_n) = -\frac{\bar{\alpha}+\mu_1}{\beta R}\xi_n + \frac{n}{\beta R}\xi_{n-1} + \frac{n(n-1)}{P\beta R}\xi_{n-2} + \frac{\bar{\alpha}}{\beta R}\xi_n \tag{8.3.9}$$

$$L(\eta_n) = \frac{\bar{\alpha}}{(1-\beta)R}\xi_n - \frac{\bar{\alpha}+\mu_2}{(1-\beta)R}\eta_n \tag{8.3.10}$$

A coupled system of linear equations (MGDEs) needs to be solved for moments of any order. We can define the Laplace transforms of the moments as

$$\hat{\xi}_n = \int_0^{\infty} e^{-sT}\xi_n\ dT\ ;\ \hat{\eta}_{\mathrm{n}} = \int_0^{\infty} e^{-sT}\eta_n\ dT \tag{8.3.11}$$

and taking Laplace transforms of (8.3.8) and (8.3.9) yields

$$G(s)\ \hat{\xi}_n = \beta R\hat{\xi}_n(0) + \frac{n(n-1)}{P}\hat{\xi}_{n-2} + n\ \hat{\xi}_{n-1} \tag{8.3.12}$$

where $G(s)$ is defined as

$$G(s) = \beta Rs + \frac{\bar{\alpha}\left[(1-\beta)Rs+\gamma_2\right]}{(1-\beta)Rs+\bar{\alpha}+\gamma_2} + \gamma_1 \tag{8.3.13}$$

By successive substitution for n = 0, 1, and 2, in (8.3.12), we obtain the following expressions

$$\xi_0 = \mathcal{L}^{-1}\left[\frac{M\beta R}{G(s)}\right] \tag{8.3.14}$$

$$\xi_1 = \mathcal{L}^{-1}\left[\frac{M\beta R}{G^2(s)}\right] \tag{8.3.15}$$

$$\xi_2 = \mathcal{L}^{-1}\left[\frac{2M\ \beta R}{P}\frac{1}{G^2(s)} + \frac{2M\ \beta R}{G^3(s)}\right] \tag{8.3.16}$$

Analytical inversion of these expressions leads to lengthy expressions, and numerical inversion is often preferable. We note that the Laplace transforms of the moments are related as

$$\hat{\eta}_n = \frac{\omega\ \hat{\xi}_n}{(1-\beta)Rs + \omega + \gamma_2} \tag{8.3.17}$$

Combining (8.3.12), (8.3.13) and (8.3.17) yields expressions for $\hat{\eta}_n$ that typically have to be inverted numerically.

As discussed in Chapter 5, the PNE model can be categorized into four different cases: non-equilibrium sorption and degradation (ND), equilibrium sorption and degradation (ED) for which $\bar{\alpha} = \infty$, and $\beta = 1$; non-equilibrium sorption and no degradation (N) where $\gamma_1 = \gamma_2 = 0$; and, equilibrium sorption and no degradation (E) where $\bar{\alpha} = \infty$, $\beta = 1$ and $\gamma_1 = \gamma_2 = 0$. The same four different combinations of model parameters R, P, β, $\bar{\alpha}$, γ_1 and γ_2 as given in Table 5.5.2 will be discussed. For each of these combinations, spatial moments were obtained corresponding to ND, ED, N and E. These four combinations of parameters do not constitute a rigorous sensitivity analysis, but provide an indication of the behaviour of spatial moments for different combinations of R, P, β, and $\bar{\alpha}$. For convenience, M is set to unity in (8.3.1).

Figure 8.3.1a shows the temporal evolution of the zeroth spatial moment ξ_0 for Case 1 described in Table 8.3.1. The figure shows four curves corresponding to ND, N, ED and E, respectively. Figures 8.3.1b, c, and d show similar results for the zeroth moments for the other three combinations of parameters in Table 5.5.2. The behaviour of the zeroth spatial moments η_0 for the four combinations of parameters can be examined in Figures 8.3.2a, b, c and d. Thus, Figures 8.3.1 and 8.3.2 account for the zeroth moments. In a similar arrangement, Figures 8.3.3a to d and 8.3.4a to d show the results for the first spatial moments ξ_1 and η_1, while Figures 8.3.5a to 8.3.5d and 8.3.6a to 8.3.6d show the temporal evolution of the second spatial moments ξ_2 and η_2.

8.3.1 Zeroth Moment

Figure 8.3.1 compares the total solute mass associated with the mobile region (ξ_0) as a function of time for each case. Under equilibrium conditions with no degradation

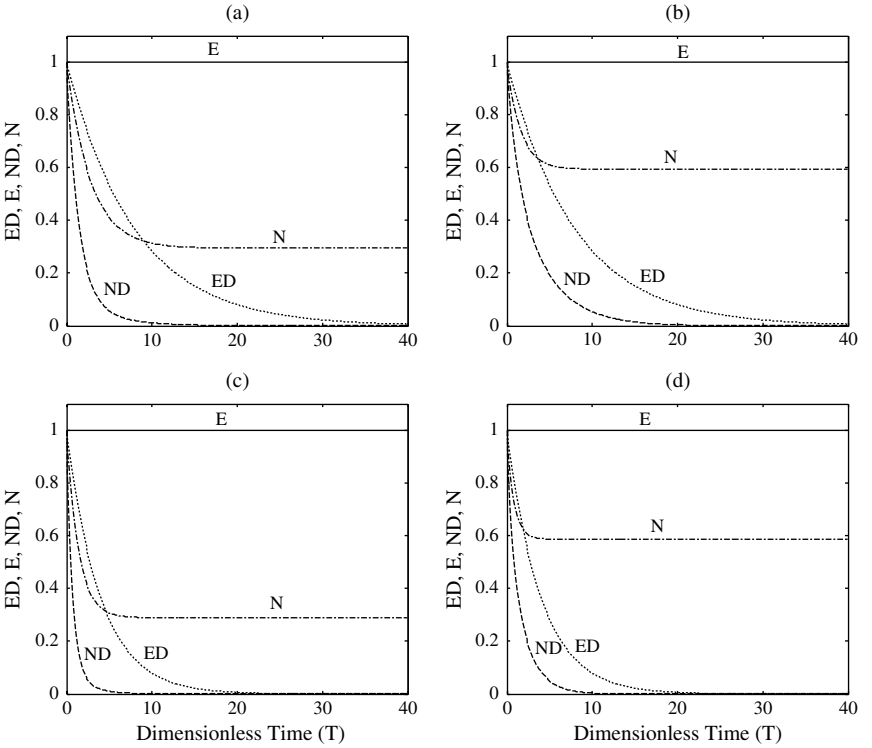

Figure 8.3.1. Behavior of the zeroth moment ξ_0 for the PNE model. Figures a, b, c, and d correspond to cases I, II, III, and IV, respectively, of Table 5.5.2. The key to the symbols is as follows: E-equilibrium and no degradation; N-nonequilibrium and no degradation; ED-equilibrium and degradation; ND-nonequilibrium and degradation as described in the text

(E) the total mass is constant over time, because there is no loss of mass from mobile phase. For equilibrium conditions, $\bar{\alpha} = \infty$, $\beta = 1$, and $\gamma_1 = \gamma_2 = 0$, and the MGDE for the nth moment in mobile phase becomes:

$$L(\xi_n) = \frac{d\xi_n}{dt} = \frac{n}{R}\xi_{n-1} + \frac{n(n-1)}{PR}\xi_{n-2} \tag{8.3.18}$$

For the zeroth moment, we set $n = 0$, and for the initial condition of (8.3.1)

$$\xi_0(t) = M = 1.0 \tag{8.3.19}$$

Consequently, Figures 8.3.1a to 8.3.1d show that $\xi_0(t)$ remains a constant for the curves designated as E. For non-equilibrium with no degradation N, the zeroth moment ξ_0 decreases with time. Initially all the mass is associated with the mobile phase. As time progresses, the solute diffuses into immobile phase and eventually the mobile and immobile concentrations are in equilibrium.

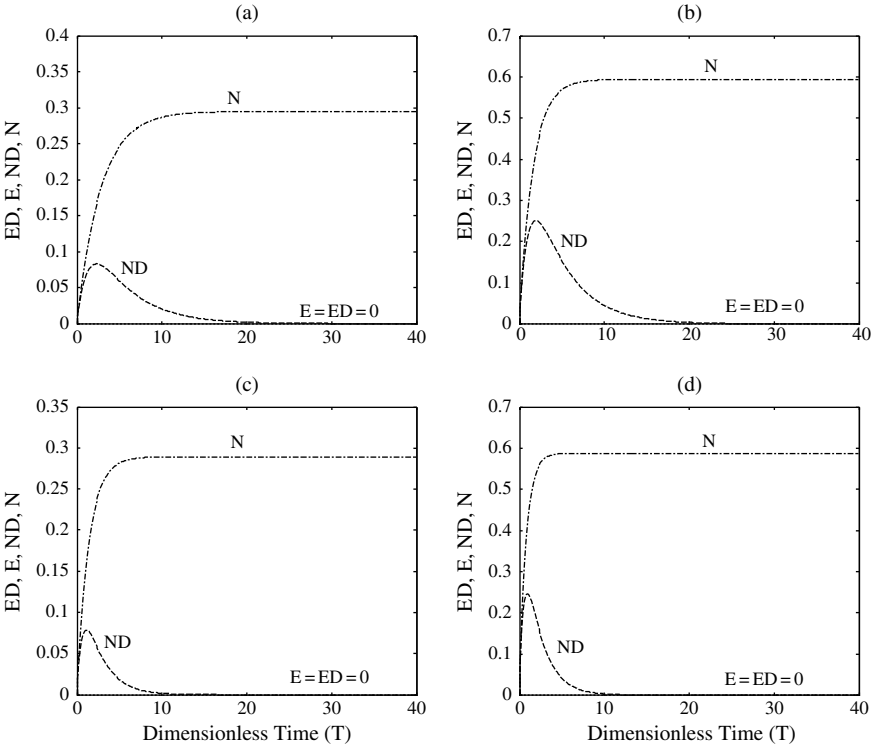

Figure 8.3.2. Behavior of the zeroth moment η_0 for the PNE model. Figures a, b, c, and d correspond to cases I, II, III, and IV, respectively, of Table 5.5.2. The key to the symbols is as follows: E-equilibrium and no degradation; N-nonequilibrium and no degradation; ED-equilibrium and degradation; ND-nonequilibrium and degradation as described in the text

For nonequilibrium with no degradation, $\gamma_1 = \gamma_2 = 0$, and the MGDEs for the zero[th] moments are

$$\frac{d\xi_0}{dt} = -\frac{\bar{\alpha}}{\beta R}\xi_0 + \frac{\bar{\alpha}}{\beta R}\eta_0 \tag{8.3.20}$$

$$\frac{d\eta_0}{dt} = \frac{\bar{\alpha}}{(1-\beta)R}\xi_0 - \frac{\bar{\alpha}}{(1-\beta)R}\eta_0 \tag{8.3.21}$$

Solving the above two eqution under (8.3.1) yields

$$\xi_0(t) = 1 - (1-\beta)(1 - e^{-\frac{\bar{\alpha}}{R\beta(1-\beta)}t}) \tag{8.3.22}$$

$$\eta_0(t) = \beta(1 - e^{-\frac{\bar{\alpha}}{R\beta(1-\beta)}t}) \tag{8.3.23}$$

And at steady state, when $t \to \infty$

$$\xi_0 = \eta_0 = \beta \tag{8.3.24}$$

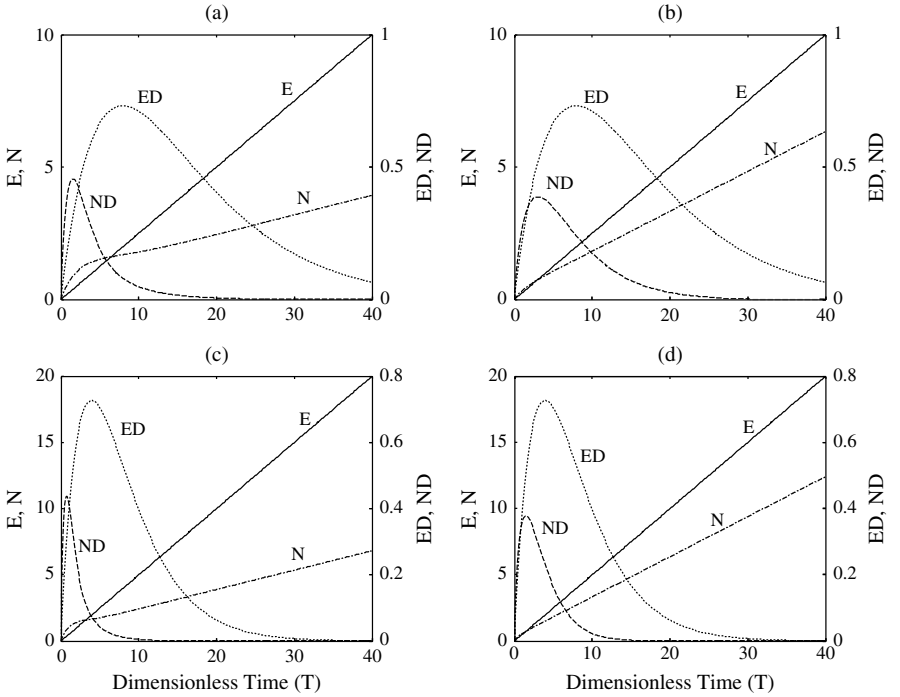

Figure 8.3.3. Behavior of the first moment ξ_1 for the PNE model. Figures a, b, c, and d correspond to cases I, II, III, and IV, respectively, of Table 5.5.2. The key to the symbols is as follows: E-equilibrium and no degradation; N-nonequilibrium and no degradation; ED-equilibrium and degradation; ND-nonequilibrium and degradation as described in the text

The curves labelled as N in Figures 8.3.1a to 8.3.1d start at 1.0 for $t = 0$, and decline asymptotically to the respective β value. Correspondingly in Figures 8.3.2a to 8.3.2d, the curves for N show that the zeroth moment η_0 starts at zero and exhibits a gradual rise to β. Under the ED conditon, the zeroth moment becomes:

$$\xi_0(t) = e^{-\frac{\gamma}{R}t} \tag{8.3.25}$$

and under the ND condition, for $\beta = 0.5$ and $\gamma_1 = \gamma_2 = \gamma$, the zeroth moment in mobile phase is found to be:

$$\xi_0(t) = \frac{e^{-\frac{4\bar{\alpha}t}{R}} - 1}{2(e^{-\frac{2\gamma t}{R}} - 1)} \tag{8.3.26}$$

The zeroth moment in immobile phase is then expressed as:

$$\eta_0(t) = \frac{e^{-\frac{4\bar{\alpha}t}{R}} - 1}{2(e^{-\frac{2\gamma t}{R}} - 1)} - e^{-\frac{4\bar{\alpha}+2\gamma}{R}t} \tag{8.3.27}$$

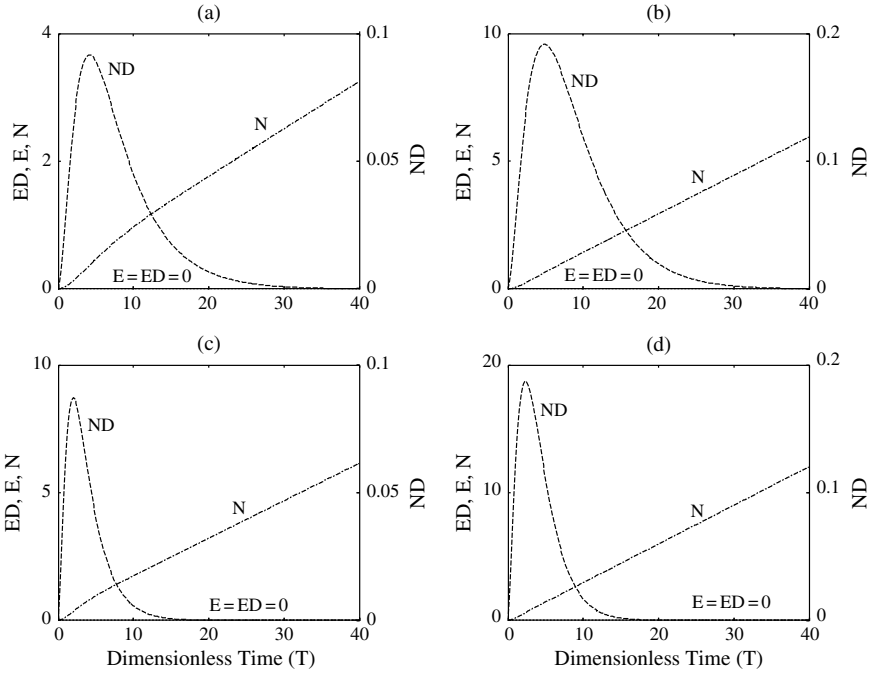

Figure 8.3.4. Behavior of the first moment η_1 for the PNE model. Figures a, b, c, and d correspond to cases I, II, III, and IV, respectively, of Table 5.5.2. The key to the symbols is as follows: E-equilibrium and no degradation; N-nonequilibrium and no degradation; ED-equilibrium and degradation; ND-nonequilibrium and degradation as described in the text

Under ED and ND conditions, loss of mass with time is evident as the curves show exponential decay. Moments in mobile phase ξ_0 for ND and ED reduce faster than for ND and ED respectively due to influence of degradation. Eventually moments for ND and ED decrease to zero. For the four combinations of parameters shown in Figures 8.3.1a to 8.3.1d, ξ_0(N) initially reduces faster than m_0(ED). However, ξ_0(N) reaches a steady value of β and ξ_0(ED) declines to zero in an exponential fashion.

When an initial decrease in solute mass in the mobile phase is observed, we are confounded with several possibilities. The initial decrease may be caused by degradation effects, in which case it depends on the degradation constant γ. If non-equilibrium is causing the initial decrease in ξ_0, then the rate of decrease is dependant on both the mass transfer coefficient $\bar{\alpha}$ and the partition coefficient β. In case of ND, both these effects combine to reduce ξ_0. Thus, the only case that can be clearly identified from zeroth moments is E, when there is no decrease in total solute mass. If accurate measurements are available over a long period of time, and the solute mass in the mobile phase achieves a non-zero equilibrium value ($= \beta$), then we may conclude that there is no degradation, and that reduction in ξ_0 is due to

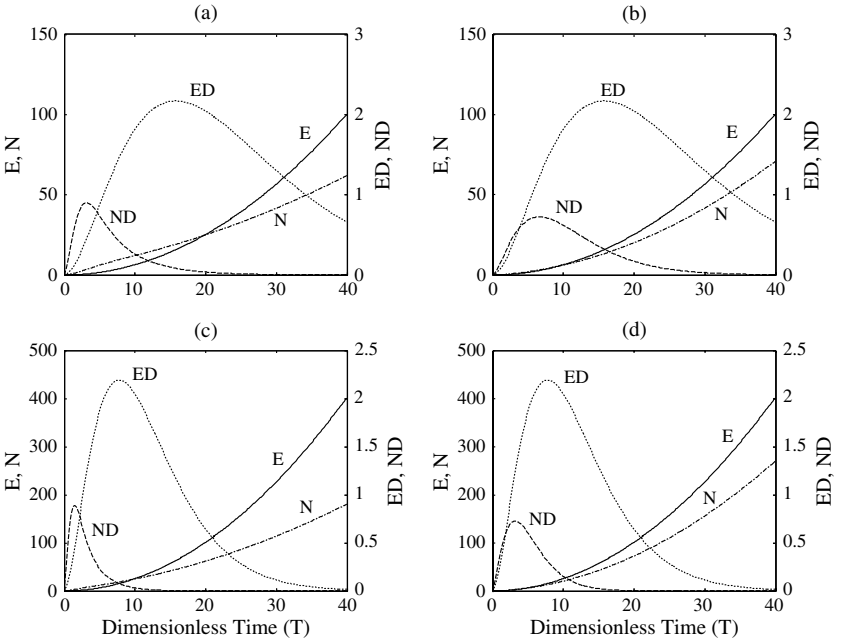

Figure 8.3.5. Behavior of the second moment ξ_2 for the PNE model. Figures a, b, c, and d correspond to cases I, II, III, and IV, respectively, of Table 5.5.2. The key to the symbols is as follows: E-equilibrium and no degradation; N-nonequilibrium and no degradation; ED-equilibrium and degradation; ND-nonequilibrium and degradation as described in the text

to non-equilibrium effects alone. This would imply that some portion of the initial solute mass is now associated with C_2. On the other hand, if long term measurements of solute concentrations show that $m_0(t)$ tends to zero, then we cannot distinguish between the effects of ED and ND. Both of them show an exponential decline to zero for $\xi_0(t)$ indicating that all the solute vanishes eventually.

It should be noted that some solutes exhibit different degradation rates depending on whether they are associated with liquid phase or solid phase (i.e. $\gamma_1 \neq \gamma_2$).

8.3.2 First Moment

Degradation reduces the first moment in mobile phase (ξ_1) for both non-equilibrium and equilibrium conditions. Absence of degradation leads to a linear increase in the first moment under both equilibrium and non-equilibrium conditions (N and E). This is demonstrated in Figures 8.3.3a to 8.3.3d, and confirmed by analytical results. The expression for first moment under equilibrium conditions (E) is:

$$\xi_1(t) = \frac{t}{R} \tag{8.3.28}$$

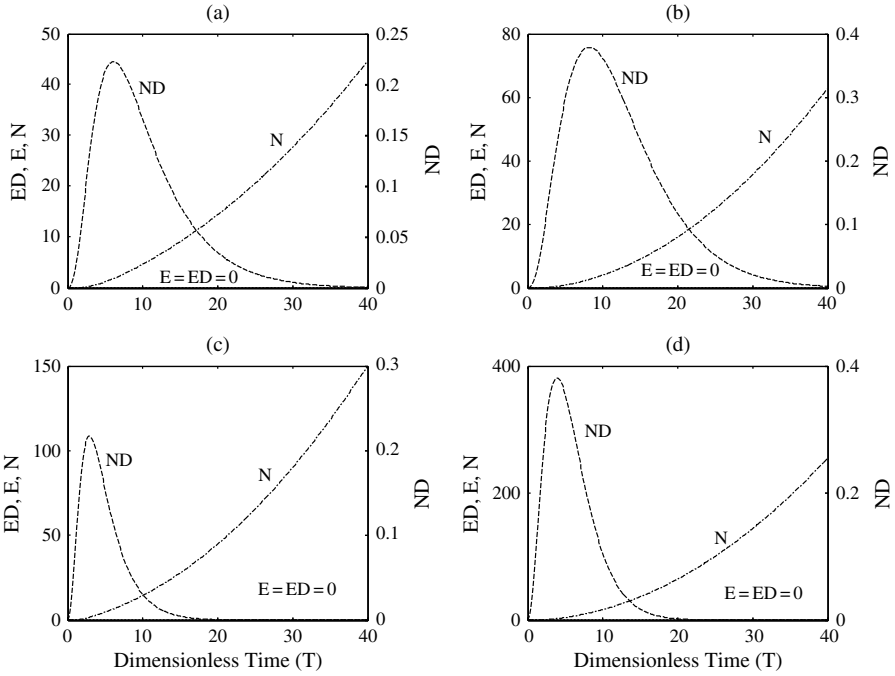

Figure 8.3.6. Behavior of the second moment η_2 for the PNE model. Figures a, b, c, and d correspond to cases I, II, III, and IV, respectively, of Table 5.5.2. The key to the symbols is as follows: E-equilibrium and no degradation; N-nonequilibrium and no degradation; ED-equilibrium and degradation; ND-nonequilibrium and degradation as described in the text

Under ED condition, the first moment can be expressed as:

$$\xi_1(t) = \frac{t}{R} e^{-\frac{\gamma}{R}t} \tag{8.3.29}$$

Comparing the ND and ED curves in Figure 8.3.3 allows us to evaluate the effects of non-equilibrium sorption in the presence of degradation. At small times, $\xi_1(\text{ND}) > \xi_1(\text{ED})$. However, as time increases, $\xi_1(\text{ED})$ becomes larger than $\xi_1(\text{ND})$. The problem of identifying which process (ND, ED or N) controls solute fate and transport cannot be resolved using the first moments either.

In Figure 8.4.4, the first moment (η_1) is zero for ED and E, as all the solute resides in the mobile phase. As $t \to \infty$, $\eta_1(\text{ND}) = \xi_1(\text{ND}) = 0$. Results in Figure 8.3.4 reaffirm our conclusions based on first spatial moments of mobile phase concentrations.

8.3.3 Second Moment

Degradation plays a similar role for second moments as it does in the zeroth and first moments. Since moments in mobile phase (ξ_2) at ND and ED (Figure 8.3.5)

are always less than ξ_2 at N and E respectively, spatial moments indicate that degradation suppresses spread of the solute mass. For smaller time, $\xi_2(\mathrm{ND})$ is higher than $\xi_2(ED)$. This relationship tends to be reversed at longer times for the cases examined in Table 5.5.2. The curves for N and E exhibit the same trend, i.e. for smaller time, $\xi_2(\mathrm{N}) > \xi_2(\mathrm{E})$ and for longer times, $\xi_2(\mathrm{N}) < \xi_2(\mathrm{E})$, implying that the reduction of the second moment at longer time might be dominated by nonequilibrium effects. Figure 8.3.6 shows $\eta_2(t)$ for the four combinations of parameters in Table 8.3.1.

Examination of Figures 8.3.1 to 8.3.6 reveals that curves for Case 1 and Case 2 are similar to each other, and so are curves for Case 3 and Case 4. This suggests that results are more sensitive to changes in P and R than they are to changes in β and $\bar{\alpha}$. However, in the case of second moments, results show more sensitivity to changes in β and $\bar{\alpha}$ than to changes in P and R. As expected, we note that

$$\xi_n(ND) < \xi_n(N)\ ;\ \xi_n(ED) < \xi_n(E) \tag{8.3.30}$$

8.4. SPATIAL MOMENTS FOR A TWO-LAYER AQUIFER

Valocchi (1988) considered the case of solute transport in a two-layer stratified aquifer to examine moment behavior at long times and the role of mixing in between the two layers in determining overall plume behavior and deviations from local equilibrium. We revisit this problem with the inclusion of a degradation term The two layers of thicknesses h_1 and h_2 have seepage velocities of V_1 and V_2 in the x-direction, respectively. The governing equations are expressed as

$$\frac{\partial c_i}{\partial t} + \frac{\rho}{\theta}\frac{\partial c_{s,i}}{\partial t} = D_{x,i}\frac{\partial^2 c_i}{\partial x^2} + D_{yi}\frac{\partial^2 c_i}{\partial y^2} + D_{zi}\frac{\partial^2 c_i}{\partial z^2} - V_i\frac{\partial c_i}{\partial x} - \mu c_i \tag{8.4.1}$$

$$\frac{\partial c_{s,i}}{\partial t} = k_r\left[k_d c_i - c_{s,i}\right] - \mu c_{s,i} \tag{8.4.2}$$

where ρ is the bulk density, θ is the uniform water content, $i = 1, 2$ denotes the layer number, C_i is the liquid phase concentration, $C_{s,i}$ is the solid phase concentration, D_{xi}, D_{yi} and D_{zi} are the hydrodynamic dispersion coefficients, and μ is the first-order degradation rate coefficient. The following boundary and initial conditions are implemented.

$$c_i, \frac{\partial c_i}{\partial x}, \frac{\partial c_i}{\partial y}, \frac{\partial c_i}{\partial z}, \frac{\partial c_{s,i}}{\partial x}, \frac{\partial c_{s,i}}{\partial y} = 0, \quad x, y \to \infty \tag{8.4.3a}$$

$$c_i(x, y, t = 0) = A\delta(x)\delta(y)\ ;\ c_{s,i}(x, y, t = 0) = 0 \tag{8.4.3b}$$

$$\frac{\partial c_i}{\partial z} = 0, \frac{\partial c_{s,i}}{\partial z} = 0, z = 0, z = H \tag{8.4.3c}$$

Furthermore, the vertical flux at the interface is assumed to be continuous. Equation (8.4.3b) implies that a total solute mass of $A\theta H$ (H is the total thickness of the

aquifer = $h_1 + h_2$) is introduced instantaneously at $t = 0$ into the aquifer throughout its depth at the origin. Valocchi (1988) defined the depth averaged concentration in each layer as

$$\bar{c}_i = \frac{1}{h_i} \int_{z_{ib}}^{z_{it}} c_i(x, y, z, t)\ dz \tag{8.4.4}$$

where z_{ib} and z_{it} refer to the bottom and top elevations for layer i. The depth-averaged concentration throughout the aquifer is

$$\bar{c}(x, y, t) = \frac{1}{H} (h_1 \bar{c}_1 + h_2 \bar{c}_2) \tag{8.4.5}$$

Integrating (8.4.1) and (8.4.2) over the thickness for each layer, the following four equations are obtained.

$$\frac{\partial \bar{c}_i}{\partial t} + \frac{\partial \bar{S}_i}{\partial t} = D_{xi} \frac{\partial^2 \bar{c}_i}{\partial x^2} + D_{yi} \frac{\partial^2 \bar{c}_i}{\partial y^2} + \frac{D_{zi}}{h_i} \left. \frac{\partial \bar{c}_i}{\partial z} \right|_{z_{ib}}^{z_{it}} - V_i \frac{\partial \bar{c}_i}{\partial x} - \gamma\ \bar{c}_i, \quad i = 1, 2 \tag{8.4.6}$$

$$\frac{\partial \bar{S}_i}{\partial t} = k_r \left[k_d \bar{c}_i \bar{S}_i \right] - \gamma\ \bar{S}_i,\ i = 1, 2 \tag{8.4.7}$$

where $S_i = \rho\ c_{s,i}/\theta$, $K_d = \rho\ K_d/\theta$ and $\gamma = \rho\mu/\theta$. Valocchi (1988) defined local moments for each layer as

$$m_{i,p,q} = \int_{-\infty}^{\infty} \int_{-\infty}^{\infty} \bar{c}_i(x, y, t)\ x^p y^q\ dx\ dy\ ,\ i = 1, 2 \tag{8.4.8}$$

$$n_{i,p,q} = \int_{-\infty}^{\infty} \int_{-\infty}^{\infty} \bar{S}_i(x, y, t)\ x^p y^q\ dx\ dy, i = 1, 2 \tag{8.4.9}$$

The global moments are defined as

$$m_{p,q}(t) = \int_{-\infty}^{\infty} \int_{-\infty}^{\infty} \bar{c}(x, y, t)\ x^p y^q\ dx\ dy = \frac{1}{H} \left(h_1 m_{1,p,q} + h_2 m_{2,p,q} \right) \tag{8.4.10}$$

Multiplying each term in (8.4.6) and (8.4.7) with $x^p y^q$and integrating over the region $-\infty \le x, y \le \infty$, one obtains the following four MGDEs

$$\frac{d}{dt} \left[m_{1,p,q} + n_{1,p,q} \right] = D_{x1} p(p-1) m_{1,p-2,q} + D_{y1} q(q-1) m_{1,p,q-2} + \frac{E_z}{h_1} \left(m_{2,p,q} - m_{1,p,q} \right) + V_1 p m_{1,p-1,q} - \gamma\ m_{1,p,q} \tag{8.4.11}$$

$$\frac{d}{dt}\left(n_{1,p,q}\right) = k_r\left[K_d m_{1,p,q} - n_{1,p,q}\right] - \gamma\, n_{1,p,q} \tag{8.4.12}$$

$$\frac{d}{dt}\left[m_{2,p,q} + n_{2,p,q}\right] = D_{x2}\; p(p-1) m_{2,p-2,q} D_{y2}\; q(q-1) m_{2,p,q-2} + \frac{E_z}{h_2}\left(m_{1,p,q} - m_{2,p,q}\right) + V_2 p m_{2,p-1,q} - \gamma\; m_{2,p,q} \tag{8.4.13}$$

$$\frac{d}{dt}\left(n_{2,p,q}\right) = k_r\left[K_d m_{2,p,q} - n_{2,p,q}\right] - \gamma\, n_{2,p,q} \tag{8.4.14}$$

where the flux term across the interface has been approximated as

$$D_{z1}\left.\frac{\partial c_1}{\partial z}\right|_{z_{1t}} = D_{z2}\left.\frac{\partial c_2}{\partial z}\right|_{z_{2b}} = \frac{E_z}{h_i}\left(\bar{c}_2 - \bar{c}_1\right) \tag{8.4.15}$$

The initial conditons for (8.4.11) to (8.4.14) are

$$m_{1,p,q} = \begin{cases} A,\ p = q = 0 \\ 0, \text{otherwise} \end{cases};\ \mathrm{n}_{1,p,q} = 0 \tag{8.4.16}$$

Defining Laplace transforms of the moments as

$$\hat{m}_{i,p,q} = \int_0^\infty e^{-st} m_{i,p,q}\ (t)\ dt,\ \ i = 1, 2 \tag{8.4.17a}$$

$$\hat{n}_{i,p,q} = \int_0^\infty e^{-st} n_{i,p,q}\ (t)\ dt,\ \ i = 1, 2 \tag{8.4.17b}$$

$$\hat{M}_{p,q} = \int_0^\infty e^{-st} M_{p,q}\ (t)\ dt = \frac{1}{H}\left[h_1 \hat{m}_{1,p,q} + h_2 \hat{m}_{2,p,q}\right] \tag{8.4.18b}$$

Taking Laplace transforms of (8.4.11) to (8.4.14) and simplifying results in the following two equations

$$G(s)\ \hat{m}_{1,p,q} - m_{1,p,q}(t=0) = D_{x1}\ p(p-1)\ \hat{m}_{1,p-2,q} + D_{y1}\ q(q-1)\ \hat{m}_{1,p,q-2} + \frac{E_z}{h_1}\left(\hat{m}_{2,p,q} - \hat{m}_{1,p,q}\right) + V_1 p\ \hat{m}_{1,p-1,q} \tag{8.4.19a}$$

$$G(s)\ \hat{m}_{2,p,q} - m_{2,p,q}(t=0) = D_{x2}\ p(p-1)\ \hat{m}_{2,p-2,q} + D_{y2}\ q(q-1)\ \hat{m}_{2,p,q-2} + \frac{E_z}{h_2}\left(\hat{m}_{1,p,q} - \hat{m}_{2,p,q}\right) + V_2 p\ \hat{m}_{2,p-1,q} \tag{8.4.19b}$$

where

$$G(s) = s\left[1 + \frac{k_r K_d}{s + k_r + \gamma}\right] + \gamma \tag{8.4.20}$$

The local and global moments are found by successive application of (8.14.19). For instance, when $p = q = 0$, one obtains under (8.4.16).

$$\hat{m}_{1,0,0} = \hat{m}_{2,0,0} = \hat{M}_{0,0} = \frac{A}{G(s)} \tag{8.4.21}$$

from which the zero-th global moment is

$$M_{0,0} = \frac{A}{R}\left[1 + K_d \exp\left(-k_r\ Rt\right)\right] \tag{8.4.22}$$

where $R = 1 + K_d$ is the retardation factor, and $\gamma = 0$. Substituting $p = 1, q = 0$ in (8.4.19) and simplfying Valocchi (1988) found

$$\hat{m}_{1,1,0} = \frac{A}{G(s) \cdot I(s)}\left[V_1 + E_z\ \bar{V}\ J/G(s)\right] \tag{8.4.23}$$

$$\hat{m}_{2,1,0} = \frac{A}{G^2(s)}\frac{\bar{V}H}{h_2} - \frac{h_1}{h_2}\hat{m}_{1,1,0} \tag{8.4.24}$$

$$\hat{M}_{1,0} = \frac{A\bar{V}}{G^2(s)} \tag{8.4.25}$$

where $\bar{V} = (h_1 V_1 + h_2 V_2)/H$ is the depth averaged velocity, $J = H/(h_1 h_2)$ and $I(s) = G(s) + E_z J$. The first global moment was given by

$$M_{1,0} = \frac{A\bar{V}}{R^2}\left\{t\left[1 + K_d^2 \exp(-k_r Rt)\right] + \frac{2K_d}{k_r R}\left[1 - \exp(-k_r Rt)\right]\right\} \tag{8.4.26}$$

Readers are referred to Valocchi (1988) for the solution to $M_{2,0,0}$ when $\gamma = 0$. The large-time results obtained by neglecting the exponential terms are reproduced here.

$$M_{0,0} = A/R \tag{8.4.27}$$

$$M_{1,0} = \frac{A\bar{V}}{R^2}\left(t + \frac{2K_d}{k_r R}\right) \tag{8.4.28}$$

$$M_{2,0} = \frac{B_1}{R} + \frac{B_2}{R^2}\left[t + \frac{2K_d}{k_r R}\right] + \frac{B_3}{R^3}\left[\frac{t^2}{2} + \frac{3K_d t}{k_r R} + \frac{3K_d(K_d - 1)}{k_r^2 R^2}\right] \tag{8.4.29}$$

where

$$B_1 = -\frac{2A\,(V_1 - V_2)^2}{H\;E_z^2\;J^2} \tag{8.4.30a}$$

$$B_2 = 2A\left[\bar{D}_x + \frac{(V_1 - V_2)^2}{H\;E_z\;J^2}\right] \tag{8.4.30b}$$

$$B_3 = 2\,A\;\bar{V}^2 \tag{8.4.30c}$$

Valocchi (1988) plotted the effective velocity (6.2.7) and effective dispersion (6.2.9) and concluded that sorption kinetics causes the total dissolved mass and effective velocity to decrease with time at a rate proportional to k_r. The plume mass in the dissolved liquid phase and the effective velocity eventually approach values corresonding to local equilibrium conditions. The overall spreading of the plume was attributed to three factors: interlayer longitudinal dispersion, intra-layer kinetics, and vertical averaging.

8.5. PERFECTLY STRATIFIED AQUIFER WITH VELOCITY VARIATION

The analysis of two-layer aquifer discussed in the previous section was extended to a perfectly stratified aquifer by Valocchi (1989). Global moments were defined as vertical averages of local moments, and effective properties were examined for large times. Here we consider a perfectly stratified aquifer with only vertical variations in the pore water velocity. We assume that there is no interaction between the layers (i.e. as if each layer acts as a streamtube), and that the Darcian flux occurs in the horizontal direction alone. The governing differential equations at the local scale for each layer are

$$\frac{\partial c}{\partial t} + \frac{\partial S}{\partial t} = D_x\frac{\partial^2 c}{\partial x^2} + D_y\frac{\partial^2 c}{\partial y^2} - V_x\frac{\partial c}{\partial x} - V_y\frac{\partial c}{\partial y} - \gamma_1 c \tag{8.5.1}$$

$$\frac{\partial s}{\partial t} = k_r[K_d c - S] - \gamma_2 S \tag{8.5.2}$$

where the definitions are the same as in Valocchi (1988, 1989), and γ_1 and γ_2 are first-order degradation rate constants in the liquid and solid phases, respectively. The initial and boundary conditions are those described in (8.4.3). Local spatial moments are defined as

$$m_{p,q} = \int_{-\infty}^{\infty}\int_{-\infty}^{\infty} c(x, y, z, t)\; x^p y^q\; dx\; dy \tag{8.5.3a}$$

$$n_{p,q} = \int_{-\infty}^{\infty}\int_{-\infty}^{\infty} S(x, y, z, t)\; x^p y^q\; dx\; dy \tag{8.5.3b}$$

The local moment generating differential equations are obtained by multiplying (8.5.1) and (8.5.2) with $x^p y^q$and integrating over $-\infty \le x, y \le \infty$ to yield

$$\frac{dm_{p,q}}{dt} + \frac{dn_{p,q}}{dt} = p(p-1)\ D_x m_{p-2,q} + q(q-1)\ D_y m_{p,q-2} + pV_x\ m_{p-1,q} + qV_y\ m_{p,q-1} - \gamma_1\ m_{p,q} \tag{8.5.4}$$

$$\frac{dn_{p,q}}{dt} = k_r\left[K_d m_{p,q} - n_{p,q}\right] - \gamma_2 n_{p,q} \tag{8.5.5}$$

with $m_{0,0}(0) = A$, and all other local moments are initially zero. Further, taking Laplace transforms of these equations yields

$$G(s)\hat{m}_{p,q} - \hat{m}_{p,q}(t=0) = p(p-1)\ D_x\ \hat{m}_{p-2,q} + q(q-1)\ D_y\ \hat{m}_{p,q-2} + pV_x\ \hat{m}_{p-1,q} + qV_y\ \hat{m}_{p,q-1} \tag{8.5.6}$$

where $\hat{m}_{p,q}$ and $\hat{n}_{p,q}$ are Laplace transforms of $m_{p,q}$ and $n_{p,q}$, respectively, and

$$G(s) = s\left[1 + \frac{k_r K_d}{s + k_r + \gamma_2}\right] + \gamma_1 \tag{8.5.7}$$

From (8.5.6), the lower order local moments are expressed as

$$m_{0,0} = A\ \mathcal{L}^{-1}\left[G^{-1}(s)\right] \tag{8.5.8a}$$

$$m_{1,0} = A\ V_x \mathcal{L}^{-1}\left[G^{-2}(s)\right] \tag{8.5.8b}$$

$$m_{0,1} = A\ V_y \mathcal{L}^{-1}\left[G^{-2}(s)\right] \tag{8.5.8c}$$

$$m_{2,0} = 2AD_x \mathcal{L}^{-1}\left[G^{-2}(s)\right] + 2AV_x^2\ \mathcal{L}^{-1}\left[G^{-3}(s)\right] \tag{8.5.8d}$$

$$m_{0,2} = 2AD_y\ \mathcal{L}^{-1}\left[G^{-2}(s)\right] + 2AV_y^2\ \mathcal{L}^{-1}\left[G^{-3}(s)\right] \tag{8.5.8e}$$

Say the velocities in each layer in the x-direction are assumed to uncorrelated and log-normally distributed with $E[\ln V_x] = \mu_v$ and $Var[\ln V] = \sigma_v^2$. Further we describe the local dispersion as

$$D_x = D_{ox} + \lambda_x V_x^k \tag{8.5.9}$$

where D_{ox} is the molecular diffusion component, and the second term expresses the contribution of mechanical disposion. Global spatial moments can be described as

$$M_{p,q}(t) = H \int_0^\infty m_{p,q}(t) f_{V_x}(V)\ dV \tag{8.5.10}$$

where $f_{V_x}(V)$ is the probability density function of V_x and H is the aquifer thickness. The lower order global moments are

$$M_{0,0} = AH\ \mathcal{L}^{-1}\left[G^{-1}(s)\right] \tag{8.5.11a}$$

$$M_{1,0} = AH\left(\mu_\nu + \sigma_\nu^2/2\right)\ \mathcal{L}^{-1}\left[G^{-2}(s)\right] \tag{8.5.11b}$$

$$M_{2,0} = 2AH\left[D_{ox} + \lambda_x\left(k\mu_\nu + k^2\sigma_\nu^2/2\right)\right]\mathcal{L}^{-1}\left[G^{-2}(s)\right] + 2AH\left(2\mu_\nu + 2\sigma_\nu^2\right)\mathcal{L}^{-1}\left[G^{-3}(s)\right] \tag{8.5.11c}$$

Similarly, $M_{0,1}$ and $M_{0,2}$ can be defined in terms of the distribution of V_y. The effective velocities and effective dispersion coefficients are defined as in Valocchi (1989) as

$$V_{eff,x} = \frac{d}{dt}\left[\frac{M_{1,0}}{M_{0,0}}\right]; \quad D_{eff,x} = \frac{d}{dt}\left[\frac{M_{2,0}}{M_{0,0}} - \left(\frac{M_{1,0}}{M_{0,0}}\right)^2\right] \tag{8.5.12}$$

Laplace transform inverses for $G^{-k}(s), k = 1, 2, 3, \ldots$ can be found from standard software packages. The expressions are too long to offer any meaningful insights, and the results have to be plotted for various cases to determine the behavior of effective properties and to study their sensitivity to various model parameters.

CHAPTER 9

MOMEMT ANALYSIS FOR COMPOUNDS UNDERGOING SEQUENTIAL DECAY CHAIN REACTIONS

9.1. INTRODUCTION

Many contaminants are known to undergo transformations into various product compounds as they migrate through soils. Examples of this type of transport in porous media are migration of radionuclides (Rogers, 1978; Gureghian and Jansen, 1983), interacting nitrogen species (Cho, 1971; Wagenet et al., 1976), organic phosphates (Castro and Rolston, 1977), and pesticides (Bromilow and Leistra, 1980). In the past, attempts have been made to derive analytical solutions for three chain members (Cho, 1971; Wagenet et al., 1976) and four chain members (van Genuchten, 1985) under different boundary conditions. Earlier studies were based on simple boundary conditions (Cho, 1971; Wagenet et al., 1976) or transport conditions where dispersion phenomenon could be neglected (Higashi and Pigford, 1980; Harada et al., 1980). This chapter presents expressions for temporal and spatial moments from the coupled one-dimensional convective dispersive transport equation for chain members under transient flow conditions. This chapter has been largely derived from the work of Parashar and Govindaraju (2006b).

9.2. GOVERNING DIFFERENTIAL EQUATIONS

We consider a semi-infinite domain in this section, with the spatial coordinate $x > 0$. The following set of differential equations constitutes a mathematical model for analysis of transport of solutes involved in sequential first-order decay reactions (van Genuchten, 1985).

$$\frac{\partial}{\partial t}(\theta C_1 + \rho S_1) = \frac{\partial}{\partial x}\left[\theta D \frac{\partial C_1}{\partial x} - qC_1\right] - k_{w,1}\theta C_1 - k_{s,1}\rho S_1 \tag{9.2.1}$$

$$\frac{\partial}{\partial t}(\theta C_i + \rho S_i) = \frac{\partial}{\partial x}\left[\theta D \frac{\partial C_i}{\partial x} - qC_i\right] + k_{w,i-1}\theta C_{i-1} + k_{s,i-1}\rho S_{i-1} - k_{w,i}\theta C_i - k_{w,j}\rho S_i, \qquad i = 1, 2, 3, \ldots \tag{9.2.2}$$

where C (ML^{-3}) is the solute concentration, S (MM^{-1}) is the adsorbed concentration, θ (L^3L^{-3}) is the water content, q (LT^{-1}) the volumetric flux, ρ (ML^{-3}) the soil bulk density, x (L) distance and t (T) time. The subscript i represents the i-th chain member. The liquid and solid phase decay constants are represented by $k_{w,i}$ and $k_{s,i}$ respectively. Although these rate constants can have different values for both chemical and microbiological degradation, for simplification purposes it has been assumed that they are identical.

$$k_{w,i} = k_{s,i} = k_i \tag{9.2.3}$$

It has been further assumed that soil system is homogeneous and that θ and q are constant in space and time. In addition, it has been assumed that adsorption may be expressed as a linear and reversible isotherm.

$$S_i = K_i C_i, i = 1, 2, 3, \ldots \tag{9.2.4}$$

where K_i ($M^{-1}L^3$) is the distribution coefficient. Equations (9.2.2) and (9.2.4) can be combined to yield

$$R_1 \frac{\partial C_1}{\partial t} = D \frac{\partial C_1^2}{\partial x^2} - V \frac{\partial C_1}{\partial x} - k_1 R_1 C_1 \tag{9.2.5}$$

$$R_i \frac{\partial C_i}{\partial t} = D \frac{\partial^2 C_i}{\partial x^2} - V \frac{\partial C_i}{\partial x} + k_{i-1} R_{i-1} C_{i-1} - k_i R_i C_i \quad i = 2, 3, \ldots \tag{9.2.6}$$

where $V\,(= q/\theta)$ is the average pore water velocity and $R_i = 1 + \frac{\rho K_i}{\theta}$ is the retardation factor. As stated in chapter 2, the flux concentration for the i-th member

$$C_{i,f} = C_i - \frac{D}{V} \frac{\partial C_i}{\partial x} \tag{9.2.7}$$

and the resident concentration obey the same set of equations. The following nondimensional variables are defined

$$C_i^* = \frac{C_{i,f}}{C_0}; P = \frac{VL}{D}; X = \frac{x}{L}; T = \frac{tV}{L}; \gamma_i = \frac{k_i L}{V} \tag{9.2.8}$$

The soil column is initially free of solute, and C_0 is the reference concentration of the inlet solution that is defined shortly. Using (9.2.8), the governing non-dimensional equations are

$$R_1 \frac{\partial C_1^*}{\partial T} = \frac{1}{P} \frac{\partial^2 C_1^*}{\partial X^2} - \frac{\partial C_1^*}{\partial X} - \gamma_1 R_1 C_1^* \tag{9.2.9}$$

$$R_i \frac{\partial C_i^*}{\partial T} = \frac{1}{P} \frac{\partial^2 C_i^*}{\partial X^2} - \frac{\partial C_i^*}{\partial X} - \gamma_i R_i C_i^* + \gamma_{i-1} R_{i-1} C_{i-1}^* \tag{9.2.10}$$

9.3. LAPLACE TRANSFORMS

The soil column is assumed to be initially free of solute, i.e. $C_i(x, 0) = 0, x \geq 0$. The Laplace transforms of the non-dimensional concentrations are defined as

$$\hat{C}_i(X; s) = \int_0^\infty e^{-sT} C_i^* (X, T)\, dT \tag{9.3.1}$$

Applying this transformation to (9.2.9) yields a second-order ordinary differential equation with constant coefficients which has the general solution

$$\hat{C}_1(X; s) = A_1 e^{m_1 X} + B_1 e^{m_2 X} \tag{9.3.2}$$

The coefficients A_1 and B_1 will depend on boundary conditions, and the exponents m_1 and m_2 are:

$$m_1 = \frac{P}{2}[1 + \alpha_1] \tag{9.3.3a}$$

$$m_2 = \frac{P}{2}[1 - \alpha_1] \tag{9.3.3b}$$

where

$$\alpha_1 = \sqrt{1 + \frac{4R_1(\gamma_1 + s)}{P}} \tag{9.3.3c}$$

Now, $\alpha_1 > 1 \Rightarrow m_1 > 0, m_2 < 0$. Therefore $A_1 = 0$ since $\hat{C}_1$ is bounded. Hence (9.3.2) reduces to

$$\hat{C}_1(X; s) = B_1 \exp\left[\frac{PX}{2}(1 - \alpha_1)\right] \tag{9.3.4}$$

We prescribe the following boundary condition

$$C_{i,f}(0, t) = \begin{cases} \frac{M}{V\theta A}\delta(t) & \text{for } i = 1 \\ 0 & \text{for } i > 1 \end{cases} \Rightarrow C_i^*(0, T) = \begin{cases} \delta(T) & \text{for } i = 1 \\ 0 & \text{for } i > 1 \end{cases} \tag{9.3.5}$$

where M is the total solute mass of the first member that is injected into the soil column whose cross-section area is A perpendicular to the flow direction, and the reference concentration C_0 in (9.2.8) is $M/\theta AL$ This implies that $\hat{C}_1(0; s) = 1$. Combining (9.3.5) and (9.3.2) results in the following expression for the transformed concentration of first member of the decay chain.

$$\hat{C}_1(X; s) = \exp\left[\frac{PX}{2}(1 - \alpha_1)\right] \tag{9.3.6}$$

Taking Laplace transform of (9.2.10) for $i = 2$, the general solution of the transform of the concentration is expressed as

$$\hat{C}_2(X; s) = B_2 \exp\left[\frac{PX}{2}(1-\alpha_2)\right] + D_2 \exp\left[\frac{PX}{2}(1-\alpha_1)\right] \tag{9.3.7}$$

where

$$\alpha_2 = \sqrt{1 + \frac{4R_2(\gamma_2 + s)}{P}} \tag{9.3.8}$$

and

$$D_2 = \frac{-\gamma_1 R_1}{\frac{1}{2}\left[\frac{P}{2}(1-\alpha_1)^2\right] - \left[\frac{P}{2}(1-\alpha_1)\right] - (\gamma_2 + S) R_2} \tag{9.3.9}$$

The Coefficient B_2 is to be determined using the boundary conditions. From (9.3.5), we obtain

$$\hat{C}_2(0, s) = 0 \tag{9.3.10}$$

and $B_2 = -D_2$. Therefore

$$\hat{C}_2(X; s) = D_2 \left\{\exp\left[\frac{PX}{2}(1-\alpha_1)\right] - \exp\left[\frac{PX}{2}(1-\alpha_2)\right]\right\} \tag{9.3.11}$$

In a similar fashion, equations for Laplace transforms of other members in the chain can be obtained from (9.2.10) as

$$\frac{1}{P}\frac{d^2\hat{C}_i}{dX^2} - \frac{d\hat{C}_i}{dx} + (\gamma_i + s) R_i \hat{C}_i = -\gamma_{i-1} R_{i-1} \hat{C}_{i-1} \tag{9.3.12}$$

9.4. TEMPORAL MOMENT ANALYSIS

As in Chapter 2, the n-th absolute temporal moment for i-th member can be written as,

$$\mu_n^{(i)} = (-1)^n \lim_{s \to 0} \left\{\frac{d^n}{ds^n}\left[\hat{C}_i(X; s)\right]\right\}, i = 1, 2, \ldots. \tag{9.4.1}$$

When computing temporal moments, it is meaningful to utilize flux concentrations (Kreft and Zuber, 1978; see also discussion in Chapter 2). For high Peclet members, flux and resident concentrations yield similar results.

Combining (9.4.1) with (9.3.6) results in the following expressions of temporal moments for the first member of the chain

$$\mu_0^{(1)} = E_1 \tag{9.4.2}$$

$$\mu_1^{(1)} = \frac{R_1 E_1}{F_1} \tag{9.4.3}$$

$$\mu_2^{(1)} = \frac{R_1^2}{PF_1^3}\left(2 + PF_1\right) E_1 \tag{9.4.4}$$

where

$$E_1 = \exp\left[\frac{P}{2}\left\{1 - \sqrt{1 + \frac{4R_1\gamma_1}{P}}\right\}\right] \tag{9.4.5}$$

and

$$F_1 = \sqrt{1 + \frac{4R_1\gamma_1}{P}} \tag{9.4.6}$$

and the expressions are derived for $X = 1$. Similarly, using (9.4.1) and (9.3.11) yields

$$\mu_0^{(2)} = \frac{-\gamma_1 R_1}{\frac{P}{4}\left(1 - F_1\right)^2 - \frac{P}{2}(1 - F_1) - R_2\gamma_2}\left(E_1 - E_2\right) \tag{9.4.7}$$

$$\mu_1^{(2)} = \frac{\gamma_1 R_1}{\frac{P}{4}\left(1 - F_1\right)^2 - \frac{P}{2}\left(1 - F_1\right) - R_2\gamma_2}\left[\frac{R_2 F_1 E_1 - R_1 F_2 E_2}{F_1 F_2}\right] - \frac{\gamma_1 R_1 M_1 \left(R_1 - R_2\right)}{\left(\gamma_1 R_1 - \gamma_2 R_2\right)^2}\left[E_1 - E_2\right] \tag{9.4.8}$$

where, now

$$E_2 = \exp\left[\frac{P}{2}\left\{1 - \sqrt{1 + \frac{4R_2\gamma_2}{P}}\right\}\right] \tag{9.4.9}$$

and

$$F_2 = \sqrt{1 + \frac{4R_2\gamma_2}{P}} \tag{9.4.10}$$

The expression for $\mu_2^{(2)}$ is rather long and is not presented here. However, behavior of the moments are studied for several cases as a function of P in Figures 9.4.1 to 9.4.6. Inspection of (9.4.5), (9.4.6), (9.4.9), and (9.4.10) reveals that as $P \to \infty$, $E_1, E_2 \in (1, 0)$ and $F_1, F_2 \to 1$.

Plots of the zero-th moment, normalized first moment, and second central moment as a function of the Peclet number (P) are presented in Figures 9.4.1 to 9.4.6 for $M = 1$ and for different nondimensional degradation rates γ_1.

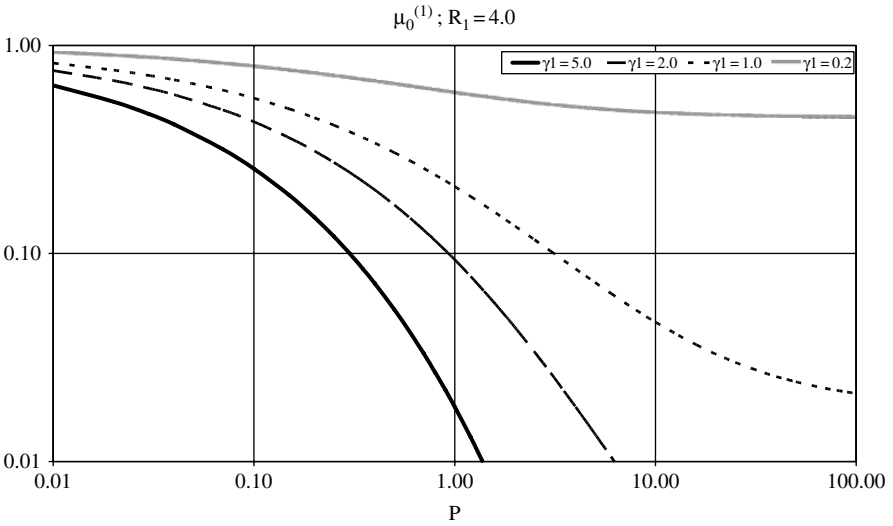

Figure 9.4.1. Zeroth temporal moment $\mu_0^{(1)}$ for first member of the chain (adapted from Parashar and Govindaraju, 2006b, with permission from Springer)

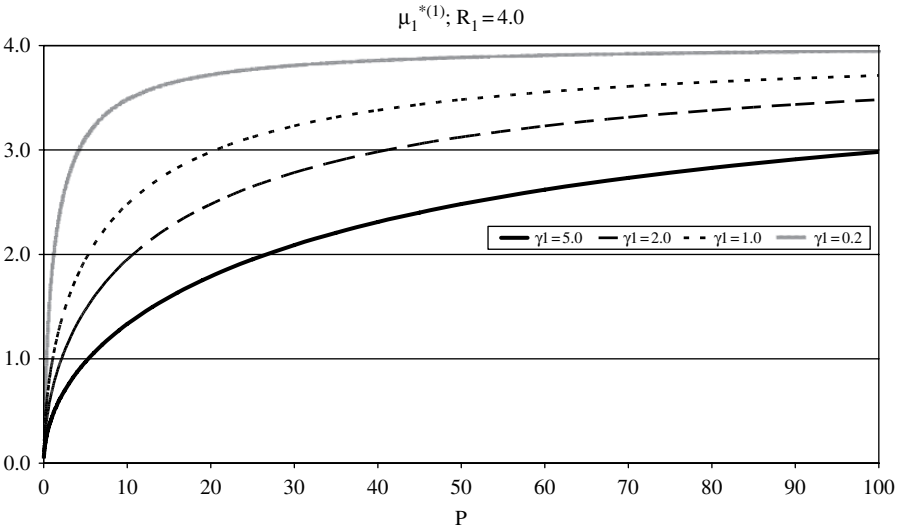

Figure 9.4.2. First temporal normalized moment $\mu_1^{*(1)}$ for first member of the chain (adapted from Parashar and Govindaraju, 2006b, with permission from Springer)

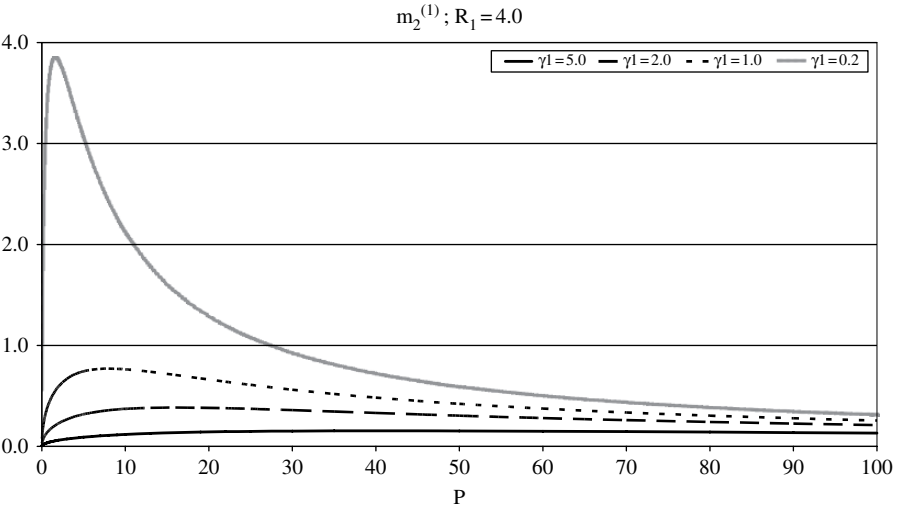

Figure 9.4.3. Temporal second central moment $m_2^{(1)}$ for first member of the chain (adapted from Parashar and Govindaraju, 2006b, with permission from Springer)

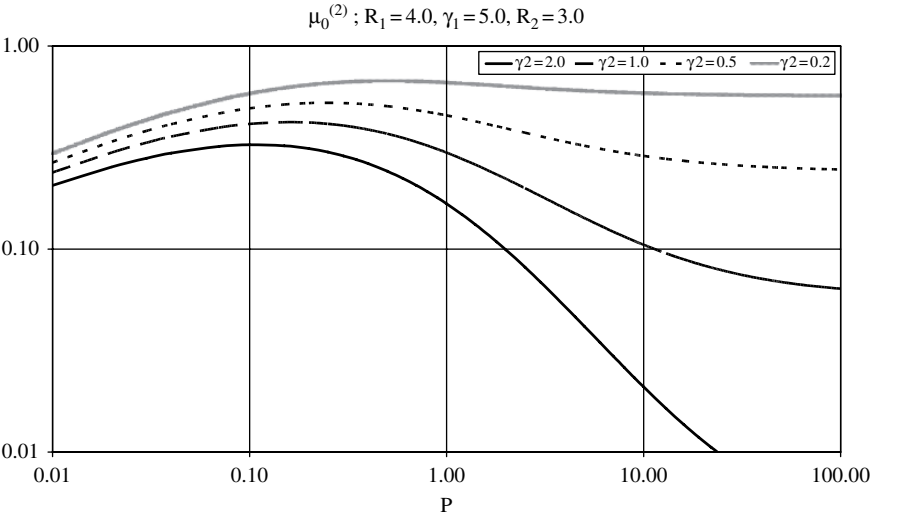

Figure 9.4.4. Zeroth temporal moment $\mu_0^{(2)}$ for second member of the chain (reproduced from Parashar and Govindaraju, 2006b, with permission from Springer)

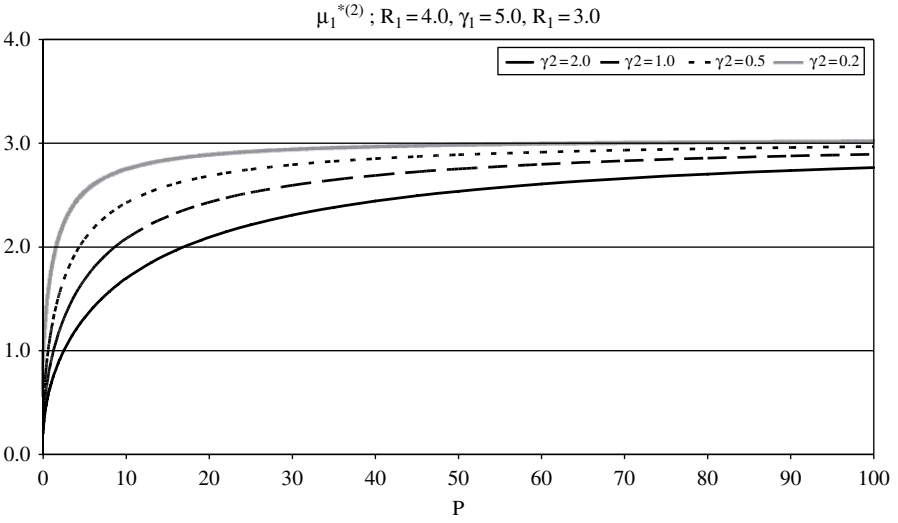

Figure 9.4.5. First temporal normalized moment $\mu_1^{*(2)}$ for second member of the chain (adapted from Parashar and Govindaraju, 2006b, with permission from Springer)

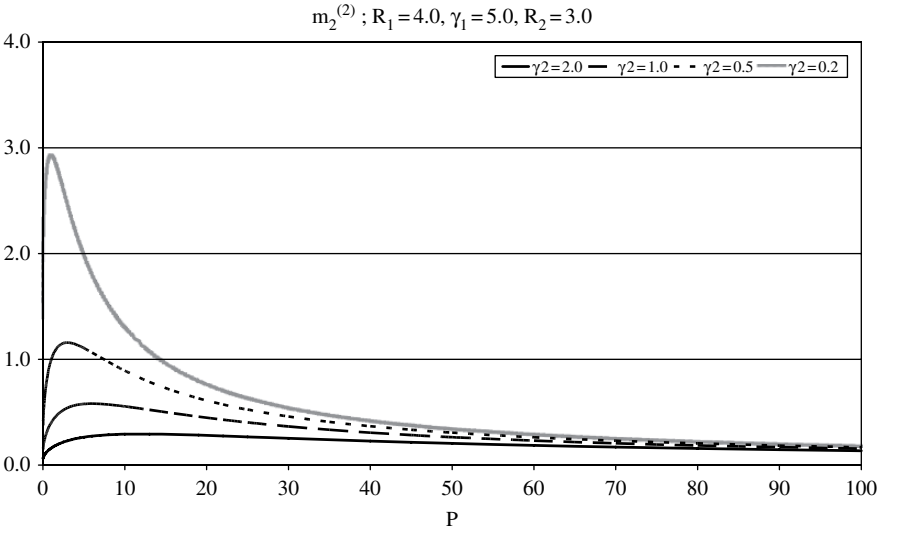

Figure 9.4.6. Temporal second central moment $m_2^{(2)}$ for second member of the chain (adapted from Parashar and Govindaraju, 2006b, with permission from Springer)

Figure 9.4.1 shows the variation of $\mu_0^{(1)}$ for different γ_1 values. As can be seen, increasing P leads to a decreasing zeroth moment. It can be shown that as P increases, the zero-th moment at $X = 1$ is given as

$$\mu_0^{(1)} = e^{-\gamma_1 R_1} \text{ for } P \to \infty \tag{9.4.11}$$

Similarly the normalized first moment $\mu_1^{(1)}$ shown in Figure 9.4.2 provides an estimate of the average travel time. With increasing Peclet number, the limiting value is

$$\frac{\mu_1^{(1)}}{\mu_0^{(1)}} = R_1 \text{ for } P \to \infty \tag{9.4.12}$$

Figure 9.4.3 shows the behavior of the second central moment $m_2^{(1)}$ for the first member of the chain. For different degradation rates γ_1, there is a particular maxima of the second central moment that is obtained. The magnitude of this maxima is greater for lower degradation rates (implying degradation inhibits spreading) and occurs for lower values of P. As P tends to infinite, the second central moment tends to zero as there is effectively no spreading of the breakthrough curve which tends to a delta function at this limit.

Figure 9.4.4 shows the variation of $\mu_0^{(2)}$ as a function of P. There is a certain value of P for which $\mu_0^{(2)}$ attains a maxima (see 9.4.4) which appears for smaller P values as γ_2 increases. For large P values, the limiting behavior of this zeroth moment is shown to be

$$\mu_0^{(2)} = \frac{\gamma_1 R_1}{\gamma_2 R_2 - \gamma_1 R_1} \left(e^{-\gamma_1 R_1} - e^{-\gamma_2 R_2} \right) \text{ for } P \to \infty \tag{9.4.13}$$

Similarly, as $P \to \infty$, the normalized first moment for the second member of the chain tends to

$$\frac{\mu_1^{(2)}}{\mu_0^{(2)}} = \frac{R_2 - R_1}{\gamma_2 R_2 - \gamma_1 R_1} - \frac{R_1 \exp(-\gamma_1 R_1) + R_2 \exp(-\gamma_2 R_2)}{\exp(-\gamma_1 R_1) - \exp(-\gamma_2 R_2)} \tag{9.4.14}$$

The behavior of the second central moment $m_2^{(2)}$ in Figure 9.4.6 is similar to $m_2^{(1)}$ with a slow decline to zero as $P \to \infty$. The location of the maxima shifts to smaller P values with lower degradation rates γ_2. In the next section, we focus on cases of very high Peclet numbers.

9.5. TEMPORAL MOMENTS FOR ADVECTIVE TRANSPORT

There are instances when only advective transport of members in a chain reaction is of interest (Harada et al. 1980; Higashi and Pigford, 1980). Further, when local dispersion is neglected, flux and resident concentrations are the same, making

temporal moment analysis mathematically simpler. From (9.2.9), (9.2.10), and (9.3.1), the governing equations for the Laplace transforms of concentrations as $P \to \infty$ are

$$sR_1\ \hat{C}_1 = -\frac{d\hat{C}_1}{dx} - \gamma_1\ R_1\ \hat{C}_1 \tag{9.5.1}$$

$$sR_i\ \hat{C}_i = -\frac{d\hat{C}_i}{dx} - \gamma_i\ R_i\ \hat{C}_i + \gamma_{i-1}\ R_{i-1}\ \hat{C}_{i-1}, \qquad i = 2, 3, \ldots \tag{9.5.2}$$

The soil column is initially free of solute, and the boundary condition of (9.3.5) is applied. The solutions to (9.5.1) and (9.5.2) are easily obtained as

$$\hat{C}_1\ (X; s) = e^{-a_1 X} \tag{9.5.3}$$

$$\hat{C}_i\ (X; s) = \gamma_{i-1}\ R_{i-1} e^{-a_i X} \int_0^X e^{-a_i y}\ \hat{C}_{i-1}(y)\ dy \tag{9.5.4}$$

where

$$a_i = (\gamma_i + s)\ R_i \tag{9.5.5}$$

Equation (9.5.4) can be solved successively to yield expressions for $\hat{C}_i(X; s)$. For a four-member chain, one obtains

$$\hat{C}_1(X; s) = e^{-a_1 X} \tag{9.5.6a}$$

$$\hat{C}_2(X; s) = \frac{\gamma_1 R_1}{(a_2 - a_1)} \left[e^{-a_1 X} - e^{-a_2 X} \right] \tag{9.5.6b}$$

$$\hat{C}_3(X; s) = \frac{\gamma_1 R_1 \gamma_2 R_2}{(a_2 - a_1)} \left[\frac{e^{-a_1 X} - e^{-a_3 X}}{a_3 - a_1} - \frac{e^{-a_2 X} - e^{-a_3 X}}{a_3 - a_2} \right] \tag{9.5.6c}$$

$$\begin{aligned} \hat{C}_4(X; s) = \frac{\gamma_1 R_1 \gamma_2 R_2 \gamma_3 R_3}{(a_2 - a_1)} \Bigg\{ & \frac{e^{-a_1 X} - e^{-a_4 X}}{(a_3 - a_1)(a_4 - a_1)} - \frac{e^{-a_3 X} - e^{-a_4 X}}{(a_3 - a_1)(a_4 - a_3)} \\ & - \frac{e^{-a_2 X} - e^{-a_4 X}}{(a_3 - a_2)(a_4 - a_2)} + \frac{e^{-a_3 X} - e^{-a_4 X}}{(a_3 - a_2)(a_4 - a_3)} \Bigg\} \end{aligned} \tag{9.5.6d}$$

Applying Aris' method as in (9.4.1), expressions for absolute moments may be generated. A few examples are given below. For notational convenience, we use $b_i = \gamma_i R_i$ and $e_i = \exp(-b_i\ X)$.

$$\mu_n^{(1)} = (R_1 X)^n e_1 \tag{9.5.7}$$

$$\mu_0^{(2)} = \frac{b_1}{b_2 - b_1}(e_1 - e_2) \tag{9.5.8a}$$

$$\mu_1^{(2)} = b_1\left[\frac{(R_2 - R_1)\,(e_1 - e_2)}{(b_2 - b_1)^2} + X\frac{R_1 e_1 - R_2 e_2}{b_2 - b_1}\right] \tag{9.5.8b}$$

$$\mu_2^{(2)} = \frac{2b_1(R_2 - R_1)^2}{(b_2 - b_1)^3}[e_1 - e_2] + \frac{2b_1(R_2 - R_1)X}{(b_2 - b_1)^2}(R_1 e_1 - R_2 e_2) + \frac{b_1 X^2}{(b_2 - b_1)}(R_1^2 e_1 - R_2^2 e_2) \tag{9.5.8c}$$

$$\mu_0^{(3)} = \frac{b_1 b_2}{(b_2 - b_1)}\left(\frac{e_1 - e_3}{b_3 - b_1} - \frac{e_2 - e_3}{b_3 - b_2}\right) \tag{9.5.9a}$$

$$\mu_1^{(3)} = b_1 b_2\left\{X\frac{R_1\ e_1 - R_3\ e_3}{A} + \frac{B(e_1 - e_3)}{A^2} + X\frac{R_3\ e_3 - R_2\ e_2}{D} + \frac{E(e_3 - e_2)}{D^2}\right\} \tag{9.5.9b}$$

where

$$A = (b_2\ - b_1)\ (b_3\ - b_1) \tag{9.5.9c}$$

$$B = b_2\ \mathrm{R}_3 + R_2\ b_3 - b_1\ \mathrm{R}_3 - R_1\ b_3 - b_1\ \mathrm{R}_2 - R_1\ b_2 + 2\ R_1 b_1 \tag{9.5.9d}$$

$$D = (b_2 - b_1)\ (b_3 - \ b_2) \tag{9.5.9e}$$

$$E = b_2\ R_3 + R_2\ b_3 - 2\ R_2\ b_2 - b_1\ R_3 - R_1\ b_3 + b_1 R_2 + R_1 b_2 \tag{9.5.9f}$$

$$\mu_0^{(4)} = b_1 b_2 b_3\left[\frac{e_1 - e_4}{(b_3 - b_1)(b_4 - b_1)} - \frac{e_3 - e_4}{(b_3 - b_1)(b_4 - b_3)} - \frac{e_2 - e_4}{(b_3 - b_2)(b_4 - b_2)} + \frac{e_3 - e_4}{(b_3 - b_2)(b_4 - b_3)}\right] \tag{9.5.10}$$

9.6. SPATIAL MOMENTS FOR COMPOUNDS UNDERGOING SEQUENTIAL FIRST-ORDER DECAY CHAIN

As mentioned previously in chapters 6 and 8, spatial moments of a solute plume have been extensively used to analyze contaminant transport (Valocchi, 1989; Dagan and Cvetkovic, 1993; Hu et al., 1995; Cunningham et al., 1999; Abulaban and Nieber, 2000; Srivastava et al., 2002). The advective-dispersive transport process for several members undergoing degradation in a decay chain is described by equations (9.2.9) and (9.2.10). However, we now consider an infinite domain ($-\infty \leq x, X \leq \infty$), with all concentrations set to zero at $x, X = \pm\infty$. Spatial moments are defined

in terms of resident concentrations that obey (9.2.9) and (9.2.10). The modified method of Aris (Aris, 1958) can be used to study the behavior of spatial moments for the members of decay chain. For the non-dimensional concentrations $C_i^*(X, T)$, the Fourier transform is defined as.

$$\mathcal{F}[C_i^*(X,T)] = \tilde{C}_i(\omega;T) = \int_{-\infty}^{\infty} e^{-j\omega X} C_i^*(X,T)dX \tag{9.6.1}$$

where ω is the Fourier transform variable. The following results involving Fourier transforms of spatial derivatives (see Chapter 3) are also useful.

$$\mathcal{F}\left[\frac{\partial}{\partial X}\{C_i^*(X,T)\}\right] = j\omega\tilde{C}_i(\omega;T) \tag{9.6.2}$$

$$\mathcal{F}\left[\frac{\partial^2}{\partial X^2}\{C_i^*(X,T)\}\right] = -\omega^2\tilde{C}_i(\omega;T) \tag{9.6.3}$$

Taking Fourier transform of equation (9.2.9) and solving the resulting ODE yields the following expression for the transform of concentration of the first member.

$$\tilde{C}_1(\omega;T) = A_1 \exp\left[\frac{-\left(\frac{\omega^2}{P} + i\omega + \gamma_1 R_1\right)}{R_1} T\right] \tag{9.6.4}$$

Here A_1 is an integration constant which will depend on the initial condition. For an aquifer of constant cross-section area A perpendicular to the flow direction, and for an instantaneous injection of mass Mat the origin, we have

$$C_i(x,0) = \begin{cases} \frac{M}{\theta A}\delta(x) & \text{for } i=1 \\ 0 & \text{for } i>1 \end{cases} \Rightarrow C_i^*(X,0) = \begin{cases} \delta(X) & \text{for } i=1 \\ 0 & \text{for } i>1 \end{cases} \tag{9.6.5}$$

Equation (9.6.4) reduces to

$$\tilde{C}_1(\omega;T) = \exp\left[\frac{-G_1}{R_1} T\right] \tag{9.6.6}$$

where

$$G_1 = \frac{\left(\frac{\omega^2}{P} + j\omega + \gamma_1 R_1\right)}{R_1} \tag{9.6.7}$$

Similarly, for the initial condition of (9.6.5)

$$\tilde{C}_2(X,0) = 0 \tag{9.6.8}$$

the following expression is obtained for concentration of the second member of the decay chain

$$\tilde{C}_2(\omega;T)=\exp\left[\frac{-G_2}{R_2}T\right]\left[\frac{\gamma_1 R_1\left[\left\{\exp\left(\frac{G_2}{R_2}-\frac{G_1}{R_1}\right)T\right\}-1\right]}{G_2-\frac{R_2G_1}{R_1}}\right] \tag{9.6.9}$$

where

$$G_2=\frac{\left(\frac{\omega^2}{P}+j\omega+\gamma_2R_2\right)}{R_2} \tag{9.6.10}$$

Formula for n-th absolute spatial moment for ith member can be written as (Aris, 1958)

$$\mu_{s,n}^{(i)}=i^n\lim_{\omega\to0}\left\{\frac{d^n}{d\omega^n}\left[\tilde{C}_i(\omega,T)\right]\right\} \tag{9.6.11}$$

Combining equations (9.6.6) and (9.6.11) results in the following expressions for the central moments of the first member of the chain.

$$m_{s,0}^{(1)}=\mu_{s,0}^{(1)}=\exp(-\gamma_1T) \tag{9.6.12}$$

$$m_{s,1}^{(1)}=\frac{\mu_{s,1}^{(1)}}{\mu_{s,0}^{(1)}}=\frac{T}{R_1} \tag{9.6.13}$$

$$m_{s,2}^{(1)}=\frac{\mu_{s,0}^{(1)}\mu_{s,2}^{(1)}-\left(\mu_{s,1}^{(1)}\right)^2}{\mu_{s,0}^{(2)}}=\frac{2T}{R_1P} \tag{9.6.14}$$

Following the same procedure, expressions for absolute and central spatial moments for second member of the decay chain are obtained from (9.6.9) and (9.6.11) as

$$m_{s,0}^{(2)}=\exp(-\gamma_2T)\left[\frac{\gamma_1R_1}{(\gamma_2-\gamma_1)R_2}\left[\exp\left\{(\gamma_2-\gamma_1)T\right\}-1\right]\right] \tag{9.6.15}$$

$$m_{s,1}^{(2)}=\frac{\mu_{s,1}^{(2)}}{\mu_{s,0}^{(2)}}=\frac{(R_1-R_2)}{(\gamma_2-\gamma_1)R_1R_2}+\frac{T}{R_1R_2}\left[R_2-\frac{(R_1-R_2)}{\exp\left\{(\gamma_2-\gamma_1)T\right\}-1}\right] \tag{9.6.16}$$

Compact expressions for $\mu_{s,2}^{(2)}$ are not available. Plots of $m_0^{(2)}$ and $m_1^{(2)}$ are presented in Figures 9.6.1 and 9.6.2, respectively. The zeroth moment for the second member (Figure 9.6.1) rises with the decay of first member, reaches a maximum and subsides because of continuing degradation. Equation (9.6.15) reveals that the position of

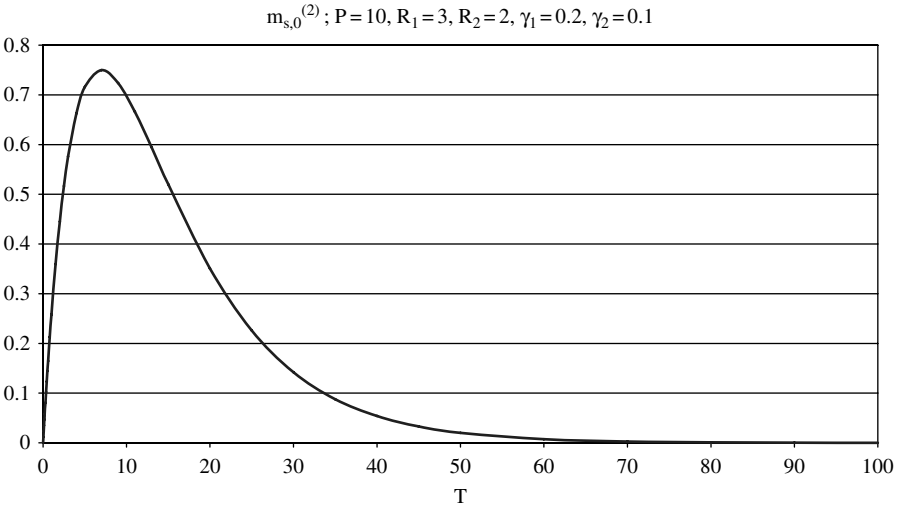

Figure 9.6.1. Zeroth spatial moment $m_{s,0}^{(2)}$ for second member of the chain (adapted from Parashar and Govindaraju, 2006b, with permission from Springer)

maxima will be primarily determined by the two degradation factors. The first central moment for second specie of the decay chain is also close to being linear in nature (Figure 9.6.2).

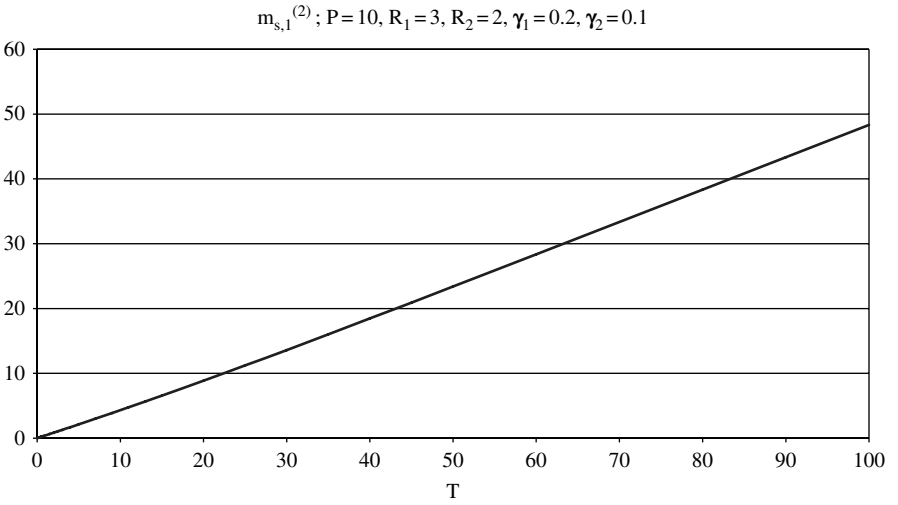

Figure 9.6.2. First spatial normalized moment $m_{s,1}^{(2)}$ for second member of the chain (adapted from Parashar and Govindaraju, 2006b, with permission from Springer)

An alternative approach for spatial moment analysis is through the use of moment generating differential equations (MGDES). From (9.2.9), (9.2.10), and (9.6.11), we obtain the following MGDEs

$$R_1 \frac{d\mu_{s,n}^{(1)}}{dT} = \frac{n(n-1)}{P}\mu_{s,n-2}^{(1)} + n\mu_{s,n-1}^{(1)} - \gamma_1 R_1 \mu_{s,n}^{(1)} \tag{9.6.22}$$

$$R_i \frac{d\mu_{s,n}^{(i)}}{dT} = \frac{n(n-1)}{P}\mu_{s,n-2}^{(i)} + n\mu_{s,n-1}^{(i)} - \gamma_i\ R_i \mu_{s,n}^{(i)} + \gamma_{i-1}\ R_{i-1}\mu_{s,n}^{(i-1)},\ \ i = 2,\ 3, \ldots \tag{9.6.23}$$

From (9.6.5), we have

$$\hat{\mu}_{s,n}^{(i)}(T=0) = \begin{cases} 1, & i=1,\ n=0 \\ 0, & \text{otherwise} \end{cases} \tag{9.6.24}$$

Now defining the Laplace transform of the spatial moment as

$$\hat{\mu}_n^{(i)} = \int_0^\infty e^{-sT}\mu_{s,n}^{(i)}(T)\ dT \tag{9.6.25}$$

and taking Laplace transforms of (9.6.22) and (9.6.23) yields

$$sR_1\hat{\mu}_n^{(1)} - R_1\mu_n^{(1)}(T=0) = \frac{n(n-1)}{P}\hat{\mu}_{n-2}^{(1)} + n\hat{\mu}_{n-1}^{(1)} - \gamma_1 R_1 \hat{\mu}_n^{(1)} \tag{9.6.26}$$

$$sR_i\hat{\mu}_n^{(i)} = \frac{n(n-1)}{P}\hat{\mu}_{n-2}^{(i)} + n\hat{\mu}_{n-1}^{(i)} - \gamma_i R_i \hat{\mu}_n + \gamma_{i-1}R_{i-1}\hat{\mu}_n^{(i-1)} \tag{9.6.27}$$

Higher order moments for different members of the decay chain can be obtained from successive application of (9.6.26) and (9.6.27). For instance,

$$\mu_{s,0}^{(1)} = \mathcal{L}^{-1}\left[\frac{1}{(s+\gamma_1)}\right] = e^{-\gamma_1 T} \tag{9.6.28a}$$

$$\mu_{s,1}^{(1)} = \frac{1}{R_1}\ \mathcal{L}^{-1}\left[\frac{1}{(s+\gamma_1)^2}\right] = \frac{1}{R_1}Te^{-\gamma_1 T} \tag{9.6.28b}$$

$$\begin{aligned}\mu_{s,2}^{(1)} &= \frac{2}{PR_1}\ \mathcal{L}^{-1}\left[\frac{1}{(s+\gamma_1)^2}\right] + \frac{2}{R_1^2}\mathcal{L}^{-1}\left[\frac{1}{(s+\gamma_1)^3}\right] \\ &= \frac{2}{PR_1}Te^{-\gamma_1 T} + \frac{1}{R_1^2}T^2 e^{-\gamma_1 T}\end{aligned} \tag{9.6.28c}$$

$$\mu_{s,0}^{(2)} = \frac{R_1\gamma_1}{R_2}\,\mathcal{L}^{-1}\left[\frac{1}{(s+\gamma_1)(s+\gamma_2)}\right] = \frac{R_1\gamma_1}{R_2(\gamma_2-\gamma_1)}\left[e^{-\gamma_1 T} - e^{-\gamma_2 T}\right] \tag{9.6.29a}$$

$$\begin{aligned}\mu_{s,1}^{(2)} &= \frac{R_1\gamma_1}{R_2^2}\,\mathcal{L}^{-1}\left[\frac{1}{(s+\gamma_1)(s+\gamma_2)^2}\right] + \frac{\gamma_1}{R_2}\,\mathcal{L}^{-1}\left[\frac{1}{(s+\gamma_2)(s+\gamma_1)^2}\right] \\ &= \frac{R_1\gamma_1}{R_2^2}\left[\frac{\left(e^{-\gamma_1 T} - e^{-\gamma_2 T}\right)}{(\gamma_2-\gamma_1)^2} - \frac{Te^{-\gamma_2 T}}{(\gamma_2-\gamma_1)}\right] \qquad (9.6.29b) \\ &\quad + \frac{\gamma_1}{R_2}\left[\frac{\left(e^{-\gamma_2 T} - e^{-\gamma_1 T}\right)}{(\gamma_1-\gamma_2)^2} - \frac{Te^{-\gamma_1 T}}{(\gamma_1-\gamma_2)}\right] \qquad (9.6.29c)\end{aligned}$$

$$\begin{aligned}\mu_{s,2}^{(2)} &= \frac{2R_1\gamma_1}{PR_2^2}\,\mathcal{L}^{-1}\left[\frac{1}{(s+\gamma_1)(s+\gamma_2)^2}\right] + \frac{2R_1\gamma_1}{R_2^3}\,\mathcal{L}^{-1}\left[\frac{1}{(s+\gamma_1)(s+\gamma_2)^3}\right] \\ &\quad + \frac{2\gamma_1}{R_2^2}\,\mathcal{L}^{-1}\left[\frac{1}{(s+\gamma_2)^2(s+\gamma_1)^2}\right] + \frac{2R_1\gamma_1}{PR_2}\,\mathcal{L}^{-1}\left[\frac{1}{(s+\gamma_1)(s+\gamma_2)}\right] \\ &\quad + \frac{2\gamma_1}{R_2}\,\mathcal{L}^{-1}\left[\frac{1}{(s+\gamma_1)^2(s+\gamma_2)}\right] \\ &= \frac{2R_1\gamma_1}{PR_2^2}\left[\frac{\left(e^{-\gamma_1 T} - e^{-\gamma_2 T}\right)}{(\gamma_2-\gamma_1)^2} - \frac{Te^{-\gamma_2 T}}{(\gamma_2-\gamma_1)}\right] \\ &\quad + \frac{2R_1\gamma_1}{R_2^3}\left[\frac{\left(e^{-\gamma_1 T} - e^{-\gamma_2 T}\right)}{(\gamma_2-\gamma_1)^3} - \frac{Te^{-\gamma_2 T}}{(\gamma_2-\gamma_1)^2} - \frac{T^2e^{-\gamma_2 T}}{2(\gamma_2-\gamma_1)}\right] \\ &\quad + \frac{2\gamma_1}{R_2^2}\left[\frac{2\left(e^{-\gamma_2 T} - e^{-\gamma_1 T}\right)}{(\gamma_2-\gamma_1)^3} + \frac{T\left(e^{-\gamma_2 T} + e^{-\gamma_1 T}\right)}{(\gamma_2-\gamma_1)^2}\right] \qquad (9.6.29d) \\ &\quad + \frac{R_1\gamma_1}{R_2(\gamma_2-\gamma_1)}\left[e^{-\gamma_1 T} - e^{-\gamma_2 T}\right] \\ &\quad + \frac{2\gamma_1}{R_2}\left[\frac{\left(e^{-\gamma_2 T} - e^{-\gamma_1 T}\right)}{(\gamma_1-\gamma_2)^2} - \frac{Te^{-\gamma_1 T}}{(\gamma_1-\gamma_2)}\right] \qquad (9.6.29e)\end{aligned}$$

As expected, (9.6.28a) and (9.6.29) are similar to (9.6.15) and (9.6.16).

CHAPTER 10

APPLICATIONS OF MOMENTS IN INTERVAL COMPUTING METHODS

10.1. GENERAL REMARKS

Interval arithmetic is useful when representing a number by two bounding values, thereby accommodating imprecise measurements. In many instances, little or no information is available regarding the probabilities of errors resulting from measurements. However, upper and lower bound values can be estimated with a certain level of confidence allowing for measurement results to be expressed as intervals. Based on this idea, Moore (1966) applied interval computing methods to error analysis. In hydrology, interval arithmetic was applied under the framework of fuzzy set theory (Dou et al., 1995; Bardossy et al., 1988, 1990) to characterize imprecise input variables such as transmissivity of an aquifer and interval (fuzzy) arithmetic was used for evaluating groundwater flow.

Heterogeneity of soil hydraulic properties has been cited as the major obstacle in predicting field-scale contaminant transport (Dagan and Bresler, 1979; Bresler and Dagan, 1979; Simmons, 1982). Given parameters with known probability distributions, traditional methods such as Monte Carlo simulations and stochastic methods appear to be the preferable means of analysis. Nevertheless, researchers, especially those who are familiar with fuzzy modeling techniques, have tried to incorporate hard data (with known probability distribution) into their modeling approach by deriving statistically based membership functions. For instance, Civanlar and Trussell (1986) attempted to construct a membership function from the probability density function of a random variable. They developed a set of criteria such that the size of the fuzzy set of a random variable could be minimized while the membership function was obtained numerically.

Interval arithmetic and interval methods can indeed be applied to deal with not just imprecise variables, but variables of known probability distributions (Zadeh, 1978). Pesonen and Hyvönen (1996) constructed probability density bounds by dividing the support of a random variable into bins of equal width. A bounded probability density function (pdf) was obtained by collecting the upper and lower bound values of the bins respectively. The authors suggested that this method provided a possible

challenge to the traditional Monte Carlo approach in characterizing probability density function (pdf).

Chan and Govindaraju (2001) employed interval arithmetic to model field-scale experiments in which model parameters of known probability distributions were characterized by interval distribution functions. In this chapter we describe and apply a methodology for finding moments in an interval computing setting. A brief introduction of interval arithmetic is provided here. A more detailed development on this topic can be found in Chan (1999).

10.2. INTERVAL ARITHMETIC OPERATIONS

Moore (1966) defined an interval number to be an ordered pair of real numbers, $[a,\ b]$, with $a < b$. Intervals consisting of exactly one point, $[a,\ a]$, are called point intervals and are denoted by a. Real arithmetic operations can be applied to interval numbers with a few exceptions. Young (1931) introduced the four basic arithmetic operations between interval numbers as follows:

$$[a, b] + [c, d] = [a + c, b + d] \tag{10.2.1}$$

$$[a, b] - [c, d] = [a - d, b - c] \tag{10.2.2}$$

$$[a, b] \cdot [c, d] = [\min(ac, ad, bc, bd), \max(ac, ad, bc, bd)] \tag{10.2.3}$$

$$[a, b]/[c, d] = [a, b] \cdot [1/d, 1/c], \text{ if } 0 \notin [c, d] \tag{10.2.4}$$

Like real arithmetic, interval addition and multiplication are both associative and commutative. However, interval subtraction and division are not the inverse operations of addition and multiplication respectively as is the case in real arithmetic. The other difference between interval and real arithmetic is that the distributive law does not always hold for interval arithmetic. For example,

$$[1, 2]([1, 2] - [1, 2]) = [1, 2]([-1, 1]) = [-2, 2],$$
$$[1, 2][1, 2] - [1, 2][1, 2] = [1, 4] - [1, 4] = [-3, 3].$$

These two expressions yield totally differently answers. By treating an interval as a set of real numbers, a so-called subdistributive law can be expressed by $A(B+C) \subseteq AB + AC$ for any intervals $A,\ B$, and C. For some special cases, however, the distributive law is valid, such as $a(B + C) = aB + aC$ when a is a point interval.

Interval arithmetic may be used to determine the upper bound and lower bound solution of a mathematical function given interval variables as inputs. In this regard, a natural interval extension is performed on the function by replacing real variables by corresponding interval variables, and also replacing real arithmetic operations by corresponding interval arithmetic operations. Due to the absence of distributive law (other than for some special cases), two rational expressions which are equivalent in real arithmetic may not be so in interval arithmetic. According to Moore (1979),

'any natural interval extension of a rational function in which each variable occurs only once (if at all) and to the first power only will compute the exact range of values providing that no division by an interval containing zero occurs.' In other words, if we have a function in the form of a polynomial or one in which a variable appears more than once, evaluation of the exact bounds of such function becomes more tedious. In such cases, simple interval arithmetic operations do not give the exact bound of values, but an optimization procedure has to be involved to search for the global maxima and minima of the function. Ratschek and Rokne (1988) showed how to combine interval methods and traditional local methods for handling of global optimization problems. It is important to note that this subdistributive problem with interval extension cannot be ignored, as it may lead to overestimation of the interval solutions.

10.3. INTERVAL DISTRIBUTION FUNCTIONS

Simlar to a Monte Carlo analysis, in the interval computing method, the cumulative distribution function (cdf) for each input variable is obtained. But instead of generating random numbers, interval computing method requires the identification of appropriate intervals on the cdf for model calculations. The idea of selecting appropriate intervals is to represent the cdf by a finite number of intervals, so-called *alpha-cuts*, which in turn form the *interval distribution function* (idf). At each alpha-cut, the governing equation can be evaluated using interval arithmetic in which the maxima and minima of the solution are found. Combining the resulting intervals from all alpha-cuts, we can obtain the complete characterization of the interval distribution function of the solution.

There is no unique way to specify intervals in a given cdf; however, we propose the following intuitive procedure. Say, X is a random variable with a certain known distribution. Then, alpha-cuts were specified by Chan and Govindaraju (2001) as:

$$X_\alpha = [x_1^{(\alpha)}, x_2^{(\alpha)}] \tag{10.3.1}$$

where $x_1^{(\alpha)}$ and $x_2^{(\alpha)}$ are the lower and upper bound values respectively, and α ranges from 0 to 1. (The superscript α of x will be omitted hereafter for ease of notation.) The resolution of alpha-cuts controls the precision of interval computing method, just as the number of random numbers does in the Monte Carlo analysis. In order to make (10.3.1) meaningful, the following conditions are imposed:

$$\begin{gathered}\alpha = \eta(x_1) = \eta(x_2) = 2F(x_1) = 2(1 - F(x_2)) \\ \text{for } 0 \le \alpha \le 1, 0 \le F(x_1) \le 0.5 \text{ and } 0.5 \le F(x_2) \le 1\end{gathered} \tag{10.3.2}$$

where $F(\cdot)$ is the cdf and $\eta(\cdot)$ is the interval density function (idf). On the other hand, the idf can be viewed as a collection of alpha-cuts. From (10.3.2), it can be seen that when $\alpha = 1$,

$$F(x_1) = F(x_2) = 0.5 \text{ and } x_1 = x_2 = \text{median}(X). \tag{10.3.3}$$

According to the conditions set forth by (10.3.2), selection of intervals should follow the steps below.

1) For $\alpha = 1$, $X_\alpha = 1 = \text{median}(X)$ where the cumulative probability of the lower bound and upper bound x is the same at 0.5. In other words, when $\alpha = 1$, the corresponding interval number is a point interval which represents the median of X.
2) For $0 \leq \alpha < 1$:
   $\Rightarrow$ x_1, the lower bound value corresponds to the cumulative probability of $\alpha/2$.
   $\Rightarrow$ x_2, the upper bound value corresponds to the cumulative probability of $1 - \alpha/2$.

Note that when $\alpha = 0$, the corresponding interval represents the support of the random variable. A graphical depiction of this approach is presented in Figure 10.3.1. An idf offers several advantages:

1) It provides a clear visualization of the interval selection and the median of the distribution (when $\alpha = 1$). This is helpful for visual comparison purposes.
2) Based on this conceptualization, the idf is defined in a probabilistic fashion as $P\left(x_1^{(\alpha)} < x \leq x_2^{(\alpha)}\right) = 1 - \alpha$.
3) Moments can be computed from idf.

Moreover, Chan and Govindaraju (2001) show that this prescription of the idf satisfies the consistency principle of possibility theory and therefore it can be used interchangeably as a membership function in a fuzzy modeling framework.

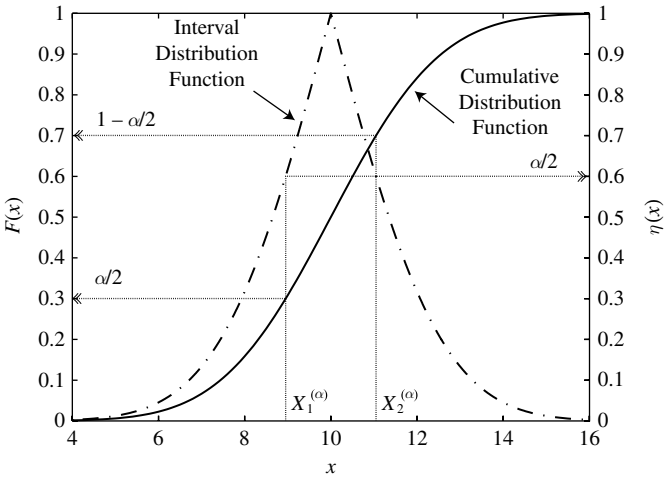

Figure 10.3.1. Schematic of interval distribution function showing its relationship to cumulative distribution function and the significance of α-cuts (adapted from Chan and Govindaraju, 2001, with permission from ASCE)

10.4. DEFINING MOMENTS FROM INTERVAL DISTRIBUTION FUNCTIONS

An interval distribution function, as a transformation of a cumulative distribution function, provides a mean for identifying appropriate intervals to be used in the interval computing technique. First we note that moments of any order can be calculated from a cumulative distribution function as (Parzen, 1960):

$$E[x^n] = \int_{-\infty}^{\infty} x^n f(x)dx = \int_0^{\infty} dy\ ny^{n-1}[1 - F(y) + (-1)^n F(-y)] \tag{10.4.1}$$

Substituting $F(\cdot)$ with α using relationship given in (10.3.2), the following equations are obtained:

$$\begin{aligned} &if\ \lambda \geq 0, \\ &\quad E[x^n] = \int_{-\infty}^{0} (-1)^{2n-1} x^{n-1} \frac{\eta(x)}{2} dx \\ &\qquad + \int_0^{\lambda} nx^{n-1}[1 - \eta(x)/2]dx + \int_{\lambda}^{\infty} nx^{n-1}\eta(x)dx \\ &if\ \lambda < 0, \qquad (10.4.2a) \\ &\quad E[x^n] = \int_{-\infty}^{\lambda} (-1)^{2n-1} x^{n-1} \frac{\eta(x)}{2} dx \\ &\qquad + \int_{\lambda}^{0} (-1)^{2n-1} x^{n-1}[1 - \eta(x)/2]dx + \int_0^{\infty} nx^{n-1}\eta(x)dx \end{aligned} \tag{10.4.2b}$$

where λ is the median of random variable X.

Some caution has to be exercised when interpreting the moments calculated from the idf, as the statistical nature of the random variable in form of an idf is not always preserved after model transformation using interval computing technique.

10.5. APPLICATION TO A REMEDIATION EXAMPLE

Phytoremediation refers to the process of remediation of contaminated sites through the use of vegetation (Banks et al., 2000). Depending on the type of plant species being used, phytoremediation can significantly increase the degradation rate of some contaminants in the soil (Shann and Boyle, 1994). Quantifying field scale remediation potential of different plant species is important for selecting the most efficient and cost effective vegetative treatment. Modeling the fate of contaminants at the field scale, however, is often difficult due to the lack of homogenous conditions over the site. Initial level of contamination varies spatially and so do other parameters that govern the transformation, degradation, and transport of contaminants.

The phytoremediation field study is first of the two examples in which the potential of interval computing method as an alternative to the Monte Carlo simulations is being assessed. Measurements of total petroleum hydrocarbon (TPH) concentration obtained from a field site established at a Gulf Coast crude oil spill location were used to evaluate interval computing techniques. The site consisted of four plots with three different vegetative treatments, namely sorghum, St. Augustine grass, and rye grass, and one unvegetated plot as a control for the experiment (see Chan, 1999). A first order degradation model was assumed to describe the local scale TPH concentration. The mean and variance of concentrations at various time steps were predicted using the interval computing method, Monte Carlo simulations, as well as stochastic solutions. Results from these various methods were compared among each other as well as with the observed data.

The phytoremediation study took place on an agricultural field. The soil at the site was characterized as low permeable, poorly drained with slow runoff. The field site encompassed an area of approximately 320 ft by 240 ft. Four plots, 60 ft by 30 ft each, were established in February 1994, and each plot was cultivated with sorghum (*Sorghum biocolor L*), rye grass (*Lolium annual*), and St. Augustine grass (*Stenotaphrum secundatum L*) respectively. The remaining plot was treated with herbicide to prevent vegetative growth and therefore was used as a control for the experiment.

Initial TPH concentrations were obtained in August 1994 and were used as the basis for an exploratory geostatistics analysis in order to evaluate the spatial variability of the site (see Nedunuri et al., 2000 for details). Placement of 20 sampling locations was designed and was identical for each plot. Sampling started August 1994 when initial concentrations were measured, and lasted until September 1996. Samples were taken every 2 months during the active growing season and every 3 months during the dormant period. As a result, TPH concentration measurements at 20 sampling locations in each plot were obtained for the 0th, 3rd, 6th, 8th, 13th, and 21st month. Preliminary data for five time points were reported in Chen (1997) and soon after, some of the samples were reanalyzed and data for the 8th month was available at a subsequent time. A soil-coring device was used to obtain samples at a depth of 6 in from the surface. Each soil sample was homogenized and TPH concentration was measured using infrared spectrometry

10.5.1 First-Order Degradation Model

Decay of TPH at the local scale, i.e. at each sampling location, was described by the first-order kinetics as follows:

$$\frac{dC}{dt} = -kC \tag{10.5.1}$$

where C is the concentration of TPH, t is the time, and k is the first-order degradation rate. This model was chosen mainly due to its simplicity. Schwab and Banks (1994) suggested that factors including root structure, nature of the organic compounds,

soil structure and compositions, and microbial activity, all have influence on the fate of the contaminant. The degradation rate, k, can therefore combine the effect from all possible contributing factors, and can be conceived as an indicator of the phytoremediation treatment effectiveness. Upon integration, the analytical solution of (10.5.1) is obtained as follows:

$$C(t) = C_0 e^{-kt} \tag{10.5.2}$$

where C_0 is the initial concentration at time zero.

10.5.2 Statistical Distributions of Degradation Rates and Initial Concentrations

In order to upscale the local model for field-scale prediction, we need to obtain or assume the statistical distributions of degradation rates and initial concentrations from field measurements.

Table 10.5.1 shows the means and variances of the degradation rates obtained for different treatments. At each sampling location, the degradation rate was estimated by a least squares linear regression on the observed concentration data based

Table 10.5.1. Degradation constant, k (1/month), of TPH at different treatment plots (from Chan, 1999)

Location	Rye Grass	St. Augustine Grass	Sorghum	Control
1	0.0105	0.0234	0.0664	−0.0348
2	0.0412	0.0090	−0.0175	0.0318
3	0.0347	0.0295	0.0174	0.0277
4	0.0473	0.0326	0.0276	0.0160
5	0.0785	−0.0407	0.0192	−0.0192
6	0.0474	0.0113	0.0490	0.0041
7	0.0517	0.0352	0.0573	0.0056
8	0.0032	0.0489	−0.0002	0.0039
9	0.0476	0.0103	0.0261	−0.0064
10	0.0638	0.0454	0.0251	0.0816
11	0.0507	−0.0022	0.0420	0.0174
12	0.0118	0.0413	0.0319	0.0108
13	0.0388	0.0156	0.0460	0.0186
14	0.0366	0.0397	0.0201	0.0220
15	0.0803	0.0450	0.0219	0.0305
16	0.0426	0.0566	0.0464	0.0278
17	0.0952	0.0351	0.0209	0.0052
18	0.0742	0.0412	−0.0544	0.0105
19	0.0589	0.0505	0.0375	0.0367
20	0.0620	0.0674	−0.0183	0.0509
Mean*	0.0489	0.0354	0.0347	0.0236
Variance*	0.00056	0.00027	0.00022	0.00039

* Mean and variance are calculated without accounting for the negative k values.

on (10.5.2). Except for the rye grass treatment, the observed concentration series at a few sampling points resulted in negative k estimates. The presence of negative values is counter-intuitive in the sense that concentration should, in general, decrease over time. However, due to the nature of destructive sampling, no identical samples could be collected at the same location. Spatial variability in the field allows higher concentration samples to be collected at a later time step, leading to the presence of negative degradation rates. As a result, data series at sampling locations with negative degradation rates were removed from the analysis; 18 data sets were left for St. Augustine Grass plot, 16 for the Sorghum plot, and 17 for the control plot.

Figure 10.5.1 displays the normal probability plots of k estimates for the four treatments. The k estimates are represented with the plot symbol '+' and the best-fit normal distribution with a superimposed straight line. By evaluating the linearity of the data, we conclude that the degradation rates for most treatments, except for the control plot, exhibit a distribution close to the normal. For the

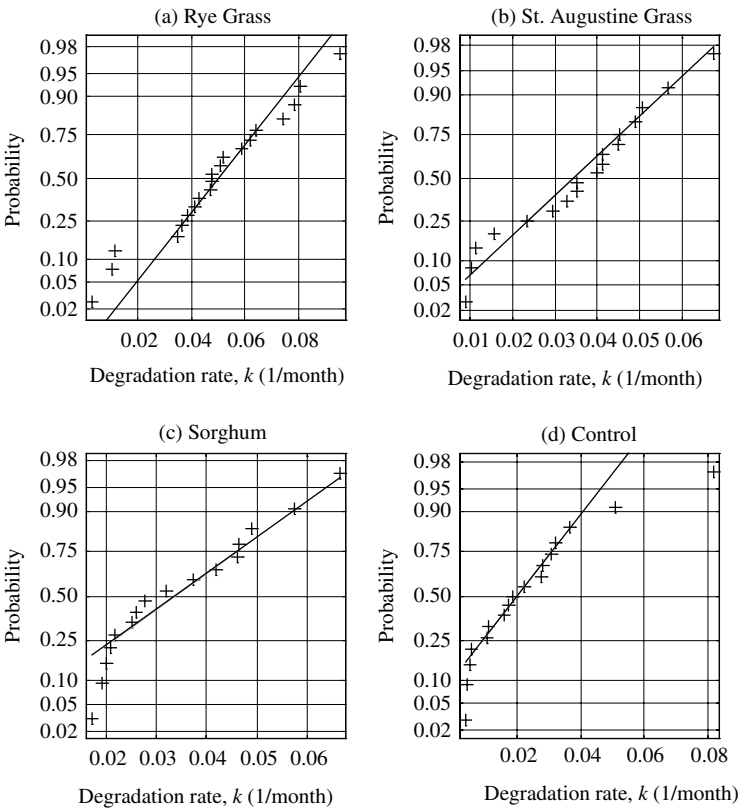

Figure 10.5.1. Normal probability plots of the degradation rates with various treatments: (a) rye grass, (b) St. Augustine grass, (c) sorghum, and (d) no treatment (control). The plot symbol '+' represents the data point while the straight line is the best-fit normal distribution (from Chan, 1999)

interval computing method, interval distribution functions of the degradation rates were generated both by interpolation from the cumulative distribution functions and by the fitting of a normal distribution. Comparisons between the interpolated and normally distributed idfs of the degradation rates are shown in Figure 10.5.2. As with the degradation rate, the initial concentration is assumed a *second-order stationary random field*. Since we are only interested in the field averages and variances of the TPH concentrations, the distribution of the initial concentrations can be also thought as being normal. The initial concentrations for different treatments are listed in Table 10.5.2.

10.5.3 Field-Scale Models

Now that the probabilistic distributions of the degradation rate and the initial concentration are assumed, the local model can be upscaled for the predictions of

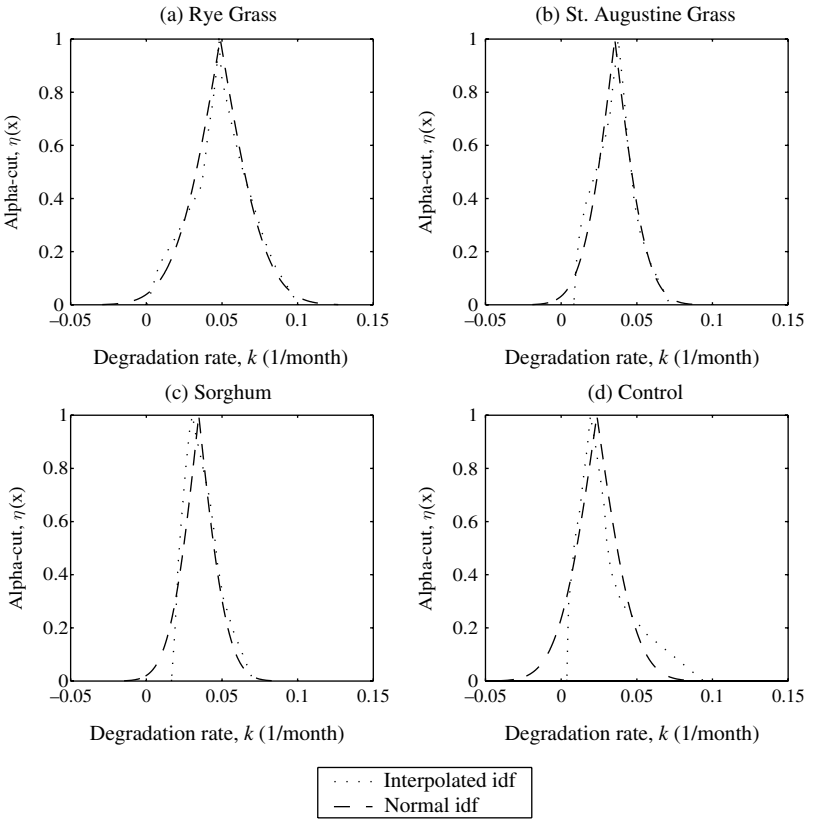

Figure 10.5.2. Comparisons between interpolated and normal interval distribution functions (idf) of the degradation rate k (from Chan, 1999)

Table 10.5.2. Initial concentration, C_0 (mg/kg), of TPH at different treatment plots (from Chan, 1999)

Location	Rye Grass	St. Augustine Grass	Sorghum	Control
1	4574.15	17671	9839.93	6459.95
2	9023.9	14248	6124.6	13440.94
3	10790.62	16709	9307.19	14501.23
4	7072.22	11751	6037.02	9282.09
5	11813.74	4070	4846.62	9099.02
6	9500.97	12384	9348.12	10828.69
7	11241.98	18993	8834.58	6939.92
8	7124.82	9905	5209.82	5616.28
9	8925.59	11521	7000.87	11816.42
10	9535.88	20687	10623.07	29141.75
11	12922.65	8818	10149.2	12444
12	6760.18	14199	17178.93	7646.04
13	7969.1	11832	7778.63	16186
14	6288.92	17818	8978.95	12148
15	12803.54	19422	10451.38	12563.07
16	11508.79	19147	17250.22	12832.77
17	13669.47	14879	6052.75	7444
18	9031.88	14837	2315.28	7074.5
19	10935	14601	10263.44	9459
20	11368.35	20637	6173.4	9396.2
Mean*	9643	15625	9621	11585
Variance*	6104191	11452297	11839713	29395149

* Mean and variance are calculated without accounting for the negative k values.

time-dependent field-scale concentration. One important assumption, however, is made to simplify the field-scale model. It is assumed that the initial concentration and the degradation rate are statistically independent of each other. Note that such assumption applies to all three methods used in the study.

For the interval computing method, the analytical expression (10.5.2) is naturally extended to an interval equation for which interval arithmetic can be used in the search for the maximum and the minimum of time-dependent field - scale concentrations at each alpha-cut. Interval distribution functions of the concentration at various time steps can be computed, and the means and variances can be obtained subsequently. An increment of 0.01 is used as the resolution of alpha-cut.

Five thousand simulations are performed in the Monte Carlo approach, assuming normal distributions for degradation rate and initial concentration. For each simulation, (10.5.2) is used to evaluate the concentration at a given time. Sample statistics are obtained based on those 5000 simulations.

For the stochastic approach, the following expressions were used to compute the first two moments of the field-scale concentration:

$$E[C(t)] = \mu_{C_0} \exp\left(\mu_k t + \frac{\sigma_k^2 t^2}{2}\right) \tag{10.5.3}$$

$$E[C^2(t)] = (\mu_{C_0}^2 + \sigma_{C_0}^2) \exp(-2\mu_k t + 2\sigma_k^2 t^2) \tag{10.5.4}$$

where μ_{C_0} and μ_k are the means of the initial concentration and the degradation rate respectively; $\sigma^2_{C_0}$ and σ^2_k are the sample variances of the initial concentration and the degradation rate respectively. Knowing the first and second moments, the variance of $C(t)$ can be computed as follows:

$$Var[C(t)] = E[C^2(t)] - E[C(t)]^2 \tag{10.5.5}$$

10.5.4 Results and Discussion

The following four cases are considered in this study:

Case 1: Interval computing method with linearly interpolated cdf (ICintrp);
Case 2: Interval computing method with fitted normal distributions (ICnorm);
Case 3: Monte Carlo simulations with fitted normal distributions (MC);
Case 4: Stochastic solutions with fitted normal distributions (Stoch);

The first moment of an interval distribution function can be geometrically interpreted as the centroid (center of gravity) of the area underneath the function curve. The first moment can be evaluated numerically using (10.4.2) given an idf. Based on the centroid interpretation of the first moment, we can treat it as an estimate of the mean of the random variable. In Figure 10.5.3, mean field-scale concentration predictions from all four cases are compared with the observed data for each treatment. In general, all cases capture the downward trend exhibited by the observed data. However, at the 8th month, the observed mean concentrations are extremely low for all treatments. Measurement error may have contributed to the lowering of the observed mean concentration. The batch of the 8th month core samples was stored for a period of time and analyzed at

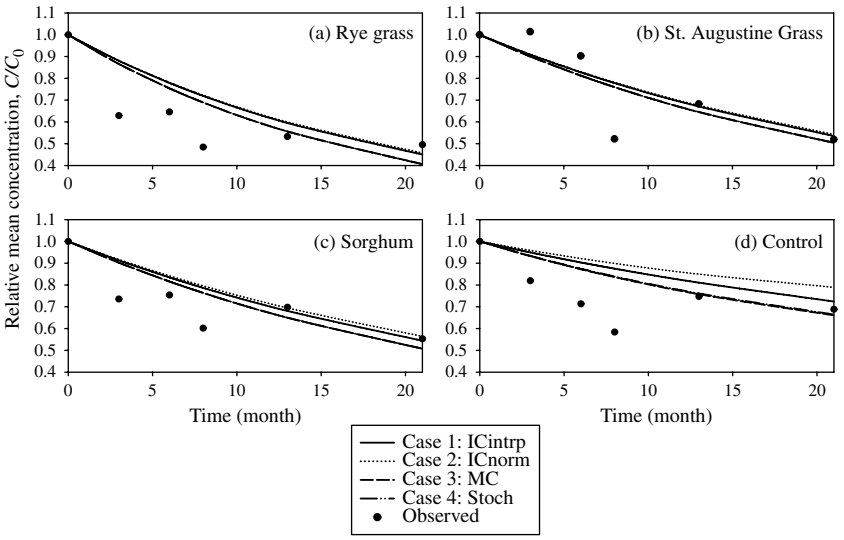

Figure 10.5.3. Relative TPH concentration as a function of time (from Chan, 1999)

a later time; as a result, natural degradation could have attenuated the concentration of TPH during the storage period. Since the low concentration is consistent across all treatments, it is believed that inconsistency in measurement and degradation of TPH are perhaps responsible for the drop in concentration. Note that this outlier has affected the model prediction in all cases by increasing the values of degradation rate estimates. As the degradation rate is used as the measure of treatment performance, such increase can lead to misleading interpretation that a treatment is more effective than it could have been. As a result, caution has to be exercised when trying to interpret the results.

Also observed from Figure 10.5.3 is that Monte Carlo simulations (Case 3) give similar results compared to the stochastic solutions (Case 4). This is expected – while the stochastic solutions provide the baseline results, the Monte Carlo method should give more closely matched results as the number of simulations increases. Another observation from the figure is that mean concentrations predicted by the interval computing method (Case 1 and 2) are slightly higher than those obtained from Monte Carlo simulations (Case 3) and stochastic solutions (Case 4). The difference is partly caused by the fact that variances, as shown in Figure 10.5.4, are overestimated using the interval computing method. To further investigate the cause of overestimation, results from Monte Carlo analysis and distributions of the observed concentrations are converted into interval distribution functions and they are superimposed on the results from interval computing method (in Figure 10.5.5). As indicated in the Figure 10.5.5, interval computing method results in wider width of intervals at almost all alpha-cuts, with discrepancy increasing at lower alpha values. This overestimation of width of the idf is more serious in the leading tail (at higher concentration). Because of the tailing effect, the variance estimated

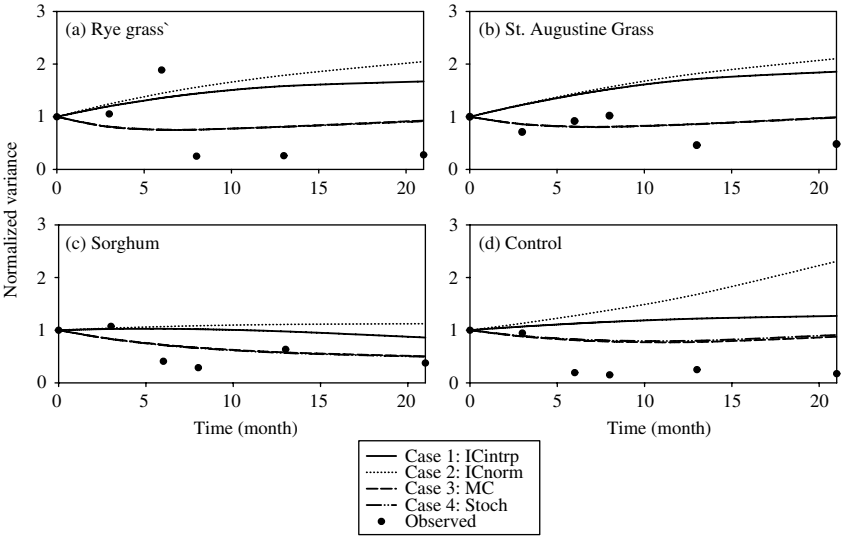

Figure 10.5.4. Normalized variance as a function of time (from Chan, 1999)

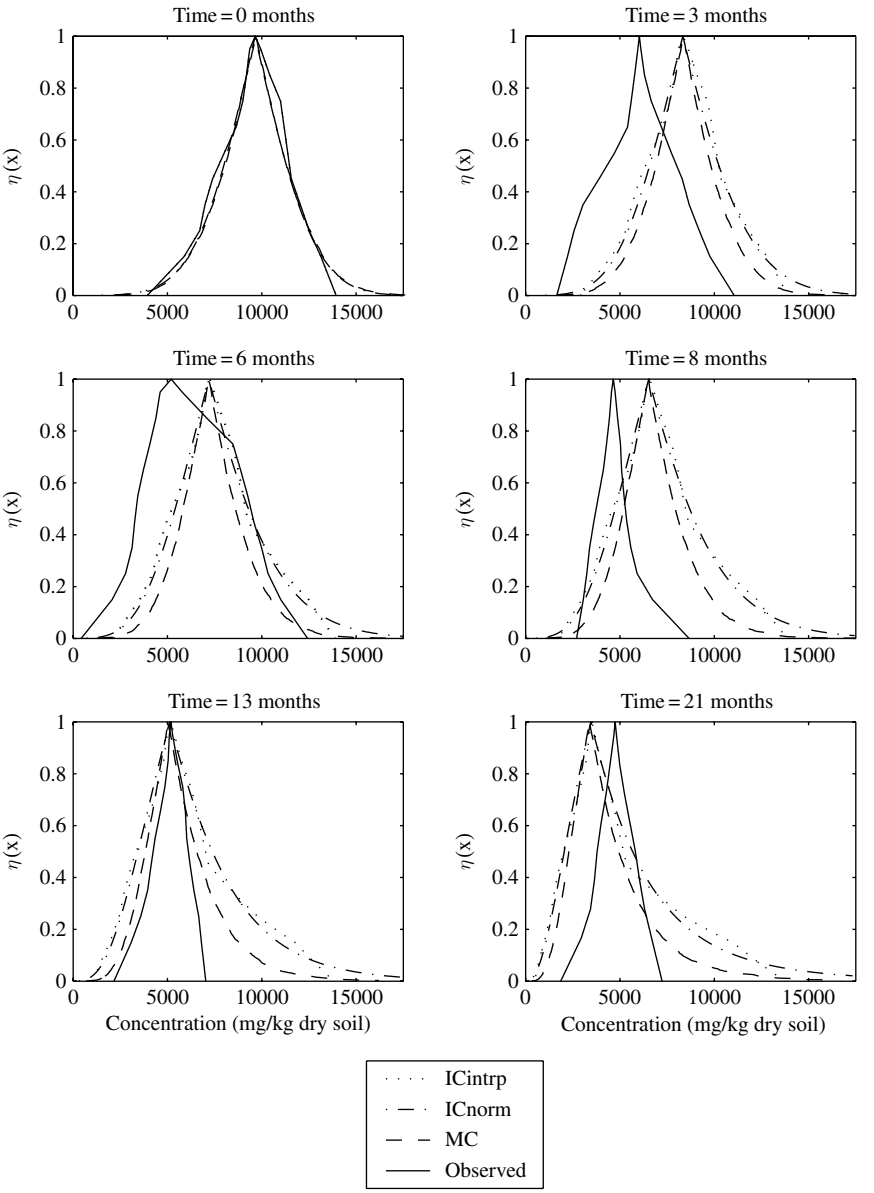

Figure 10.5.5. Interval distribution function of TPH concentrations at different time after start of Rye Grass treatment (from Chan, 1999)

from the idf is biased towards a higher value, resulting in overestimation of mean concentration by the interval computing method. Chan (1999) hypothesized that it is the nature of the interval arithmetic and the computation approach that leads to a wider hull. In the interval computing method, we are only interested in obtaining the upper and lower bound of the solution at each alpha-cut. During this computational process, certain information, such as the distribution within the interval, is lost. The discarded information could have led to the overestimation we observed in the results, especially in the variance prediction.The more serious overestimation in the leading tail may also be compounded by the exponential nature of the local-scale model behavior. To obtain the upper bound solution at an alpha-cut, the governing equation takes on the maximum of C_0 and minimum of k. With k being negative, $C(t)$ will grow larger as time increases. Despite the poor performance of the method in estimating variances, it is generally successful in predicting the mean behavior of time-dependent concentrations and more importantly the hull of the solution as shown in Figure 10.5.6 (with concentration data at 8th month being an exception).

Although all methods are generally able to predict the trend of the mean behavior, they all have trouble estimating the field-scale variances of the concentration. As shown in Figure 10.5.4, except for the sorghum plot where the stochastic solutions and the Monte Carlo method are able to capture the lowering trend of the variances, the variances of other treatments are poorly predicted by all methods. For the interval computing method, the reasons for failure in overestimating variances have been discussed in the earlier paragraphs. In addition, poor predictions in variances indicate the inadequacy of the models in replicating field conditions effectively. Efforts had been attempted in a study by Nedunuri et al. (2000) to incorporate the spatial variability in a stochastic framework. They had somewhat better estimates of the variance when the nature of spatial variability was included explicitly through variograms. Further research is, therefore, warranted in finding a way to integrate spatial variability into the interval computing method.

The computational requirement of interval computing method is proportional to the resolution of alpha-cut which in turn controls the precision of the method. In other words, the resolution of alpha-cut is important in controlling the computational time and the precision as well. Similar to Monte Carlo simulations, more the precision desired (by increasing the resolution), the higher the computational time required. Unlike Monte Carlo simulations, however, the number of intervals required to adequately represent a distribution can be far less than the number of realizations needed for Monte Carlo simulations. As a result, the number of model evaluations performed by the interval computing method can be, in theory, far less than that carried out by Monte Carlo simulations. Thus, the interval computing method is expected to be more efficient computationally than Monte Carlo simulations. However, in this study, the interval computing method does not outperform Monte Carlo simulations due to the simplicity of the model as well as the time-consuming numerical integration required for the computation of moments from the idfs. In the next example (potassium chloride transport field study), the efficiency of interval

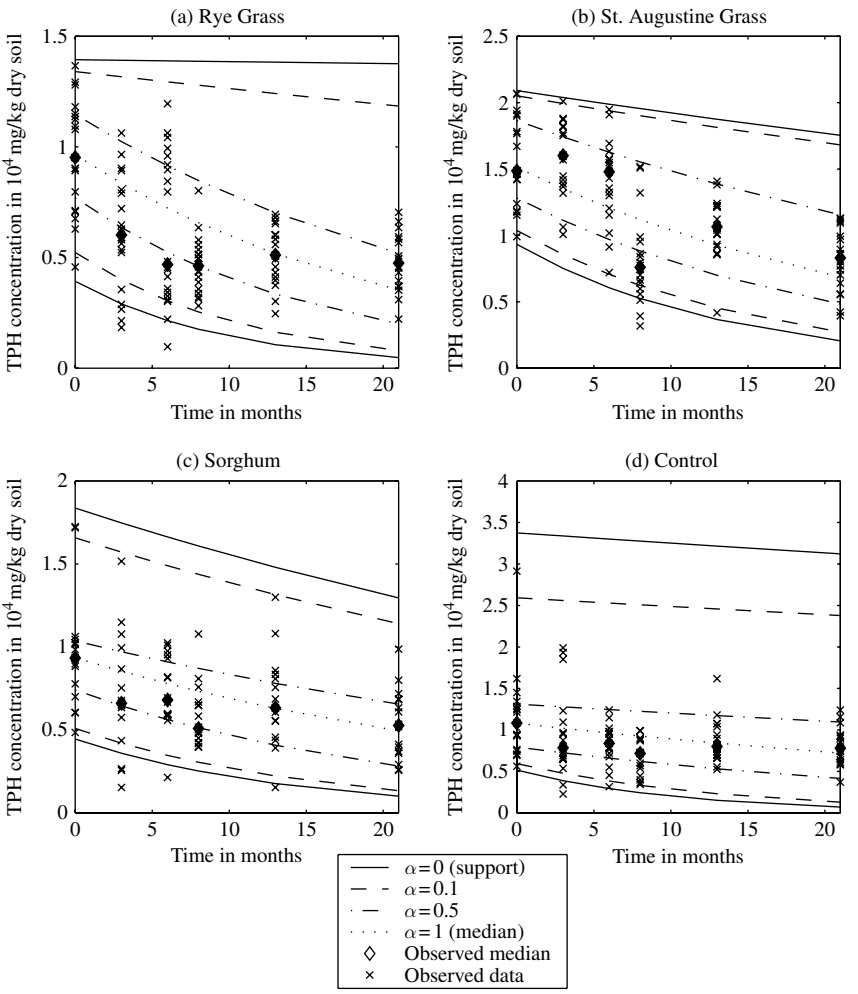

Figure 10.5.6. Predicted TPH concentration intervals at various alpha-cuts using interval computing method (Case 1) (from Chan, 1999)

computing method will be demonstrated with greater success as the model grows in complexity and involves heavier computation.

10.6. APPLICATION TO SOLUTE TRANSPORT EXPERIMENT

Solute transport in soils is often treated as a stochastic-advective phenomenon due to soil heterogeneity (see Section 4.7). Dispersion at pore-scale is negligible but field-scale dispersion results from the probability distribution of travel time due to the heterogeneous distributions of soil properties. Utilizing data from a field site

at University of California, Davis, a stochastic advective transport approach was adopted by Chan and Govindaraju (2001) to develop moments of travel times and concentrations for one-dimensional vertical solute transport in soils; however, the interval computing method was introduced as an alternative to numerical evaluations of the model. In order to evaluate the validity of the interval computing method, comparisons of interval distribution functions of travel times were made against Monte Carlo simulations, theoretical solutions, and experimental observations. The time-depth dependent mean solute concentration (i.e. the first moment) over the field was also evaluated based on the probability distribution of travel time using the three different methods. Results were compared against each method as well as with the experimental observations. In this section, we describe the work of Chan and Govindaraju (2001).

10.6.1 Description of the Solute Transport Experiment

The original intent of the experiment was to evaluate the use of time domain reflectometer (TDR) for estimating solute travel time and surface flux in field-scale soils (Koos, 1994). The same data were utilized to investigate and validate the effectiveness of interval computing method in evaluating a stochastic advective solute transport model.

The experiment was conducted on a University of California, Davis, field site that consisted of 24 plots, each 2.5 m square in size. Twelve sets of TDR rods at 15-, 30-, and 45-cm depths were instrumented at each plot. Three neutron probes were installed to measure the soil water content at eight different depths (15, 30, 45, 60, 120, 180, 240, and 300 cm). Also, two porous solution samplers ranging in depths from 30 to 300 cm were used to monitor solute movement. To allow ponding at each plot, dikes were constructed at the plot boundary and water was continuously added to the soil surface except during the application of potassium chloride (KCl) pulse. Upon reaching steady state for the soil water content, a 5-cm pulse of KCl solution with a concentration of 170 meq/L was applied to the plot followed by clean water application at the same rate. Monitoring of KCl transport continued until the concentration tailed off at 300-cm depth. The plot infiltration rate was measured during the experiment by ceasing the water supply to the plot and timing the rate of drop of the ponded water height. Local infiltration rate was calculated using measurements from the 15-cm TDR probes. Solution sampler data were used to generate the mean break through curve at each depth. Experimental details are available in Koos (1994).

10.6.2 Advective Solute Transport in Vadose Zone

The advective transport equation for a solute traveling through a vertically heterogeneous soil under unsteady and nonunifrom soil water flow is given as

(Simmons, 1982)

$$\frac{\partial C(z,t)}{\partial t} + \frac{q(z,t)}{\theta(z,t)}\frac{\partial C(z,t)}{\partial z} = 0 \tag{10.6.1}$$

where C is the solute concentration, z is the depth (downward positive), t is the time, q is the local Darcy flux in vertical direction, and θ is the local volumetric water content. Using the method of characteristics, Wilson and Gelhar (1981) derived the following characteristic equation:

$$u(z,t) = \int_0^z \theta(\xi,t)d\xi - \int_0^t q(0,\tau)d\tau \tag{10.6.2}$$

where the first term in on the right hand side of the equation is the soil water storage $\Phi(z)$:

$$\Phi(z) = \int_0^z \theta(\xi,t)d\xi \tag{10.6.3}$$

and the second term is the cumulative infiltration. For a constant surface flux q_0, the cumulative infiltration $Q(t)$ becomes

$$Q(t) = \int_0^t q(0,\tau)d\tau = q_0 t \tag{10.6.4}$$

By setting $u(z,\ t) = 0$ in (12.6.2), the location of the solute front can be obtained. Assuming steady state, the time it takes for water to reach a depth z, as denoted by $T(z)$, is

$$T(z) = \frac{\int_0^z \theta(\xi)d\xi}{q_0} = \frac{\Phi(z)}{q_0} \tag{10.6.5}$$

Knowing the solute travel time, the time-depth dependent solute concentration can be expressed in terms of Heaviside step function provided that C_0 is the solute concentration at the surface inlet.

$$C(z,t) = C_0 H[t - T(z)] \tag{10.6.6}$$

If the solute application at the soil surface is a rectangular pulse loading of duration t_0, then

$$C(z,t) = C_0\{H[t - T(z)] - H[t - T(z) - t_0]\} \tag{10.6.7}$$

This may be restated as

$$C(z,t) = C_0\{H[q_0 t - \Phi(z)] - H[q_0 t - Q_0 - \Phi(z)]\} \tag{10.6.8}$$

where $Q_0 = q_0 t_0$ is the depth of the pulse application (5 cm). Kavvas et al. (1996) argued that the above expression is valid when q_0 is available (i.e. the expression is conditioned on q_0 being available). As in their study, we assume that $\Phi(z)$ and q_0 are independent.

10.6.3 Field-Scale Model using Interval Computing Method

Field-scale distributions of both solute travel time and solute concentration can be obtained through the upscaling of (10.6.5) and (10.6.8) and the use of interval computing method. The local volumetric water content was parameterized using an exponential expression:

$$\theta(z) = ae^{-bz} \tag{10.6.9}$$

By fitting (10.6.9) to the water content data from neutron probes in the experiment, 24 values of constants a and b were obtained respectively. Normal probability plots were generated for a and b as shown in Figure 10.6.1. From the linearity of the plots, we assume that a and b both follow a normal distribution.

Although the plot infiltration rate was measured in the experiment, the local infiltration rate calculated from 15-cm TDR measurements was used as the surface flux q_0 because TDR measurements provided more data points, thus a more realistic measure of the field-scale variability. A normal probability plot for log q_0 is shown in Figure 10.6.1 to demonstrate that q_0 is distributed in a lognormal fashion. Table 10.6.1 shows the means and standard deviations of a, b, and log q_0. Based on the statistics given in the table, interval density function (idf) for each variable was obtained by the procedure described in Section 10.3. Combining (10.6.5) and parameterized θ in (10.6.9), field-scale solute travel time is given by the follow expression:

$$T(z) = \frac{\int_0^z \theta(\xi)d\xi}{q_0} = \frac{q}{bq_0}(1 - e^{-bz}) \tag{10.6.10}$$

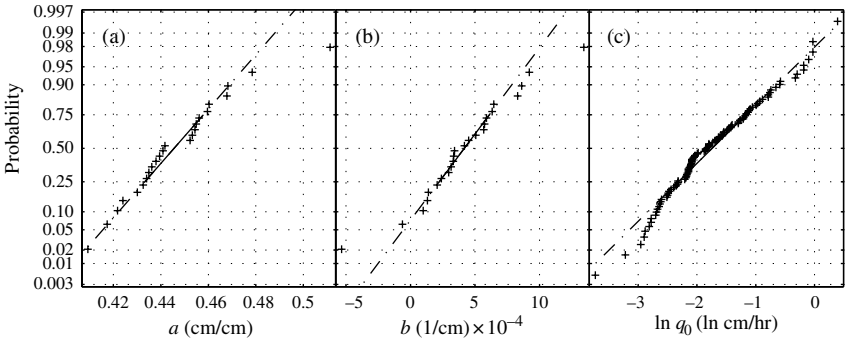

Figure 10.6.1. Normal probability plots of parameters a, b, and ln q_0 (from Chan and Govindaraju, 2001, with permission from ASCE). The plot symbol '+' represents the data point and the straight line is the best-fit normal distribution

Table 10.6.1. Best-fit parameters for volumetric water content θ based on (10.6.9) and lognormally distributed surface flux q_0 (from Chan and Govindaraju, 2001, with permission from ASCE)

	a	b	log q_0
Mean	0.45	4.2×10^{-4}	−1.73
Standard deviation	0.02	3.7×10^{-4}	0.82

From (10.6.8) the field solute concentration becomes

$$C(z,t) = C_0 \left\{ H\left[Q(t) - \frac{a}{b}\left(1 - e^{-bz}\right)\right] - H\left[Q(t) - Q_0 - \frac{a}{b}\left(1 - e^{-bz}\right)\right]\right\} \tag{10.6.11}$$

Equations (10.6.10) and (10.6.11) can now be untilized for analysis by interval arithmetic based on the random nature of a, b and q_0. Note that during the parameterization of θ, the procedure for interval computing method did not call for the consideration of spatial variability of θ in the field. The variability in the solute travel time and solute concentration is the direct result of distribution in θ and q_0.

10.6.4 Stochastic Advective Solute Transport

In Chapter 4, we discussed stochastic stream tube models. Here we briefly describe an application where the flow properties in the streamtube vary with location. To compute the mean field-scale solute concentration, we need to first develop the pdfs of soil water storage $\Phi(z)$ and cumulative infiltration $Q(t)$. From the pdfs of $\Phi(z)$ and $Q(t)$, the cdf of solute travel time $T(z)$ can be determined. Finally, the expression for expected value of the solute concentration can be obtained based on (10.6.8).

Kavvas et al. (1996) derived the following explicit solution for the Fokker-Planck equation which can approximate the pdf of $\Phi(z)$:

$$f(\Phi) = \frac{1}{\sqrt{4\pi B(z)}} \exp\left\{ -\frac{1}{2} \frac{[\Phi - G(z)]^2}{2B(z)} \right\} \tag{10.6.12}$$

where $B(z)$ and $G(z)$ are given by

$$B(z) = \int_0^z du \int_0^u d\xi \mathrm{cov}[\theta(u); \theta(u-\xi)] \tag{10.6.13}$$

$$G(z) = \int_0^z \langle \theta(\xi) \rangle \, d\xi = \langle \Phi(z) \rangle \tag{10.6.14}$$

From (10.6.12), it is obvious that $\Phi(z)$ is a Gaussian distribution with $G(z)$ as the mean and $2B(z)$ as the variance.

According to (10.6.4), cumulative infiltration $Q(t)$ is a function of time and local surface flux q_0. Thus, we can determine the pdf of $Q(t)$ from that of q_0. As shown in the previous section, q_0 is lognormal. If $y = \ln q_0$ with mean μ_y and variance σ_y^2, then from (1.1.13)

$$f[Q(t)] = f(y) \left| \frac{dy}{dQ(t)} \right| = \frac{f(y)}{Q(t)} \tag{10.6.15}$$

Now that the pdfs of $\Phi(z)$ and $Q(t)$ are determined, the cdf of solute travel time $T(z)$ can be derived based on (10.6.2). The probability of solute travel time at a depth z being equal to or less than a specified time t is equivalent to the probability of the solute front to be located at a depth greater than z before time t. In terms of (10.6.3), the solute front would pass depth z when the cumulative infiltration exceeded the soil water storage at time t. Thus, we can write the cdf of $T(z)$ as

$$P[T(z) < t] = P[\Phi(z) < Q(t)] \tag{10.6.16}$$

Substituting from (10.6.12) to (10.6.15) in (10.6.16), one obtains

$$P[T(z) < t] = \int_0^\infty S\left(\frac{Q(t) - G(z)}{\sqrt{2B(z)}} \right) f[Q(t)] dQ(t) \tag{10.6.17}$$

where $S(\cdot)$ is the conditional cdf of a standard normal distribution:

$$S(\delta) = \begin{cases} 0, & \delta \le 0 \\ \int_0^\delta \frac{1}{\sqrt{2\pi}} \exp\left(-\frac{x^2}{2}\right) dx, & \delta > 0 \end{cases} \tag{10.6.18}$$

Similarly, $P[T(z) < t - t_0]$ can be written as

$$P[T(z) < t - t_0] = \int_0^\infty S\left(\frac{Q(t) - Q_0 - G(z)}{\sqrt{2B(z)}} \right) f[Q(t)] dQ(t) \tag{10.6.19}$$

Using (10.6.17) and (10.6.19) in equation (10.6.11) yields

$$\begin{aligned} \langle C(z,t) \rangle = & C_0 \left\{ \int_0^\infty S\left(\frac{Q(t) - G(z)}{\sqrt{2B(z)}} \right) f[Q(t)] dQ(t) \right. \\ & \left. - \int_0^\infty S\left(\frac{Q(t) - Q_0 - G(z)}{\sqrt{2B(z)}} \right) f[Q(t)] dQ(t) \right\} \end{aligned} \tag{10.6.20}$$

After the equations to evaluate the cdf of solute travel time and the mean solute concentration are developed, one can apply the model to predict the results of the experiment by constructing the necessary pdfs of $\Phi(z)$ and $Q(t)$ from the experimental observations. Similar to interval computing method, an exponential

function was used (Chan and Govindaraju, 2001) to parameterize the water content $\theta(z)$. But in this stochastic approach, the spatial variability of $\theta(z)$ is accounted for; as a result, not only do we have to obtain the mean water content function, we also need to have the covariance structure of water content in z (vertical) direction. The mean, variance, and covariance functions for $\theta(z)$ were parameterized as

$$\langle \theta(z) \rangle = a_\mu e^{b_\mu z} \tag{10.6.21a}$$

$$\mathrm{var}[\theta(z)] = a_v e^{b_v z} \tag{10.6.21b}$$

$$\mathrm{cov}[\theta(z), \theta(z-\xi)] = \mathrm{var}[\theta(z)] \cdot e^{b_c|\xi|} \tag{10.6.21c}$$

The spatial covariance in (10.6.21c) was estimated from the experimental data as:

$$\begin{aligned}\mathrm{cov}[\theta(z_j), \theta(z_j - \xi_k)] = &\frac{1}{N}\sum_{i=1}^{N}[\theta_i(z_j, t) - \langle (z_j, t)\rangle] \\ &\cdot [\theta_i(z_j - \xi_k, t) - \langle (z_j - \xi_k, t)\rangle]\end{aligned} \tag{10.6.22}$$

where ξ is the separation distance. Table 10.6.2 lists the parameters in (6.21) estimated by least squares fitting of the equations on the field observations. With the complete parameterization of water content, the mean function $G(z)$ and the covariance function $B(z)$ can be rewritten in terms of the estimated parameters in Table 10.6.2 as:

$$G(z) = \frac{a_\mu}{b_\mu}(1 - e^{b_\mu z}) \tag{10.6.23}$$

and

$$B(z) = \frac{a_v}{b_c b_v}(1 - e^{b_v z}) \tag{10.6.24}$$

respectively. The surface flux q_0 on the other hand, as already mentioned earlier, has a lognormal distribution, and the mean and variance of log q_0 are given in Table 10.6.1. From (10.6.15), the pdf of soil water storage $Q(t)$ is given as:

$$f[Q(t)] = \frac{1}{\sqrt{2\pi}\sigma_y Q(t)} \exp\left\{ -\left[\ln\frac{Q(t)}{t} - \mu_y\right]^2 \Big/ 2\sigma_y^2 \right\} \tag{10.6.25}$$

Table 10.6.2. Parameterization for mean, variance and covariance functions in stochastic approach (adapted from Chan and Govindaraju, 2001, with permission from ASCE)

	a	b
Mean function	0.45	-3.9×10^{-4}
Variance function	2.6×10^{-4}	8.7×10^{-3}
Covariance function	N.A.	-0.01

10.6.5 Results and Discussion

Following Chan and Govindaraju (2001), results of solute travel time distribution and the breakthrough curve of mean solute concentration computed by the following methods are presented and compared against each other and with the field observations:

a) Interval computing method
b) Monte Carlo simulations
c) Stochastic theories

In the interval computing approach, an alpha-cut resolution of 0.0005 was set throughout the model calculations. A smaller increment was used in this example than in the previous one because a higher degree of accuracy in computing the first moment was needed to generate the mean breakthrough curve.

Monte Carlo simulations serve as a base comparison for the interval computing method. Instead of constructing idfs for water content parameters a, b and surface flux q_0, random numbers were generated according to the assumed distributions, i.e., a and b are normally distributed and q_0 is lognormal. A much higher number of simulations ($\sim 50,000$) was needed in this case due to the oscillations observed in the breakthrough curve resulting from inadequate number of simulations.

In the stochastic approach, Chan and Govindaraju (2001) computed positive infinite integrals, (10.6.17–20), numerically in the MATLAB environment. The infinite integrals were approximated by computing finite integrals using an adaptive recursive Newton-Cotes 8-panel rule with large upper limit. The upper limit was set to a sufficiently large number without compromising the accuracy of the integration.

Figure 10.6.2 show the observed breakthrough curves at 30-, 60-, 120-, 180-, 240- and 300-cm depths respectively. On the same graphs, the predicted mean breakthrough curves from interval computing method, Monte Carlo simulations, and stochastic theories are also shown.The results and implications from these figures were discussed by Chan and Govindaraju (2001).

When comparing the predictions from interval computing method with those from Monte Carlo simulations and stochastic theories, interval computing method tends to produce slightly smaller peaks. Although Figure 10.6.2 only shows the breakthrough to a upper time limit of 1400 hours, it is expected that the loss in area due to smaller peak is compensated by a more pronounced tailing effect. Evidence of this can be seen in Figure 10.6.2 where interval computing method predicted higher concentrations at the tail of the breakthrough curve. As depth increases, the predicted time to peak by interval computing method becomes smaller compared with results from other methods. The more intense tailing and the shift in peaking time are caused by overestimation of variance in computing the distribution of travel times. At smaller depths, the overestimation in travel time is greater at the leading tail of the idf; thus, the tailing effect in the breakthrough curve is more obvious. However, as depth increases, overestimation at the left side of the idf becomes bigger, and that translates into a shift in the peak.

The computation of moments from interval computing method showed promise as an alternative to conventional stochastic computations. Surprisingly, due to the

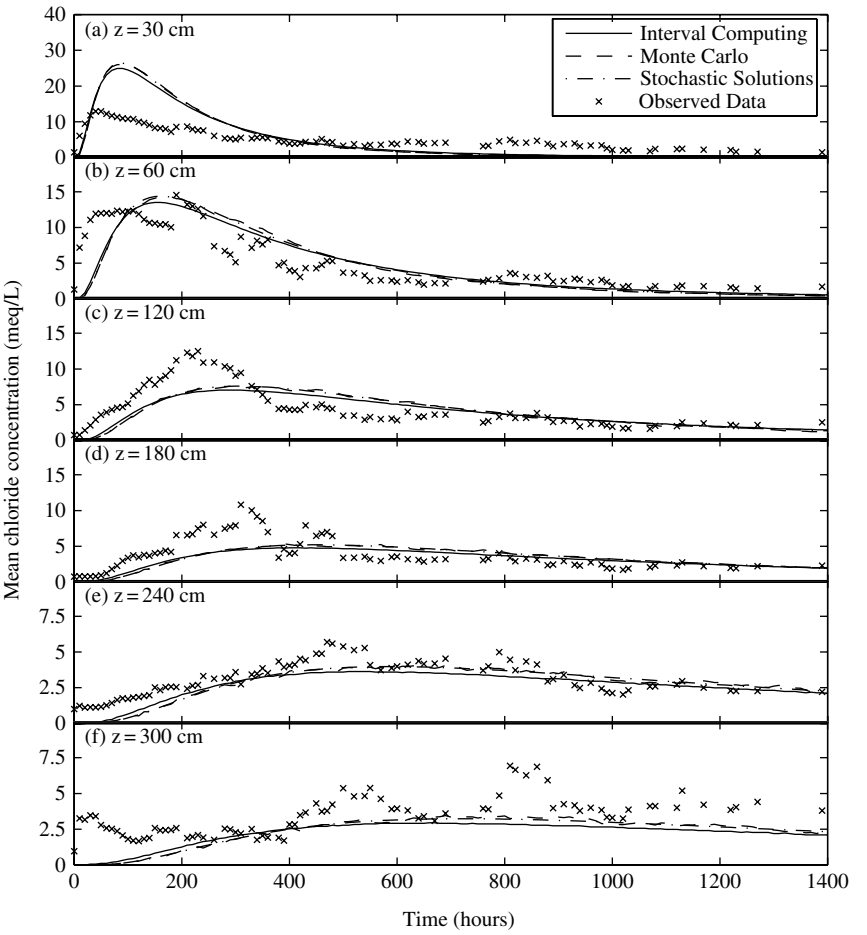

Figure 10.6.2. Comparison of predicted and observed mean solute concentrations at field scale at: (a) 30-cm depth; (b) 60-cm depth; (c) 120-cm depth; (d) 180-cm depth; (e) 240-cm depth; (f) 300-cm depth (from Chan and Govindaraju, 2001, with permission from ASCE)

requirement of evaluating infinite integrals with iterations, the stochastic approach required the most computing time out of the three methods studied. As a large number of simulations was performed in the Monte Carlo approach (Chan and Govindaraju, 2001), interval computing method with an alpha resolution of 0.0005 was more efficient. Again, the efficiency of interval computing method was hampered by the time-consuming task in computing the moments; otherwise the method would have a clear advantage with less computation requirement.

CHAPTER 11

MOMENT ANALYSIS FOR SUBSURFACE STORM FLOW

11.1. INTRODUCTION

Subsurface drainage and associated contaminant transport forms an important element of stream water quality, especially during dry-weather flows where this mechanism is primarily responsible for maintaining streamflow. Beven (1981) points out that subsurface flow is the dominant mechanism of hydrologic response when soils possess a high permeability inherently, or the soil structure has macropores and preferential flow paths. Further, when steep gradients exist either because of slope on the hillslopes or because of groundwater mounds, subsurface flow and associated contaminant transport become important. A proper analysis of the flow problem involves a combined solution of Richards equation for unsaturated vertical flow combined with unconfined saturated flow to describe the horizontal component. However such an approach would typically require a numerical solution.

The problem of tile drain flow can also be cast as one of subsurface drainage. However, for simplicity, this approach has largely ignored the unsaturated flow that acts as recharge to the water table. Consequently, the focus has been on finding simplified solutions of unconfined saturated flow using the Boussinesq equation (Childs, 1971; Chapman and Dressler, 1984; Brutsaert and El-Kadi, 1986). Steady state solutions have been investigated by Yates et al. (1985), while Brutsaert (1994) linearized this equation to develop the unit response from subsurface flow. Beven (1981, 1982) and Germann and Beven (1985) analyzed this problem using the kinematic wave approximation, however this technique is only applicable for unconfined flows with a steep impermeable layer at the bottom. Stagnitti et al. (1986) used an approximation of Richards equation along a slope and found the model performance to be in reasonable agreement with the two-dimensional solution of Richards equation and experimental observations. Mizumura (2002), Schmidt (2002) and Govindaraju (2003) have used simplified models based on series expansions. In the context of subsurface flow to tile drains, steady state (Van der Ploeg et al., 1999) and transient solutions (Youngs, 1999) have been discussed in the literature.

Transfer functions have been commonly employed to model solute transport through soils (Jury, 1982; Jury et al., 1982; Jury et al., 1986; White et al., 1986; Sposito et al., 1986). The basic argument behind using transfer functions is that field soils are very complex because of heterogeneity in hydraulic properties, presence of preferential flow paths, impeding layers, and other factors. As a result, characterization of spatial variability becomes all but impossible, thereby rendering mechanistic and stochastic models to be of limited use. As discussed in Chapter 4, transfer functions have been based on the idea of developing a travel time probability density function (pdf) of solute particles from source to a control plane.

In this chapter, we will seek analytical solutions under suitable approximations to develop process-based transfer functions and associated moments. The goals of this chapter are to study mathematical models for tile drain response to rainfall events using a mechanistic approach leading to the development of transfer functions, and to present expressions for moments. The travel time pdfs of water and solute molecules are often assumed to be similar, so that similar analyses could be implemented for solute breakthrough curves.

We adopt the hydraulic theory of ground water (Dupuit, 1863) for unsteady flow in unconfined aquifers as given by Boussinesq (1877). Using Figure 11.1.1 as a definition sketch, the horizontal water flux throughout the saturated thickness is given as

$$q = -Kh\left[\frac{\partial h}{\partial x}cos\gamma + sin\gamma\right] \tag{11.1.1}$$

where q is the flow rate in the x-direction per unit width of the aquifer, K is the saturated hydraulic conductivity, γ is the angle determining the slope of the impermeable layer at the bottom, and $h(x, t)$ is the saturated thickness as shown in Figure 11.1.1. Combining (11.1.1) with the continuity equation

$$S\frac{\partial h}{\partial t} + \frac{\partial q}{\partial x} = 0 \tag{11.1.2}$$

yields the Boussinesq equation (Brutsaert, 1994)

$$\frac{\partial h}{\partial t} = \frac{K}{S}\left[\cos\gamma\frac{\partial}{\partial x}\left(h\frac{\partial h}{\partial x}\right) + \sin\gamma\frac{\partial h}{\partial x}\right] \tag{11.1.3}$$

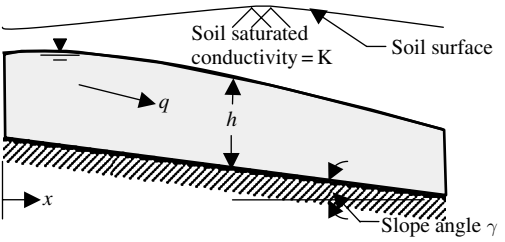

Figure 11.1.1. Definition sketch for subsurface flow along a sloping surface

where S is the porosity that is available for drainage from saturated conditions.

Equation (11.1.3) is nonlinear and does not admit analytical solutions in general, and simplifications have been sought for different approaches. The kinematic wave approach (Henderson and Wooding, 1964; Beven, 1981, 1982; Germann and Beven, 1985) ignores the gradient term in (11.1.1), so that flow occurs only by gravity, and would not be applicable for cases of a horizontal impermeable base.

11.2. MOMENTS FOR LINEARIZED SUBSURFACE DRAINAGE WITH NO RECHARGE

Brutsaert (1994) presented a linearized solution to (11.1.3) under the end conditions of

$$h(x,0) = D, \quad 0 < x < L \tag{11.2.1}$$

$$h(0,t) = 0, \quad t > 0 \tag{11.2.2}$$

$$q(L,t) = 0, \quad t > 0 \tag{11.2.3}$$

The boundary condition of (11.2.3) implies a no flow condition at $x = L$ suggesting the presence of a subsurface divide. The boundary condition of (11.2.2) imposes a zero thickness of saturated flow which is a good approximation when $D\tan\gamma << L$, a condition that is easily met in most cases. The focus is on obtaining a good representation of the outflow rate from the aquifer. Brutsaert (1994) linearized the expression for the flux (11.1.1) as

$$q = -\left[KpD\cos\gamma\frac{\partial h}{\partial x} + Kh\ \sin\gamma\right] \tag{11.2.4}$$

where p is a factor to account for linearization, i.e. $pD \simeq h$. Brutsaert and Nieber (1977) suggest a value of $p = 1/3$, while a value of $p = 1/2$ is perhaps more reasonable for flow between two parallel channels. Defining new variables $\beta = D - h$, $\tilde{K} = KpD\cos\gamma/S$, and $U = K\sin\gamma/S$, the linearized equation has the same form as the advection–dispersion equation

$$\frac{\partial\beta}{\partial t} = \tilde{K}\frac{\partial^2\beta}{\partial x^2} + U\frac{\partial\beta}{\partial x} \tag{11.2.5}$$

and the boundary conditions are

$$\beta(x,0) = 0, \quad 0 < x < L \tag{11.2.6}$$

$$\beta(0,t) = D, \quad t > 0 \tag{11.2.7}$$

$$\tilde{K}\frac{\partial\beta(L,t)}{\partial x} = U(D-\beta), \quad t > 0 \tag{11.2.8}$$

Defining the Laplace transform of β as

$$\hat{\beta}(x; s) = \int_0^\infty e^{-st}\beta(x, t)dt \tag{11.2.9}$$

Equation (11.2.5) becomes

$$\tilde{K}\frac{d^2\hat{\beta}}{dx^2} + U\frac{d\hat{\beta}}{dx} - s\hat{\beta} = 0 \tag{11.2.10}$$

and the boundary conditions are

$$\hat{\beta}(0; s) = D/s \tag{11.2.11}$$

$$\tilde{K}\frac{d\hat{\beta}(L; s)}{dx} = U\left(\frac{D}{s} - \hat{\beta}\right) \tag{11.2.12}$$

The solution for $\hat{\beta}(x; s)$ is provided by Brutsaert (1994) as

$$\begin{aligned}\hat{\beta}(x; s) = De^{-a(L-x)}\{&[be^{aL} - 2a\sinh(bL)]\cosh[b(L-x)] \\ &+ [2a\cosh(bL) - ae^{aL}]\sinh[b(L-x)]\}/\{s[b\cosh(bL) - a\sinh(bL)]\}\end{aligned} \tag{11.2.13}$$

where $a = -U/2\tilde{K}$ and $b = \left[\left(\frac{U}{2\tilde{K}}\right)^2 + \left(\frac{S}{\tilde{K}}\right)\right]^{1/2}$.

Brutsaert (1994) found the inverse Laplace transform of $\hat{\beta}(x; s)$ and used it to estimate the out flow discharge at $x = 0$ as

$$q(0, t) = \frac{2D\tilde{K}S}{L^3}\sum_{n=1}^{\infty}\frac{z_n^2[(2e^{-aL}\cos z_n) - 1]\exp[-\tilde{K}(z_n^2/L^2 + U^2/4\tilde{K}^2)t]}{[z_n^2/L^2 + U^2/(4\tilde{K}^2) + U/(2\tilde{K}L)]} \tag{11.2.14}$$

where the z_n are the roots of the equation

$$\tan z = \frac{z}{aL} \tag{11.2.15}$$

Since the outflow discharge is treated as the hydrologic response, it is useful to construct the moments of this function. As in Chapter 5, absolute temporal moments are defined about the origin as

$$\mu_n = \int_0^\infty t^n q(0, t)dt \tag{11.2.16}$$

Given the complicated nature of $q(0, t)$ in (11.2.14), Aris' method can be adopted. Defining the Laplace transform of $q(0, t)$ as

$$\hat{q}(s) = \int_0^\infty e^{-st}q(0, t)dt \tag{11.2.17}$$

we have

$$\mu_n = (-1)^n \frac{d^n}{ds^n} [\hat{q}(s)] |_{s=0} \tag{11.2.18}$$

From (11.2.14), taking Laplace transforms

$$\hat{q}(s) = \tilde{K} S \frac{d\hat{\beta}(x; s)}{dx} |_{x=0} \tag{11.2.19}$$

Using this analysis and setting $b_0 = -a$, Brutsaert (1994) obtained the following expressions for the first few moments

$$\mu_0 = -SDL \tag{11.2.20}$$

$$\mu_1 = \frac{-SD}{4b_0^3 \tilde{K}} \left[b_0 L e^{-2b_0 L} + b_0^2 L^2 - e^{-b_0 L} \sin h(b_0 L) \right] \tag{11.2.21}$$

$$\mu_2 = \frac{SD}{4b_0^5 \tilde{K}^2} \left[-\frac{1}{3} b_0^3 L^3 - b_0^2 L^2 - \left(\frac{1}{2} + \frac{5}{2} e^{-2b_0 L} \right) + b_0 L \left(\frac{1}{2} - 2e^{-2b_0 L} - \frac{1}{2} e^{-4b_0 L} \right) + \frac{3}{4} - \frac{1}{2} e^{-2b_0 L} - \frac{1}{4} e^{-4b_0 L} \right] \tag{11.2.22}$$

For a horizontal slope ($\gamma = 0$), the solution for subsurface drainage simplifies to (DIngman, 2002)

$$q(0, t) = \frac{D^2 K}{L} \sum_{i=1}^{\infty} exp \left[-\frac{(2i-1)^2 \pi^2 KD}{8L^2 S} t \right] \tag{11.2.23}$$

Since successive terms decrease in importance very rapidly, a fairly good approximation is available with retention of only the first term as

$$q(0, t) \tilde{-} \frac{D^2 K}{L} exp \left[-\frac{1 \cdot 23 KD}{L^2 S} t \right] \tag{11.2.24}$$

If (11.2.23) is used to calculate moments of the outflow discharge, then we obtain

$$\mu_0 = \frac{8SLD}{\pi^2} \sum_{i=1}^{\infty} \frac{1}{(2i-1)^2} \tag{11.2.25}$$

$$\mu_1 = \frac{64L^3 S^2}{\pi^4 K} \sum_{i=1}^{\infty} \frac{1}{(2i-1)^4} \tag{11.2.26}$$

$$\mu_2 = \frac{1024L^5 S^3}{\pi^6 K^2 D} \sum_{i=1}^{\infty} \frac{1}{(2i-1)^6} \tag{11.2.27}$$

The analysis can be further simplified in the case of very steep and thin aquifers. This generally implies that all the flow lines, including the water table, are parallel to the impermeable bottom. We know that the total volume of water available for drainage at any time is

$$\forall = SLh \tag{11.2.28}$$

where $h(x, t) = h(t)$. The discharge from the aquifer is given as

$$q(0, t) = Kh(t) \tan \gamma \tag{11.2.29}$$

From overall continuity we have

$$\frac{d\forall}{dt} = -q(0, t) \tag{11.2.30}$$

so that hillslope drainage is given by

$$q(0, t) = KD \tan \gamma \exp\left(-\frac{Ktan\gamma}{SL} t\right) \tag{11.2.31}$$

where we have used the condition $h(t = 0) = D$. The moments for this case are obtained as

$$\mu_0 = SLD \tag{11.2.32}$$

$$\mu_1 = \frac{DS^2L^2}{Ktan\gamma} \tag{11.2.33}$$

$$\mu_2 = \frac{2DS^3L^3}{K^2tan^2\gamma} \tag{11.2.34}$$

One should keep in mind that (11.2.23), (11.2.24) and (11.2.31) are not probability density functions, unless properly normalized with their respective zero-th moments.

11.3. SUBSURFACE DRAINAGE WITH LATERAL INFLOW

The previous section dealt with subsurface drainage from a slope initially filled to a constant depth D as in (11.2.1). In this section, we consider the problem of subsurface drainage when the water table receives recharge from infiltrating and redistributing water. Henderson and Wooding (1964) had analyzed the problem of Boussinesq equation with lateral inflow assumed constant under the kinematic wave approximation. This was further extended by Beven (1981), who defined a dimensionless parameter to determine the conditions when the kimematic wave approximation would be valid. Beven (1982) extended the analysis of subsurface storm flow using this approach to include vertical unsaturated flow contributions

to the saturated horizontal flow. However, this study utilized a pre-defined form of variation of soil properties in the vertical direction, and is also not amenable to moment analysis.

Here we analyze the problem of subsurface drainage in the context of water movement to tile drains. These are very commonly used in croplands. Constructed of clay tiles or corrugated plastic, these drain pipes are used to transfer excess water from the subsurface to an outlet, typically a surface drainage ditch. These systems are also known to expedite the transport of nutrients and pesticides to surface waters, and their presence affects the hydrologic response of the watershed in a significant manner. Depending on factors such as soil type, storm characteristics, and topography, tile drains can either increase or decrease the peak flow at the outlet of the watershed. Once again, the expectation is that water and solute molecules will follow similar paths, so that tile drain hydrographs serve as a surrogate for breakthrough curves.

We assume a horizontal bottom for simplicity as in Figure 11.3.1, and incorporate a recharge rate $i(t)$. For this case, Boussinesq's equation (11.1.3) is written as

$$S\frac{\partial h}{\partial t} = \frac{\partial}{\partial x}\left(Kh\frac{\partial h}{\partial x}\right) + i \tag{11.3.1}$$

under the following end conditions

$$\frac{\partial h}{\partial x} = 0 \; at \; x = 0 \tag{11.3.2a}$$

$$h(L, t) = a \tag{11.3.2b}$$

$$h(x, 0) = a \tag{11.3.2c}$$

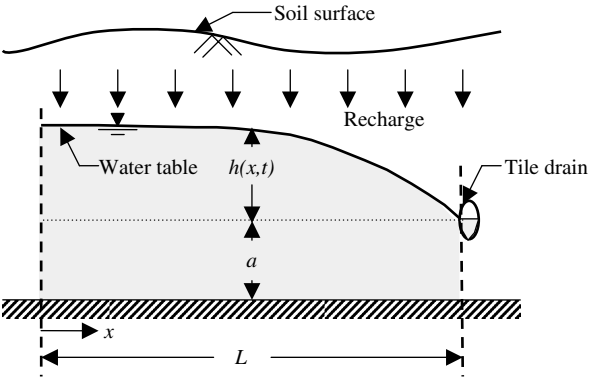

Figure 11.3.1. Schematic picture of the tile drain problem and parameter definition (vertical scale has been exaggerated)

Following Schmidt (2002), the following dimensionless quantities are defined

$$X = \frac{x}{L}; H = \frac{h}{LS}; T = \frac{tK}{L}; A = \frac{a}{LS}; \lambda = \frac{i}{KS^2}; \overline{Q} = \frac{Q}{iL} \tag{11.3.3}$$

Substituting these non-dimensional parameters into (11.3.1), the non-dimensional governing differential equation becomes,

$$\frac{\partial H}{\partial T} = \frac{\partial}{\partial X}\left(H\frac{\partial H}{\partial X}\right) + \lambda \tag{11.3.4}$$

As (11.3.4) is nonlinear, exact analytical solutions are not available for arbitrary λ. A Fourier cosine series (see Chapter 3) is adopted as a trial solution to represent the non-dimensional height of the water table (Govindaraju et al., 1988; Mizumura, 2002; Schmidt, 2002; Govindaraju, 2003) as

$$H(X, T) = A + \sum_{n=1}^{N} H_n(T)\cos\left(\frac{2n-1}{2}\pi X\right) \tag{11.3.5}$$

with N tending to ∞. From (11.3.5), the one-term approximation to the Fourier series solution ($N = 1$) can be written as follows,

$$H(X, T) = A + H_1(T)\cos\left(\frac{\pi X}{2}\right) \tag{11.3.6}$$

The partial derivative of H with respect to T can be substituted into (11.3.4) and integrated from $X = 0$ to $X = 1$. The solution of the resulting equation defines the maximum water table height as a function of T as

$$H_1(T) = \frac{2\lambda}{\pi A} - \frac{2}{\pi A}\left(\lambda - \frac{\pi A}{2}H_0\right)e^{\frac{-\pi^2 A}{4}(T-T_0)} \tag{11.3.7}$$

where, $H_0 = H_1(T_0)$. The dimensionless discharge at the tile drain is found by substituting the non-dimensional parameters into Darcy's equation (11.1.1) for $\gamma = 0$,

$$\overline{Q} = \frac{\pi A}{2\lambda}H_1(T) \tag{11.3.8}$$

It is expected that the series solution of (11.3.5) will converge rapidly. Setting $N = 2$ in (11.3.5), the dimensionless water table height is,

$$H(X, T) = A + H_1(T)\cos\left(\frac{\pi X}{2}\right) + H_2(T)\cos\left(\frac{3\pi X}{2}\right) \tag{11.3.9}$$

Similar to the one-term solution, the partial derivative of (11.3.9) with respect to T can be substituted into (11.3.4) and integrated from $X = 0$ to $X = 1$, to yield

$$\frac{2}{\pi}\frac{\partial H_1}{\partial T} - \frac{2}{3\pi}\frac{\partial H_2}{\partial T} = A\left(\frac{-\pi}{2}H_1 + \frac{3\pi}{2}H_2\right) + \lambda \tag{11.3.10}$$

Since there are two unknowns, H_1 and H_2 a second equation is needed. This equation is found by again substituting (11.3.9) into (11.3.4) and then integrating from $X = 0.5$ to $X = 1.0$. After integration and simplification, the following expression is obtained,

$$\frac{\sqrt{2}}{\pi}\frac{\partial H_1}{\partial T} + \frac{\sqrt{2}}{3\pi}\frac{\partial H_2}{\partial T} = \frac{-\pi}{4}H_1^2 + \frac{3\pi}{4}H_2^2 - \frac{\pi}{2}H_1H_2 - \frac{\pi A}{2\sqrt{2}}H_1 - \frac{3\pi A}{2\sqrt{2}}H_2 + \frac{\lambda}{2} \tag{11.3.11}$$

Equations (11.3.10) and (11.3.11) can be solved using the method of finite differences in time. In what follows, the superscripts T_1 and $T_2 (T_2 > T_1)$ indicate values at the beginning and end of a time step $\Delta T (= T_2 - T_1)$. The finite difference solution utilizes a weighting factor Φ (note, $0.5 < \Phi \leq 1.0$ for unconditional stability). Schmidt (2002) found expressions for $H_1^{T_2}$ and $H_2^{T_2}$ as,

$$H_2^{T_2} = \alpha^* H_1^{T_2} + \beta \tag{11.3.12}$$

where,

$$\alpha^* = \frac{\dfrac{-2}{\pi\Delta T} - \dfrac{A\pi\Phi}{2}}{\dfrac{-2}{3\pi\Delta T} - \dfrac{3\pi A\Phi}{2}} \tag{11.3.13}$$

$$\beta = \frac{\left(\dfrac{2}{\pi\Delta T} - \dfrac{A\pi}{2}(1-\Phi)\right)H_1^{T_1} + \left(\dfrac{3\pi A(1-\Phi)}{2} - \dfrac{2}{3\pi\Delta T}\right)H_2^{T_1} + \Phi\lambda^{T_2} + (1-\Phi)\lambda^{T_1}}{\dfrac{-2}{3\pi\Delta T} - \dfrac{3\pi A\Phi}{2}} \tag{11.3.14}$$

Note that A and λ in the above expressions are the dimensionless quantities defined in (11.3.3). The solution for $H_1^{T_2}$ is a quadratic equation in the form of (Schmidt, 2002)

$$H_1^{T_2} = \frac{-b + \sqrt{b^2 - 4ac}}{2a} \tag{11.3.15}$$

where,

$$a = \frac{\pi\Phi}{4}\left(-3\alpha^{*^2} + 2\alpha^* + 1\right) \tag{11.3.16a}$$

$$b = \frac{\sqrt{2}}{\pi\Delta T}\left(1 + \frac{\alpha^*}{3}\right) + \frac{\pi\Phi}{2}\left(\beta + \frac{A}{\sqrt{2}} + \frac{3A\alpha^*}{\sqrt{2}} - 3\beta\alpha^*\right) \tag{11.3.16b}$$

$$c = \frac{\pi(1-\Phi)}{4}\left[\left(H_1^2\right)^{T_1} - 3\left(H_2^2\right)^{T_1}\right] + \left(\frac{3\pi A(1-\Phi)}{2\sqrt{2}} - \frac{\sqrt{2}}{3\pi\Delta T}\right)H_2^{T_1} + \left(\frac{\pi A(1-\Phi)}{2\sqrt{2}} - \frac{\sqrt{2}}{\pi\Delta T}\right)H_1^{T_1} + \frac{\pi(1-\Phi)}{2}H_1^{T_1}H_2^{T_1} + \frac{\sqrt{2}\beta}{3\pi\Delta T} - \frac{3\pi\Phi\beta^2}{4} + \frac{3\pi A\Phi\beta}{2\sqrt{2}} - \frac{\Phi\lambda^{T_2}}{2} - \frac{(1-\Phi)\lambda^{T_1}}{2} \tag{11.3.16c}$$

The process of solving for the flow rate at the tile drain follows the same logic used in the one-term solution. The dimensionless discharge can be expressed in terms of $H_1(T)$ and $H_2(T)$ as,

$$\overline{Q} = \frac{A\pi}{2\lambda}\left[H_1(T) - 3H_2(T)\right] \tag{11.3.17}$$

The performance of the one- and two- term Fourier approximations was evaluated in detail by Stillman et al. (2006)

11.4. TRANSFER FUNCTION APPROACH FOR SUBSURFACE DRAINAGE

11.4.1 Theoretical Development

We now develop a transfer function for the problem described in the previous section by following Arabi et al. (2006). Earlier, Utermann et al. (1990) utilized a combination of two gamma functions (for preferential flow paths and for matrix flow) for the travel time pdf of vertical unsaturated solute movement. This was convoluted with an exponential travel time pdf for solute movement in the horizontal saturated portion towards the tile drain to develop the overall transfer function for application to solute movement at the field scale. Using this model, simulations were conducted for several pesticides under hypothetical soils to interpret the results in the context of a screening model.

Here we initially follow the Fourier series solution approach of the previous section. We deal with prediction of the hydrograph alone to illustrate this method. Rather than assuming a distribution based purely on fitting to experimental data, wedemonstrate how the transfer function may be developed from an approximate

analysis of the problem so that parameters of the model can be more easily interpreted in terms of averaged properties at the field scale. The transfer function of Utermann et al. (1990) allows for a fraction of solute to arrive at the tile drain immediately after water is applied on the soil surface. However, the water that is applied at the soil surface does not reach the tile drain immediately even when preferential flow paths are engaged, and nor does the associated solute. There is a time lag, in the order of hours, before the tile drain hydrograph is initiated in response to rainfall events. This time lag can be explicitly represented into the transfer function for water movement, as shown in this section.

Adopting a hydraulic approach for unsteady unconfined flow, the water flux in the x-direction throughout the saturated thickness is given by (see Figure 11.3.1)

$$Q(x,t) = -K(h+a)\frac{\partial h}{\partial x} \tag{11.4.1}$$

We again express the flow depth, h, in the form of an infinite Fourier series.

$$h(x,t) = a + \sum_{n=1}^{\infty} h_n(t)\cos\frac{n\pi x}{2L} \tag{11.4.2}$$

In practice, only the first few terms of the infinite series are adopted in (11.4.2). Schmidt (2002) studied this problem in detail, and specifically examined the role of higher terms. It was concluded that the solution obtained for $n = 1$ was adequate, as including higher terms changed the solution to a small degree only. In any case, these higher order corrections tend to be smaller than the 'noise' exhibited by field observations. Therefore, for simplicity, the following approximate model is adopted

$$h(x,t) \cong a + h_1(t)\cos\frac{\pi x}{2L} \tag{11.4.3}$$

Furthermore, in order to develop the transfer function, the unit response of the horizontal saturated flow component is achieved by setting $i(t) = \delta(t)$, i.e. a Dirac input, in (11.3.1). This implies that a unit volume of water is instantaneously added per unit area over the water table. Then substitution of (11.4.3) into (11.3.1) and integrating under the end conditions of (11.3.2) yields the tile drain response to an instantaneous unit depth of water in terms of an exponential pdf as (Govindaraju, 2003; Arabi et al., 2006)

$$q(t) = L\tilde{A}\exp(-\tilde{A}t) \tag{11.4.4}$$

where the parameter $\tilde{A}$ is

$$\tilde{A} = \frac{\pi^2 Ka}{4SL^2} \tag{11.4.5}$$

Utermann et al. (1990) also adopted an exponential distribution to model the resident time distribution of solute particles in the saturated flow part.

In order to relate the tile drain response to infiltrated water, the next step is to determine the lateral inflow function $i(t)$ that would result if a certain depth of water,W, were to instantaneously infiltrate into the soil at the soil surface. A sharp front model may be used to determine the depth to the wetting front during redistribution, and to estimate the water flux to the water table. The unsaturated soil hydraulic conductivity is described by a power-law relationship (Charbeneau, 2000),

$$K\left(S_e\right) = KS_e^{\varepsilon} \tag{11.4.6}$$

where S_e is a normalized soil water content defined by the ratio,

$$S_e = \frac{\theta - \theta_{init}}{\theta_s - \theta_{init}} \tag{11.4.7}$$

In the expression above, θ is the volumetric soil water content, θ_{init} is the soil water content at which drainage by macropore flow will cease, θ_s is the saturated water content, and the exponent ε is a model parameter. Just before redistribution starts, the soil is saturated to a depth $z_{in} = \frac{W}{\theta_s - \theta_{init}}$, where W is the infiltrated volume expressed as a depth. From redistribution theory of a sharp front, the value of S_e decreases as the wetting front progresses deeper into the soil. If at a certain time after redistribution begins, the wetting front is at a depth z_f, then the normalized water content is,

$$S_e = \frac{W}{\left(\theta_s - \theta_{init}\right) z_f} = \frac{W}{z_f \Delta\theta}, \;\; z \le z_f \tag{11.4.8}$$

where $\Delta\theta$ is defined as $\theta_s - \theta_{init}$. Since the total volume of redistributed water remains constant during redistribution, the continuity equation is

$$\frac{dW}{dt} = 0 \tag{11.4.9}$$

Darcy's law for the sharp front model takes the form

$$K(S_e)dt = \Delta\theta.S_e.dz_f \tag{11.4.10}$$

Using (11.4.6) to solve (11.4.9) and (11.4.10), and then using the value of S_e from (11.4.8), the time for the wetting front to reach a control plane at a depth z from the soil surface is,

$$t_0 = \left(\frac{W}{\varepsilon K}\right)\left[\left(\frac{1}{S_e}\right)^{\varepsilon} - 1\right] \tag{11.4.11}$$

Equation (11.4.11) clearly shows the time lag that would occur for water that has infiltrated during a rainfall event to start contributing to horizontal saturated flow.

Once the wetting front has reached the water table, the recharge rate i can be found as a function of time and depth to the water table z,

$$i(t) = \frac{\Delta\theta K z}{W\left[1^{+}\frac{\varepsilon K t}{W}\right]^{1+\frac{1}{\varepsilon}}} \tag{11.4.12}$$

It is this recharge rate that acts as a source in (11.3.1) governing saturated water flow towards the tile. It is noted that $\frac{\varepsilon K t}{W} >> 1$, which is easily satisfied especially for $t > t_0$, so that the lateral inflow function can be compactly represented as

$$i(t) = \begin{cases} 0, & t < t_0 \\ \dfrac{B}{t^g}, & t \geq t_0 \end{cases} \tag{11.4.13}$$

with t_0 defined as in (11.4.11), and

$$B = \frac{\Delta\theta . z}{\varepsilon^g K^{1/\varepsilon}} W^{1/\varepsilon}, \; g = 1 + 1/\varepsilon \tag{11.4.14}$$

Thus for a given depth of infiltrated water W, the lateral inflow function to saturated flow is proportional to $W^{1/\varepsilon}$. This implies that the lateral inflow function can be scaled and superimposed in terms of $W^{1/\varepsilon}$ for multiple rainfall/infiltration events.

The tile drain hydrograph for an infiltrated depth of water W can now be obtained from convolution as

$$Q(t) = \int_{t_0}^{t} i(\tau) q(t-\tau) d\tau = \int_{t_0}^{t} \frac{LB}{\tau^g} \tilde{A} \exp\left\{-\tilde{A}(t-\tau)\right\} d\tau, \; t > t_0 \tag{11.4.15}$$

This integral has no closed form solution for arbitrary values of g in (11.4.14). Given that (11.4.6) is in the form of the Brooks-Corey model, ε can be written as (Rawls et al., 1993)

$$\varepsilon = 3 + \frac{2}{\tilde{\lambda}} \tag{11.4.16}$$

where $\tilde{\lambda}$ is soil water retention parameter that can theoretically range from 0 to 1, but exceeds 0.5 in only very sandy soils. Consequently, the value of $g \to 1.0$ for most soils, and in fact achieves a high value of only 1.14 for very sandy soils. For $g = 1$, the tile drain response to a volume of water W that instantaneously infiltrates into the soil at $t = 0$ is given by

$$\begin{aligned} \underset{g \to 1}{Q(t)} &= \int_{t_0}^{t} \frac{LB'}{\tau} \tilde{A} \exp\left\{-\tilde{A}(t-\tau)\right\} d\tau \\ &= LB' \tilde{A} \exp(-\tilde{A}t) \left\{ \ln(\frac{t}{t_0}) + \sum_{n=1}^{\infty} \frac{\tilde{A}^n (t^n - t_0^n)}{n.n!} \right\}, \quad t > t_0 \end{aligned} \tag{11.4.17}$$

where B' with units of length, has the same magnitude as B when $g = 1$. Equation (11.4.17) is still quite complicated for practical use. It is observed that $\tilde{A} << 1$, (as an example, a conservative estimate using K = 0.1 m/h, a = 1.0m, L = 5.0m, S= 0.2, yields $\tilde{A}$ = 0.05/h), and combined with the negative exponential term, the infinite sum converges very rapidly. For practical purposes the first term of the series is all that is required, so that the response can be approximated by the simple expression

$$\underset{g\to 1}{Q(t)} = \begin{cases} 0, & t < t_0 \\ C\exp(-\tilde{A}t)\left\{\ln\left(\frac{t}{t_0}\right) + \tilde{A}(t-t_0)\right\}, & t \geq t_0 \end{cases} \tag{11.4.18}$$

where $C = LB'\tilde{A}$. Equation (11.4.18) is a three-parameter model of the tile drain response to an instantaneously infiltrated depth of W. It should be noted that C is a scaling parameter. While the analysis resorts to approximations, it serves the useful purpose of determining the form of the transfer function, as opposed to assuming an arbitrary distribution.

11.4.2 Moments and Experimental Results

Arabi et al. (2006) examined the utility of (11.4.18) as a viable transfer function. The Purdue Water Quality Field Station (WQFS), located at the Agronomy Research Center in West Lafayette, IN, is an experimental research facility used to study water quality impacts associated with agricultural practices. The soil at the WQFS is a silty clay loam with glacial till at approximately 2 m below the surface. Among other types of tile drain layouts, the station contains a group of 48 plots, each of which contains a 10 m × 24 m clay lysimeter. About 15 years ago, slurry walls were put in place to create a hydrologically isolated 'box' for each plot so that (11.3.2a) is applicable. For the experimental conditions, the dimensions corresponding to Figure 11.3.1 are $L = 5\,\text{m}$, $a = 0.53\,\text{m}$, and the depth to the water table $z = 1\,\text{m}$. To account for the convergence of flow lines near the tile drain, an equivalent 'ditch depth,' as proposed by Van der Molen and Wesseling (1991), was used in place of the actual depth a from the tile drain to the impervious barrier below.

A set of observed events (hyetograph and recorded tile-drain flow) were selected from the available WQFS data for analysis as indicated in Table 11.4.1 (Arabi et al., 2006). These events contain a mixture of single-burst and multiple-burst rainfall hyetographs. A burst is defined as a series of consecutive hourly rainfall pulses.

To construct the model, the event hyetograph was subdivided into bursts. Since the tile plots satisfy the water balance criterion, the total volume of rainfall for each burst was used for the infiltration volume. Using (11.4.11), the time for the wetting front to reach the water table was calculated, as well as the time-dependent recharge (11.4.12).

The procedure described above allows for the computation of a tile-drain hydrograph resulting from a single burst of rainfall assumed to occur instantaneously at the center of mass of the rainfall hyetograph. Once completed, the hydrographs

Table 11.4.1. Summary of precipitation events

Event	1	2	3	4	5
Date	2/20/1997	3/13/1997	4/8/2002	5/11/2002	5/9/2002
Total Precip.(cm)	3.05	2.97	2.39	3.16	1.14
Number of Bursts	3	1	2	2	1
Flow Duration (hr)	64	54	32	62	17
t_0 (hr): First Burst	4	7	8	6	2
t_0 (hr): Second Burst	11	–	19	22	–
t_0 (hr): Third Burst	31	–	–	–	–
C (cm^2/hr): First Burst	2647000	7687000	3610000	1042000	561600
C (cm^2/hr: Second Burst	90760	–	402500	935100	–
C (cm^2/hr): Third Burst	241700	–	–	–	–

Adapted from Arabi et al., 2006, with permission from Wiley

from individual bursts in an event were superimposed to create a single tile-drain hydrograph for the event.

We now compare model results with data from several events at the Water Quality Field Station (WQFS). A moment-based analysis was adopted for parameter estimation. The $n-$th temporal moment of the tile drain response about time t_0 for an infiltrated depth of water W is

$$\mu_n = \int_{t_0}^{\infty} (t-t_0)^n Q(t)dt = \int_{t_0}^{\infty} (t-t_0)^n C\exp(-\tilde{A}t)\left\{\ln\left(\frac{t}{t_0}\right)+\tilde{A}(t-t_0)\right\}dt \tag{11.4.19}$$

Expressions for the first few temporal moments are obtained as

$$\mu_0 = C\left\{\frac{1}{\tilde{A}}\exp(-\tilde{A}t_0)+\frac{Ei(\tilde{A}t_0)}{\tilde{A}}\right\} \tag{11.4.20}$$

$$\mu_1 = C\left\{\frac{3}{\tilde{A}^2}\exp(-\tilde{A}t_0)+\frac{Ei(\tilde{A}t_0)}{\tilde{A}^2}-\frac{Ei(\tilde{A}t_0)}{\tilde{A}}t_0\right\} \tag{11.4.21}$$

$$\mu_2 = C\left\{\begin{array}{l}\frac{9}{\tilde{A}^3}\exp(-\tilde{A}t_0)-\frac{t_0}{\tilde{A}^2}\exp(-\tilde{A}t_0)- \\ \frac{2t_0}{\tilde{A}^2}Ei(\tilde{A}t_0)+\frac{{t_0}^2}{\tilde{A}}Ei(\tilde{A}t_0)+\frac{2}{\tilde{A}^3}Ei(\tilde{A}t_0)\end{array}\right\} \tag{11.4.22}$$

where $Ei(x)$ is exponential integral and is defined as

$$Ei(x) = \int_x^{\infty}\frac{\exp(t)}{t}dt \tag{11.4.23}$$

The n^{th} normalized moment is defined as (Chapter 5)

$$\mu_n^* = \frac{\mu_n}{\mu_0} \tag{11.4.24}$$

and the second central moment is given by

$$m_2 = \mu_2^* - (\mu_1^*)^2 \tag{11.4.25}$$

The corresponding experimental moments were obtained by numerical integration of the observed data for flow discharge using (11.4.20) and the trapezoidal rule.

Since the transfer function model (11.4.19) is approximate, the parameter C was utilized to equate the zero-th theoretical and experimental moments. Event 2 (of 03/13/1997) was used for calibration (see Figure 11.4.1). Data from plots 13 and 18 were averaged to form the experimental data set for calibration. Arabi et al. (2006) equated the first normalized moment to obtain $\tilde{A}$ and estimated it to be 0.265 h^{-1} for this site. The value of C was obtained from (11.4.21).

Subsequently, Figure 11.4.2 shows the performance of the model in the validation mode. For each of these events, the t_0 value was obtained from observations, the C value was selected from the total amount of water that infiltrated the soil and was recovered in the tile drain hydrograph (which is equal to the total volume of rainfall as there was no surface runoff for these events), and the value of $\tilde{A}$ was maintained at 0.265 hr^{-1} as obtained from calibration. In these figures, tile-drain hydrographs from different plots are shown, along with a curve labeled 'observed' that shows the averaged hydrograph from all the plots. The tile drain hydrograph from the proposed model is also shown in these figures. Examination of these figures indicates that the model is able to replicate the observed results fairly well.

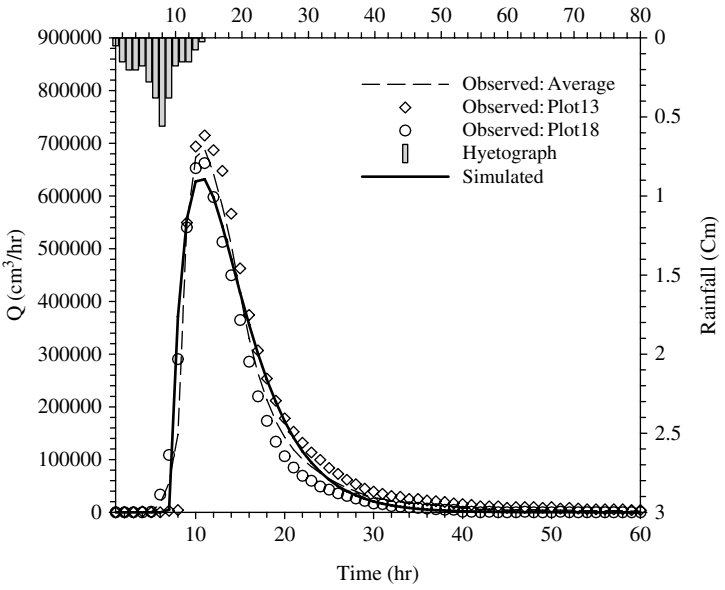

Figure 11.4.1. Comparison of predicted and observed tile drain hydrographs for Even 2 in calibration mode (adapted from Arabi et al., 2006, with permission from Wiley)

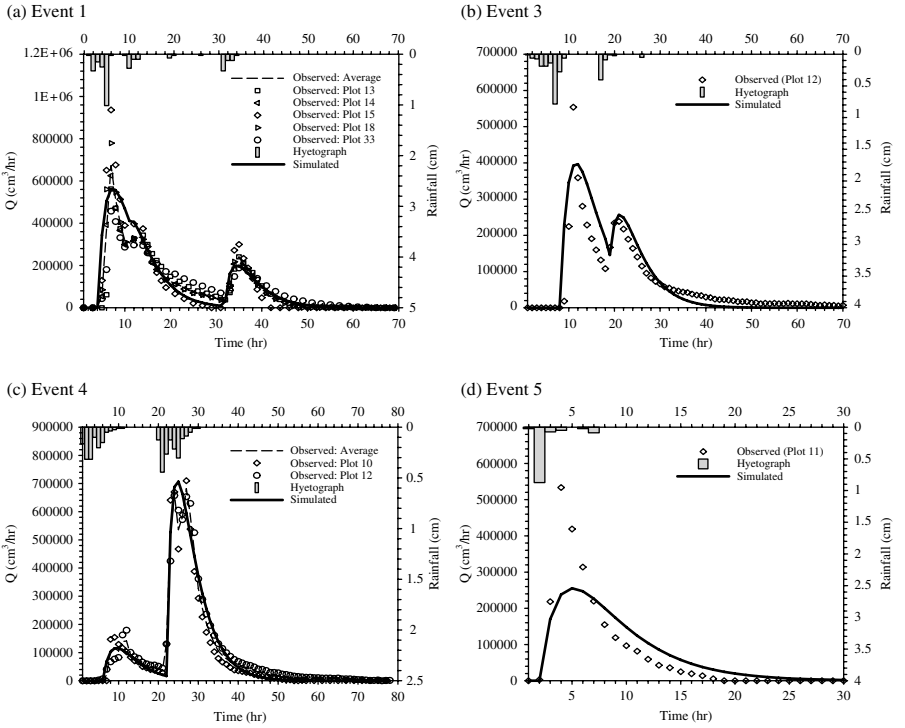

Figure 11.4.2. Comparison of predicted and observed hydrographs for the validation events (adapted from Arabi et al., 2006, with permission from Wiley)

Table 11.4.1 shows basic properties of each event, and the parameter values used for generating the model results.

Arabi et al. (2006) discuss Figures 11.4.1 and 11.4.2 in detail, and conclude that the simple model of (11.4.18) holds promise despite its simplicity. Use of such simple models as a local scale solution would likely help in upscaling to larger heterogeneous tile-drained watersheds.

CHAPTER 12

CONSTRUCTING CONCENTRATION DISTRIBUTIONS FROM MOMENTS

In solute fate and mobility studies, it is often of interest to know the concentration of a solute at any time or any location. This requires that a *continuous solute concentration function* $c(z, t)$ in time (t) and depth (z) be available. Solute concentration distribution as a function of time is called the solute breakthrough curve (BTC) and as a function of soil depth is called the concentration profile (CP). Direct measurement of a BTC or CP is one way to obtain a $c(z, t)$ function. However, it may not be always feasible to make such measurements. Even if it is possible, the measured data is at best discrete. Traditionally, a continuous BTC or a CP may be constructed through these discrete data points if parameters of an *a priori* assumed solute transport model are known. However, as pointed out earlier, formulation of a transport model is difficult for many practical scenarios. Without prior knowledge of a solute transport model, it is possible to draw a continuous curve through observed concentration values using moments if the solute input function is finite. Finite input requirement results from the fact that it is not possible to obtain moments if the $c(z, t)$ function is not a probability distribution. In addition to discrete concentration data, a method of reconstruction of a BTC or a CP from known moments is needed for some specific scenarios where moments may be more readily available than concentration data.

12.1. PROBLEM DEFINITION

Construction of a BTC or a CP from their moments is similar to the classical moment problem first posed by the mathematician T. Stieltjes in 1894. The Stieltjes moment problem consists of obtaining a real or complex valued function $p(x)$ from the sequence $\{\mu_n\}$ with $n = 0,\ 1,\ 2,\ \ldots$ of real or complex numbers such that the domain of $p(x)$ is the interval between 0 and ∞ and μ_n is the n-th moment

$$\mu_n = \int_0^\infty x^n p(x) dx; \quad n = 0, 1, 2, \ldots \tag{12.1.1}$$

of $p(x)$ (Talenti, 1987). Two other form of the moment problem are obtained by changing the interval for the random variable x to range from $-\infty$ to $+\infty$

(Hamburger Moment Problem) and 0 to 1 (Hausdorff Moment Problem, HMP). In Chapter 5, we discussed that both the BTC and CP can be viewed as a probability distribution function (pdf) and the time scale (in temporal moment) or the space scale (in spatial moment) in the dimensionless form would range from 0 to 1 satisfying the requirements for the HMP.

Although a unique solution to the moment problem may be desired, there is no unique method to estimate $p(x)$ from μ_n (Novi Inverardi et al., 2005). The HMP is an ill-posed inverse problem. Formal mathematical proof of this aspect is described in Talenti (1987). A simple mathematical illustration can be seen with the moments of the probability distribution:

$$p(x) = \frac{1}{x\sqrt{2}\pi} \exp[0.5(\ln x)^2]\{1 + a \sin[2\pi \ln(x)]\} \tag{12.1.2}$$

where a is a parameter defined in the interval $[-1, +1]$. It can be shown that the first six moments of this distribution are given by the sequence $\{e^{0.5}, e^{2}, e^{4.5}, e^{8}, e^{12.5}, e^{18}\}$ and are not dependent on the parameter a. In fact, none of the moments of the above distribution depend on the parameter a (Au-Yeung, 2003).

Mathematical analyses of the moment problem suggest that the necessary and sufficient conditions required for the Hamburger, Stieltjes, and Hausdorf moment problems are:

$$D(\mu_0, \mu_1, \mu_2, \ldots, \mu_{2k}) > 0 \qquad k = 0, 1, 2 \ldots \tag{12.1.3}$$

$$\begin{cases} D(\mu_0, \mu_1, \mu_2, \ldots, \mu_{2k} \geq 0 & k = 0, 1, 2 \ldots \\ D(\mu_1, \mu_2, \mu_3, \ldots, \mu_{2k+1}) \geq 0 & k = 0, 1, 2 \ldots \end{cases} \tag{12.1.4}$$

and

$$\begin{cases} D(\mu_0, \mu_1, \mu_2, \ldots, \mu_{2k}) \geq 0 & k = 0, 1, 2 \ldots \\ D(\mu_1, \mu_2, \mu_3, \ldots, \mu_{2k+1}) \geq 0 & k = 0, 1, 2 \ldots \\ D(\mu_0 - \mu_1, \mu_1 - \mu_2, \ldots, \mu_{2k-1} - \mu_{2k}) \geq 0 & k = 0, 1, 2 \ldots \\ D(\mu_1 - \mu_2, \mu_2 - \mu_3, \ldots, \mu_{2k} - \mu_{2k+1}) \geq 0 & k = 0, 1, 2 \ldots \end{cases} \tag{12.1.5}$$

respectively, where D is the Hankel determinant of the moment sequence:

$$D(\mu_0, \mu_1, \mu_2, \ldots, \mu_{2k}) = \begin{vmatrix} \mu_0 & \mu_1 & \mu_2 & \ldots & \mu_k \\ \mu_1 & \mu_2 & \mu_3 & \ldots & \mu_{k+1} \\ . & . & . & \ldots & . \\ \mu_k & \mu_{k+1} & \mu_{k+2} & \ldots & \mu_{2k} \end{vmatrix} \tag{12.1.6}$$

The moment problem becomes determinate when the smallest eigenvalue of the Hankel matrix tends to zero as k approaches infinity (Berg et al., 2002). A simpler

condition for the existence of a unique distribution for the Hamburger moment problem is the Carleman criterion:

$$\sum_{k=1}^{\infty}(\mu_{2k})^{-\frac{1}{2k}} = \infty \tag{12.1.7}$$

Given the ill-posed nature of the problem, construction of $p(x)$ from moments becomes challenging. A satisfactory evaluation of an ill-posed problem requires full set of data including the information on noise and *a priori* information on solution (Talenti, 1987). A solute transport problem generally lacks such information. In general, a BTC or a CP at discrete measurement points is available often without prior knowledge of the contributing flow domain, flow boundaries, or the nature of processes involved. Construction of $p(x)$ from μ_n values is also influenced by the numerical errors involved in μ_n estimation from inherently noisy and incomplete data. Estimation of $p(x)$ itself from a set of basis functions may have numerical instabilities. Under such conditions, finite moments of the discretely measured BTC or CP may be utilized to reconstruct the full-scale BTC or the CP. Ideally, one likes to obtain positive $p(x)$ values with least numerical oscillation. Methods available for such reconstruction may be broadly divided into three groups:

a) Density Matching Method: Here, different statistical density functions are matched with the observed densities through moments
b) Polynomial Summation Method: Here, the desired pdf is expressed as a sum of polynomials of degree N
c) Maximum Entropy Method: The maximization of appropriate entropy functional leads to an expression for the desired pdf.

Some of these approaches are described in the following sections.

12.2. DENSITY MATCHING METHODS

In this method, an assumed probability distribution function is parameterized such that the moments for this distribution match known moments for a specific scenario. Different families of pdfs have been used for this purpose. The Pearson family of curves can assume a wide range of shapes and is commonly applied to estimate a density function using moments. One of the limitations of the Pearson type densities is that only two parameters are used for matching densities requiring only two moments. In addition to the Pearson type densities, Johnson density, and Generalized Lambda Distribution (Au-Yeung, 2003) have also been used for reconstructing pdfs.

12.3. POLYNOMIAL SUMMATION METHODS

12.3.1 Gram-Charlier and Edgeworth Series Approach

The application of orthogonal polynomials to moment problems is based on Pade's approximants (Mead and Papanicolaou, 1984). The technique essentially consists of selecting an appropriate set of basis functions such that a series expansion

of the desired function converges rapidly. For example, one of the widely used polynomial summation approaches is based on the Gram-Charlier Series (GCS) of Type A involving Hermite polynomials (Kendall and Stuart, 1977). In the GCS approach, a density function is expanded in terms of normal density and its derivatives (Bowers, 1966). Hermite polynomial H_n is widely used for constructing chromatographic elution curves (Kubin, 1965; Kucera, 1965; Habel et al., 2002). Recently, Di Marco and Bombi (2001) have summarized several forms of Gram-Charlier series used in chromatographic literature. A chromatographic elution curve is similar to solute BTCs observed in soil. Das et al. (2002) recently showed that Hermite polynomial approach may also be used to construct a solute BTC. The Hermite polynomial approach is similar to the Edgeworth form of Type A series, which was derived using the theory of elementary errors. The Edgeworth form of the series has been applied in hydrologic studies (Chatwin, 1970; Guven et al., 1984).

In the GCS approach, it is assumed that the pdf approaching a Gaussian distribution may be approximated by a truncated sum of orthonormal polynomials such as Hermite polynomials, H_n (Abramowitz and Stegun, 1964):

$$C(\tau) = \sum_{n=0}^{\infty} h_n H_n(\tau)\alpha(\tau) \tag{12.3.1}$$

where $\alpha(\tau)$ is given by (Olive and Grimalt, 1991),

$$\alpha(\tau) = \frac{1}{\sqrt{\pi}} \exp(-\tau^2) \tag{12.3.2}$$

The parameter τ in equation (12.3.2) is the standard normal random variable around the first normal moment μ_1^* and is defined by:

$$\tau = \frac{y - \mu_1^*}{\sqrt{2m_2}} \tag{12.3.3}$$

where m_2 is the second central moment and y represents the time coordinate t for temporal moments and space coordinate x for the spatial moments. The coefficients of H_n are determined from moments of a distribution.

A detailed derivation of equation (12.3.1) is available in Kendall and Stuart (1977). For completeness, we briefly reproduce a few steps of the derivation. Repeated differentiation of equation (12.3.2) shows that the n-th derivative of $\alpha(\tau)$ is a product of a polynomial equation of order n and the function $\alpha(\tau)$ itself. For example, the first three derivatives of $\alpha(\tau)$ yield the following expressions for the derivatives:

$$\begin{aligned} D^1\alpha(\tau) &= (-1)2\tau\alpha(\tau) \\ D^2\alpha(\tau) &= (-1)^2(4\tau^2 - 2)\alpha(\tau) \\ D^3\alpha(\tau) &= (-1)^3(8\tau^3 - 12\tau)\alpha(\tau) \end{aligned} \tag{12.3.4}$$

Equation (12.3.4) shows that the n-th derivative of $\alpha(\tau)$ yields the coefficient for $\alpha(\tau)$, which is a polynomial equation of degree n. This polynomial equation is the Hermite polynomial:

$$(-1)^n D^n \alpha(\tau) = (-1)^n H_n(\tau)\alpha(\tau) \tag{12.3.5}$$

The Taylor series expansion of $\alpha(\tau - u)$ around a variable u and substitution of equation (12.3.5) into the resulting expression leads to

$$\begin{aligned}\alpha(\tau - u) &= \exp(u\tau - \frac{u^2}{2})\alpha(\tau) \\ &= \sum_{j=0}^{\infty} \frac{u^j}{j!}(-1)^j D^j \alpha(\tau) \\ &= \sum_{j=0}^{\infty} \frac{u^j}{j!} H_j(\tau)\alpha(\tau)\end{aligned} \tag{12.3.6}$$

A series expansion of $exp(u\tau - u^2/2)$ term and rearrangement of the coefficients of $\frac{u^j}{j!}$ terms results in specific expressions for the Hermite polynomial for any order n:

$$H_n(\tau) = \sum_{j=0}^{l} \frac{(-1)^j n!}{j!(n-2j)!}(2\tau)^{n-2j} \tag{12.3.7}$$

where $l = n/2$ if n is an even integer and $l = (n-1)/2$ if n is an odd integer. The coefficients h_n in equation (12.3.1) are obtained by multiplying H_r to both sides of equation (12.3.1) and integrating the results in the interval $(-\infty, +\infty)$

$$\int_{-\infty}^{\infty} C(\tau)H_r(\tau)d\tau = \int_{-\infty}^{\infty} \sum_{n=0}^{\infty} h_n H_n(\tau)H_r(\tau)\alpha(\tau)d\tau \tag{12.3.8}$$

Using the orthonormal property of the Hermite polynomial

$$\int_{-\infty}^{\infty} H_r(\tau)H_n(\tau)\alpha(\tau)d\tau = \begin{cases} 0 & n \neq r \\ 2^n n! & n = r \end{cases} \tag{12.3.9}$$

Equation (12.3.8) for $r = n$ simplifies to (Sansone, 1991)

$$\int_{-\infty}^{\infty} C(\tau)H_n(\tau)d\tau = \int_{-\infty}^{\infty} \sum_{n=0}^{\infty} h_n H_n(\tau)H_n(\tau)\alpha(\tau)d\tau = 2^n n! h_n \tag{12.3.10}$$

or

$$h_n = \frac{1}{2^n n!} \int_{-\infty}^{\infty} C(y)H_n\left(\frac{y - \mu_1^*}{\sqrt{2m_2}}\right)\frac{dy}{\sqrt{2m_2}} \tag{12.3.11}$$

Equation (12.3.11) provides a way to estimate the coefficients h_n in terms of moments. It may also be represented in series form:

$$h_n = \frac{\mu_0}{\sqrt{m_2}} \sum_{k=0}^{l} \frac{(-1)^k m_{n-2k} {m_2}^k}{2^k k!(n-2k)!(2m_2)^{n/2}} \tag{12.3.12}$$

The Hermite polynomial function H_n and the coefficients h_n expanded in this fashion may be substituted into equation (12.3.1) to obtain the concentration profile $C(\tau)$. The first six terms of these functions are listed in Table 12.3.1. The selection of the order depends on the skewness of the experimental Pdf. Lupini and Tirabassi (1983) suggested the order $n = 4$ for constructing a Pdf. Di Marco and Bombi (2001) have reported a range of 3–8 for the Gram-Charlier Series expansion and 2–8 for the Edgeworth-Cramer series. With $n = 4$, the Gram-Charlier expansions includes both the skewness and kurtosis parameters for constructing the Pdf allowing some flexibility over a normal density.

The Gram-Charlier (and Edgeworth) expansion efficiently yields the BTC for solutes exhibiting diffusion and fast exchange processes but is very sensitive to the BTCs that show even slight tailing (Vidal-Madjar and Guiochon, 1977). These conditions yield BTCs resembling normal distribution. However, being a polynomial approximation, the GCS method has the drawback of yielding negative values for certain moment combinations. Moreover, it is also not easy to know for which specific analytic condition one obtains a negative density. Some limiting conditions are available to obtain positive densities (Rubinstein, 1998; Jondeau and Rockinger, 2001). Jondeau and Rockinger (2001) have proposed a condition to guarantee positive definiteness of the underlying densities through a numerical method. In addition to negative densities, the GCS approach also yields multimodal densities.

12.3.2 Expansion Methods Based on other Polynomials

Other orthogonal polynomials such as Laguerre polynomials (Bowers, 1966), Legendre polynomials (Talenti, 1987), Pollackzek polynomials (Scalas and Viano, 1993) among others have been used to represent a density function. Similar to the GCS approach, coefficients for these polynomial functions are also estimated using

Table 12.3.1. First six terms of the Hermite polynomials and their coefficients (adapted from Das et al., 2002, with permission from ASCE Press)

$h_0 = \frac{\mu_0}{\sqrt{2m_2}}$	$H_0 = 1$
$h_1 = h_2 = 0$	H_1 and H_2 are not needed in the calculation as $h_1 = h_2 = 0$
$h_3 = \frac{\mu_0 m_3}{3!\,(2m_2)^2}$	$H_3 = (2\tau)^3 - 6(2\tau)$
$h_4 = \frac{\mu_0 \left(m_4 - 3m_2^2\right)}{4!\,(2m_2)^{5/2}}$	$H_4 = (2\tau)^4 - 12(2\tau)^2 + 12$
$h_5 = \frac{\mu_0 \left(m_5 - 10m_3 m_2\right)}{5!\,(2m_2)^3}$	$H_5 = (2\tau)^5 - 20(2\tau)^3 + 60(2\tau)$

moments. For example, Talenti (1987) provided a simple algorithm to construct pdf from known moments using Legendre polynomials:

$$P_N(x) = \sum_{n=0}^{N} \lambda_n L(x) \tag{12.3.13}$$

where $L_0(x)$, $L_1(x)$, $L_2(x), \ldots$ are shifted Legendre polynomials and $\lambda_0, \lambda_1, \lambda_2, \ldots, \lambda_n$ are Fourier-Legendre coefficients given by:

$$\lambda_n = \sum_{j=1}^{n} C_{nj}\mu_j; \qquad n = 0, 1, 2, \ldots, N \tag{12.3.14}$$

The coefficients C_{nj} are those of the shifted Legendre polynomials given by the formula:

$$C_{nj} = (2n+1)^{\frac{1}{2}}(-1)^j \binom{n}{j}\binom{n+j}{j} \tag{12.3.15}$$

Legendre polynomials can also be efficiently estimated by an iterative procedure (Abramowitz and Stegun, 1964):

$$C_{00} = 1; \quad C_{n0} = (2n+1)^{\frac{1}{2}}; \quad C_{nj} = C_{n(j-1)}\left(1+\frac{n}{j}\right)\left(\frac{n+1}{j}-1\right) \tag{12.3.16}$$

where $n = 1, 2, \ldots$ and $j = 1, 2, \ldots$

12.4. MAXIMUM ENTROPY (MAXENT) METHOD

The classical entropy maximization problem (Shannon, 1948; Jaynes, 1957) consists of determining a probability density function $p(x)$ from its moments. Shannon (1948) used the calculus of variations technique to define the entropy of a probability density function:

$$W = -\int_a^b p(x)\ln[p(x)]dx \tag{12.4.1}$$

The maximization of entropy problem amounts to maximizing W subject to constraints in form of

$$E\{\phi_n(x)\} = \int_a^b \phi_n(x)p(x)dx = a_n \qquad n = 0, 1, ..., N \tag{12.4.2}$$

where a_n is the expected value of $p(x)$. By assuming different functional forms for $\phi_n(x)$, one may get different types of moments from equation (12.4.2). Generally, $\phi_n(x)$ are either powers of x or the logarithm of x. When $\phi_n(x) = x^n$, equation (12.4.2) results in absolute moments of $p(x)$ as defined in

equation (12.1.1); $a_n = \mu_n$. These are also referred to as *geometrical moments. Trigonometrical moments* result when $\phi_n(x) = exp(-jnwx)$, where j is the imaginary number and w is the angular frequency. These moments are the Fourier components of $p(x)$.

The classical solution of maximum entropy problem is accomplished by defining the entropy functional S of $p(x)$ with appropriate Lagrange multipliers:

$$S[p(x)] = -\int_a^b [p(x)\ln[p(x)] - p(x)]dx + \sum_{n=0}^{N} \lambda_n \left(\int_a^b \phi_n(x)p(x)dx - a_n \right) \tag{12.4.3}$$

Maximization of the above entropy functional is done by setting the derivative of S with respect to unknown density $p(x)$ to zero:

$$\frac{\partial}{\partial[p(x)]} S[p(x)] = 0 \Rightarrow P_N(x) = \exp\left(-\sum_{n=0}^{N} \lambda_n \phi_n(x) \right) \tag{12.4.4}$$

The Lagrange multipliers λ_n are estimated by minimizing the error between observed $p(x)$ and computed $P_N(x)$ from N finite moments. This requires that equation (12.4.4) must satisfy $N+1$ constraints:

$$\int_a^b \phi_n(x)P_N(x)dx = a_n; \quad n = 0, 1, 2, \ldots, N \tag{12.4.5}$$

Stated explicitly, the Lagrange parameters $\lambda = [\lambda_0, \ \lambda_1, \ldots, \lambda_N]$ are obtained by solving the following $N+1$ equations:

$$G_n(\boldsymbol{\lambda}) = \int_a^b \phi_n(x) \exp\left(-\sum_{n=0}^{N} \lambda_n \phi_n(x) \right) dx = a_n \tag{12.4.6}$$

The bold face for $\boldsymbol{\lambda}$ in equation (12.4.6) indicates that $\boldsymbol{\lambda}$ is a vector quantity. Equation (12.4.4) together with constraints in equation (12.4.6) forms a set of non-linear equations of polynomial order. Exact solution to this problem is not available. Standard optimization methods, such as Newton's method (Zellner and Highfield, 1988), may be used to estimate $p(x)$. For example, the Taylor series expansion of $G_n(\boldsymbol{\lambda})$ around trial values of $\boldsymbol{\lambda}^0$ with a first-order approximation may be given as

$$G_n(\boldsymbol{\lambda}) \cong G_n(\boldsymbol{\lambda}^0) + (\boldsymbol{\lambda} - \boldsymbol{\lambda}^0)'\nabla G_n(\boldsymbol{\lambda})\big|_{\boldsymbol{\lambda}=\boldsymbol{\lambda}^0} = a_n \tag{12.4.7}$$

Noting the vectors $\boldsymbol{\delta}$ and $\mathbf{v}$ by

$$\boldsymbol{\delta} = \boldsymbol{\lambda} - \boldsymbol{\lambda}^0 \tag{12.4.8}$$

$$\boldsymbol{v} = [a_0 - G_0(\boldsymbol{\lambda}^0), a_1 - G_1(\boldsymbol{\lambda}^0), \ldots, a_N - G_N(\boldsymbol{\lambda}^0)] \tag{12.4.9}$$

and the matrix $\mathbf{H}$ by

$$\mathbf{H} = [h_{n,k}] = \left(\frac{\partial G_n(\boldsymbol{\lambda})}{\partial \lambda_k} \right)_{\boldsymbol{\lambda}=\boldsymbol{\lambda}^0} \qquad n, k = 0, 1, \ldots, N \tag{12.4.10}$$

the equation (12.4.7) becomes

$$\mathbf{H}\boldsymbol{\delta} = \mathbf{v} \tag{12.4.11}$$

This system is solved for $\boldsymbol{\delta}$ from which one can get a new estimate for $\boldsymbol{\lambda} = \boldsymbol{\lambda}^0 + \boldsymbol{\delta}$. This process is repeated in Newton's method until $\boldsymbol{\delta}$ becomes very small. Note that the Hankel matrix $\mathbf{H}$ in equation (12.4.11) is non-singular and thus, the solution of this equation would converge. Mohammad-Djafari (1991) provided the following algorithm to solve equation (12.4.11):

1. Define the range and discretization step for x
2. Write a function to calculate $\phi_{\mathrm{n}}(\mathrm{x})$
3. Initialize the iterative procedure with initial guesses λ^0
4. Calculate $\mathbf{H}$ matrix
5. Solve equation (12.4.11) to obtain $\boldsymbol{\delta}$
6. Calculate $\boldsymbol{\lambda} = \boldsymbol{\lambda}^0 + \boldsymbol{\delta}$
7. Repeat steps 3 to 6 until $\boldsymbol{\delta}$ becomes negligible

The iterative approach outlined above is useful in getting the solution to the MAXENT problem when only few moments are considered and when $\boldsymbol{\lambda}^0$ are close to true $\boldsymbol{\lambda}$. Several more efficient methods than the above Newton's method may be found in the literature (for example, see Ormoneit and White, 1999; Bandyopadhyay et al., 2005).

12.4.1 Geometrical Moments

Geometrical moments defined in equation (12.1.1) result when we assume $\phi_n(x) = x^n$. The solution to the maximum entropy problem in this case becomes

$$P_N(x) = \exp\left(-\sum_{n=0}^{N} \lambda_n x^n \right) \tag{12.4.12}$$

with the Lagrange parameters $\boldsymbol{\lambda} = [\lambda_0, \ \lambda_1, \ldots, \lambda_N]$ obtained by solving the constraint equations:

$$G_n(\boldsymbol{\lambda}) = \int_0^1 x^n \exp\left(-\sum_{n=0}^{N} \lambda_n x^n \right) dx = \mu_n \tag{12.4.13}$$

With these definitions, it is assumed that the zeroth moment is unity. Thus, $P(x)$ should be so chosen to have its mass equal to unity. Although equation (12.4.12) and (12.4.13) have been solved for $n > 4$, the first five moments ($n = 4$) are generally used to estimate $\mathrm{P}_N(x)$.

Harvey and Gorelick (1995) observed that because of fat tails commonly associated with the BTCs, the above entropy method fails to capture measured BTCs, which are skewed. In particular, they observed that some values of λ_n do not appear to exist because of the fat tails. These authors suggested that the log-transform of the maximum entropy function provides better estimates for the BTC. By transforming the maximum entropy function to $ln(x)$, these authors obtained:

$$P_N(x) = \frac{1}{x} \exp\left[-\sum_{n=0}^{N} \lambda_n (\ln x)^n \right] \tag{12.4.14}$$

Harvey and Gorelick (1995) have used equation (12.4.14) to reconstruct skewed BTCs.

12.5. EXAMPLE CALCULATIONS

To illustrate the application of the above methods, we tested the GCS and the maximum entropy (ME) approaches on two datasets collected from miscible displacement experiments of Das (1996) and Langner et al. (1999). The BTC for the tritiated water shown in Figure 12.5.1 (open squares) was obtained from

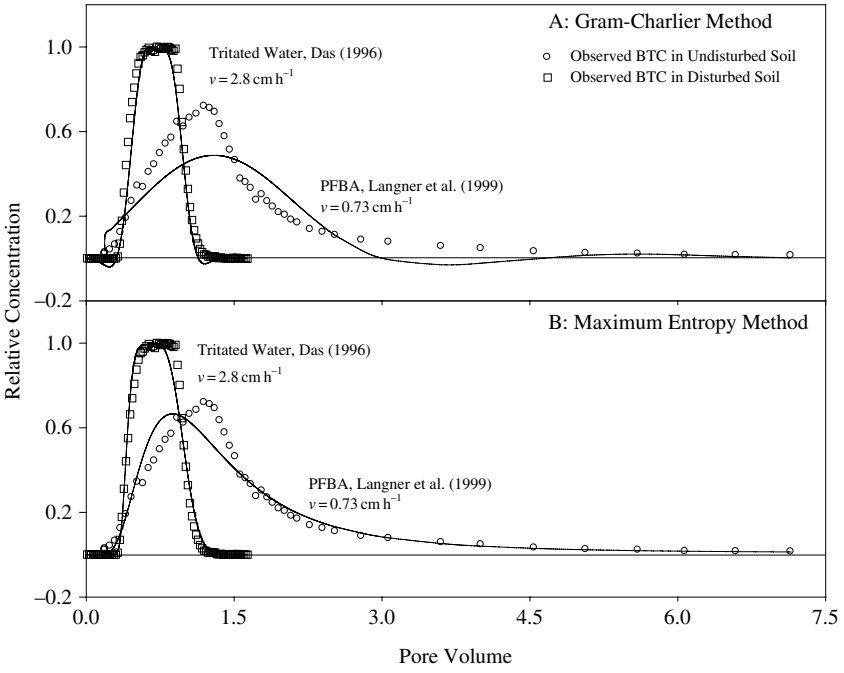

Figure 12.5.1. Observed and predicted BTCs using the Gram-Charlier Series approach (A) and the Maximum Entropy approach (B) for tritiated water (open squares) and pentafluorobenzoic acid (open circles)

the saturated flow experiment (Das, 1996) conducted at a pore water velocity of 2.8 cm h^{-1}. The BTC for the pentafluorobenzoic acid (PFBA) shown in Figure 12.5.1 (open circles) was obtained from the unsaturated flow experiment (Langner et al., 1999) conducted at a pore water velocity of 0.73 cm h^{-1}. We have shown the predicted BTCs using the GCS approach and the ME approaches in Figures 12.5.1A and B, respectively. It may be observed that as long as the process is Gaussian, the simple GCS approach (or the ME approach) can effectively predict the observed BTC. As shown by Harvey and Gorelick (1995), the log-transformed form of ME approach effectively describes the BTCs with long tails.

Figure 12.5.1 also shows that the GCS approach may yield negative and multimodal densities. It also does not describe the skewed BTCs effectively. The ME approach, on the other hand, describes the tail end of the BTC reasonably well, yet it fails to match observed concentrations around the peak areas. Tari and Telek (2005) evaluated different estimation methods and showed that the accuracy of constructing a density function increases as more and more number of moments are used to estimate a density. These authors showed that although one could use as many as 29 moments for constructing a normal pdf, there is not much gain in accuracy beyond 19 moments. In our examples, only few moments were used. In the ME approach, we used the first 5 moments and in the GCS approach, we used the first nine moments. Even with these few moments, we observed lack of uniqueness while constructing the BTCs.

REFERENCES

Abramowitz M, Stegun IA, eds. (1964) Handbook of mathematical functions with formulas, graphs, and mathematical tables, US Government Printing Office, Washington, DC., p 1046

Abulaban A, Nieber JL (2000) Modeling the effects of nonlinear equilibrium sorption on the transport of solute plumes in saturated heterogeneous porous media, *Adv. Water Resour.* 23(8):893–905

Arabi M, Stillman JS, Govindaraju RS (2006) A process-based transfer function approach to model tile drain hydrographs. *Hydrol. Process*., 20:3105–3117

Aris R (1956) On the dispersion of a solute in a fluid flowing through a tube. *Proc. Royal Soc. London, Ser. A*, 235:67–77

Aris R (1958) On the dispersion of linear kinematic waves. *Proc. Royal Soc. London, Ser. A*, 245:268–277

Au-Yeung SWM (2003) Finding probability distributions from moments. *MS Thesis* Submitted to Imperial College of Science, Technology, and Medicine, Univ. London

Baehr AL, Hoag GE, Marley MC (1989) Removing volatile contaminants from the unsaturated zone by inducing advective air-phase transport. *J. Contam. Hydrol*., 4(1):1–26

Bandyopadhyay K, Bhattacharya AK, Biswas P, and Drabold DA. (2005) Maximum entropy and the problem of moments: a stable algorithm. *Phys. Rev. E.* 71,057701-04

Banks MK., Govindaraju RS, Ashwab AP, Kukalow P, Finn J (2000) *Phytoremediation of Hydrocarbon-Contaminated Soils*, series edited by Fiorenza S, Oubre CL, Ward CH, Lewis Publishers, New York, pp 164

Bardossy A, Bogardi I and Kelly WE (1988) Imprecise (fuzzy) information in geostatistics, *Math. Geol*., 20(4):287–311

—— (1990) Kriging with imprecise (fuzzy) variograms, II, Application, *Math. Geol*., 22(1):81–94

Bear J (1979) *Hydraulics of Groundwater*, McGraw-Hill, Inc., New York, pp 569

Beltman WHJ, Boesten JJTI, van der Zee SEATM (1995) Analytical modeling of pesticide transport from the soil surface to a drinking water well, *J. Hydrol*. 169:209–228

Berg C, Chen Y, Ismail MEH (2002) Small eigenvalues of large Hankel matrices: the indeterminate case, *Math. Scand*. 91(1):67–81

Berglund S (1997) Aquifer remediation by pumping: a model for stochastic-advective transport with nonaqueous liquid dissolution, *Water Resour. Res*. 30(4):649–661

Beven K (1981) Kinematic subsurface flow, *Water Resour. Res*., 17(5):1419–1424

—— (1982) On subsurface stormflow: predictions with simple kinematic theory for saturated and unsaturated flows, *Water Resour. Res*., 18(6):1627–1633

Bird R, Stewart B, Lightfoot EN (1960) *Transport Phenomena*, John Wiley and Sons, Inc., Madison, WI

Bischoff KB (1960) Notes on the diffusion-type model for longitudinal mixing in flow, *Chemical Engrg. Sci*., 12:69

Boussinesq J (1877) Essai sur la theorie des eaux courantes. *Mem. Acad. Sci. Inst. France*, 23(1):252–260

Bowers NL (1966) Expansion of probability density functions as a sum of gamma densities with applications in risk theory. *Trans. Soc. Actuaries*. 18:125–147

Brenner H (1980) A general theory of Taylor dispersion phenomena, *Physicochem. Hydrodyn*. l:91–123

Brenner H and Adler PM (1982) Dispersion resulting from flow through spatially periodic porous media, II Surface and intraparticle transport, *Philos. Trans. R. Soc. London, Ser. A*, 307:149–200

Bresler E, Dagan G (1979) Solute dispersion in unsaturated heterogeneous soil at field scale, II, Applications, *Soil Sci. Soc. Am. J*. 43:467–472

Bromilow RH, Leistra M (1980) Measured and simulated behavior of aldicarb and its oxidation products in fallow soils, *Pestic. Sci*., 11(4):389–395

Bronson R (1973) *Modern Introductory Differential Equations*, Schaum's Outline Series in Mathematics, McGraw Hill, New York, p 306

Brown BD, Rolston DE (1980) Transport and transformation of methyl bromide in soils, *Soil Sci*., 130(2):68–75

Brusseau ML (1991) Transport of Organic Chemicals by Gas Advection in Structured or Heterogeneous Porous Media: Development of a Model and Application to Column Experiments, *Water Resources Res*., 27(12):3189–3199

Brusseau ML, Jessup RE, Rao PSC (1990) Sorption kinetics of organic chemicals: Evaluation of gas-purge and miscible-displacement techniques, *Environ. Sci. Technol*., 24(5):727–735

Brusseau ML, Rao PSC (1989) Sorption nonideality during organic contaminant transport in porous media, *CRC Crit. Rev. Environ. Control*, 19(1):33–39

Brutsaert W, (1994) The unit response of groundwater outflow from a hillslope. *Water Resour. Res*., 30(10):2759–2763

Brutsaert W and El-Kadi A (1986) Interpretation of an unconfined groundwater flow experiment, *Water Resour. Res*., 22(3):419–422

Brutsaert W and Nieber J, (1977) Regionalized drought flow hydrographs from a mature glaciated plateau, *Water Resour. Res*., 13:637–643

Buxton DS, Green RE (1987) Desorption and leachability of DBCP residues in soils, *Agronomy Abstracts*, American Society of Agronomy, Madison, WI, p 167

Cameron DR. and Klute A (1977) Convective-dispersive solute transport with a combined equilibrium and kinetic adsorption model, *Water Resour. Res*., 13(1):183–188

Castro CL, Rolston DE (1977) Organic phosphate transport and hydrolysis in soil: theoretical and experimental evaluation, *Soil Sci. Soc. America Jour*., 41(6):1085–1092

Chan TP (1999) Interval computing applications in quantifying field-scale experiments, *M.S. Thesis*, School of Civil Engineering, Purdue University, p 82

Chan TP, Govindaraju RS (2001) Analyzing vertical field-scale solute movement by applying interval computing methods to the stochastic-convective transport model, *ASCE Journal of Hydrol. Eng*., 6(6):480–489

Chan TP., and Govindaraju RS (2006) A stochastic-convective transport model for NAPL dissolution with degradation in heterogeneous porous media, *Journal of Contaminant Hydrology*, 87:253–276

Chapman TG. and Dressler RF (1984) Unsteady shallow groundwater flow over a curved impermeable boundary. *Water Resour. Res*., 20(10):1427–1434

Charbeneau R, (2000) *Groundwater Hydraulics and Pollutant Transport*. Prentice Hall, NJ, p 593

Chatwin PC (1970) The approach to normality of the concentration distribution of solute in a solvent flowing along a straight pipe. *J. Fluid Mech*. 51:321–352

Chen Z (1997) Phytoremediation of Total Petroleum Hydrocarbons, *Ph.D Dissertation*, Dept. of Civil Engineering, Kansas State University, Manhattan, KS

Childs EC (1971) Drainage of groundwater resting on a sloping bed. *Water Resour. Res*., 7(5):1256–1263

Cho CM (1971) Convective transport of ammonium with nitrification in soil, *Can. Jour. Soil Sci*., 51(3):339–350

Civanlar MR and Trussell HJ (1986) Constructing membership functions using statistical data, *Fuzzy Sets. Sys*., 18:1–13

Clements WC (1969) Determination of the parameters of the longitudinal dispersion model from experimental data, *Chemical Engrg. Sci*., 24:957–963

Coats KH Smith BD (1956) Dead end pore volume and dispersion in porous media, *Soc. Pet. Eng. J*., 4:73–84

Crank J (1975) *The Mathematics of Diffusion*, 2nd ed., Oxford University Press, New York

Cunningham JA, Roberts PV (1998) Use of temporal moments to investigate the effects of nonuniform grain-size distribution on the transport of sorbing solutes, *Water Resour. Res*., 34:1415–1425

Cunningham JA, Werth CJ, Reinhard M, Roberts PV (1997a) Effects of grain-scale mass transfer on the transport of volatile organics through sediments 1. Model Development, *Water Resources Res*., 33(12):2713–2726

—— (1997b) Effects of grain-scale mass transfer on the transport of volatile organics through sediments 2. Column Results, *Water Resources Res*., 33(12):2727–2740

Cunningham JA, Goltz MN, Roberts PV (1999) Simplified expressions for spatial moments of groundwater contaminant plumes, *ASCE J. Hydrologic Eng*., 4(4):377–380

Dagan G (1982) Stochastic modeling of groundwater flow by unconditional and conditional probabilities, 2, The solute transport, *Water Resour. Res*., 18:835–848

—— (1986) Statistical theory of groundwater flow and transport: pore to laboratory, laboratory to formation, and formation to regional scale, *Water Resour. Res*., 22(9):120S-134S

Dagan G, Brelser E (1979) Solute dispersion in unsaturated heterogeneous soil at field scale, I, Theory, *Soil Sci. Soc. Am. J*., 43:461–467

Dagan G, Cvetkovic V (1993) Spatial moments of a kinetically sorbing solute plume in a heterogeneous aquifer, *Water Resour. Res*., 29(12):4053–4061

Dagan G and Nguyen V (1989) A comparison of travel time and concentration approaches to modeling of transport by groundwater, *J. Contam. Hydrol*., 4:79–91

Danckwerts PV (1953) Continuous flow systems: distribution of residence times, Chemical Engrg. Sci., 2:1–18

Das BS (1996) Nonequilibrium sorption and degradation of organic solutes in soil, *Ph.D. Diss*., Kansas State University, Manhattan, KS, p 229

Das BS, Govindaraju RS, Kluitenberg GJ, Valocchi AJ, Wraith JM (2002) Theory and applications of time moment analysis to study the fate of reactive transport in soils, in *Stochastic Methods in Subsurface Contaminant Hydrology* (ed. Govindaraju RS), ASCE Press, 239–279

Das BS, Kluitenberg GJ (1996) Moment analysis to estimate degradation rate constants from leaching experiments, *Soil Sci. Soc. Am. J*., 60:1724–1731

Das BS, Wraith JM, Kluitenberg GJ, Langner HM, Shouse PJ, Inskeep WP (2005) Evaluation of mass recovery impacts on transport parameters using least-squares optimization and moment analysis, *Soil Sci. Soc. Am. J*., 69:1209–1216

Di Marco VB, Bombi GG (2001) Mathematical functions for the representation of chromatographic peaks. *J. Chromatography A*, 931:1–30

Diaz RD, Loague K (2000) Regional-scale leaching assessments for Tenerife: effect of data uncertainties, *J. Environ. Qual*., 29:835–847

Dingman SL (2002) Physical Hydrology, Prentice Hall, Upper Saddle River, New Jersey, p 646

Dou C, Woldt W, Bogardi I and Dahab M (1995) Steady state goundwater flow simulation with imprecise parameters, *Water Resour. Res*, 31(11):2709–2719

Dupuit J (1863) Etudes theoriques et pratiques sue le movement des eaux dans les canax decouverts et a travers les terrains permeables, ed. 2, Dunod, Paris

Espinoza C, Valocchi AJ (1997) Stochastic analysis of one-dimensional transport of kinetically adsorbing solutes in chemically heterogeneous aquifers, *Water Resour. Res*., 33: 2429–2445

Fahim MA, Wakao SM (1982) Parameter estimation from tracer response measurements, *Chem. Engg. J*., 25:1–8

Fox RF (1975) A generalized theory of multiplicative stochastic theories using cumulant techniques, *J. Mathematical Physics*, 16:289–297

—— (1976) Critique of the generalized cumulant expansion method, *J. mathematical Physics*, 17:1148–1153

Freyberg DL (1986) A natural gradient experiment on solute transport in sand aquifer, 2, Spatial moments and the advection and dispersion of nonreactive tracers, *Water Resour. Res*., 22:2031–2046

Gaber HM, Inskeep WP, Comfort SD, Wraith JM (1995) Nonequilibrium transport of atrazine through large intact soil cores, *Soil Sci. Soc. Am. J*., 59:60–67

Gamerdinger AP, Wagenet RJ, Van Genuchten MT (1990) Application of two-site/two-region models for studying simultaneous nonequilibrium transport and degradation of pesticides, *Soil Sci. Soc. Am. J*., 54:957–963

Gangwal SK., Hudgins RR, Bryson AW, Silveston PL (1971) Interpretation of chromatic peaks by Fourier analysis, *Can. J. Chemical Engrg*., 49:113

Garabedian PS, LeBlanc DR, Gelhar LW, Celia MA (1991) Large-Scale natural gradient tracer test in sand and gravel, Cape Cod, Massachusetts, 2, Analysis of spatial moments for a nonreactive tracer, *Water Resour. Res*., 27:911–924

Gardiner CW (1985) *Handbook of Stochastic Methods*, Springer-Verlag, New York, p 442

Gelhar LW, Axness CL (1983) Three-dimensional stochastic analysis of macrodispersion in aquifers, *Water Resour. Res*., 19:161–180

Germann PF,. Beven K, (1985) Kinematic wave approximation to infiltration into soils with sorbing macropores, *Water Resour. Res*., 21 (7), 990–996

Gierke JS, Hutzler NJ, Crittenden JC (1990) Modeling the movements of Volatile Organic Chemicals in Columns of Unsaturated Soil, *Water Resources Res*., 26(7):1529–1547

Gierke JS, Hutzler NJ, McKenzie DB (1992) Vapor transport in unsaturated soil columns: implications for vapor extraction, *Water Resources Res*., 28(2):323–335

Ginn TR (2002) Streamtube ensemble techniques for subsurface multicomponent reactive transport, in *Stochastic Methods in Subsurface Contaminant Hydrology*, Govindaraju RS (ed.), ASCE Press, 169–238

Goltz MN, Roberts PV (1987) Using the method of moments to analyze three-dimensional diffusion-limited solute transport from temporal and spatial perspectives, *Water Resour. Res*., 23(8):1575–1585

Govindaraju RS. (2003) Discussion on "drought flow from hillslope" by Mizumura K, *ASCE Journal of Hydrologic Engineering*, 8(6):370–372

Govindaraju RS, Jones SE, Kavvas ML (1988) On the Diffusion Wave Model for Overland Flow, 1, Solution for Steep Slopes. *Water Resou. Res*., 24(5):734–744

Govindaraju RS, Das BS, Kluitenberg GJ (1996) Cumulant-based analysis of concentration data from soil-column studies for system identification, *ASCE J. Hydrol. Eng*., 1:46–48

Govindaraju RS, Morbidelli R, Corradini C (2001) Areal infiltration modeling over soils with spatially correlated hydraulic conductivities, *ASCE Jour. Hydro. Eng*., 6(2):150–158

Greenwood JA., Landwehr JM, Matalas NC, Wallis JR (1979) Probability weighted moments: definition and relation to parameters of several distributions expressable in inverse form, *Water Resour. Res*., 15:1049–1054

Griffioen JW, Barry DA, Parlange J-Y (1998) Interpretation of the two-region model parameters, *Water Resour. Res*. 34(3):373–384

Gureghian AB, Jansen G (1983) LAYFLO: A one dimensional semianalytical model for the migration of a three-member decay chain in a multilayered geologic medium, *Tech. Rep. ONWI-466, Office of Nuclear Waste Isolation*, Battelle Memorial Institute, Columbus, OH, p 83

Guven O, Molz FJ, Melville JG (1984) An analysis dispersion in a stratified aquifer, *Water Resour. Res*., 209: 1337–1354

Haas CN (1996) Moment analysis of tracer experiments, *J. Environ. Eng*., 122:1121–1123

Habel F, Mendoza C, Bagtzoglou AC. (2002) Solute transport in open channel flows and porous streambeds. *Adv. Water Resour*. 25: 455–469

Haggerty R, Gorelick SM (1995) Multiple-rate mass transfer for modeling diffusion and surface reactions in media with pore-scale heterogeneity, *Water Resour. Res*., 31(1): 2383–2400

Hantush MM, Mariño MA, Islam MR (2000) Models for leaching of pesticides in soils and groundwater, *J. Hydrol*. 227:66–83

Hantush MM, Mariño MA (1998) Interlayer diffusive transfer and transport of contaminants in stratified formation. I: Theory, *ASCE J. Hydrol. Eng*., 3(4):232–240

Hantush MM, Govindaraju RS, Marino MA, Zhang Z (2002) Screening model for volatile pollutants in dual porosity soils, *J. Hydrol*., 260:58–72

Hantush MM. and Govindaraju RS (2003) Theoretical development and analytical solutions for transport of volatile organic compounds in dual porosity soils, *J. Hydrol*., 279:18–42

Harada M, Chambre PL, Foglia M, Higashi K, Iwamoto F, Leung D, Pigford TH, Ding T (1980) Migration of radionuclides through sorbing media, analytical solutions – I, *Rep. no. LBL-10500 (UC-11), Lawrence Berkeley Laboratory*, Univ. California, Berkeley, p 245

Harvey FC, Gorelick SM (1995) Temporal moment-generating equations: modeling transport and mass transfer in heterogeneous aquifers, *Water Resour. Res*., 31:1895–1911

Henderson FM, Wooding RA (1964) Overland flow and groundwater flow from a steady rainfall of a finite duration, *J. Geophys. Res*., 69(8):1531–1540

Higashi K, Pigford TH (1980) Analytical models for migration of radionuclides in geologic sorbing media, *Jour. Nucl. Sci. and Techn*., 17(9):700–709

Hoffman DL, Rolston DE (1980) Transport of organic phosphate in soil as affected by soil type, *Soil Sci. Soc. Am. J*., 44:46–52

Horn FJM (1971) Calculation of dispersion coefficients by means of moments, *AIChE J*., 17:613–620

Hosking JRM (1986) The theory of probability weighted moments, *Research Rep. RC12210*, IBM Research Division, Yorktown Heights, New York

Hosking JRM, Wallis JR (1997) *Regional Frequency Analysis*, Cambridge University Press, New York, p 224

Hu BX, Deng FW, Cushman JW (1995) Nonlocal reactive transport with physical and chemical heterogeneity: Linear nonequilibrium sorption with random K_d, *Water Resour. Res*., 31(9):2239–2252

Hutzler NJ, Gierke JS, Krause LC (1989) Movement of Volatile Organic Chemicals in Soils, *Soil Sci. Soc. Am. J*., Special Publication no. 22:373–403

Jacobsen OH, Leij FJ, van Genuchten MT (1992) Parameter determination for chloride and tritium transport in undisturbed lysimeters during steady flow, *Nordic Hydrol*., 23:89–104

Jawitz JW (2004) Moments of truncated continuous univariate distributions, *Adv. Water Resour*., 27:269–281

Jawitz JW, Fure AD, Demmy GG, Berglund S, Rao PSC (2005) Groundwater contaminant flux reduction resulting from nonaqueous phase liquid mass reduction. *Water Resour. Res*., 41, W10408, doi:10.1029/2004WR003825

Jaynes ET (1957) Information theory and statistical mechanics. *Phys. Rev*., 106:361–373

Johnson Wilson RL, Palmer CD, Keely JF (1987) Mass transfer of organics between soil, water and vapor phases: Implication for monitoring, biodegradation and remediation, in *Proceedings of the NWWA/API Conference on Petroleum Hydrocarbons and Organic chemicals in Groundwater-Prevention, Detention and Restoration*, National Water Well Association, Dublin, OH, pp 493–507

Jondeau E, Rockinger M (2001) Gram-Charlier Densities. *J. Economic Dynamics and Control*, 25:1457–1483

Jury WA (1982) Simulation of solute transport with a transfer function model, *Water Resour. Res*., 18; 363–368

—— (1986) Mathematical derivation of chemical transport equations, in *Vadose Zone Modeling of Organic Pollutants*, Hern SC and Melancon SM (eds.), Lewis Publishers, Chelsea, MI

Jury WA, Gardner WR, Gardner WH (1991) *Soil Physics*, John Wiley & Sons. Inc. New York. p 328

Jury WA, Roth K (1990) *Transfer Functions and Solute Movement through Soil*, Birkhauser, Boston, p 226

Jury WA, Russo D, Streile G, and El Abd H (1990) Evaluation of volatilization by organic chemicals residing below the soil surface, *Water Resources Res*., 26(1):13–20

Jury WA, Spencer WF, Farmer WJ (1983) Behavior assessment model for trace organics in soil: I. Model description, *J. Environ. Qual*., 12(4):558–564

Jury WA, Sposito G (1985) Field calibration and validation of solute transport models for the unsaturated zone, *Soil Sci. Soc. Am. J*., 49:1331–1341

Jury WA, Sposito G, White RE (1986) A transfer function model of solute transport through soil: 1. Fundamental concepts. *Water Resour. Res*., 22(2):243–247

Jury WA, Stolzy LH., Shouse P (1982) A field-test of the transfer-function model for predicting solute transport. *Water Resour. Res*., 18(2): 369–375

Jury WA and Utermann J (1992) Solute transport through layered soil profiles: zero and perfect travel time correlation models, *Transport in Porous Media*, 8:277–297

Kamra SK, Lennartz B, Van Genuchten MT, Widmoser P (2001) Evaluating nonequilibrium solute transport in soil columns, *J. Contam. Hydrol*. 48:189–212

Kaufmann A, Gupta MM (1991) *Introduction to Fuzzy Arithmetic: Theory and Applications*, Van Nostrand Reinhold, New York

Kavvas ML, Chen Z-Q, Govindaraju RS, Rolston DE, Koos T, Karakas A, Or D, Jones S, Biggar J (1996) Probability distribution of solute travel time for convective transport in field-scale soils under unsteady and nonuniform flows, *Water Resources Research*, 32(4):875–889

Kendall M, Stuart A (1977) *The Advanced Theory of Statistics*, Vol. 1, 4th ed., MacMillan, New York, p 472

Khan MA, Liang T (1989) Mapping pesticide contamination potential, *Environmental Management*, 13:233–242

Koos TG (1994) Evaluating TDR for estimating solute travel time and surface flux in field soils, *Masters Thesis*, Department of Land, Air and Water Resources, University of California, Davis, Davis, CA

Kreft A, Zuber A (1978) On the physical meaning of the dispersion equation and its solutions for different initial and boundary conditions, *Chem. Eng. Sci*. 33:1471–1480

Kubin M (1965) Beitrag zur theorie der chromatographie. Collection Czechoslov. *Chem. Commun*., 30:1104–1118

Kubo R (1962) Generalized cumulant expansion method, *J. Phys. Soc. Japan*, 17:1100–1120

Kucera E (1965) Contribution to the theory of chromatography linear non-equilibrium elution chromatography, *J. Chromatog*., 19:237–248

Langner HW, Gaber HM, Wraith JM, Huwe B, Inskeep WP (1999) Preferential flow through intact soil cores: effects of matric head, *Soil Sci. Soc. Am. J*., 63:1591–1598

Laskowski DA, Goring CAI, McCall PJ, Swann RL (1982) Terrestrial Environment, in *R. A. Conway (ed) Environmental Risk Analysis for Chemicals*. Van Nostrand Reinhold Co., NY, 198–240

LeBlanc DR, Garabedian SP, Hess KM, Gelher LW, Quadri RD, Stollenwerk KG, Wood WW (1991) Large-scale natural gradient tracer test in sand and gravel, Cape Cod, MA, 1, Experimental design and observed tracer movement, *Water Resour. Res*., 27: 895–910

Leij FJ, Dane JH (1991) Solute transport in a two-layer medium investigated with time moments, *Soil Sci. Soc. Am. J*., 55:1529–1535

Leij FJ, Priesack E, Schaap MG (2000) Solute transport modeled with Green's functions with applications to persistent solute sources, *J. Contam. Hydrol*., 41:155–173

Li L, Barry DA, Culligan-Hensley PJ, Bajracharya K (1994) Mass transfer in soils with local stratification of hydraulic conductivity, *Water Resour. Res*., 30(11):2891–2900

Lindstrom FT, Haque R, Freed VH, Boersma L (1967) Theory on the movement of some herbicides in soils: linear diffusion and convection of chemicals in soil, *Environ. Sci. Tecnhol*., 1:561–565

Loague K, Bernknopf RL, Giambelluca TW, Green RE (1995) The impact of data uncertainty upon regional scale leaching assessments of non-point source pollutants, *Applications of GIS to the modeling of non-point source pollutants in the vadose zone*, ASA-CSSA-SSSA Bouyoucos Conference, Mission In, Riverside, CA

Lupini R and Tirabassi T (1983) Solution of the advection-diffusion method by the moments method. *Atmospheric Environ*. 17:965–971

Marle C, Simandoux P, Pacsirsky J, Gaulier C (1967) Etude du desplacement de fluides miscibles en milieu poreux stratifie, *Rev. Inst. Fr. Pet*., 22(2):272–294

Mead LR, Papanicolaou N (1984) Maximum entropy in the problem of moments. *J. Math. Phys*., 25:2404–2417

Meeks YJ and Dean JD (1990) Evaluating ground-water vulnerability to pesticides, *ASCE Journal Water Resources Planning and Management*, 116(5):693–707

Meeron E (1957) Series expansion of distribution functions in multicomponent fluid systems, *J. Chemical Phys*., 27:1238–1246

Mishra BK Misra C (1990) Simulation of nitrogen breakthrough curves stemming from leaching of ammonium nitrate through soil, J. Hydrol., 115:377–384

Misra C, Mishra BK (1977) Miscible displacement of nitrate and chloride under field conditions, *Soil Sci. Soc. Am. J*., 41:496–499

Mizumura K (2002) Drought flow from hillslope. *ASCE J. Hydrolog. Engrg*., 7(2):109–115

Mohammad-Djafari A (1992) A Matlab program to calculate the maximum entropy distributions, Presented at the *11th International Workshop on Maximum Entropy and Bayesian Methods (MaxEnt91)*, Laramie, Wyoming, USA, 1991), Appeared in Maximum Entropy and Bayesian Methods, Kluwer Academic Publishers, Grandy TW (ed.), pp 221–233

Moore RE (1966) *Interval Analysis*, Prentice-Hall, Englewood Cliffs, NY

Moore RE (1979) *Methods and Applications of Interval Analysis*, Society for Industrial and Applied Mathematics, Philadelphia, PA

Mulla DJ, Perillo CA, Cogger CG (1996) A site specific farm scale GIS approach for reducing ground water contamination by pesticides, *J. Environ. Qual*., 25(3):419–425

Nahar N (1998) Influence of first-order degradation on spatial moment analysis of the convection-dispersion equation with kinetic sorption, *M.S. Thesis*, submitted to School of Civil Engineering, Purdue University, p 73

Nedunuri KV, Govindaraju RS, Banks MK, Schwab AP, Chen Z (2000) Evaluation of phytoremediation for field-scale degradation of total petroleum hydrocarbons, *ASCE Jour. of Envir. Engg*., 126(6):483–490

Nkedi-Kizza P, Bigger JW, Selim HM, van Genuchten MT, Wierenga PJ, Davidson JM, Nielsen DR (1984) On the equivalence of two conceptual models for describing ion exchange during transport through an aggregated soil, *Water Resour. Res*., 20:1123–1130

Ogata A, Banks RB (1961) A solution of the differential equation of longitudinal dispersion in porous media, *United States Geol. Surv. Prof. Paper 411-A*

Olive J, Grimalt JO (1991) Gram-Charlier and Edgeworth-Cramer series in the characterization of chromatographic peaks. *Analytica Chemica Acta*, 249:337–348

Ormoneit D, White H (1999) An efficient algorithm to compute maximum entropy densities. *Econometric Reviews*, 18:127–140

Ostergaard K, Michelsen ML (1969) On the use of the imperfect tracer pulse method for determination of hold-up and axial mixing, *Can. J. Chem. Engg*., 47:107–112

Parashar R (2003) Moment analysis for some solute transport models in porous media, *M.S. Thesis*, School of Civil Engineering, Purdue University, p 89

Parashar R, Govindaraju RS (2006a) Evaluation of effective parameters for volatile organic compounds in porous media with mobile air phase, *Transport in Porous Media*, 63: 349–362

—— (2006b) Moment analysis for compounds undergoing sequential first-order decay chain reactions, *Stochastic Environmental Research and Risk Assessment*, 20:95–105

Parashar R, Govindaraju RS, Hantush M (2007) Temporal moment analysis for volatile organic compounds in dual-porosity media: loss fractions and effective parameters, ASCE J. Env. Engrg, accepted for publication

Parker JC, Valocchi AJ (1986) Constraints on the validity of equilibrium and first-order kinetic transport models in structured soils, *Water Resour. Res*., 22(3):399–407

Parker JC, van Genuchten MT (1984) Flux-averaged and volume-averaged concentrations in continuum approaches to solute transport, *Water Resour. Res., 20*:866–872

Parzen E (1960) *Modern Probability Theory and Its Applications*, John Wiley, New York

Pesonen J, Hyvönen E (1996) Interval approach challenges Monte Carlo simulation, *Reliable Computing*, 2(2):155–160

Press WH., Flannery BP, Teukolsky SA, Vetterling WT (1988) *Numerical Recipes in Pascal: The Art of Scientific Computing*, Cambridge University Press, Cambridge

Rao PSC, Hornsby AG, Jessup RE (1985) Indices for ranking the potential for pesticide contamination of groundwater, *Proc. Soil Crop Sci. Soc. Fla*., 44:1–8

Rao PSC, Jawitz JW (2003) Comment on "steady state mass transfer from single-component dense nonaqueous phase liquids in uniform flow fields" by Sale TC and McWhorter DB, *Water Resour. Res*. 39(3):1068, doi:10.1029/2001WR000599

Rao PSC., Rolston DE, Jessup RE, Davidson JM (1980) Solute transport in aggregated porous media. Theoretical and experimental evaluation, *Soil Sci. Soc. Am. J*., 44:1139–1146

Rasmuson A, Gimmi T, and Fluhler H (1990) Modeling reactive gas uptake, transport, and transportation in aggregated soils, *Soil Sci. Soc. Am. J*., 54(5):1206–1213

Rasmuson A, Neretnieks I (1980) Exact solution of a model for diffusion in particles and longitudinal dispersion in packed beds, *AIChE. J*., 26:686–690

Ratschek H, Rokne J (1988) *New Computer Methods for Global Optimization*, Ellis Horwood, West Sussex, England

Rawls WJ (1983) Estimating soil bulk density from particle size analysis and organic matter content, *Soil Science*, 135(2):123–125

Rawls WJ, Ahuja LR, Brakensiek DL, Shirmohammadi A, (1993) Infiltration and soil water movement. In *Handbook of Hydrology*, (ed. Maidment DR), McGraw-Hill Inc. 5.1–5.51

Risler PD, Wraith JM, Gaber HM (1996) Solute transport under transient flow conditions estimated using time domain reflectometry, *Soil Sci. Soc. Am. J*. 60:1297–1305

Roberts PV, Goltz MN, Mackay DM (1986) A natural gradient experiment on solute transport in a sand aquifer, 3, Retardation estimates and mass balances for organic solutes, *Water Resour. Res*., 23:2047–2058

Rogers VC (1978) Migration of radionuclide chains in groundwater, *Nucl. Techn*., 40(3): 315–320

Rosen JB (1952) Kinetics of a fixed bed system for solid diffusion into spherical particles, *J. Chem. Phys*., 20(3):387–394

Rubin Y, Cushey MA, Wilson A (1997) The moments of the breakthrough curves of instantaneously and kinetically sorbing solutes in heterogeneous geologic media: Predictions and parameter inference from field measurements, *Water Resour. Res*. 33:2465–2481

Rubinstein M, (1998) Edgeworth binomial trees. *J. of Derivatives*, 5:20–27

Sansone G (1991) *Orthogonal Functions*. Dover Publications, Inc., New York, p 411

Sardin M, Schweich D, Leij FJ, van Genuchten MT (1991) Modeling the nonequilibrium transport of linearly interacting solutes in porous media: a review, *Water Resour. Res*., 27:2287–2307

Sauty, J-P (1980) Analysis of hydrodispersive transfer in aquifers, *Water Resour. Res*., 16(1):145–158

Scalas E, Viano GA (1993) The Hausdorff moments in statistical mechanics. *J. Math. Phys*. 35:5781–5800

Schmidt J (2002) A model for transient flow to a subsurface tile drain. M.S. Thesis, School of Civil Engineering, Purdue University, p 165

Schwab AP and Banks MK (1994) Biologically mediated dissipation of polyaromatic hydrocarbons in the root zone, *Bioremediation through Rhizosphere Technology, ACS Symposium Series 563*, (ed. Anderson TA and Coats JR), *American Chemical Society*, Washington, DC, pp 132–141

Selim HM, Davidson JM, Mansell RS (1976) Evaluation of a two-site adsorption-desorption model for describing solute transport in soils, in *Proceedings of the Summer Computer Simulation Conference*, Washington, DC., Simulation Councils, La Jolla, Calif, 444–448

Selim HM, Davidson JM, Rao PSC (1977) Transport of reactive solutes through multilayered soils, *Soil Sci. Soc. Am. J*., 41:3–10

Shann JR, Boyle JJ (1994) Influence of plant species on in situ rhizosphere degradation, *Bioremediation through Rhizosphere Technology, ACS Symposium Series 563*, Anderson TA, Coats JR (eds.), 70–81, *American Chemical Society*, Washington, DC

Shannon CE (1948) A mathematical theory of communication. *Bell System Tech. J*. 27: 379–423

Shapiro M, Brenner H (1988) Dispersion of a chemically reactive solute in a spatially periodic model of a porous medium, *Chem. Engg. Sci*., 43:551–571

Shukla S, Mostaghimi S, Shanholt VO, Collins MC, Ross BB (2000) A county-level assessment of ground water contamination by pesticides, Ground Water Monit. Rem., 20(1):104–119

Simmons CS (1982) A stochastic-convective transport representation of dispersion in one-dimensional porous media systems, *Water Resources Research*, 18(4):1193–1214

—— (1986a) A generalization of one dimensional solute transport: a stochastic-convective flow conceptualization, *Proc. of 6th Ann. AGU Front Range Branch Hydrology Days*, Hydrol. Days Pub, Fort Collins, CO

—— (1986b) Scale dependent effective dispersion coefficients for one-dimensional solute transport, *Proc. of 6th Ann. AGU Front Range Branch Hydrology Days*, Hydrol. Days Pub., Fort Collins, CO

Skopp J (1985) Analysis of solute movement in structured soils, *Journal Series*, Nebraska Agricultural Station, paper 7430, Lincoln

Smith JA, Chiou CT, Kammer JA, Kile DE (1990) Effect of soil moisture on the sorption of tricholoroethene vapor to vadose zone soil at Picatinny arsenal, New Jersey, *Environ. Sci. Technol*., 24(5):676–683

Spitz, K, and Moreno, J (1996). *A Practial Guide to Groundwater and Solute Transport Modeling*. John Wiley & Sons, New York

Sposito G, White RE, Darrah PR, Jury WA, (1986) Transfer function model of solute transport through soil. 3. The convection-dispersion equation, *Water Resour. Res*., 22(2):255–262

Srivastava R, Sharma PK, Brusseau ML (2002) Spatial moments for reactive transport in heterogeneous porous media, *ASCE J. Hydrol. Eng*., 7(4):336–341

Stagnitti F, Parlange MB, Steenhuis TS, Parlange J-Y (1986) Drainage from a uniform soil layer on a hillslope, *Water Resour. Res*., 22(5):631–634

Stillman JS, Haws NW, Govindaraju RS, Rao PSC (2006) A model for transient flow to a subsurface tile drain under macropore-dominated flow conditions, *J. Hydrol*., 317:49–62

Sudicky EA (1986) A natural gradient experiment on solute transport in a sand aquifer: spatial variability of hydraulic conductivity and its role in the dispersion process, *Water Resour. Res*., 22:2069–2082

Talenti G (1987) Recovering a function from a finite number of moments. *Inverse Problems*, 3:501–517

Tari A, Telek M (2005) Numerical behaviour of the moment based estimation algorithms. Paper presented in the Workshop on *Preformability Modeling of Computer and Communication Systems, PMCCS*, Torino, Italy

Toride N, Leij FJ, van Genuchten MT (1993) A comprehensive set of analytical solutions for nonequilibrium solute transport with first-order decay and zero-order production, *Water Resour. Res*., 29,2167–2182

—— (1995) The CXTFIT code for estimating transport parameters from laboratory or field tracer experiments, *Res. Rep. No. 137*, U.S. Salinity Laboratory, ARS, U.S.D.A., Riverside, CA

Turner GA (1972) *Heat and Concentration Waves*. Academic Press, New York

Utermann J, Kladivko EJ, Jury WA (1990) Evaluating pesticide migration in tile-drained soils with a transfer function model. *J. Environ. Qual*. 19(4):707–714

Van der Molen WH. and Wesseling J (1991) A solution in closed form and a series solution to replace the tables for thickness of the equivalent layer in Hooghoudt's drain spacing formula. *Agric. Water Manage*, 19:1–16

Valocchi AJ (1985) Validity of the local equilibrium assumption for modeling sorbing transport through homogeneous soils, *Water Resour. Res*., 21:808–820

—— (1988) Theoretical analysis of deviations from local equilibrium during sorbing solute transport through idealized stratified aquifers, *J. Contam. Hydrol*., 2:191–207

—— (1989) Spatial moment analysis of the transport of kinetically adsorbing solutes through stratified aquifers. *Water Resour. Res*., 25:273–279

Van der Ploeg RR, Horton R, Kirkham D (1999) Steady flow to drains and wells, in *Agricultural Drainage*, Skaggs RW, Van Schilfgaarde J (eds.), Monograph 38, ASA, Madison, WI

van Genuchten MT (1985) Convective-dispersive transport of solutes involved in sequential first order decay reactions, *Computers and Geosciences*, 11(2):129–147

van Genuchten M. Th, Wagenet RJ (1989) Two-site/two-region models for pesticide transport and degradation: theoretical development and analytical solutions, *Soil Sci. Soc. Am. J*., 53:1303–1310

van Genuchten M. Th, Leij FJ (1991) Mathematical analysis of one dimensional solute transport in a layered soil profile, *Soil. Sc. Soc. Am. J*. 55:944–953

van Genuchten M. Th, Dalton FN (1986) Models for simulating salt movement in aggregated field soils, *Geoderma*, 38:165–183

van Genuchten M. Th, Wierenga PJ (1976) Mass transfer studies in sorbing porous media I. analytical solutions, *Soil Sci. Soc. Am. Proc*., 40(4). 473–480

van Genuchten M. Th (1974) Mass transfer studies in sorbing porous media, *Ph.D. Diss*. New Mexico State Univ., Las Cruces (Diss. Abstr. 75–11005)

van der Werf HMG (1996) Assessing the impact of pesticides on the environment, *Agricultural, Ecosystems and Environment*, 60:81–96

van der Zee SEATM, Boesten JJTI (1991) Effects of soil heterogeneity on pesticide leaching to groundwater, *Water Resour. Res*., 27(12):3051–3063

Vidal-Madjar, Guiochon CG (1977) Experimental characterization of elution profiles in gas chromatography using central statistical moments: study of the relationship between these moments and mass transfer kinetics in the column. *J. Chromatography*. 142:61–86

Villermaux J (1981) Theory of linear chromatography. In: Rodrigues AE, D

Tondeur (Editors), *Percolation Processes: Theory and Applications*. Sijthoff & Noordhoff, The Hague, 83–140

Wagenet RJ, Biggar JW, Nielsen DR (1976) Analytical solutions of miscible displacement equations describing the sequential microbiological transformations of urea, ammonium and nitrate: *Research Rep. no. 6001, Dep. of Water Science and Engineering*, Univ. California, Davis, p 53

Wagenet RJ, Rao PSC (1990) Modeling pesticide fate in soils, in: *Pesticides in the Soil Environment: Processes, Impacts, and Modeling*, SSSA Book Series, 2:351–399

Wilson DE, Montgomery RE, Sheller MR (1987) A mathematical model for removing volatile subsurface hydrocarbons by miscible displacement, *Water Air Soil Pollut*., 33:231–255

Wilson DJ, Clarke AN, Clarke JH (1988) Soil clean up by in-situ aeration, I, Mathematical modeling, *Sep. Sci. Technol*., 23(10–11), 991–1037

Wilson JL, Gelhar LW (1981) Analysis of longitudinal dispersion in unsaturated flow, 1, The analytical method, *Water Resour. Res*., 17(1):122–130

White RE, Dyson JS, Haigh RA, Jury WA, Sposito G, (1986) A transfer function model of solute transport through soil. 2. Illustrative applications. *Water Resour. Res*., 22(2): 248–254

Wraith JM, Comfort SD, Woodbury BL, Inskeep WP (1993) A simplified waveform analysis approach for monitoring solute transport using time-domain reflectometry, Soil Sci. Soc. Am. J., 57:637–642

Wraith JM, Das BS (1998) Monitoring soil water and ionic solute distributions using time-domain reflectometry, *Soil & Tillage Research*, Special Issue: State of the art in soil physics and in soil technology of anthropic soils, 47:145–150

Yates SR, Warrick AW, Lomen DO, (1985) Hillsope seepage: an analytical solution to a nonlinear Dupuit-Forchheimer problem. *Water Resour. Res*., 21(3):331–336

Yates SR, Papiernik SK, Gao F, Gan J (2000) Analytical solutions for the transport of volatile organic chemicals in unsaturated layered system, *Water Resour. Res*., 36(8):1993–2000

Young RC (1931) The algebra of many-valued quantities, *Math. Annalen*, 104:260–290

Youngs EG (1999) Non-steady flow to drains, in *Agricultural Drainage*, Skaggs RW., J. Van Schilfgaarde (ed.), Monograph 38, ASA, Madison, WI

Zadeh LA (1978) Fuzzy sets as a basis for a theory of possibility, *Fuzzy Sets Sys*., 1:3–28

Zellner A, Highfield RA (1988) Calculation of maximum entropy distribution and approximations of marginal posterior distributions. *J. Econometrics*, 37:195–209

INDEX

Water Science and Technology Library

1. A.S. Eikum and R.W. Seabloom (eds.): *Alternative Wastewater Treatment*. Low-Cost Small Systems, Research and Development. Proceedings of the Conference held in Oslo, Norway (7–10 September 1981). 1982 ISBN 90-277-1430-4
2. W. Brutsaert and G.H. Jirka (eds.): *Gas Transfer at Water Surfaces*. 1984 ISBN 90-277-1697-8
3. D.A. Kraijenhoff and J.R. Moll (eds.): *River Flow Modelling and Forecasting*. 1986 ISBN 90-277-2082-7
4. World Meteorological Organization (ed.): *Microprocessors in Operational Hydrology*. Proceedings of a Conference held in Geneva (4–5 September 1984). 1986 ISBN 90-277-2156-4
5. J. N.ěmec: *Hydrological Forecasting*. Design and Operation of Hydrological Forecasting Systems. 1986 ISBN 90-277-2259-5
6. V.K. Gupta, I. Rodríguez-Iturbe and E.F. Wood (eds.): *Scale Problems in Hydrology*. Runoff Generation and Basin Response. 1986 ISBN 90-277-2258-7
7. D.C. Major and H.E. Schwarz: *Large-Scale Regional Water Resources Planning*. The North Atlantic Regional Study. 1990 ISBN 0-7923-0711-9
8. W.H. Hager: *Energy Dissipators and Hydraulic Jump*. 1992 ISBN 0-7923-1508-1
9. V.P. Singh and M. Fiorentino (eds.): *Entropy and Energy Dissipation in Water Resources*. 1992 ISBN 0-7923-1696-7
10. K.W. Hipel (ed.): *Stochastic and Statistical Methods in Hydrology and Environmental Engineering*. A Four Volume Work Resulting from the International Conference in Honour of Professor T.E. Unny (21–23 June 1993). 1994
    10/1: Extreme values: floods and droughts ISBN 0-7923-2756-X
    10/2: Stochastic and statistical modelling with groundwater and surface water applications ISBN 0-7923-2757-8
    10/3: Time series analysis in hydrology and environmental engineering ISBN 0-7923-2758-6
    10/4: Effective environmental management for sustainable development ISBN 0-7923-2759-4
    Set 10/1–10/4: ISBN 0-7923-2760-8
11. S.N. Rodionov: *Global and Regional Climate Interaction: The Caspian Sea Experience*. 1994 ISBN 0-7923-2784-5
12. A. Peters, G. Wittum, B. Herrling, U. Meissner, C.A. Brebbia, W.G. Gray and G.F. Pinder (eds.): *Computational Methods in Water Resources X*. 1994
    Set 12/1–12/2: ISBN 0-7923-2937-6
13. C.B. Vreugdenhil: *Numerical Methods for Shallow-Water Flow*. 1994 ISBN 0-7923-3164-8
14. E. Cabrera and A.F. Vela (eds.): *Improving Efficiency and Reliability in Water Distribution Systems*. 1995 ISBN 0-7923-3536-8
15. V.P. Singh (ed.): *Environmental Hydrology*. 1995 ISBN 0-7923-3549-X
16. V.P. Singh and B. Kumar (eds.): *Proceedings of the International Conference on Hydrology and Water Resources* (New Delhi, 1993). 1996
    16/1: Surface-water hydrology ISBN 0-7923-3650-X
    16/2: Subsurface-water hydrology ISBN 0-7923-3651-8

Water Science and Technology Library

16/3: Water-quality hydrology ISBN 0-7923-3652-6
16/4: Water resources planning and management ISBN 0-7923-3653-4
Set 16/1–16/4 ISBN 0-7923-3654-2

17. V.P. Singh: *Dam Breach Modeling Technology*. 1996 ISBN 0-7923-3925-8
18. Z. Kaczmarek, K.M. Strzepek, L. Somlyódy and V. Priazhinskaya (eds.): *Water Resources Management in the Face of Climatic/Hydrologic Uncertainties*. 1996 ISBN 0-7923-3927-4
19. V.P. Singh and W.H. Hager (eds.): *Environmental Hydraulics*. 1996 ISBN 0-7923-3983-5
20. G.B. Engelen and F.H. Kloosterman: *Hydrological Systems Analysis*. Methods and Applications. 1996 ISBN 0-7923-3986-X
21. A.S. Issar and S.D. Resnick (eds.): *Runoff, Infiltration and Subsurface Flow of Water in Arid and Semi-Arid Regions*. 1996 ISBN 0-7923-4034-5
22. M.B. Abbott and J.C. Refsgaard (eds.): *Distributed Hydrological Modelling*. 1996 ISBN 0-7923-4042-6
23. J. Gottlieb and P. DuChateau (eds.): *Parameter Identification and Inverse Problems in Hydrology, Geology and Ecology*. 1996 ISBN 0-7923-4089-2
24. V.P. Singh (ed.): *Hydrology of Disasters*. 1996 ISBN 0-7923-4092-2
25. A. Gianguzza, E. Pelizzetti and S. Sammartano (eds.): *Marine Chemistry*. An Environmental Analytical Chemistry Approach. 1997 ISBN 0-7923-4622-X
26. V.P. Singh and M. Fiorentino (eds.): *Geographical Information Systems in Hydrology*. 1996 ISBN 0-7923-4226-7
27. N.B. Harmancioglu, V.P. Singh and M.N. Alpaslan (eds.): *Environmental Data Management*. 1998 ISBN 0-7923-4857-5
28. G. Gambolati (ed.): *CENAS. Coastline Evolution of the Upper Adriatic Sea Due to Sea Level Rise and Natural and Anthropogenic Land Subsidence*. 1998 ISBN 0-7923-5119-3
29. D. Stephenson: *Water Supply Management*. 1998 ISBN 0-7923-5136-3
30. V.P. Singh: *Entropy-Based Parameter Estimation in Hydrology*. 1998 ISBN 0-7923-5224-6
31. A.S. Issar and N. Brown (eds.): *Water, Environment and Society in Times of Climatic Change*. 1998 ISBN 0-7923-5282-3
32. E. Cabrera and J. García-Serra (eds.): *Drought Management Planning in Water Supply Systems*. 1999 ISBN 0-7923-5294-7
33. N.B. Harmancioglu, O. Fistikoglu, S.D. Ozkul, V.P. Singh and M.N. Alpaslan: *Water Quality Monitoring Network Design*. 1999 ISBN 0-7923-5506-7
34. I. Stober and K. Bucher (eds): *Hydrogeology of Crystalline Rocks*. 2000 ISBN 0-7923-6082-6
35. J.S. Whitmore: *Drought Management on Farmland*. 2000 ISBN 0-7923-5998-4
36. R.S. Govindaraju and A. Ramachandra Rao (eds.): *Artificial Neural Networks in Hydrology*. 2000 ISBN 0-7923-6226-8
37. P. Singh and V.P. Singh: *Snow and Glacier Hydrology*. 2001 ISBN 0-7923-6767-7
38. B.E. Vieux: *Distributed Hydrologic Modeling Using GIS*. 2001 ISBN 0-7923-7002-3
39. I.V. Nagy, K. Asante-Duah and I. Zsuffa: *Hydrological Dimensioning and Operation of Reservoirs*. Practical Design Concepts and Principles. 2002 ISBN 1-4020-0438-9

40. I. Stober and K. Bucher (eds.): *Water-Rock Interaction*. 2002 ISBN 1-4020-0497-4
41. M. Shahin: *Hydrology and Water Resources of Africa*. 2002 ISBN 1-4020-0866-X
42. S.K. Mishra and V.P. Singh: *Soil Conservation Service Curve Number (SCS-CN) Methodology*. 2003 ISBN 1-4020-1132-6
43. C. Ray, G. Melin and R.B. Linsky (eds.): *Riverbank Filtration*. Improving Source-Water Quality. 2003 ISBN 1-4020-1133-4
44. G. Rossi, A. Cancelliere, L.S. Pereira, T. Oweis, M. Shatanawi and A. Zairi (eds.): *Tools for Drought Mitigation in Mediterranean Regions*. 2003 ISBN 1-4020-1140-7
45. A. Ramachandra Rao, K.H. Hamed and H.-L. Chen: *Nonstationarities in Hydrologic and Environmental Time Series*. 2003 ISBN 1-4020-1297-7
46. D.E. Agthe, R.B. Billings and N. Buras (eds.): *Managing Urban Water Supply*. 2003 ISBN 1-4020-1720-0
47. V.P. Singh, N. Sharma and C.S.P. Ojha (eds.): *The Brahmaputra Basin Water Resources*. 2004 ISBN 1-4020-1737-5
48. B.E. Vieux: *Distributed Hydrologic Modeling Using GIS. Second Edition*. 2004 ISBN 1-4020-2459-2
49. M. Monirul Qader Mirza (ed.): *The Ganges Water Diversion: Environmental Effects and Implications*. 2004 ISBN 1-4020-2479-7
50. Y. Rubin and S.S. Hubbard (eds.): *Hydrogeophysics*. 2005 ISBN 1-4020-3101-7
51. K.H. Johannesson (ed.): *Rare Earth Elements in Groundwater Flow Systems*. 2005 ISBN 1-4020-3233-1
52. R.S. Harmon (ed.): *The Río Chagres, Panama*. A Multidisciplinary Profile of a Tropical Watershed. 2005 ISBN 1-4020-3298-6
53. To be published.
54. V. Badescu, R.S. Cathcart and R.D. Schuiling (eds): Macro-Engineering: A Challenge for the Future. 2006 ISBN 1-4020-3739-2
55. To be published.
56. G. Salvadori, C. De Michele, N.T. Kottegoda and R. Renzo: *Extremes in Nature*. An Approach to Using Copulas. 2007 ISBN 1-4020-4414-3
57. S.K. Jain, R.K. Agarwal and V.P. Singh: *Hydrology and Water Resources of India*. 2007 ISBN 1-4020-4414-4
58. To be published.
59. M. Shahin: *Water Resources and Hydrometeorology of the Arab Region*. 2007 ISBN 1-4020-4577-8
60. To be published.
61. R.S. Govindaraju and B.S. Das: *Moment Analysis for Subsurface Hydrologic Applications*. 2007 ISBN 978-1-4020-5751-9